THE QCD AND STANDARD MODEL WORKING GROUP:

Summary Report

Conveners:

S. Catani[1], M. Dittmar[2], J. Huston[3], D. Soper[4], S. Tapprogge[5]

Working Group:

P. Aurenche[6], C. Balázs[7], R. D. Ball[8], T. Binoth[6], E. Boos[9], J. Collins[10], V. del Duca[1], M. Fontannaz[11], S. Frixione[1], J.P. Guillet[6], G. Heinrich[11], V. Ilyin[9], Y. Kato[12], K. Odagiri[13], F. Paige[14], E. Pilon[6], A. Pukhov[9], I. Puljak[15,16], A. Semenov[9], A. Skatchkova[9], V. Tano[17], W.K. Tung[3], W. Vogelsang[18], M. Werlen[6], D. Zeppenfeld[1,19].

[1] CERN, Theory Division, CH-1211 Geneva 23, Switzerland
[2] Institute for Particle Physics (IPP), ETH Zurich, CH-8093 Zurich, Switzerland
[3] Physics Dept., Michigan State University, East Lansing, MI 48824 USA
[4] Institute of Theoretical Science, University of Oregon, Eugene, Oregon 97403 USA
[5] CERN, EP Division, CH-1211 Geneva 23, Switzerland
[6] LAPTH, BP 110, F–74941 Annecy le Vieux Cedex, France.
[7] Department of Physics and Astronomy, University of Hawaii, Honolulu, HI, 96822 USA
[8] Department of Physics and Astronomy, University of Edinburgh, EH9 3JZ, Scotland
[9] Institute of Nuclear Physics, MSU, 119899 Moscow, Russia
[10] Department of Physics, Penn State University, University Park, PA 16802, USA
[11] Laboratoire de Physique Théorique, Université de Paris XI, Batiment 210, F-91405, Orsay Cedex, France
[12] Kogakuin University, Shinjuku, Tokyo 163-8677, Japan
[13] Rutherford Appleton Laboratory, Chilton, Didcot, Oxon OX11 0QX, UK
[14] Physics Department, Brookhaven National Laboratory, Upton, NY 11973, USA
[15] Laboratoire de Physique Nucléaire et des Houtes Energies, Ecole Polytechnique, 91128 Palaiseau, France
[16] University of Split, 21000 Split, Croatia
[17] Technische Hochschule Aachen, III Physikalisches Institut, Sommerfeldestrasse 26-28, D-52-56 Aachen, Germany; MPI fuer Physik, Foehringer Ring , 80805 Muenchen
[18] C.N. Yang Institute for Theoretical Physics, SUNY Stony Brook, Stony Brook, New York 11794, USA
[19] Department of Physics, University of Wisconsin, Madison, WI 53706, USA

Report of the QCD/SM working group for the Workshop "Physics at TeV Colliders", Les Houches, France 8–18 June 1999.

CONTENTS

Introduction

The Les Houches Workshop on Physics at TeV Colliders took place from June 8-18, 1999. One of the three working groups at Les Houches concentrated on QCD issues, both at the Tevatron Collider and at the LHC. Besides the interest in QCD in its own right, QCD dynamics plays an important role in the production mechanisms for any new physics processes that might be observed at either collider, as well as any processes that may form backgrounds to the new physics. As might be expected, there was a great deal of overlap with the other two working groups, and especially with the Higgs working group.

To provide a more specific focus, each day at Les Houches was devoted to a specific topic. The topic and speakers are listed below:

- Thursday: parton distibutions (W.K. Tung, R. Ball)
- Friday: photons (E. Pilon, M. Fontannaz, S. Frixione); jet definitions (J. Huston, D. Zeppenfeld)
- Saturday: Monte Carlos (F. Paige, J.Collins, K. Odagiri, Y. Kato, E. Boos, A. Skatchkova, V. Ilyin)
- Monday: joint meeting with Higgs group (C. Balazs)
- Tuesday: (re)summation (C. Balazs)
- Wednesday: direct photons and pions (P. Aurenche), heavy flavor (S. Frixione)
- Thursday: N^{n}LO (V. del Duca, G. Henrich)

This writeup for the QCD working group is not intended to be a comprehensive summary of all of the QCD issues currently important in high energy physics, or expected to be important for the LHC. Rather, we have chosen to concentrate in detail on a few selected topics and to summarize in a pedagogical manner the current status and the progress expected in the near future. The expertise of the people attending the workshop, and the timeliness of the issues, resulted in a great deal of concentration on resummation calculations, and their relation to Monte Carlos. This is also reflected in the writeup. The writeup is organized into chapters that roughly follow the organization shown above. Preceding the discussion of the individual topics is a general introduction to QCD phenomenology relevant for the LHC, by S. Catani.

Joey Huston (for the Working Group).

Acknowledgements:
We would like to thank the organizers of the workshop for the pleasant and stimulating atmosphere. Les Houches is a beautiful place to do physics; we should do this every two years.

Aspects of QCD, from the Tevatron to the LHC

S. Catani

Abstract

This contribution presents a selection of the topics (parton densities, fixed-order calculations, parton showers, soft-gluon resummation) discussed in my introductory lectures at the Workshop and includes a pedagogical overview of the corresponding theoretical tools.

1 Introduction

The production cross sections for all the processes at hadron-collider experiments are controlled by strong interaction physics and, hence, by its underlying field theory, QCD (see recent overviews in Refs. [1, 2, 3, 4]). Studies of QCD at the Tevatron and the LHC have two main purposes [5, 6, 7]. First, they are important to test the predictions of QCD, to measure its fundamental parameters (e.g. the strong coupling α_S) and to extract quantitative information on its non-perturbative dynamics (e.g. the distribution of partons in the proton). Second, they are relevant to a precise estimate of the background to other Standard Model processes and to signals of new physics.

This contribution is not a comprehensive review of QCD at high-energy hadron colliders. It is based on a selection of the topics presented in my introductory lectures at this Workshop. The selection highlights the QCD subjects that were most discussed during the Workshop and includes a pedagogical overview of some of the corresponding theoretical tools.

After the introduction of the general theoretical framework, I summarize in Sect. 2 the present knowledge on the parton densities and its impact on QCD predictions for hard-scattering processes at the Tevatron and the LHC. In Sect. 3, I then discuss some issues related to processes that are sensitive to the gluon density and, hence, to its determination. Section 4 presents a dictionary of different approaches (fixed-order expansions, resummed calculations, parton showers) to perturbative QCD calculations. The dictionary continues in Sect. 5, where I review soft-gluon resummation and discuss some recent phenomenological applications of threshold resummation to hadron collisions.

The QCD framework to describe any inclusive hard-scattering process,

$$h_1(p_1) + h_2(p_2) \to H(Q, \{\ldots\}) + X \quad , \tag{1}$$

in hadron–hadron collisions is based on perturbation theory and on the factorization theorem of mass singularities. The corresponding cross section is computed by using the factorization formula [8]

$$\sigma(p_1,p_2;Q,\{\ldots\}) = \sum_{a,b}\int_{x_{\min}}^{1} dx_1\,dx_2\,f_{a/h_1}(x_1,\mu_F^2)\,f_{b/h_2}(x_2,\mu_F^2)\,\hat{\sigma}_{ab}(x_1p_1,x_2p_2;Q,\{\ldots\};\mu_F^2) + \mathcal{O}\left((\Lambda_{QCD}/Q)^p\right) \quad . \tag{2}$$

The colliding hadrons h_1 and h_2 have momenta p_1 and p_2, H denotes the triggered hard probe (vector bosons, jets, heavy quarks, Higgs bosons, SUSY particles and so on) and X stands for any unobserved particle produced by the collision. The typical scale Q of the scattering process is set by the invariant mass or the transverse momentum of the hard probe, and the notation $\{\ldots\}$ stands for any other relevant scale and kinematic variable of the process. For instance, in the case of W production we have $Q = M_W$ and $\{\ldots\} = \{Q_\perp, y, \ldots\}$, where $M_W, Q_\perp$ and y are the mass of the vector boson, its transverse momentum and its rapidity, respectively.

The factorization formula (2) involves the convolution of the partonic cross sections $\hat{\sigma}_{ab}$ (where $a,b = q,\bar{q},g$) and the parton distributions $f_{a/h}(x,\mu_F^2)$ of the colliding hadrons. If the hard probe H is a hadron or a photon, the factorization formula has to include an additional convolution with the corresponding parton fragmentation function $d_{a/H}(z,\mu_F^2)$.

The term $\mathcal{O}\left((\Lambda_{QCD}/Q)^p\right)$ on the right-hand side of Eq. (2) generically denotes non-perturbative contributions (hadronization effects, multiparton interactions, contributions of the soft underlying event, and so on). Provided the hard-scattering process (1) is sufficiently inclusive[1], $\hat{\sigma}_{ab}$ is computable as a power series expansion in $\alpha_S(Q^2)$ and the non-perturbative contributions are (small) power-suppressed corrections (i.e. the power p is positive) as long as the hard-scattering scale Q is larger than few hundred MeV, the typical size of the QCD scale Λ_{QCD}.

The parton densities $f_{a/h}(x,\mu_F^2)$ are phenomenological distributions that describe how partons are bounded in the colliding hadrons. Although they are not calculable in QCD perturbation theory, the parton densities are universal (process-independent) quantities. The scale μ_F is a factorization scale introduced in Eq. (2) to separate the bound-state effects from the perturbative interactions of the partons. The physical cross section $\sigma(p_1,p_2;Q,\{\ldots\})$ does not depend on this arbitrary scale, but parton densities and partonic cross sections separately depend on μ_F. In particular, higher-order contributions to $\hat{\sigma}_{ab}(x_1p_1,x_2p_2;Q,\{\ldots\};\mu_F^2)$ contain corrections of relative order $(\alpha_S(Q^2)\ln Q^2/\mu_F^2)^n$. If μ_F is very different from Q, these corrections become large and spoil the reliability of the perturbative expansion. Thus, in practical applications of the factorization formula (2), the scale μ_F is set approximately equal to the hard scale Q and variations of μ_F around this central value are used to estimate the uncertainty of the perturbative expansion.

The lower limit $x_{\min}$ of the integrations over the parton momentum fractions x_1 and x_2, as well as the values of x_1 and x_2 that dominate the convolution integral in Eq. (2), are controlled by the kinematics of the hard-scattering process. Typically we have $x_{\min} \gtrsim Q^2/S$,

[1] More precisely, it has to be defined in an infrared- and collinear-safe manner.

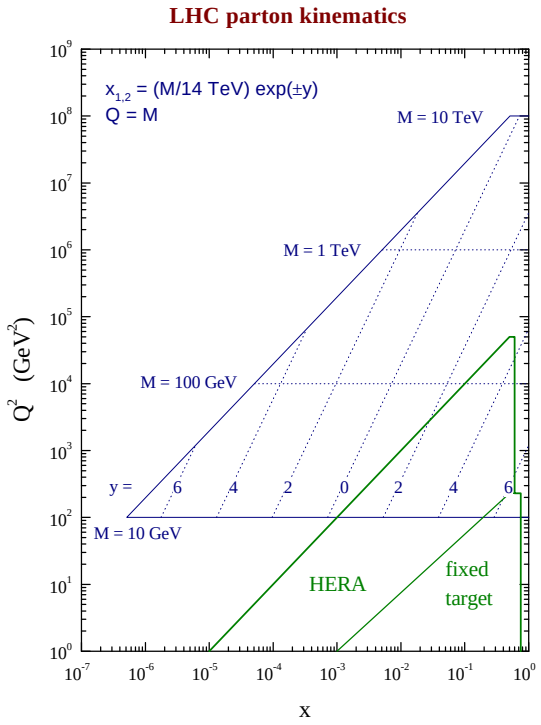

Figure 1: The (x, Q^2) plane of the parton kinematics for the production of a heavy system of invariant mass M and rapidity y at LHC, HERA and fixed-target experiments.

where $S = (p_1 + p_2)^2$ is the square of the centre-of-mass energy of the collision. If the hard probe is a state of invariant mass M and rapidity y, the dominant values of the momentum fractions are $x_{1,2} \sim (Me^{\pm y})/\sqrt{S}$ (see Fig. 1). Thus varying M and y at fixed $\sqrt{S}$, we are sensitive to partons with different momentum fractions. Increasing $\sqrt{S}$ the parton densities are probed in a kinematic range that extends towards larger values of Q and smaller values of $x_{1,2}$.

2 Parton densities

The parton densities are an essential ingredient to study hard-scattering collisions. Once the partonic cross sections have been perturbatively computed, cross section measurements can be used to determine the parton densities. Then, they can in turn be used to predict cross sections for other hard-scattering processes.

The dependence of the parton densities[2] $f_a(x, \mu^2)$ on the momentum fraction x and their absolute value at any fixed scale μ are not computable in perturbation theory. However, the scale dependence is perturbatively controlled by the DGLAP evolution equation [9]

$$\frac{d\, f_a(x,\mu^2)}{d \ln \mu^2} = \sum_b \int_x^1 \frac{dz}{z}\, P_{ab}(\alpha_S(\mu^2), z)\, f_a(x/z, \mu^2) \quad . \tag{3}$$

[2]In the following the parton densities of the proton $f_{a/p}$ are simply denoted by f_a and those of the antiproton are obtained by using charge-conjugation invariance, i.e. $f_{a/\bar{p}} = f_{\bar{a}/p} = f_{\bar{a}}$.

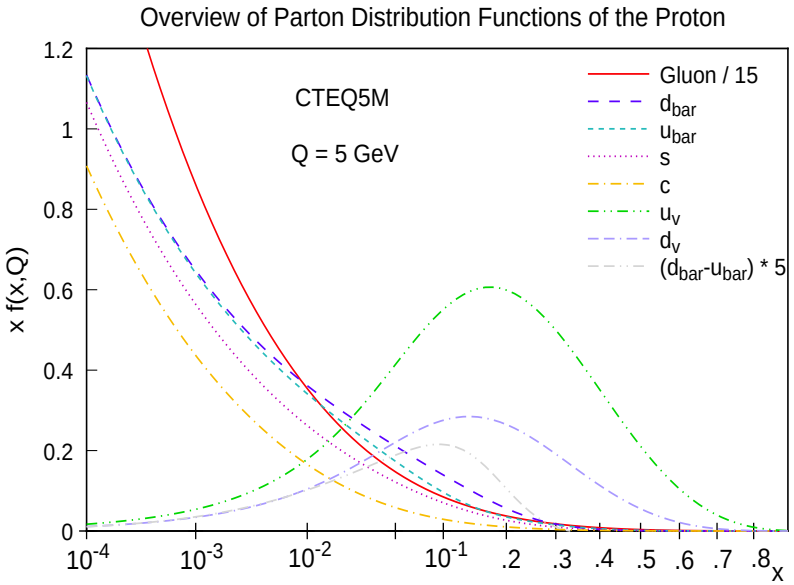

Figure 2: Typical x-shape of the parton densities (set CTEQ5M at $Q = 5$ GeV).

The kernels $P_{ab}(\alpha_S, z)$ are the Altarelli–Parisi (AP) splitting functions. As the partonic cross sections in Eq. (2), the AP splitting functions can be computed as a power series expansion in α_S:

$$P_{ab}(\alpha_S, z) = \alpha_S P_{ab}^{(LO)}(z) + \alpha_S^2 P_{ab}^{(NLO)}(z) + \alpha_S^3 P_{ab}^{(NNLO)}(z) + \mathcal{O}(\alpha_S^4) \quad . \tag{4}$$

The leading order (LO) and next-to-leading order (NLO) terms $P_{ab}^{(LO)}(z)$ and $P_{ab}^{(NLO)}(z)$ in the expansion are known [10]. These first two terms are used in most of the QCD studies. Having determined $f_a(x, Q_0^2)$ at a given input scale $\mu = Q_0$, the evolution equation (3) can be used to compute the parton densities at different perturbative scales μ and larger values of x.

The parton densities are determined by performing global fits [11] to data from deep-inelastic scattering (DIS), Drell–Yan (DY), prompt-photon and jet production. The method consists in parametrizing the parton densities at some input scale Q_0 and then adjusting the parameters to fit the data. The parameters are usually constrained by imposing the positivity of the parton densities ($f_a(x, \mu^2) \geq 0$) and the momentum sum rule ($\sum_a \int_0^1 dx\, x\, f_a(x, \mu^2) = 1$).

The present knowledge on the parton densities of the proton is reviewed in Refs. [7, 12, 13]. Their typical behaviour is shown in Fig. 2. All densities decrease at large x. At small x the valence quark densities vanish and the gluon density dominates. The sea-quark densities also increase at small x because they are driven by the strong rise of the gluon density and the splitting of gluons in $q\bar{q}$ pairs. Note that the quark densities are not flavour-symmetric either in the valence sector ($u_v \neq d_v$) or in the sea sector ($\bar{u} \neq \bar{d}$).

In addition to having the best estimate of the parton densities, it is important to quantify the corresponding uncertainty. This is a difficult issue. The uncertainty depends on the kinematic range in x and Q^2. Moreover, it cannot be reliably estimated by simply comparing the parton densities obtained by different global fits. In fact, a lot of common systematic

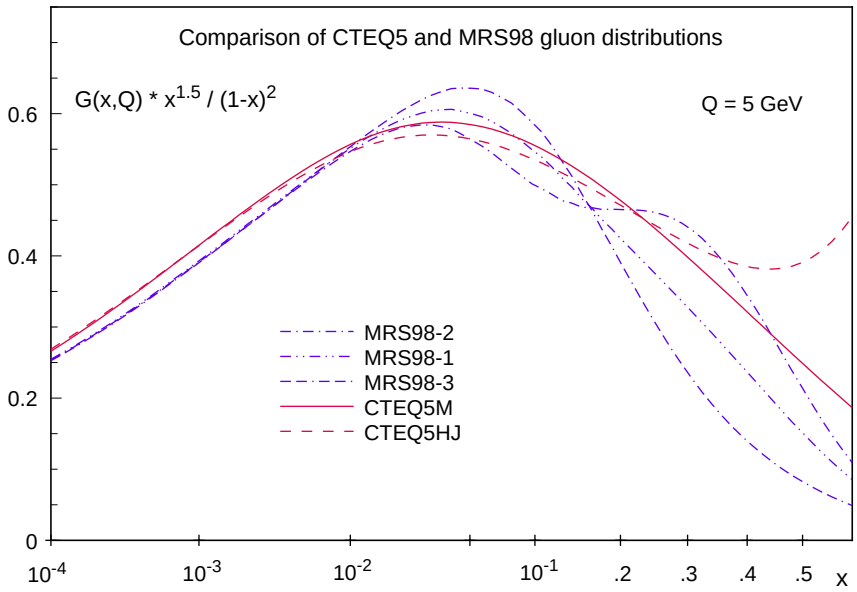

Figure 3: Comparison between the gluon densities of the CTEQ and MRST groups.

and common assumptions affect the global-fit procedures. Recent attempts to obtain parton densities with error bands that take into account correlations between experimental errors are described in Refs. [7, 13]. Some important theoretical uncertainties that are still to be understood are also discussed in Ref. [7].

The overall conclusion is that the quark densities[3] are reasonably well constrained and determined by DIS and DY processes, while the gluon density is certainly more uncertain [11, 17]. At small x ($x \lesssim 10^{-3}$), the gluon density f_g is at present constrained by a *single* process, namely DIS at HERA. Thus, large higher-order corrections of the type $(\alpha_S \ln 1/x)^n$ could possibly affect the extraction of f_g. *Assuming* that f_g is well determined at small x, the momentum sum rule reasonably constrains f_g at intermediate values of x ($x \sim 10^{-2}$). Jet production at the Tevatron at low to moderate values of the jet transverse energy E_T can also be useful in constraining the gluon distribution in the range $0.05 \lesssim x \lesssim 0.2$. At large x ($x \gtrsim 10^{-1}$), the most sensitive process to f_g is prompt-photon production. Since, at present, prompt-photon data are not well described/predicted by perturbative QCD calculations, they cannot be used for a precise determination of f_g. Further discussion on these points is given in Sect. 3.

The conclusion that the gluon density is not well known can also be drawn by inspection (see Fig. 3) of the differences between the most updated analyses performed by the CTEQ Collaboration and the MRST group.

The differences between the MRST gluons and the CTEQ ones are due to the fact that the two groups used different data sets. The various gluon densities are very similar at small x, because in this region both groups used the HERA data. The MRST group includes prompt-photon data in the global fit: these data constrain the gluon directly at $x \gtrsim 10^{-1}$

[3]Uncertainties on the determination of the quark densities at very high x are discussed in Refs. [14, 15, 16].

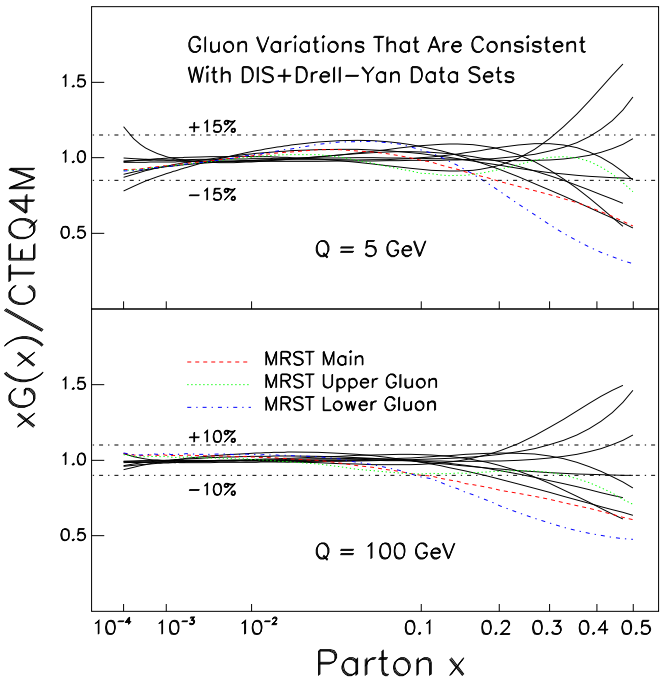

Figure 4: A picture of the gluon density uncertainty. The continuous (black) lines refer to gluon densities that are constrained only by DIS and DY data. The dashed (coloured) lines refer to gluon densities of the MRST group, which uses also prompt-photon data.

and indirectly (by the momentum sum rule) at $x \sim 10^{-2}$. The CTEQ group does not use prompt-photon data, but it includes Tevatron data on the one-jet inclusive cross section. These data give a good constraint on f_g in the region $0.05 \lesssim x \lesssim 0.2$.

There are also differences within the MRST and CTEQ sets. The various gluon densities of the MRST set correspond to different values of the non-perturbative transverse-momentum smearing that can be introduced to describe the differences among the prompt-photon data that are available at several centre-of-mass energies. The CTEQ5M and CTEQ5HJ gluons correspond to different assumptions on the parametrization of the functional form of $f_g(x, Q_0^2)$ at large x; the CTEQ5M set corresponds to the minimum-χ^2 solution of the fit while the CTEQ5HJ set (with a slightly higher χ^2) provides the best fit to the high-E_T tail of the CDF *and* D0 jet cross sections.

This brief illustration shows that the differences in the most recent parton densities are mainly due to either inconsistencies between data sets and/or poor theoretical understanding of them. A more quantitative picture of the dependence on x and Q^2 of the gluon density uncertainty is presented in Fig. 4.

We can see that the DIS and DY data sets weakly constrain f_g for $x \gtrsim 10^{-1}$. Since the AP splitting functions lead to negative scaling violation at large x, when $f_g(x, Q^2)$ is evolved at larger scales Q according to Eq. (3) the gluon uncertainty is diluted: it propagates at smaller values of x and its size is reduced at fixed x.

Figure 5 shows the typical predictions for hard-scattering cross sections at the Tevatron

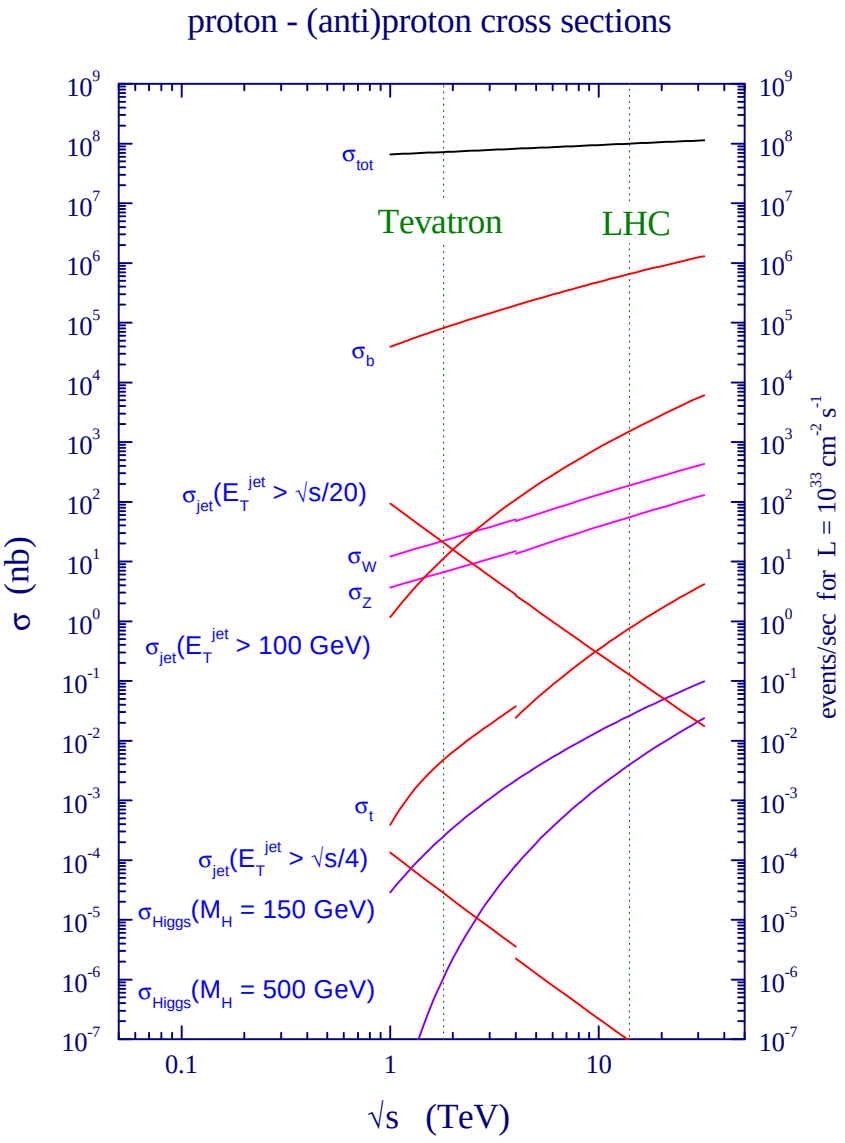

Figure 5: QCD predictions for hard-scattering cross sections at the Tevatron and the LHC.

and the LHC, as obtained by using the parton densities of the MRST set. These predictions have to be supplemented with the corresponding uncertainties [7] coming from the determination of the parton densities and from perturbative corrections beyond the NLO. Owing to the increased centre-of-mass energy and to QCD scaling violation (see Fig. 4), the kinematic region with small uncertainties is larger at the LHC than at the Tevatron.

For most of the QCD processes at the LHC, the uncertainty from the parton densities is smaller than $\pm 10\%$ and, in particular, it is smaller than the uncertainty from higher-order corrections. Some relevant exceptions are the single-jet, W/Z and top quark cross sections. In the case of the single-jet inclusive cross section at high E_T ($E_T \gtrsim 2$ TeV), the uncertainty from the poorly known gluon density at high x is larger than that ($\sim \pm 10\%$) from higher-order corrections. The W and Z production cross sections are dominated by $q\bar{q}$ annihilation. Since the quark densities are well known, the ensuing uncertainty on the W/Z cross section is small ($\sim \pm 5\%$). Nonetheless, in this case the uncertainty from higher-order corrections is even smaller, since the partonic cross sections for the DY process are known [18] at the next-to-next-to-leading order (NNLO) in perturbation theory. In the case of top-quark production at the LHC, the gluon channel dominates and leads to an uncertainty of $\pm 10\%$ on the total cross section. Also for this process, however, the perturbative component is known beyond the NLO. Including all-order resummation of soft-gluon contributions [19], the estimated uncertainty from unknown higher-order corrections is approximately $\pm 5\%$ [19, 7].

3 The gluon density issue

At present, the processes[4] that are, in principle, most sensitive to the gluon density are DIS at HERA, b-quark production at the Tevatron, and prompt-photon production at fixed-target experiments. These processes constrain f_g for $x \lesssim 10^{-3}$, $x \sim 10^{-3}$–10^{-2} and $x \gtrsim 10^{-1}$, respectively. Nonetheless, the gluon density is, in practice, not well determined. The issue (or, perhaps, the puzzle) is that from a phenomenological viewpoint the standard theory, namely perturbative QCD at NLO, works pretty well for $x \lesssim 10^{-3}$ but not so well at larger values of x, while from theoretical arguments we should expect just the opposite to happen. This issue is discussed below mainly in its perturbative aspects. We should however keep it in mind that all these processes are dominated by hard-scattering scales Q of the order of few GeV. Different types of non-perturbative contributions can thus be important.

From the study of DIS at HERA we can extract information on the gluon and sea-quark densities of the proton. The main steps in the QCD analysis of the structure functions at small values of the Bjorken variable x are the following. The measurement of the proton structure function $F_2(x, Q^2) \sim q_S(x, Q^2)$ directly determines the sea-quark density $q_S = x(f_q + f_{\bar{q}})$. Then, the DGLAP evolution equation (3) or, more precisely, the following equations (the symbol $\otimes$ denotes the convolution integral with respect to x):

$$dF_2(x, Q^2)/d\ln Q^2 \quad \sim \quad P_{qq} \otimes q_S + P_{qg} \otimes g \quad , \tag{5}$$

[4]The rôle of jet production at the Tevatron has briefly been recalled in Sect. 2, and it is discussed in detail in Ref. [12].

$$dg(x,Q^2)/d\ln Q^2 \;\; \sim \;\; P_{gq} \otimes q_S + P_{gg} \otimes g \;\; , \tag{6}$$

are used to extract a gluon density $g(x,Q^2) = xf_g(x,Q^2)$ that agrees with the measured scaling violation in $dF_2(x,Q^2)/d\ln Q^2$ (according to Eq. (5)) and fulfils the self-consistency equation (6).

The perturbative-QCD ingredients in this analysis are the AP splitting functions $P_{ab}(\alpha_S, x)$. Once they are known (and only then), the non-perturbative gluon density can be determined.

The standard perturbative-QCD framework to extract $g(x,Q^2)$ consists in using the truncation of the AP splitting functions at the NLO. This approach has been extensively compared with structure function data over the last few years and it gives a good description of the HERA data, down to low values of $Q^2 \sim 2\,\mathrm{GeV}^2$. The NLO QCD fits simply require a slightly steep input gluon density at these low momentum scales. Typically [11], we have $g(x,Q_0^2) \sim x^{-\lambda}$, with $\lambda \sim 0.2$ at $Q_0^2 \sim 2\,\mathrm{GeV}^2$, and the data constrain $g(x,Q_0^2)$ with an uncertainty of approximately $\pm 20\%$.

Although it is phenomenologically successful, the NLO approach is not fully satisfactory from a theoretical viewpoint. The truncation of the splitting functions at a fixed perturbative order is equivalent to assuming that the dominant dynamical mechanism leading to scaling violations is the evolution of parton cascades with strongly-ordered transverse momenta. However, at high energy this evolution takes place over large rapidity intervals ($\Delta y \sim \ln 1/x$) and diffusion in transverse momentum becomes relevant. Formally, this implies that higher-order corrections to $P_{ab}(\alpha_S, x)$ are logarithmically enhanced:

$$P_{ab}(\alpha_S, x) \sim \frac{\alpha_S}{x} + \frac{\alpha_S}{x}\,(\alpha_S \ln x) + \ldots + \frac{\alpha_S}{x}\,(\alpha_S \ln x)^n + \ldots \;\; . \tag{7}$$

At asymptotically small values of x, resummation of these corrections is mandatory to obtain reliable predictions.

Small-x resummation is, in general, accomplished by the BFKL equation [20]. In the context of structure-function calculations, the BFKL equation provides us with improved expressions of the AP splitting functions $P_{ab}(\alpha_S, x)$, in which the leading logarithmic (LL) terms $(\alpha_S \ln x)^n$, the next-to-leading logarithmic (NLL) terms $\alpha_S(\alpha_S \ln x)^n$, and so forth, are systematically summed to all orders n in α_S. The present theoretical status of small-x resummation is discussed in Ref. [7]. Since in the small-x region the gluon channel dominates, only the gluon splitting functions P_{gg} and P_{gq} contain LL contributions. These are known [20, 21] to be positive but numerically smaller than naively expected (the approach to the asymptotic regime is much delayed by cancellations of logarithmic corrections that occur at the first perturbative orders in P_{gg} and P_{gq}). The NLL terms in the quark splitting functions P_{qg} and P_{qq} are known [22] and turn out to be positive and large. A very important progress is the recent calculation [23, 24] of the NLL terms in P_{gg}, which are found to be negative and large. The complete NLL terms in P_{gq} are still unknown.

The results of Refs. [23, 24], the large size of the NLL terms and the alternating sign (from the LL to the NLL order and from the gluon to the quark channel) of the resummed small-x contributions have prompted a lot of activity (see the list of references in Ref. [7]) on the conceptual basis and the phenomenological implications of small-x resummation. This

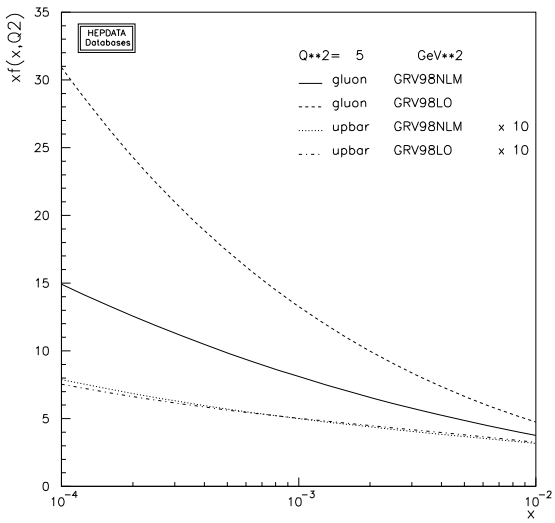

Figure 6: Comparison between the LO (GRV98LO) and NLO (GRV98NLM) GRV parametrizations of the gluon and sea-quark densities at $Q^2 = 5$ GeV^2.

activity is still in progress and definite quantitative conclusions on the impact of small-x resummation at HERA cannot be drawn yet.

At the same time, the capability of the fixed-order approach to produce a good description of the proton structure function $F_2(x, Q^2)$ at HERA cannot be used to conclude that the small-x behaviour of the gluon density is certainly well determined. In fact, by comparing LO and NLO results, we could argue that the ensuing theoretical uncertainty on f_g is sizeable [4]. Going from LO to NLO, we can obtain stable predictions for F_2, but we have to vary the gluon density a lot. As shown in Fig. 6, the NLO gluon density sizeably differs from its LO parametrization, not only in absolute normalization but also in x-shape. For instance, at $x = 10^{-4}$ and $Q^2 = 5$ GeV^2 the NLO gluon is a factor of 2 smaller than the LO gluon. This can be understood [25] from the fact that the scaling violation of F_2 is produced by the convolution $P_{qg} \otimes g$ (see the right-hand side of Eq. (5)). The quark splitting function P_{qg} behaves as

$$P_{qg}(\alpha_{\rm S}, x) \simeq \alpha_{\rm S} P_{qg}^{(LO)}(x) \left[1 + 2.2 \frac{C_A \alpha_{\rm S}}{\pi} \frac{1}{x} + \ldots\right] \quad , \tag{8}$$

where the LO term $P_{qg}^{(LO)}(x)$ is flat at small x, whereas the NLO correction is steep. To obtain a stable evolution of F_2, the NLO steepness of P_{qg} has to be compensated by a gluon density that is less steep at NLO than at LO. This has to be kept in mind when concluding on the importance of small-x resummation because the NLO steepness of P_{qg} is the lowest-order manifestation of BFKL dynamics in the quark channel.

In the large-x region, there is a well-known correlation between $\alpha_{\rm S}$ and f_g. At small x, there is an analogous strong correlation between the x-shapes of P_{qg} and f_g. In the fixed-order QCD analysis of F_2, large NLO perturbative corrections at small x can be balanced by the extreme flexibility of parton density parametrizations. It is difficult to disentangle this correlation between process-dependent perturbative contributions and non-perturbative parton densities from the study of a single quantity, as in the case of F_2 at HERA. The

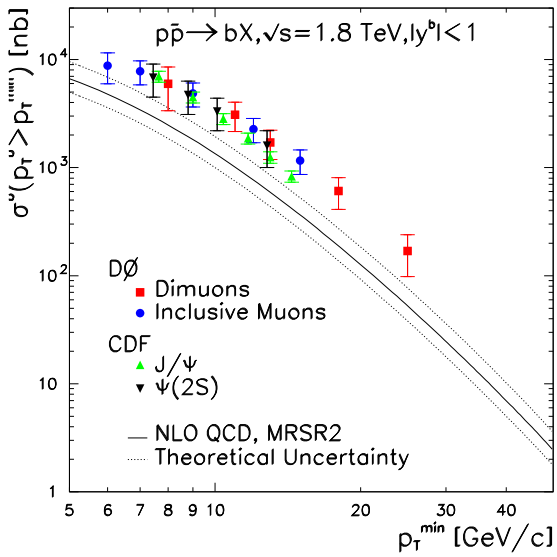

Figure 7: Comparison between Tevatron data and NLO QCD for b-quark production [27]. The band is obtained by varying factorization and renormalization scales in the NLO calculation.

uncertainty on the gluon density at small x, as estimated from the NLO QCD fits of the HERA data, is evidently only a lower limit on the actual uncertainty on f_g.

The production of b quarks at the Tevatron is also sensitive to the gluon density at relatively small values of x. The comparison between Tevatron data and perturbative-QCD predictions at NLO [26] is shown in Fig. 7. Using standard sets of parton densities, the theoretical predictions typically underestimate the measured cross section by a factor of 2. This certainly is disappointing, although justifiable by the large theoretical uncertainty of the perturbative calculation [28]. A lower limit on this uncertainty can be estimated by studying the scale dependence and the convergence of the perturbative expansion. Varying the factorization and renormalization scales by a factor of four around the b-quark mass m_b, the NLO cross section varies by a factor of almost 2 at the Tevatron and by a factor of 4–5 at the LHC [7]. Similar factors are obtained by considering the ratio of the NLO and LO cross sections.

The present theoretical predictions for b-quark production at hadron colliders certainly need to be improved [7]. Since the hard scale $Q \sim m_b$ is not very large, a possible improvement regards estimates of non-perturbative contributions (for instance, effects of the fragmentation of the b-quark and of the intrinsic transverse momentum of the colliding partons). As for the evaluation of perturbative contributions at higher orders, the resummation of logarithmic terms of the type $\alpha_S^n \ln^n(p_t/m_b)$ is important [29] when the transverse momentum p_t of the b quark is much larger than m_b. The resummation of small-x logarithmic contributions $\alpha_S^n \ln^n x$ can also be relevant, because $x \sim 2m_b/\sqrt{S}$ is as small as $\sim 10^{-3}$ at the Tevatron and as $\sim 10^{-4}$ at the LHC. The theoretical tool to perform this resummation, namely the $k_\perp$-factorization approach [30], is available. Updated phenomenological studies based on this tool and on the information from small-x DIS at HERA would be interesting.

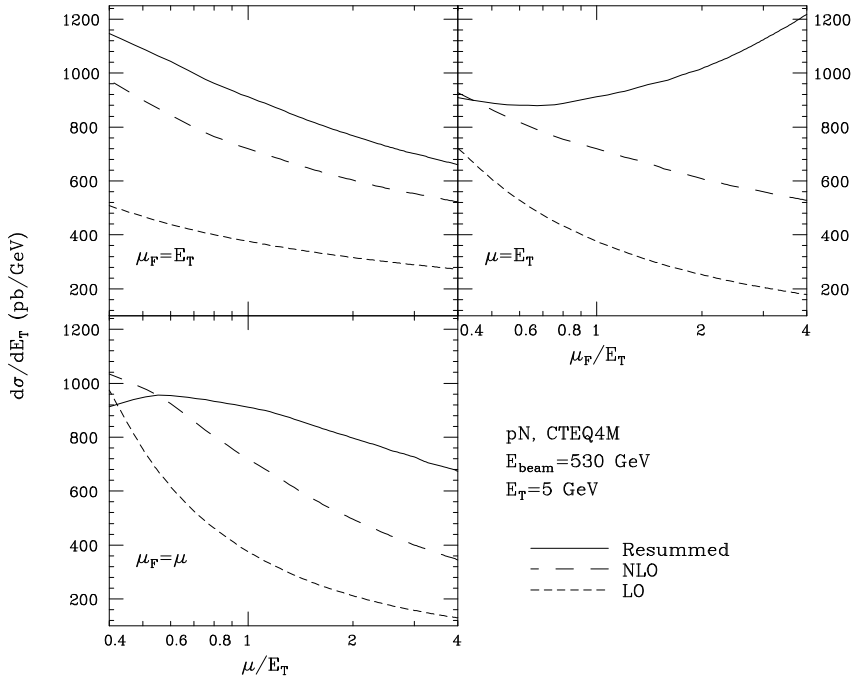

Figure 8: The dependence on the factorization (μ_F) and renormalization ($\mu_R = \mu$) scale of the LO and NLO prompt-photon cross section $d\sigma/dE_T$ in pN collisions at $E_T = 5$ GeV and $\sqrt{S} = 31.6$ GeV. The resummed calculation is discussed in Sect. 5.

Prompt-photon production at fixed-target experiments is sensitive to the behaviour of the gluon density at large x ($x \gtrsim 0.1$). The theoretical predictions for this process, however, are not very accurate. Figure 8 shows the factorization- and renormalization-scale dependence of the perturbative cross section for the case of the E706 kinematics. If the scale is varied by a factor of 4 around the transverse energy E_T of the prompt photon, the LO cross section varies by a factor of almost 4. Going to NLO [31] the situation improves, but not very much, because the NLO cross section still varies by a factor of about 2.

A detailed comparison between NLO QCD calculations and data from the ISR and fixed-target experiments has recently been performed in Ref. [32]. As shown in Fig. 9, the overall agreement with the theory is not satisfactory, even taking into account the uncertainty coming from scale variations in the theoretical predictions. Modifications of the gluon density can improve the agreement with some data sets only at the expense of having larger disagreement with other data sets. The differences between experiments at similar centre-of-mass energies (see, for instance, E706 pBe/530 at $\sqrt{S} = 31.6$ GeV and WA70 pp at $\sqrt{S} = 23$ GeV) are much larger than expected from perturbative scaling violations. This can possibly suggest [32] inconsistencies of experimental origin.

Another (not necessarily alternative) origin of the differences between data and theory could be the presence of non-perturbative effects that are not included in the NLO perturbative calculation. This explanation has been put forward in Refs. [33, 34] by introducing some amount of intrinsic[5] transverse momentum $\langle k_\perp \rangle$ of the colliding partons. Owing to

[5]To be precise, in Ref. [34] the $\langle k_\perp \rangle$ of the colliding partons is not called 'intrinsic', but it is more

the steeply falling E_T distribution ($d\sigma/dE_T \propto 1/E_T^7$) of the prompt photon, even a small transverse-momentum kick[6] can indeed produce a large effect on the cross section, in particular, at small values of E_T. Phenomenological investigations [34] show that this additional $\langle k_\perp \rangle$ kick can lead to a better agreement between calculations and data. The E706 data suggest the value $\langle k_\perp \rangle \sim 1.2$ GeV, the WA70 data prefer no $\langle k_\perp \rangle$, and the UA6 data in the intermediate range of centre-of-mass energy ($\sqrt{S} = 24.3$ GeV) may prefer an intermediate value of $\langle k_\perp \rangle$. Similar conclusions are obtained in the analysis by the MRST group [11].

A precise physical understanding of $\langle k_\perp \rangle$ effects is still missing. On one side, since the amount of $\langle k_\perp \rangle$ suggested by prompt-photon data varies with $\sqrt{S}$, it is difficult to argue that the transverse momentum is really 'intrinsic' and has an entirely non-perturbative origin. On the other side, in the case of the inclusive production of a single photon, a similar effect cannot be justified by higher-order *logarithmic* corrections produced by perturbative soft-gluon radiation (see Sect. 5). A lot of model-dependent assumptions (and ensuing uncertainties) certainly enter in the present implementations of the $\langle k_\perp \rangle$ kick. A general framework to *consistently* include non-perturbative transverse-momentum effects in perturbative calculations is not yet available. Recent proposals with this aim are presented in Refs. [35] and [36].

Further studies on the consistency between different prompt-photon experiments and on the issue of intrinsic-$\langle k_\perp \rangle$ effects in hadron–hadron collisions are necessary. Owing to the present theoretical (and, possibly, experimental) uncertainties, it is difficult to use prompt-photon data to accurately determine the gluon density at large x. Other recent theoretical improvements, such as soft-gluon resummation, of the perturbative calculations for prompt-photon production at large $x_T = 2E_T/\sqrt{S}$ are discussed in Sect. 5.

Studies of other single-particle inclusive cross sections, such as π^0 cross sections [34, 37, 38], can be valuable to constrain the parton densities and could possibly help to clarify some of the experimental and theoretical issues arisen by prompt-photon production.

4 Partonic cross sections: fixed-order expansions, resummed calculations, parton showers

The calculation of hard-scattering cross sections according to the factorization formula (2) requires the knowledge of the partonic cross sections $\hat{\sigma}$, besides that of the parton densities. The partonic cross sections are usually computed by truncating their perturbative expansion at a fixed order in α_S:

$$\begin{aligned}\hat{\sigma}(p_1,p_2;Q,\{Q_1,\ldots\};\mu_F^2) = \alpha_S^k(\mu_R^2) \Big\{ & \hat{\sigma}^{(LO)}(p_1,p_2;Q,\{Q_1,\ldots\}) \\ & + \alpha_S(\mu_R^2)\ \hat{\sigma}^{(NLO)}(p_1,p_2;Q,\{Q_1,\ldots\};\mu_R^2;\mu_F^2) \\ & + \alpha_S^2(\mu_R^2)\ \hat{\sigma}^{(NNLO)}(p_1,p_2;Q,\{Q_1,\ldots\};\mu_R^2;\mu_F^2) + \ldots \Big\}\ . \end{aligned} \tag{9}$$

generically called the $\langle k_\perp \rangle$ 'from initial-state soft-gluon radiation'.

[6] The E_T distribution of the single-photon is not calculable down to $E_T = 0$ or, in other words, $d\sigma/dE_T$ is not integrable in the entire kinematic range of E_T. Thus, the intrinsic $\langle k_\perp \rangle$ of the incoming partons does not simply produce a shift of events from the low-E_T to the high-E_T region. For this reason, the terminology '$\langle k_\perp \rangle$ kick' seems to be more appropriate than '$\langle k_\perp \rangle$ smearing'.

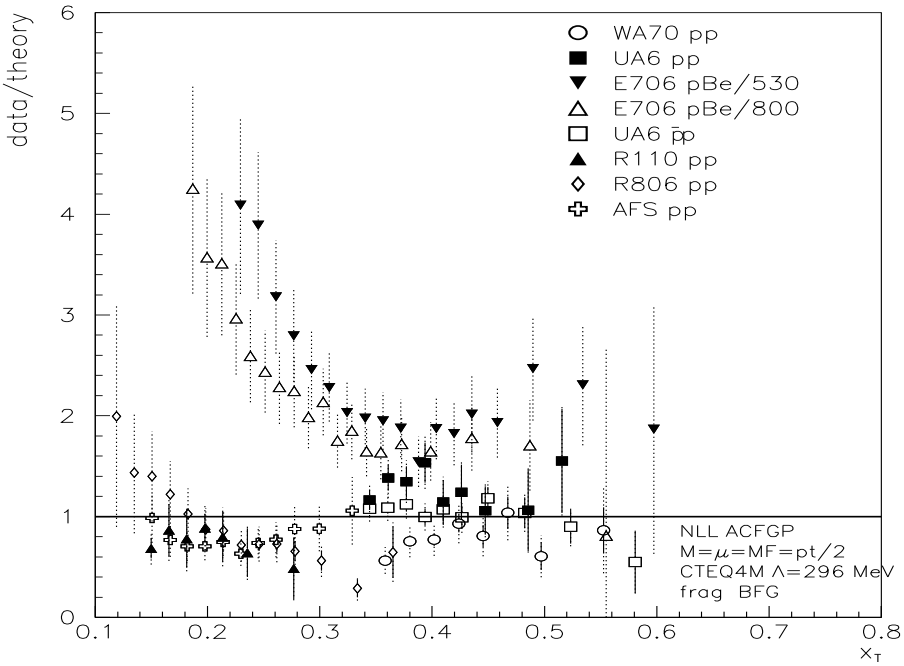

Figure 9: A comparison between NLO QCD calculations and data from the ISR and fixed-target experiments for the prompt-photon distribution $d\sigma/dE_T$ ($x_T = 2E_T/\sqrt{S}$).

The scale μ_R is the arbitrary renormalization scale introduced to define the perturbative expansion. Although the 'exact' partonic cross section on the left-hand side of Eq. (9) does not depend on μ_R, each term on the right-hand side (and, hence, any fixed-order truncation) separately depends on it.

The LO (or tree-level) term $\hat{\sigma}^{(LO)}$ gives only an estimate of the order of magnitude of the partonic cross section, because at this order α_S is not unambiguously defined. Equivalently, we can say that since $\hat{\sigma}^{(LO)}$ does not depend on μ_R, the size of its contribution can be varied quite arbitrarily by changing μ_R in its coefficient $\alpha_S^k(\mu_R^2)$. The strong coupling α_S can be precisely defined only starting from NLO. A 'reliable' estimate of the central value of $\hat{\sigma}$ thus requires the knowledge of (at least) the NLO term $\hat{\sigma}^{(NLO)}$. This term explicitly depends on μ_R and this dependence begins to compensate that of $\alpha_S(\mu_R^2)$.

In general, the n-th term in the curly bracket of Eq. (9) contains contributions of the type $(\alpha_S(\mu_R^2)\ln Q/\mu_R)^n$. If μ_R is very different from the hard scale Q, these contributions become large and spoil the reliability of the truncated expansion (9). Thus, in practical applications the scale μ_R should be set approximately equal to the hard scale Q. As mentioned in Sect. 3, variations of μ_R around this central value are typically used to set a lower limit on the theoretical uncertainty of the perturbative calculation.

A better estimate of the accuracy of any perturbative expansion is obtained by considering the effect of removing the last perturbative term that has been computed. Since α_S can be precisely defined only at NLO, this procedure can consistently be applied to Eq. (9) only as from its NNLO term. A 'reliable' estimate of the theoretical error on $\hat{\sigma}$ thus requires the knowledge of the NNLO term $\hat{\sigma}^{(NNLO)}$ in Eq. (9).

The LO and NLO approximations of $\hat{\sigma}$ are used at present in (most of) the fixed-order QCD calculations. Prospects towards NNLO calculations of partonic cross sections and AP splitting functions are reviewed in Refs. [7, 39].

The fixed-order expansion (9) provides us with a well-defined and systematic framework to compute the partonic cross section $\hat{\sigma}(p_1, p_2; Q, \{Q_1, \ldots\}; \mu_F^2)$ of any hard-scattering process that is sufficiently inclusive or, more precisely, that is defined in an infrared- and collinear-safe manner. However, the fixed-order expansion is reliable only when all the kinematical scales $Q, \{Q_1, \ldots\}$ are of the same order of magnitude. When the hard-scattering process involves two (or several) very different scales, say $Q_1 \gg Q$, the $\mathrm{N}^n\mathrm{LO}$ term in Eq. (9) can contain double- and single-logarithmic contributions of the type $(\alpha_\mathrm{S} L^2)^n$ and $(\alpha_\mathrm{S} L)^n$ with $L = \ln(Q_1/Q) \gg 1$. These terms spoil the reliability of the fixed-order expansion and have to be summed to all orders by systematically defining logarithmic expansions (resummed calculations).

Typical large logarithms, $L = \ln Q/Q_0$, are those related to the evolution of the parton densities from a low input scale Q_0 to the hard-scattering scale Q. These logarithms are produced by collinear radiation from the colliding partons and give single-logarithmic contributions. They never explicitly appear in the calculation of the partonic cross section, because they are systematically (LO, NLO and so forth) resummed in the evolved parton densities $f(x, Q^2)$ by using the DGLAP equation (3).

Different large logarithms, $L = \ln Q/\sqrt{S}$, appear when the centre-of-mass energy $\sqrt{S}$ of the collision is much larger than the hard scale Q. These small-x ($x = Q/\sqrt{S}$) logarithms are produced by multiple radiation over the wide rapidity range that is available at large energy. They usually give single-logarithmic contributions that can be resummed by using the BFKL equation. BFKL resummation is relevant to DIS structure functions at small values of the Bjorken variable x (see Sect. 3) and it can also be important at the LHC for the production of b quarks and of prompt photons at relatively low E_T.

Another class of large logarithms is associated to the bremsstrahlung spectrum of soft gluons. Since soft gluons can be radiated collinearly, they give rise to double-logarithmic contributions to the partonic cross section:

$$\hat{\sigma} \sim \alpha_\mathrm{S}^k \hat{\sigma}^{(LO)} \left\{ 1 + \sum_{n=1}^{\infty} \alpha_\mathrm{S}^n \left(C_{2n}^{(n)} L^{2n} + C_{2n-1}^{(n)} L^{2n-1} + C_{2n-2}^{(n)} L^{2n-2} + \ldots \right) \right\} \quad . \tag{10}$$

Soft-gluon resummation is discussed in Sect. 5.

A related approach to evaluate higher-order contributions to the partonic cross sections is based on Monte Carlo parton showers (see [40] and the updated list of references in [6, 7]). Rather than computing exactly $\hat{\sigma}^{(NLO)}$, $\hat{\sigma}^{(NNLO)}$ and so forth, the parton shower gives an all-order approximation of the partonic cross section in the soft and collinear regions. In this respect, the computation of the partonic cross sections performed by parton showers is somehow similar to that obtained by soft-gluon resummed calculations. There is, however, an important conceptual difference between the two approaches. This difference and the limits of applicability of the parton-shower method are briefly recalled below. Apart from these limits, parton-shower calculations can give some advantages. Multiparton kinematics can be treated exactly. The parton shower can be supplemented with models of non-perturbative

effects (hadronization, intrinsic $k_\perp$, soft underlying event) to provide a complete description of the hard-scattering process at the hadron level.

For a given cross section, resummed calculations can in principle be performed to any logarithmic accuracy. The logarithmic accuracy achievable by parton showers is instead intrinsically limited by quantum mechanics. The parton-shower algorithms are probabilistic. Starting from the LO cross section, the parton shower generates multiparton final states according to a probability distribution that approximates the *square* of the QCD matrix elements. The approximation is based on the universal (process-independent) factorization properties of multiparton matrix elements in the soft and collinear limits. Although the matrix element does factorize, its square contains quantum interferences, which are not positive-definite and, in general, cannot be used to define probability distributions. To leading infrared accuracy, this problem is overcome by exploiting QCD coherence (see Refs. [40, 41, 42] and referencees therein): soft gluons radiated at large angle from the partons involved in the LO subprocess destructively interfere. This quantum mechanical effect can be simply implemented by enforcing an angular-ordering constraint on the phase space available for the parton shower evolution. Thus, angular-ordered parton showers can *consistently* compute the first two dominant towers ($\alpha_{\rm S}^n L^{2n}$ and $\alpha_{\rm S}^n L^{2n-1}$) of logarithmic contributions in Eq. (10). However, parton showers contain also some subleading logarithmic contributions. For instance, they correctly compute the single-logarithmic terms $\alpha_{\rm S}^n L^n$ of purely collinear origin that lead to the LO evolution of the parton densities. Moreover, as discussed in Ref. [43] by a comparison with resummed calculations, in the case of hard-scattering processes whose LO subprocess involves two coloured partons (e.g. DIS or DY production), angular-ordered parton showers have a higher logarithmic accuracy: they can consistently evaluate the LL and NLL terms in Eq. (15). The extension of parton-shower algorithms to higher logarithmic accuracy is not necessarily feasible and is, in any case, challenging.

Of course, because of quantum interferences and quantum fluctuations, the probabilistic parton-shower approach cannot be used to systematically perform exact calculations at NLO, NNLO and so forth. Nonetheless, important progress has been made to include matrix element corrections in parton shower algorithms [44–47]. The purpose is to consider the multiparton configurations generated by parton showering from the LO matrix element and to correct them in the hard (non-soft and non-collinear) region by using the exact expressions of the higher-order matrix elements. Hard matrix element corrections to parton showers have been implemented for top quark decay [48] and for production of W, Z and DY lepton pairs [49, 50, 51]. The same techniques could be applied to other processes, as, for instance, production of Higgs boson [52] and vector-boson pairs [7].

Note also that, at present, angular-ordered parton showers cannot be considered as true 'next-to-leading' tools, even where their logarithmic accuracy is concerned. The consistent computation of the first two towers of logarithmic contributions in Eq. (10) is not sufficient for this purpose. For instance, to precisely introduce an NLO definition of $\alpha_{\rm S}$, we should control all the terms obtained by the replacement $\alpha_{\rm S} \to \alpha_{\rm S} + c\ \alpha_{\rm S}^2 + \mathcal{O}(\alpha_{\rm S}^3)$. When it is introduced in the towers of double-logarithmic terms $\alpha_{\rm S}^n L^{2n}$ of Eq. (10), this replacement leads to contributions of the type $\alpha_{\rm S}^{n+1} L^{2n} \sim \alpha_{\rm S}^n L^{2n-2}$. Since these contributions are not fully computable at present, the parameter $\alpha_{\rm S}$ used in the parton showers corresponds to a

simple LO parametrization of QCD running coupling.

5 Soft-gluon resummation

Double-logarithmic contributions due to soft gluons arise in all the kinematic configurations where radiation of real and virtual partons is highly unbalanced (see Ref. [53] and references therein). For instance, this happens in the case of transverse-momentum distributions at low transverse momentum, in the case of hard-scattering production near threshold or when the structure of the final state is investigated with high resolution (internal jet structure, shape variables).

Soft-gluon resummation for jet shapes has been extensively studied and applied to hadronic final states produced by e^+e^- annihilation [1, 4, 54]. Applications to hadron–hadron collisions have just begun to appear [55] and have a large, yet uncovered, potential (from $\alpha_{\rm S}$ determinations to studies of non-perturbative dynamics).

Transverse-momentum logarithms, $L = \ln Q^2/\boldsymbol{Q}_\perp^2$, occur in the distribution of transverse momentum $\boldsymbol{Q}_\perp$ of systems with high mass Q ($Q \gg Q_\perp$) that are produced with a vanishing $\boldsymbol{Q}_\perp$ in the LO subprocess. Examples of such systems are DY lepton pairs, lepton pairs produced by W and Z decay, heavy quark–antiquark pairs, photon pairs and Higgs bosons. In these processes the LO transverse-momentum distribution is sharply peaked around $\boldsymbol{Q}_\perp = 0$ ($d\hat{\sigma}/d^2\boldsymbol{Q}_\perp \propto \delta^{(2)}(\boldsymbol{Q}_\perp)$). If the heavy system is produced with $\boldsymbol{Q}_\perp^2 \ll Q^2$, the emission of real radiation at higher orders is strongly suppressed and cannot balance the virtual contributions. The ensuing logarithms, $L = \ln Q^2/\boldsymbol{Q}_\perp^2$, diverge order by order when $\boldsymbol{Q}_\perp \to 0$, but after all-order resummation they leads to a finite smearing of the LO distribution.

Threshold logarithms, $L = \ln(1-x)$, occur when the tagged final state produced by the hard scattering is forced to carry a very large fraction x ($x \to 1$) of the available centre-of-mass energy $\sqrt{S}$. Also in this case, the radiative tail of real emission is stronly suppressed at higher perturbative orders. Oustanding examples of hard processes near threshold are DIS at large x (here x is the Bjorken variable), production of DY lepton pairs with large invariant mass Q ($x = Q/\sqrt{S}$), production of heavy quark–antiquark pairs ($x = 2m_Q/\sqrt{S}$), production of single jets and single photons at large transverse energy E_T ($x = 2E_T/\sqrt{S}$).

To emphasize the difference between transverse-momentum logarithms and threshold logarithms generated by soft gluons, it can be instructive to consider prompt-photon production. In the case of production of a *photon pair*[7] with invariant mass squared $Q^2 = (p_1^{(\gamma)} + p_2^{(\gamma)})^2$ and *total* transverse momentum $\boldsymbol{Q}_\perp = \boldsymbol{p}_{1\perp}^{(\gamma)} + \boldsymbol{p}_{2\perp}^{(\gamma)}$, transverse-momentum logarithms and threshold logarithms appear when $\boldsymbol{Q}_\perp^2 \ll Q^2$ and $\boldsymbol{Q}_\perp^2 \sim (S/4 - Q^2)$, respectively. However, in the case of production of a *single photon* with transverse energy (or, equivalently, transverse momentum) E_T, soft gluons can produce logarithms only in the threshold region $x_T = 2E_T/\sqrt{S} \to 1$. If the prompt photon has a transverse energy that is not close[8] to its threshold value, the emission of accompanying radiation is not kinematically suppressed and

[7] The same discussion applies to the production of a DY lepton pair.

[8] Eventually, when $x_T \ll 1$, higher-order corrections are single-logarithmically enhanced. This small-x logarithms, $(\alpha_{\rm S} \ln x_T)^n$, have to be taken into account by BFKL resummation.

there are no soft logarithms analogous to those in the transverse-momentum distribution of a photon pair. In particular, there are no double-logarithmic contributions of the type $(\alpha_{\rm S} \ln^2 E_T^2/S)^n$, and perturbative soft gluons are not distinguishable from perturbative hard gluons.

Studies of soft-gluon resummation for transverse-momentum distributions at low transverse momentum and for hard-scattering production near threshold started two decades ago [42, 56]. The physical bases for a systematic all-order summation of the soft-gluon contributions are dynamics and kinematics factorizations [53]. The first factorization follows from gauge invariance and unitarity: in the soft limit, multigluon amplitudes fulfil factorization formulae given in terms of universal (process-independent) soft contributions. The second factorization regards kinematics and strongly depends on the actual cross section to be evaluated. *If*, in the appropriate soft limit, the multiparton phase space for this cross section can be written in a factorized way, resummation is analytically feasible in form of *generalized exponentiation* of the universal soft contributions that appear in the factorization formulae of the QCD amplitudes.

Note that the phase space depends in a non-trivial way on multigluon configurations and, in general, is not factorizable in single-particle contributions[9]. Moreover, even when phase-space factorization is achievable, it does not always occur in the space of the kinematic variables where the cross section is defined. Usually, it is necessary to introduce a conjugate space to overcome phase-space constraints. This is the case for transverse-momentum distributions and hard-scattering production near threshold. The relevant kinematical constraint for $\boldsymbol{Q}_\perp$-distributions is (two-dimensional) transverse-momentum conservation and it can be factorized by performing a Fourier transformation. Soft-gluon resummation for $\boldsymbol{Q}_\perp$-distributions is thus carried out in $\boldsymbol{b}$-space [60, 61], where the impact parameter $\boldsymbol{b}$ is the variable conjugate to $\boldsymbol{Q}_\perp$ via the Fourier transformation. Analogously, the relevant kinematical constraint for hard-scattering production near threshold is (one-dimensional) energy conservation and it can be factorized by working in N-moment space [62, 63], N being the variable conjugate to the threshold variable x (energy fraction) via a Mellin or Laplace transformation.

Using a short-hand notation, the general structure of the partonic cross section $\hat{\sigma}$ after summation of soft-gluon contributions is

$$\hat{\sigma} = \hat{\sigma}_{\rm res.} + \hat{\sigma}_{\rm rem.} \ . \tag{11}$$

The term $\hat{\sigma}_{\rm res.}$ embodies the all-order resummation, while the remainder $\hat{\sigma}_{\rm rem.}$ contains no large logarithmic contributions. The latter has the form

$$\hat{\sigma}_{\rm rem.} = \hat{\sigma}^{\rm (f.o.)} - \left[\, \hat{\sigma}_{\rm res.} \,\right]^{\rm (f.o.)} \quad , \tag{12}$$

and it is obtained from $\hat{\sigma}^{\rm (f.o.)}$, the truncation of the perturbative expansion for $\hat{\sigma}$ at a given fixed order (LO, NLO, ...), by subtracting the corresponding truncation $[\hat{\sigma}_{\rm res.}]^{\rm (f.o.)}$ of the

[9] In the case of jet cross sections, for instance, phase-space factorization depends on the detailed definition of jets and it can easily be violated [57]. Some jet algorithms, such as the $k_\perp$-algorithm [58, 59], have better factorization properties.

resummed part. Thus, the expression on the right-hand side of Eq. (11) includes soft-gluon logarithms to all orders and it is *matched* to the exact (with no logarithmic approximation) fixed-order calculation. It represents an improved perturbative calculation that is everywhere as good as the fixed-order result, and much better in the kinematics regions where the soft-gluon logarithms become large ($\alpha_{\rm S} L \sim 1$). Eventually, when $\alpha_{\rm S} L \gtrsim 1$, the resummed perturbative contributions are of the same size as the non-perturbative contributions and the effect of the latter has to be implemented in the resummed calculation.

The resummed cross section has the following typical form:

$$\hat{\sigma}_{\rm res.} = \alpha_{\rm S}^k \int_{\rm inv.} \hat{\sigma}^{(LO)} \cdot C \cdot S \; , \tag{13}$$

where the integral $\int_{\rm inv.}$ denotes the inverse tranformation from the conjugate space where resummation is actually carried out. Methods to perform the inverse transformation are discussed in Refs. [64] and [65] for $Q_\perp$-resummation and threshold resummation, respectively. The C term has the perturbative expansion

$$C = 1 + C_1 \, \alpha_{\rm S} + C_2 \, \alpha_{\rm S}^2 + \ldots \tag{14}$$

and contains all the constant contributions in the limit $L \to \infty$ (the coefficients $C_1, C_2, \ldots$ do not depend on the conjugate variable). The singular dependence on L (more precisely, on the logarithm $\tilde{L}$ of the conjugate variable) is entirely *exponentiated* in the factor S:

$$S = \exp \left\{ L \; g_1(\alpha_{\rm S} L) + g_2(\alpha_{\rm S} L) + \alpha_{\rm S} \; g_3(\alpha_{\rm S} L) + \ldots \right\} \quad . \tag{15}$$

In the exponent, the function $L \, g_1$ resums all the leading logarithmic (LL) contributions $\alpha_{\rm S}^n L^{n+1}$, while g_2 contains the next-to-leading logarithmic (NLL) terms $\alpha_{\rm S}^n L^n$ and so forth[10] (all the functions g_i are normalized as $g_i(\lambda = 0) = 0$). Note that the LL terms are formally suppressed by a power of $\alpha_{\rm S}$ with respect to the NLL terms, and so forth for the successive classes of logarithmic terms. Thus, this logarithmic expansion is as systematic as the fixed-order expansion in Eq. (9). In particular, using a matched NLL+NLO calculation, we can consistently *i*) introduce a precise definition (say $\overline{\rm MS}$) of $\alpha_{\rm S}(\mu)$ and *ii*) investigate the theoretical accuracy of the calculation by studying its renormalization-scale dependence.

The structure of the exponentiated resummed calculations discussed so far has to be contrasted with that obtained by organizing the logarithmic expansion on the right-hand side of Eq. (10) in terms of towers as

$$\hat{\sigma} \sim \alpha_{\rm S}^k \hat{\sigma}^{(LO)} \left\{ t_1(\alpha_{\rm S} L^2) + \alpha_{\rm S} L \; t_2(\alpha_{\rm S} L^2) + \alpha_{\rm S}^2 L^2 \; t_3(\alpha_{\rm S} L^2) + \ldots \right\} \quad , \tag{16}$$

where the double-logarithmic function $t_1(\alpha_{\rm S} L^2)$ and the successive functions are normalized as $t_i(0) = {\rm const}$. While the ratio of two successive terms in the exponent of Eq. (15) is

[10] To compare this notation with that of Ref. [66], we can notice that our functions g_i are obtained by the straightforward integration over $\overline{\mu}$ of the functions $A(\alpha_{\rm S}(\overline{\mu}))$ and $B(\alpha_{\rm S}(\overline{\mu}))$ of Ref. [66]. In particular, our terms g_1, g_2, g_3 are not to be confused with the non-perturbative parameters of the same name used in Ref. [66].

formally of the order of α_S, the ratio of two successive towers in Eq. (16) is formally of the order of $\alpha_S L$. In other words, the tower expansion sums the double-logarithmic terms $(\alpha_S L^2)^n$, then the terms $\alpha_S^n L^{2n-1} \sim \alpha_S L (\alpha_S L^2)^{n-1}$, and so forth; it thus assumes that the resummation procedure is carried out with respect to the large parameter $\alpha_S L^2$ ($\alpha_S L^2 \lesssim 1$). On the contrary, in Eq. (15) the large parameter is $\alpha_S L \lesssim 1$. The tower expansion allows us to formally extend the applicability of perturbative QCD to the region $L \lesssim 1/\sqrt{\alpha_S}$, and exponentiation extends it to the wider region $L \lesssim 1/\alpha_S$. This fact can also be argued by comparing the amount of information on the logarithmic terms that is included in the truncation of Eqs. (15) and (16) at some logarithmic accuracy. The reader can easily check that, after matching to the NLO (LO) calculation as in Eq. (11), the NLL (LL) result of Eq. (15) contains all the logarithms of the first *four* (*two*) towers in Eq. (16) (and many more logarithmic terms).

In the case of $Q_\perp$-distributions, full NLL resummation has been performed for lepton pairs, W and Z bosons produced by the DY mechanism [61, 67] and for Higgs bosons produced by gluon fusion [68]. Corresponding resummed calculations are discussed in Refs. [52, 66] and references therein.

Threshold logarithms in hadron collisions have been resummed to NLL accuracy for DIS and DY production [62, 63, 43, 69] and for Higgs boson production [70]. Recent theoretical progress [71, 72, 19] regards the extension of NLL resummation to processes produced by LO hard-scattering of more than two coloured partons, such as heavy-quark hadroproduction [71, 19] and leptoproduction [73], as well as prompt-photon [74–77], quarkonium [78] and vector-boson [79] production.

An important feature of threshold resummation is that the resummed soft-gluon contributions regard the partonic cross section rather than the hadronic cross section. This fact has two main consequences: *i*) soft-gluon contributions can be sizeable long before the threshold region in the hadronic cross section is actually approached, and *ii*) the resummation effects typically enhance the fixed-order perturbative calculations.

The first consequence follows from the fact that the evolution of the parton densities sizeably reduces the energy that is available in the partonic hard-scattering subprocess. Thus, the partonic cross section $\hat{\sigma}$ in the factorization formula (2) is typically evaluated much closer to threshold than the hadronic cross section. In other words, the parton densities are strongly suppressed at large x (typically, when $x \to 1$, $f(x,\mu^2) \sim (1-x)^\eta$ with $\eta \sim 3$ and $\eta \sim 6$ for valence quarks and sea-quarks or gluons, respectively); after integration over them, the dominant value of the square of the partonic centre-of-mass energy $\langle \hat{s} \rangle = \langle x_1 x_2 \rangle S$ is therefore substantially smaller than the corresponding hadronic value S.

The second consequence, which depends on the actual definition of the parton densities, follows from the fact that the resummed contributions are those soft-gluon effects that are left at the partonic level after factorization of the parton densities. After having absorbed part of the full soft-gluon contributions in the customary definitions (for instance, those in the $\overline{\rm MS}$ or DIS factorization schemes) of the parton densities, it turns out that the residual effect in the partonic cross section is positive and tends to enhance the perturbative predictions.

A quantitative illustration of these consequences is given below by discussing top-quark and prompt-photon production. The discussion also shows another relevant feature of

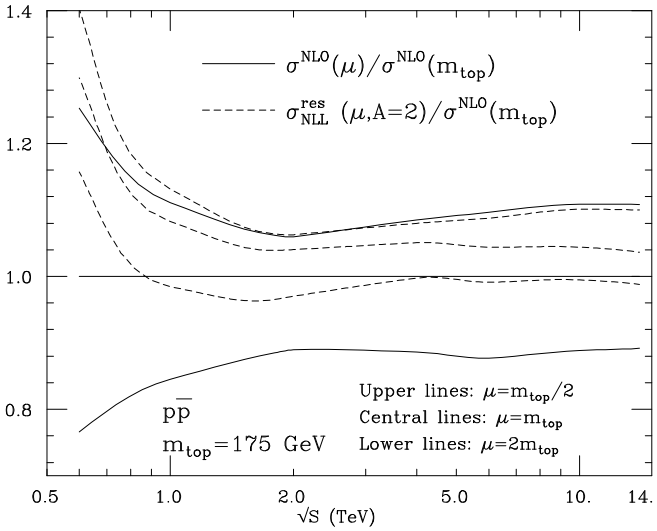

Figure 10: The $t\bar{t}$ production cross section in $p\bar{p}$ collisions as a function of $\sqrt{S}$. The solid lines represent the NLO results for different choices ($\mu = m_t/2$ and $\mu = 2m_t$) of the renormalization/factorization scale $\mu = \mu_R = \mu_F$, normalized to the result with $\mu = m_t$. The dashed lines represent the NLO+NLL results for different choices of μ ($\mu = m_t/2, m_t$ and $2m_t$), normalized to the NLO result with $\mu = m_t$.

NLO+NLL calculations, namely, their increased stability with respect to scale variations.

The effects of soft-gluon resummation on the top-quark production cross sections at hadron colliders have been studied in Refs. [19, 80–83]. In the case of $p\bar{p}$ collisions, the comparison between QCD predictions at NLO and those after NLL resummation is shown in Fig. 10 [19]. At the Tevatron the resummation effects are not very large and the NLO cross section is increased by about 4%. This had to be expected because the top quark is not produced very close to threshold ($x = 2m_t/\sqrt{S} \sim 0.2$, at the Tevatron). Note, however, that the dependence on the factorization/renormalization scale of the theoretical cross section is reduced by a factor of almost 2 by including NLL resummation. More precisely, the scale dependence ($\sim \pm 5\%$) of the NLO+NLL calculation becomes comparable to that obtained by using different sets of parton densities [11]. Combining linearly scale and parton density uncertainties, the NLO+NLL cross section is $\sigma_{t\bar{t}} = 5.0 \pm 0.6$, with $m_t = 175$ GeV and $\sqrt{S} = 1.8$ TeV [19].

At the LHC ($x = 2m_t/\sqrt{S} \sim 0.03$) the top quark is produced less close to the hadronic threshold than at the Tevatron. However this is compensated by the fact that the gluon channel[11] is more important at the LHC. As a result, the effect of including soft-gluon resummation to NLL accuracy is very similar: the NLO cross section is enhanced by $\sim$ 5% and its scale dependence is reduced from $\sim \pm 10\%$ to $\sim \pm 5\%$. Note, however, that

[11]Since f_g is steeper than f_q at large x, partonic cross sections in gluon subprocesses are typically closer to threshold than in quark subprocesses. Moreover, the intensity of soft-gluon radiation from gluons is larger than that from quarks by a factor of $\sim C_A/C_F \sim 2$.

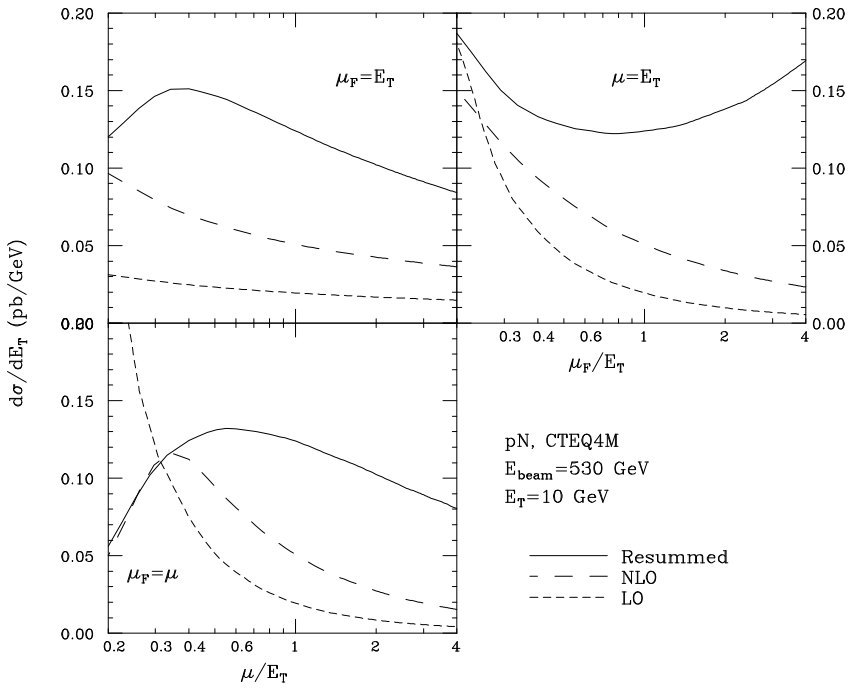

Figure 11: The dependence on the factorization (μ_F) and renormalization ($\mu_R = \mu$) scale of the prompt-photon cross section $d\sigma/dE_T$ in pN collisions at $E_T = 10$ GeV and $\sqrt{S} = 31.6$ GeV. The short-dashed, long-dashed and solid lines are respectively the results at LO, NLO and after NLO+NLL resummation.

the uncertainty ($\sim \pm 10\%$) coming from the parton (gluon) densities is larger than at the Tevatron [7].

Similar qualitative results are obtained [76] when NLL resummation is applied to prompt-photon production at fixed-target experiments. The scale dependence of the theoretical calculation is highly reduced and the resummed NLL contributions lead to large corrections at high $x_T = 2E_T/\sqrt{S}$ (and smaller corrections at lower x_T). Of course, the impact of soft-gluon resummation is quantitatively more sizeable in prompt-photon production than in top-quark production, because x_T can be as large as 0.6, the hard scale E_T is much smaller than m_t (thus, $\alpha_S(E_T) > \alpha_S(m_t)$) and the gluon channel is always important. The scale dependence of the theoretical cross section for the E706 kinematics is shown in Fig. 11. Fixing $\mu_R = \mu_F = \mu$ and varying μ in the range $E_T/2 < \mu < 2E_T$ with $E_T = 10$ GeV, the cross section varies by a factor of ~ 6 at LO, by a factor of ~ 4 at NLO and by a factor of ~ 1.3 after NLL resummation. The highly reduced scale dependence of the NLO+NLL cross section is also visible in Fig. 12, which, in particular, shows that when $E_T = 10$ GeV and $E_{\rm beam} = 530$ GeV the central value (i.e. with $\mu = E_T$) of the NLO cross section increases by a factor of ~ 2.5 after NLL resummation. As expected, the size of these effects is reduced by increasing $\sqrt{S}$ at fixed E_T (see Fig. 12) or by decreasing E_T at fixed $\sqrt{S}$ (see Fig. 8).

The comparison with the E706 data shown in Fig. 13 suggests that the NLO+NLL calculation can help to better understand prompt-photon production at large x_T. Note,

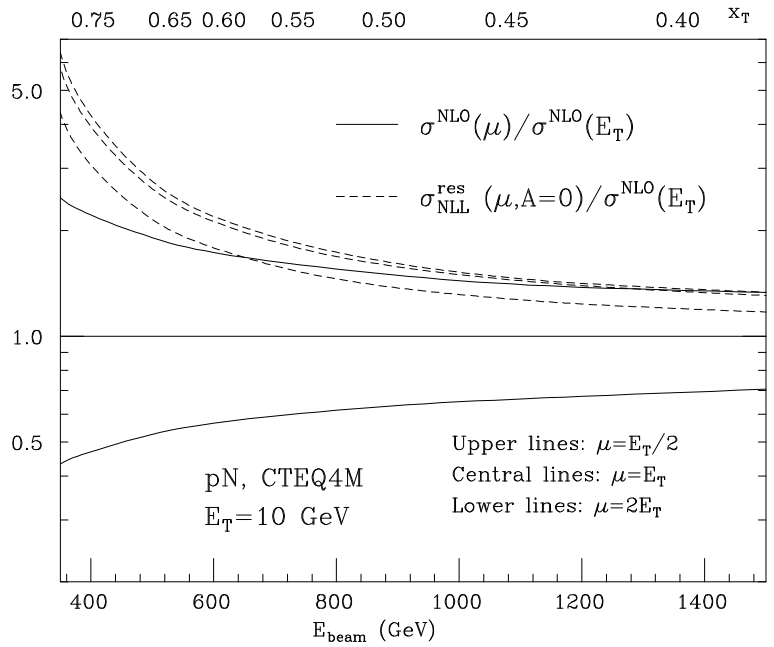

Figure 12: The prompt-photon cross section $d\sigma/dE_T$ in pN collisions at $E_T = 10$ GeV as a function of the energy $E_{\rm beam}$ of the proton beam. The solid lines represent the NLO results for different choices ($\mu = E_T/2$ and $\mu = 2E_T$) of the renormalization/factorization scale $\mu = \mu_R = \mu_F$, normalized to the result with $\mu = E_T$. The dashed lines represent the NLO+NLL results for different choices of μ ($\mu = E_T/2, E_T$ and $2E_T$), normalized to the NLO result with $\mu = E_T$.

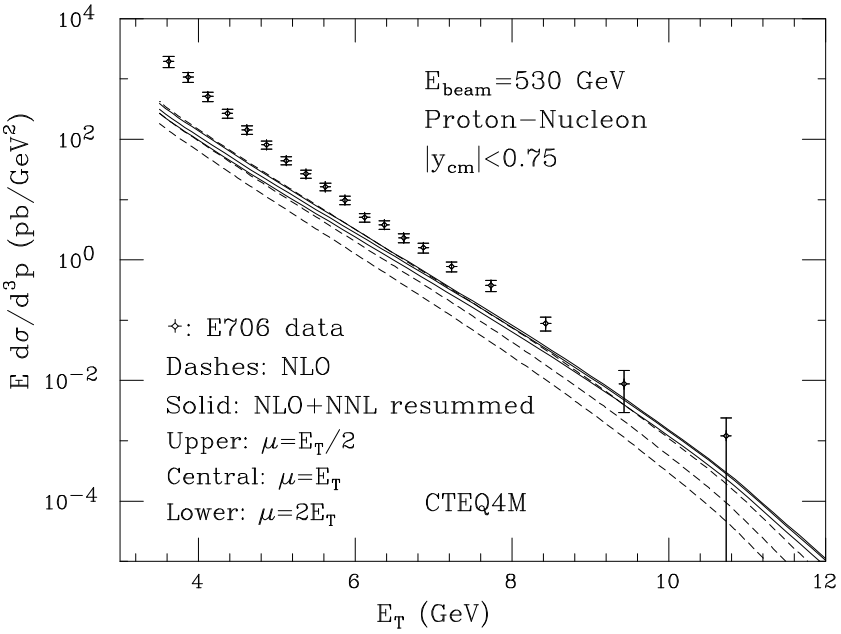

Figure 13: E706 prompt-photon data compared with theoretical calculations, which use the parton densities of the set CTEQ4 and GRV photon fragmentation functions. The solid and dashed lines correspond to the NLO+NLL and pure NLO calculations, respectively.

however, that this comparison has to be regarded as preliminary in several respects [76]. In particular, the parton densities used in Fig. 13 are those extracted from NLO fits. Owing to the soft-gluon enhancement at large x_T, refitting the parton densities may lead to a smaller f_g at large x and, consequently (because of the momentum sum rule), a larger f_g at intermediate x. As a result, this procedure could somehow increase the theoretical cross section also at smaller values of x_T.

Soft-gluon resummation at NLL accuracy is now available for all the processes (namely, DIS, DY and prompt-photon production) that are typically used to perform global fits to parton densities. A detailed extraction/evolution of parton densities by consistently using NLL resummed calculations is thus nowadays feasible.

6 Other topics

The activity of the QCD Working Group at this Workshop has also been devoted to other topics, such as automatic computation of matrix elements and LO cross sections for multiparticle processes at high-energy colliders, definition and properties of jets algorithms, definition of isolated photons and related NLO calculations. Corresponding contributions are included in these Proceedings.

Other studies performed during this Workshop have a large overlap with the activity of the related Workshops at FERMILAB and CERN and can be found in those Proceed-

ings [6, 7].

Acknowledgements. This work was supported in part by the EU Fourth Framework Programme "Training and Mobility of Researchers", Network "Quantum Chromodynamics and the Deep Structure of Elementary Particles", contract FMRX–CT98–0194 (DG 12 – MIHT). I would like to thank the members of the Local Organizing Committee for the excellent Workshop.

References

1. M.L. Mangano, plenary talk at the *1999 International Europhysics Conference on High Energy Physics* Tampere, Finland, 15–21 July 1999, preprint CERN-TH/99-337 (hep-ph/9911256), to appear in the Proceedings, and references therein.

2. B.R. Webber, plenary talk at the *19th International Symposium on Lepton-Photon Interactions at High-Energies, LP 99*, Stanford, California, 9–14 Aug 1999, preprint CERN-TH/99-387 (hep-ph/9912292), to appear in the Proceedings, and references therein.

3. J. Huston, in Proc. of the *29th International Conference on High-Energy Physics, ICHEP 98*, eds. A. Astbury, D. Axen and J. Robinson (World Scientific, Singapore, 1999), vol. 1, p. 283, and references therein.

4. S. Catani, hep-ph/9712442, in Proc. of the *XVIII International Symposium on Lepton-Photon Interactions, LP97*, eds. A. De Roeck and A. Wagner (World Scientific, Singapore, 1998), p. 147, and references therein.

5. G. Jarlskog and D. Rein eds., Proc. of ECFA LHC Workshop, report CERN 90-10 (December 1990); ATLAS Coll., ATLAS TDR 15, report CERN/LHCC/99-15 (May 1999).

6. Proceedings of the Workshop on *Physics at the Tevatron in Run II*, Fermilab, 2000 (to appear). See: http://www-theory.fnal.gov/people/ellis/QCDWB/QCDWB.html

7. Proceedings of the Workshop on *Standard Model Physics (and more) at the LHC*, CERN 1999 (to appear). See: http://home.cern.ch/˜mlm/lhc99/lhcworkshop.html

8. See J.C. Collins, D.E. Soper and G. Sterman, in *Perturbative Quantum Chromodynamics*, ed. A.H. Mueller (World Scientific, Singapore, 1989), p. 1, and references therein.

9. V.N. Gribov and L.N. Lipatov, Sov. J. Nucl. Phys. 15 (1972) 438, 675; G. Altarelli and G. Parisi, Nucl. Phys. B126 (1977) 298; Yu.L. Dokshitzer, Sov. Phys. JETP 46 (1977) 641.

10. E. G. Floratos, D. A. Ross and C. T. Sachrajda, Nucl. Phys. B129 (1977) 66, E ibid. B139 (1978) 545, Nucl. Phys. B152 (1979) 493; A. Gonzalez-Arroyo, C. Lopez and F. J. Yndurain, Nucl. Phys. B153 (1979) 161; A. Gonzalez-Arroyo and C. Lopez, Nucl. Phys. B166 (1980) 429; G. Curci, W. Furmanski and R. Petronzio, Nucl. Phys. B175 (1980) 27; W. Furmanski and R. Petronzio, Phys. Lett. B97 (1980) 437; E. G. Floratos, C. Kounnas and R. Lacaze, Nucl. Phys. B192 (1981) 417.

11. A.D. Martin, R.G. Roberts, W.J. Stirling and R.S. Thorne, Eur. Phys. J. C4 (1998) 463, Phys. Lett. 443B (1998) 301, preprint DTP-99-64 (hep-ph/9907231); M. Glück, E. Reya and A. Vogt, Eur. Phys. J. C5 (1998) 461; H.L. Lai et al., Eur. Phys. J. C12 (2000) 375.

12. LHC Guide to Parton Distribution Functions and Cross Sections, ATLAS note ATL-PHYS-99-008, http://www.pa.msu.edu/~huston/lhc/lhc_pdfnote.ps .

13. R.D. Ball and J. Huston, in these Proceedings, and references therein.

14. U.K. Yang and A. Bodek, Phys. Rev. Lett. 82 (1999) 2467, preprint UR-1581 (hep-ex/9908058).

15. W. Melnitchouk, I.R. Afnan, F. Bissey and A.W. Thomas, preprint ADP-99-47-T384 (hep-ex/9912001).

16. S. Kuhlmann et al., hep-ph/9912283.

17. J. Huston et al., Phys. Rev. D 58 (1998) 114034.

18. R. Hamberg, W.L. van Neerven and T. Matsuura, Nucl. Phys. B359 (1991) 343; W.L. van Neerven and E.B. Zijlstra, Nucl. Phys. B382 (1992) 11.

19. R. Bonciani, S. Catani, M.L. Mangano and P. Nason, Nucl. Phys. B529 (1998) 424.

20. L.N. Lipatov, Sov. J. Nucl. Phys. 23 (1976) 338; E.A. Kuraev, L.N. Lipatov and V.S. Fadin, Sov. Phys. JETP 45 (1977) 199; Ya. Balitskii and L.N. Lipatov, Sov. J. Nucl. Phys. 28 (1978) 822.

21. T. Jaroszewicz, Phys. Lett. 116B (1982) 291.

22. S. Catani and F. Hautmann, Phys. Lett. 315B (1993) 157, Nucl. Phys. B427 (1994) 475.

23. V.S. Fadin and L.N. Lipatov, Sov. J. Nucl. Phys. 50 (1989) 712, Phys. Lett. 429B (1998) 127.

24. M. Ciafaloni and G. Camici, Nucl. Phys. B496 (1997) 305, Phys. Lett. 430B (1998) 349.

25. S. Catani, Z. Phys. C70 (1996) 263, Z. Phys. C75 (1997) 665.

26. P. Nason, S. Dawson and R.K. Ellis, Nucl. Phys. B303 (1988) 607; W. Beenakker, H. Kuijf, W.L. van Neerven and J. Smith, Phys. Rev. D 40 (1989) 54; M.L. Mangano, P. Nason and G. Ridolfi, Nucl. Phys. B373 (1992) 295.

27. M. Baarmand, talk presented at the Workshop on *Standard Model Physics (and more) at the LHC*, CERN, January 1999.
See: http://home.cern.ch/n/nason/www/lhc99/14-01-99/program-1-14-99

28. S. Frixione, M.L. Mangano, P. Nason and G. Ridolfi, in *Heavy Flavours II*, eds. A.J. Buras and M. Lindner (World Scientific, Singapore, 1998), p. 609, and references therein.

29. M. Cacciari, M. Greco and P. Nason, JHEP 05 (1998) 007; F.I. Olness, R.J. Scalise and Wu-Ki Tung, Phys. Rev. D 59 (1999) 014506.

30. S. Catani, M. Ciafaloni and F. Hautmann, Phys. Lett. 242B (1990) 97, Nucl. Phys. B366 (1991) 135; J.C. Collins and R.K. Ellis, Nucl. Phys. B360 (1991) 3; E.M. Levin, M.G. Ryskin, Yu.M. Shabel'skii and A.G. Shuvaev, Sov. J. Nucl. Phys. 53 (1991) 657.

31. P. Aurenche, R. Baier, M. Fontannaz and D. Schiff, Nucl. Phys. B297 (1988) 661; H. Baer, J. Ohnemus and J.F. Owens, Phys. Rev. D 42 (1990) 61; P. Aurenche, R. Baier and M. Fontannaz, Phys. Rev. D 42 (1990) 1440; L.E. Gordon and W. Vogelsang, Phys. Rev. D 48 (1993) 3136.

32. P. Aurenche, M. Fontannaz, J.Ph. Guillet, B. Kniehl, E. Pilon and M. Werlen, Eur. Phys. J. C9 (1999) 107.

33. E706 Coll., L. Apanasevich et al., Phys. Rev. Lett. 81 (1998) 2642.

34. L. Apanasevich et al., Phys. Rev. D 59 (1999) 074007.

35. M.A. Kimber, A.D. Martin and M.G. Ryskin, Eur. Phys. J. C12 (2000) 655.

36. E. Laenen, G. Sterman and W. Vogelsang, preprint YITP-99-69 (hep-ph/0002078).

37. P. Aurenche, M. Fontannaz, J.P. Guillet, B.A. Kniehl and M. Werlen, preprint LAPTH-751-99 (hep-ph/9910252).

38. J. Huston et al., paper in preparation.

39. V. Del Duca and G. Heinrich, in these Proceedings, and references therein.

40. R.K. Ellis, W.J. Stirling and B.R. Webber, *QCD and Collider Physics* (Cambridge University Press, Cambridge, 1996) and references therein.

41. Yu.L. Dokshitzer, V.A. Khoze, A.H. Mueller and S.I. Troian, *Basics of Perturbative QCD* (Editions Frontières, Gif-sur-Yvette, 1991) and references therein.

42. A. Bassetto, M. Ciafaloni and G. Marchesini, Phys. Rep. 100 (1983) 201, and references therein.

43. S. Catani, G. Marchesini and B.R. Webber, Nucl. Phys. B349 (1991) 635.

44. M.H. Seymour, Comput. Phys. Commun. 90 (1995) 95.

45. J. Andre and T. Sjostrand, Phys. Rev. D57 (1998) 5767.

46. C. Friberg and T. Sjostrand, in Proc. of the Workshop *Monte Carlo Generators for HERA Physics*, eds. T.A. Doyle, G. Grindhammer, G. Ingelman and H. Jung, (DESY, Hamburg, 1999), p. 181.

47. J.C. Collins, hep-ph/0001040 and in these Proceedings.

48. G. Corcella and M.H. Seymour, Phys. Lett. 442B (1998) 417.

49. G. Miu and T. Sjostrand, Phys. Lett. 449B (1999) 313.

50. S. Mrenna, preprint UCD-99-4 (hep-ph/9902471).

51. G. Corcella and M.H. Seymour, preprint RAL-TR-1999-051 (hep-ph/9908388).

52. C. Balazs, J. Huston and I. Puljak, preprint FERMILAB-PUB-00-032-T (hep-ph/0002032), and in these Proceedings.

53. G. Sterman, in Proc. *10th Topical Workshop on Proton-Antiproton Collider Physics*, eds. R. Raja and J. Yoh (AIP Press, New York, 1996), p. 608; S. Catani, Nucl. Phys. Proc. Suppl. 54A (1997) 107, and in Proc of the *32nd Rencontres de Moriond: QCD and High-Energy Hadronic Interactions*, ed. J. Tran Than Van (Editions Frontières, Paris, 1997), p. 331.

54. S. Catani, G. Turnock, B.R. Webber and L. Trentadue, Nucl. Phys. B407 (1993) 3.

55. M.H. Seymour, Nucl. Phys. B513 (1998) 269; J.R. Forshaw and M.H. Seymour, JHEP 09 (1999) 009.

56. Yu.L. Dokshitzer, D.I. Diakonov and S.I. Troian, Phys. Rep. 58 (1980) 269, and references therein.

57. N. Brown and W.J. Stirling, Phys. Lett. 252B (1990) 657.

58. S. Catani, Yu.L. Dokshitzer, M. Olsson, G. Turnock and B.R. Webber, Phys. Lett. 269B (1991) 432.

59. S. Catani, Yu.L. Dokshitzer and B.R. Webber, Phys. Lett. 285B (1992) 291; S. Catani, Yu.L. Dokshitzer, M.H. Seymour and B.R. Webber, Nucl. Phys. B406 (1993) 187; S.D. Ellis and D.E. Soper, Phys. Rev. D 48 (1993) 3160.

60. G. Parisi and R. Petronzio, Nucl. Phys. B154 (1979) 427.

61. J.C. Collins, D.E. Soper and G. Sterman, Nucl. Phys. B250 (1985) 199.

62. G. Sterman, Nucl. Phys. B281 (1987) 310.

63. S. Catani and L. Trentadue, Nucl. Phys. B327 (1989) 323, Nucl. Phys. B353 (1991) 183.

64. J.C. Collins and D.E. Soper, Nucl. Phys. B197 (1982) 446.

65. S. Catani, M.L. Mangano, P. Nason and L. Trentadue, Nucl. Phys. B478 (1996) 273.

66. C. Balázs, J.C. Collins and D.E. Soper, in these Proceedings.

67. J. Kodaira and L. Trentadue, Phys. Lett. 112B (1982) 66, Phys. Lett. 123B (1983) 335; C.T.H. Davies, B.R. Webber and W.J. Stirling, Nucl. Phys. B256 (1985) 413.

68. S. Catani, E. D'Emilio and L. Trentadue, Phys. Lett. 211B (1988) 335; R.P. Kauffman, Phys. Rev. D 45 (1992) 1512.

69. H. Contopanagos, E. Laenen and G. Sterman, Nucl. Phys. B484 (1997) 303.

70. M. Kramer, E. Laenen and M. Spira, Nucl. Phys. B511 (1998) 523.

71. N. Kidonakis and G. Sterman, Phys. Lett. 387B (1996) 867, Nucl. Phys. B505 (1997) 321.

72. N. Kidonakis, G. Oderda and G. Sterman, Nucl. Phys. B531 (1998) 365.

73. E. Laenen and S. Moch, Phys. Rev. D 59 (1999) 034027.

74. E. Laenen, G. Oderda and G. Sterman, Phys. Lett. 438B (1998) 173.

75. S. Catani, M.L. Mangano and P. Nason, JHEP 07 (1998) 024.

76. S. Catani, M.L. Mangano, P. Nason, C. Oleari and W. Vogelsang, JHEP 03 (1999) 025.

77. N. Kidonakis and J.F. Owens, preprint FSU-HEP-991216 (hep-ph/9912388).

78. M. Cacciari, preprint CERN-TH/99-312 (hep-ph/9910412).

79. N. Kidonakis and V. Del Duca, preprint FSU-HEP-991123 (hep-ph/9911460).

80. E. Laenen, J. Smith and W.L. van Neerven, Nucl. Phys. B369 (1992) 543, Phys. Lett. 321B (1994) 254.

81. E. Berger and H. Contopanagos, Phys. Rev. D 54 (1996) 3085, Phys. Rev. D 57 (1998) 253.

82. S. Catani, M.L. Mangano, P. Nason and L. Trentadue, Phys. Lett. 378B (1996) 329.

83. N. Kidonakis, preprint EDINBURGH-99-4 (hep-ph/9904507).

Partons for the LHC

R.D. Ball [12] and J. Huston

Abstract

We discuss some of the experimental, theoretical and methodological issues in the determination of parton distributions with meaningful error estimates, and their impact on physical cross sections to be measured at the Tevatron and LHC.

1 Introduction

The calculation of production cross sections at the Tevatron and LHC, for both interesting physics processes and their backgrounds, relies upon a knowledge of the distribution of the momentum fraction x of the partons in a proton at the relevant scale. These parton distribution functions (pdfs) are at present determined by global fits to data from deep inelastic scattering (DIS), Drell-Yan (DY), and jet and direct photon production at current energy ranges. Two groups, CTEQ and MRS, provide semi-regular updates to their best-fit parton distributions when new data and/or theoretical developments become available. The newest pdfs, in most cases, currently provide the single most accurate overall description of the world's data, and should be utlilized in preference to older pdf sets. The most recent sets from the two groups are CTEQ5 [1] and MRST [2].

In this contribution we will discuss the data sets used in the fits, the way in which the fits are performed in practice (in particular, issues such as the parametrization of initial distributions, the solution of the evolution equations, and scheme dependence), and the main uncertainties in the fitted pdfs due to uncertain or incomplete experimental data. In particular, we will concentrate on the difficulties involved in determining the gluon distribution through direct photons or jets. We then move on to discuss more general issues which may affect future pdf determinations: the inclusion of correlated systematics and the difficulties involved in combining these for different experiments, purely theoretical uncertainties arising from the limitations of NLO perturbative QCD, and finally, methodological uncertainties such as the dependence on the form of the parametrization and the assumption of Gaussian error propagation. We conclude with a summary of the progress that might be made before the LHC turns on, and the role of LHC data in determining pdfs.

[12] Royal Society University Research Fellow.

2 Processes Involved in Global Analysis Fits

Lepton-lepton, lepton-hadron and hadron-hadron interactions probe complementary aspects of perturbative QCD (pQCD). Lepton-lepton processes provide clean measurements of $\alpha_s(Q^2)$ and of the fragmentation functions of partons into hadrons. Measurements of deep-inelastic scattering (DIS) structure functions (F_2, F_3) in lepton-hadron scattering and of lepton pair production cross sections in hadron-hadron collisions are the main source of information on the quark distributions $q^a(x,Q)$ inside hadrons. Scaling violations in deep inelastic processes give some information about the gluon distribution $g(x,Q)$. Furthermore the gluon distribution function enters directly (i.e. at leading order) in hadron-hadron scattering processes with direct photon and jet final states. Modern global parton distribution fits are carried out to next-to-leading (NLO) order which allows $\alpha_s(Q^2), q^a(x,Q)$ and $g(x,Q)$ to all mix and contribute in the theoretical formulae for all processes. Nevertheless, the broad picture described above still holds to some degree in global pdf analyses.

In pQCD, the gluon distribution is always accompanied by a factor of α_s, in both the hard scattering cross sections and in the evolution equations for parton distributions. Thus, determination of α_s and the gluon distribution is, in general, a strongly coupled problem. One can determine α_s separately from e^+e^- or determine α_s and $g(x,Q)$ jointly in a global pdf analysis. In the latter case, though, the coupling of α_s and the gluon distribution may not lead to a unique solution for either (see for example the discussion in the CTEQ4 paper where good fits were obtained to a global analysis data set, including the inclusive jet data, for a wide range of α_s values [3].)

Currently, the world average value of $\alpha_s(M_Z)$ is 0.119 ± 0.004 [4]. This is in agreement with the average value from LEP, while the DIS experiments prefer a slightly smaller value (of the order of $0.116-0.118$)). Since global pdf analyses are dominated by the high statistics DIS data, they would tend to favor the values of α_s closer to the lower DIS values. The more logical approach is to adopt the world average value of $\alpha_s(M_Z)$ and concentrate on the determination of the pdfs. This is what both CTEQ and MRS currently do. [13]

The data from DIS, DY, direct photon and jet processes utilized in pdf fits cover a wide range in x and $Q \equiv \sqrt{Q^2}$. The kinematic 'map' in the (x,Q) plane of the data points used in a recent parton distribution function analyses is shown in Figure 1. The HERA data (H1+ZEUS) are predominantly at low x, while the fixed target DIS and DY data are at higher x. There is considerable overlap, however, with the degree of overlap increasing with time as the statistics of the HERA experiments increases. DGLAP-based NLO pQCD provides an accurate description of the data (and of the evolution of the parton distributions) over the entire kinematic range shown. At very low x and Q^2, DGLAP evolution is believed to be no longer applicable due to unresummed small x logarithms. Similarly at very large x there are significant contributions from unresummed soft logarithms (logarithms of $1-x$). However, no evidence for such corrections is seen in the current range of data; thus all global analyses use conventional DGLAP evolution of pdfs.

[13] One can either quote a value of $\alpha_s(M_Z)$ or the value of $\Lambda^{\overline{MS}}$. In the latter case, however, the number of flavors has to be clearly specified, since the value of α_s (and not $\Lambda^{\overline{MS}}$) has to be continuous across flavor thresholds.

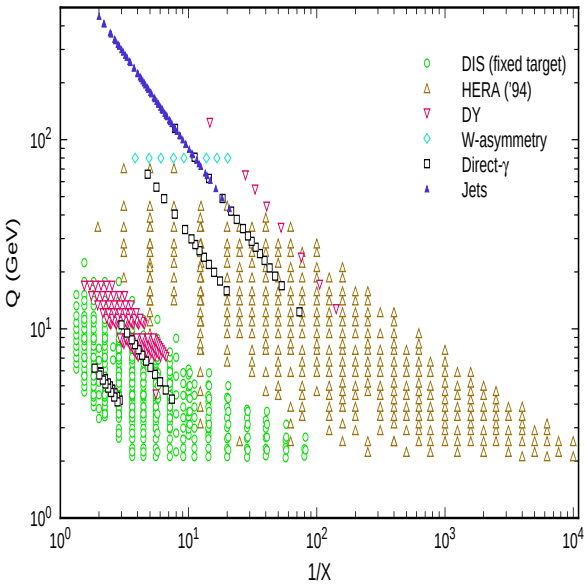

Figure 1: The kinematic map in the (x, Q) plane of data points used in the CTEQ5 analysis.

There is a remarkable consistency between the data in the pdf fits and the NLO QCD theory fit to them. Over 1300 data points are shown in Figure 1 and the χ^2/d.o.f. for the fit of theory to data is on the order of one.

Parton distributions determined at a given x and Q^2 propagate down to lower x values at higher Q^2 values. The accuracy of the extrapolation to higher Q^2 depends both on the accuracy of the original measurement and any uncertainty on $\alpha_s(Q^2)$. For the structure function F_2, the typical measurement uncertainty at medium to large x is on the order of $\pm 3\%$. At large x, the DGLAP equation for F_2 can be approximated as $\frac{\partial F_2}{\partial \log\ Q^2} = \alpha_s(Q^2) P^{qq} \otimes F_2$. There is an extrapolation uncertainty of around $\pm 5\%$ in F_2 from low to high Q^2 (10^5 GeV^2) from the uncertainty in α_s. Evolved distributions are also susceptible to uncertainties from an anomalously large contribution to F_2 near x values of 1. Such a contribution may not be evident in fixed target measurements at low x and low Q^2, but may influence higher Q^2 measurements [5].

For comparison, the kinematics appropriate for the production of a state of mass M and rapidity y at the LHC is shown in Figure 2 [6]. For example, to produce a state of mass 100 GeV and rapidity 2 requires partons with x values between 0.05 and 0.001 at a Q^2 value of 10^4 GeV^2. Also shown in the figure is another view of the kinematic coverage of the fixed target and HERA experiments used in pdf fits. It can be seen that parton distributions determined from these experiments are sufficient to predict most LHC cross-sections of interest, provided that DGLAP evolution at small and large x is sufficiently reliable.

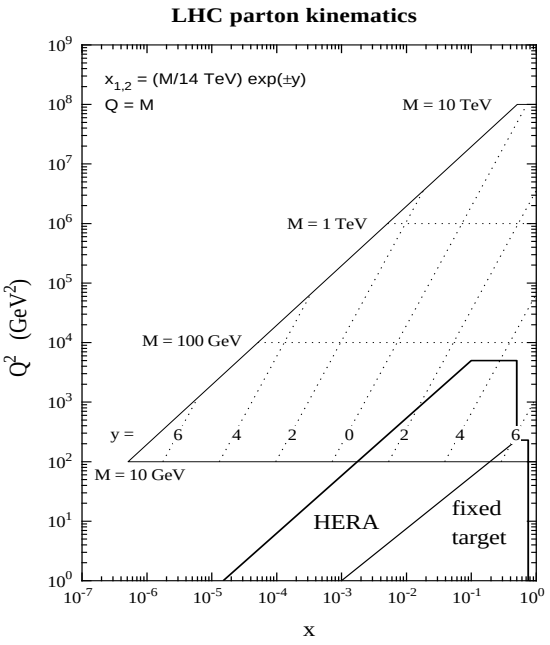

Figure 2: A plot of LHC parton kinematics in (x, Q^2) space. Also shown are the reach of fixed target and HERA experiments.

3 Evolution, Schemes and Parametrizations

3.1 Evolution Codes

In order to fit the initial pdfs to experimental data they need to be evolved up to the correct scale by solving the DGLAP equations either to LO or NLO. The evolution can be carried out in either moment space or configuration space: both MRS and CTEQ use configuration space codes. Improvements have been made in the CTEQ and MRST evolution programs so that both now agree with the 'DESY standard' evolution prescription [7]. The CTEQ and MRST packages should be able to carry out the evolution using NLO DGLAP to an accuracy of a few percent over the LHC kinematic range, except perhaps at very large and very small x. Note that the theoretical predictions for the W and Z total cross sections at the LHC may have uncertainties of less than 5%[8]. This puts a great demand for the pdf evolution to have accuracies of better than a few percent, since any error on a pdf gets doubled in the cross section calculation. Mellin space codes might be the answer here.

A global pdf analysis carried out at next-to-leading order needs to be performed in a specific renormalization and factorization scheme. The evolution kernels are in a specific scheme and to maintain consistency, any hard scattering cross section calculations used for the input processes or utilizing the resulting pdfs need to also have been implemented in that same renormalization scheme. Almost universally, the $\overline{MS}$ scheme is used: pdfs are also available in the DIS scheme, a fixed flavor scheme (as in ref.[9]) and several schemes that differ in their specific treatment of the charm quark mass [10, 11].

It is also possible to use only leading-order matrix element calculations in the global fits which results in leading-order parton distribution functions. Such pdfs are preferred when leading order matrix element calculations (such as Monte Carlo programs like `HERWIG` [12] and `PYTHIA` [13]) are used. The differences between LO and NLO pdfs, though, are formally NLO; thus, the additional error introduced by using a NLO pdf with `HERWIG` rather than a LO pdf, for example, should not be significant, in principle, and NLO pdfs can be used when no LO alternatives are available. The accuracy of current DIS/DY data is such that the χ^2 values for LO fits are noticeably worse than those from the NLO fits: the data are sensitive to the differences between LO and NLO partonic cross-sections and evolution kernels.

3.2 Parametrization of Initial Distributions

All current global analyses use a generic form for the parametrization of both the quark and gluon distributions at some reference value Q_0:

$$f(x, Q_0) = a_0 x^{a_1} (1-x)^{a_2} P(x; a_3, ...). \tag{1}$$

The reference value Q_0 is usually chosen in the range of $1-2$ GeV. The parameter a_1 is associated with small-x behaviour while a_2 is associated with large-x valence counting rules. In some pdf fits, $a_1^{\rm gluon}$ has been tied to $a_1^{\rm seaquark}$; in more recent fits like CTEQ4, CTEQ5 and MRST, the two small x exponents are allowed to vary independently. The current statistical power of the low x and Q^2 DIS data from HERA warrants this separation.

The first two factors, in general, are not sufficient to describe either quark or gluon distributions. The term $P(x; a_3, ...)$ is a suitably chosen smooth function, depending on one or more parameters, that adds more flexibility to the pdf parametrization. In general, both the number of free parameters and the functional form can have an influence on the global fit. For example, the MRS group traditionally uses $P_{MRS}(x; a_3, a_4) = 1 + a_3\sqrt{x} + a_4 x$. The CTEQ3 pdf used $P_{CTEQ3} = 1 + a_3 x$ while CTEQ2, CTEQ4 and CTEQ5 all use the more general form $P_{CTEQ2,4,5} = 1 + a_3 x^{a_4}$. The flexibility in the latter form, for example, makes possible the larger gluon at high x observed in the CTEQ4HJ pdf.

Although the pdfs determined from global analyses should, in principle, be universal, in practice they could depend on the choice of data sets, and in particular on the choice of Q_{cut} values that specify the minimum hard physical scale $(Q, p_T, ..)$ required for data points to be included in the fit.

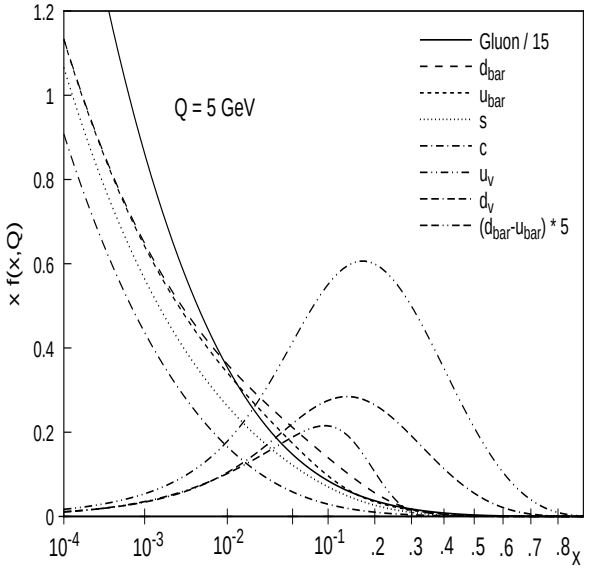

Figure 3: The parton distributions from the CTEQ5 set plotted at a Q value of 5 GeV.

The parton distributions from the recent CTEQ pdf release are plotted in Figure 3 at a Q value of 5 GeV. The gluon distribution is largest at small x values while the valence quark distributions dominate at higher x.

3.3 Evolution in time and Q^2

As discussed in the introduction, the MRS and CTEQ groups provide semi-regular updates to their parton distributions as new data and/or theory becomes available. The latest parton distributions are the most accurate and should be used in preference to previous pdfs. However, in some cases calculations using older pdfs are necessary: for example, until

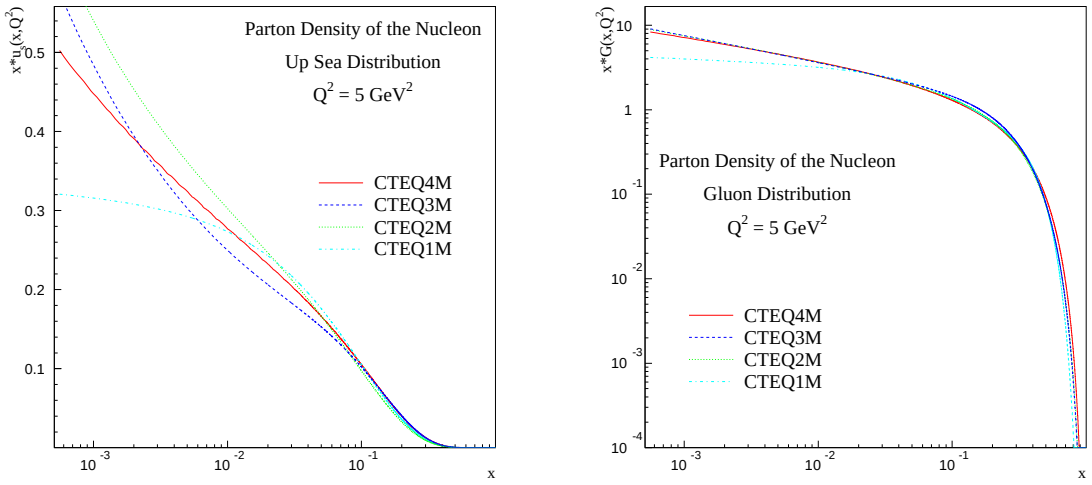

Figure 4: The up sea quark and gluon parton distributions from the CTEQ1-4 sets plotted at a Q^2 value of 5 GeV^2.

recently [14] none of the more recent pdfs were implemented in PYTHIA, and most comparisons in the ATLAS TDR have been made with the CTEQ2L pdf (the default pdf in PYTHIA version 5.7).

A comparison of the CTEQ1M [14], CTEQ2M [15], CTEQ3M [16] and CTEQ4M [3] parton distributions (in particular the up sea quark and gluon distributions) are shown in Figure 4, at a Q^2 value of 5 GeV^2. The CTEQ2-4 up quark sea distributions are substantially steeper than that of CTEQ1, reflecting the influence of the HERA data. A similar effect is seen with the gluon distribution. There is little change in the valence distributions.

The up sea quark and gluon distributions are shown in Figure 5 at a larger Q^2 value of 10^4 GeV^2. Evolution has evened out many of the differences observed at lower Q^2 values. A Q^2 value of 10^4 GeV^2 corresponds to a mass scale at the LHC of about 100 GeV.

The effects of evolution are examined in more detail in Figure 6 where the up sea quark and gluon distributions are plotted at Q^2 values of 2, 10, 50, 10^4 and 10^6 GeV^2. There are two interesting features that can be noted. Most of the evolution takes place at low Q^2 and there is little evolution for x values in the vicinity of 0.1. In contrast, at large x value the distributions decrease by an order of magnitude from the lowest to the highest Q^2 value, while at small x they increase by an order of magnitude.

[14] In the most recent version of PYTHIA (6.1), the CTEQ5 pdf's are available.

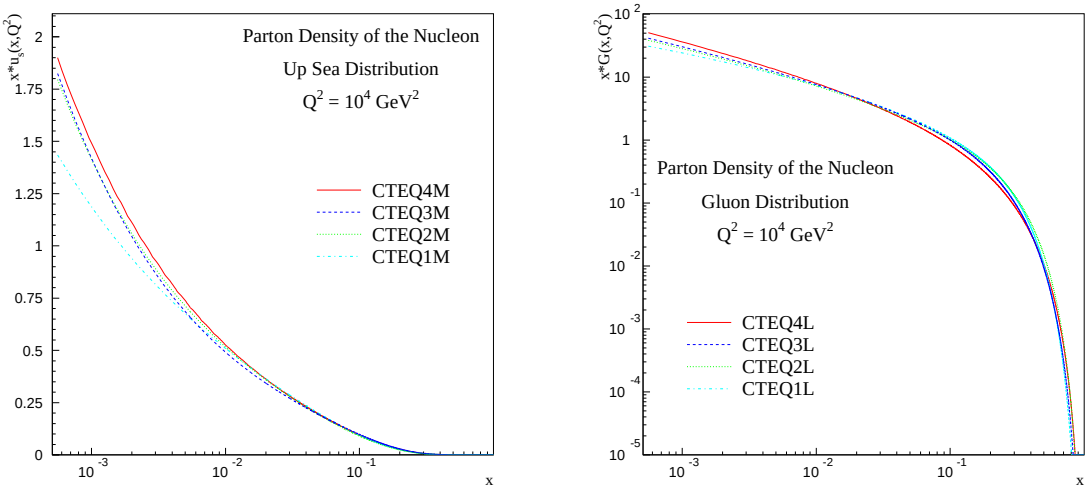

Figure 5: The up sea quark and gluon parton distributions from the CTEQ1-4 sets plotted at a Q^2 value of 10^4 GeV^2.

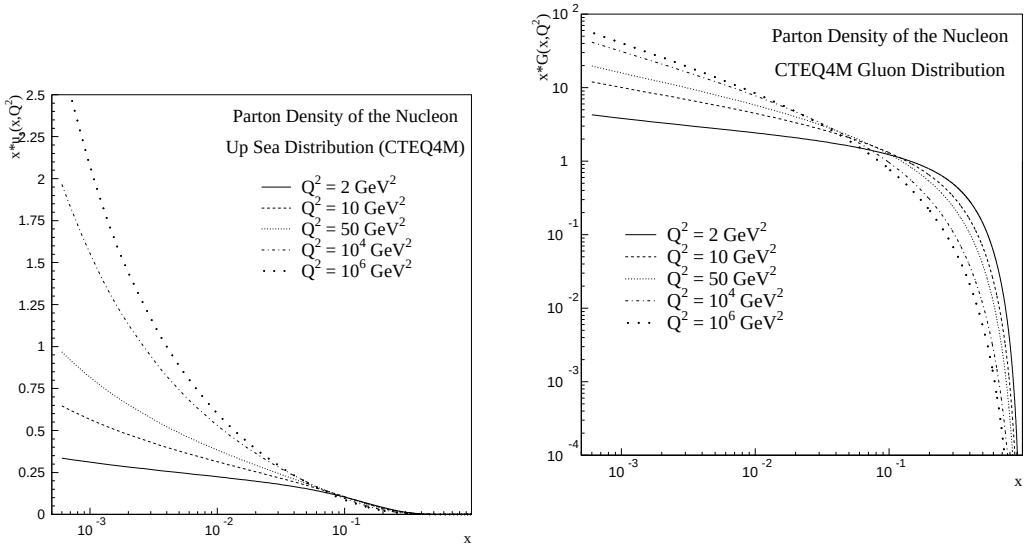

Figure 6: The up sea quark and gluon distributions from CTEQ4M shown at five different Q^2

4 Estimating Uncertainties

In addition to having the best estimates for the values of the pdfs in a given kinematic range, it is also important to understand the allowed range of variation of the pdfs, i.e. their uncertainties. The crudest method of estimating parton distribution uncertainties is to compare different published parton distributions. This is unreliable since most published sets of parton distributions (for example from CTEQ and MRS) adopt similar assumptions and the differences between the sets do not fully explore the full range uncertainties that actually exist. Here and in the next section we concentrate on estimating the uncertainties due to to the limitations of available data sets.

The sum of the quark distributions $\Sigma(q(x) + \overline{q}(x))$ is, in general, well-determined over a wide range of x and Q^2. As stated above, the quark distributions are predominantly determined by the DIS and DY data sets which have large statistics, and systematic errors in the few percent range ($\pm 3\%$ for $10^{-4} < x < 0.75$). Thus the sum of the quark distributions is basically known to a similar accuracy. The individual quark flavors, though, may have a greater uncertainty than the sum. This can be important, for example, in predicting distributions that depend on specific quark flavors, like the W asymmetry distribution [17] and the W rapidity distribution.

Information on the $\overline{d}$ and $\overline{u}$ distributions comes, at small x, from HERA and at medium x from fixed target DY production on H_2 and D_2 targets. It is now well-established [18, 19] that the $\overline{d}$ and $\overline{u}$ distributions are not the same. The difference in these distributions between the CTEQ4M and CTEQ5M pdfs is due primarily to the influence of the data from the E866 experiment. It is worth noting that our detailed knowledge of $\overline{d}/\overline{u}$ is limited primarily to the x region (.03-.35) covered by E866.

The strange quark sea is determined from dimuon production in ν DIS (CCFR[20]), with the strange quark distribution $(s + \overline{s})$ being approximately $\frac{1}{2}(\overline{u} + \overline{d})$. The charm and bottom quark distributions are calculated perturbatively from gluon splitting for given masses of m_c and m_b. (See also the previous discussion on schemes.)

Current information on d/u at large x comes from fixed target DY production on H_2 and D_2 and the lepton asymmetry in W production at the Tevatron. In the CTEQ5 and MRST fits, the NMC D_2/H_2 data are used to constrain the large x d quark distribution in this way. Bodek and Yang have argued that the D_2 data need to be corrected for nuclear binding effects, which would lead to a larger d/u ratio at large x (and thus a larger d quark distribution as the u quark distribution is well-determined from DIS) [21]. The need for the nuclear binding corrections is still an open question [22]. The larger d quark distribution would lead to an increase in the high E_T Tevatron jet cross section of about 10%. A similar excess would be expected for high E_T jet production at the LHC.

The parton distribution with the greatest uncertainty is the gluon distribution, simply because it does not couple directly to an external probe. The LHC is essentially a gluon-gluon collider and many hadron-collider signatures of physics both within and beyond that Standard Model involve gluons in the initial state. Thus, it is very important to estimate the theoretical uncertainty due to the uncertainty in the gluon distribution.

The gluon distribution can be determined indirectly at low x by measuring the scaling

violations in the quark distributions ($\partial F_2/\partial \log Q^2$), but a direct measurement is necessary at moderate to high x. Direct photon production has long been regarded as potentially the most useful source of information on the gluon distribution with fixed target direct photon data, especially from the experiment WA70 [23], being used in a number of global analyses. However, as will be discussed in the next section, there are a number of theoretical complications with the use of direct photon data.

The momentum fraction of the proton carried by quarks is determined very well from DIS data; at a Q_0 value of 1.6 GeV, in the CTEQ4 analysis for example, the momentum fraction carried by quarks is 58% with an uncertainty of $\pm 2\%$. Thus, the momentum fraction carried by gluons is 42% with a similar uncertainty. This constraint is important; if the gluon distribution increases in one x range, momentum conservation forces it to decrease in another x range. Thus, if the gluon flux in the x range from 0.01 to 0.3 were to decrease by 20%, the gluon flux would have to increase by a fairly dramatic amount in the other x ranges to compensate. For example, if this compensation were to come in the high x region, the gluon distribution would have to double.

A simple way of estimating the uncertainty in the gluon distribution is to systematically vary the gluon parameters in a global analysis and then look for incompatibilities with the data sets that make up the global analysis database. This study has been carried out by CTEQ using only DIS and Drell-Yan data where the theoretical and experimental systematic errors are under good control [24]. Except at larger values of $x(x > 0.2 - 0.3)$, the variation in the gluon distributions is less than 15% at low values of Q^2, decreasing to less than 10% at high values: as noted earlier, evolution is the great equalizer for parton distributions. Note that the DIS and DY datasets used in this analysis do not provide any strong constraints on the gluon distribution at high values of x. This study used the CTEQ4 value of α_s (i.e. 0.116). If α_s is varied in the range from 0.113 to 0.122, the gluon distribution varies by 3% for $x < 0.15$.

In order to assess the range of predictions for hadronic cross sections, it is more important to know the uncertainties in the gluon-gluon and gluon-quark luminosity functions at the appropriate kinematic region (in $\tau = x_1 x_2 = \hat{s}/s$) rather than the uncertainties in the parton distributions themselves. Therefore it is useful to define the relevant integrated parton-parton luminosity functions: for example the gluon-gluon luminosity function can be defined as:

$$\tau \frac{dL}{d\tau} = \int_\tau^1 \frac{dx}{x} g(x, Q^2) g(\tau/x, Q^2). \tag{2}$$

This quantity is directly proportional to the cross section for s-channel production of a single particle and it also gives a good estimate for more complicated production mechanisms. In Figure 7 is shown the range of allowed gluon-gluon luminosities (normalized to the CTEQ4M values) for the variations discussed above. Here, Q^2 is taken to be τs, which naturally takes the Q^2 dependence of the gluon distribution into account as one changes $\sqrt{\tau}$. The top region is for the LHC and the bottom is for the Tevatron. Above a $\sqrt{\tau}$ value of 0.1, the allowed variation grows dramatically; this indicates the need for more information about the gluon distribution at large x than provided by the DIS and DY data sets used in this analysis.

In analogy with the discussion of gluon-gluon luminosities, one can also study the gluon-

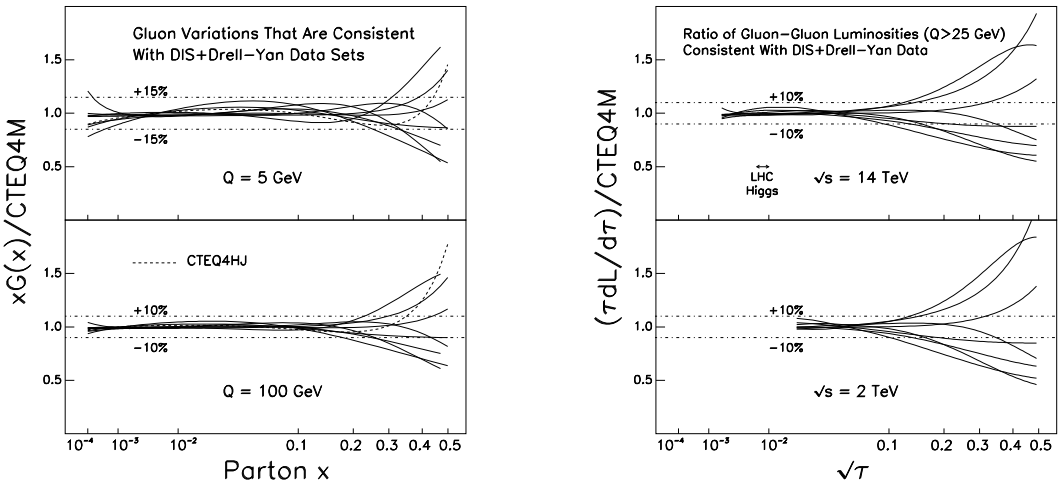

Figure 7: The ratio of gluon distributions consistent with the DIS and DY data sets to the gluon distributions from CTEQ4M. The gluon distribution from CTEQ4HJ is also shown for comparison. In the second figure are shown the corresponding allowable variations in the integrated gluon-gluon luminosity as a function of $\sqrt{\tau}$.

Table 1: The parton-parton luminosity uncertainty as a function of $\sqrt{\tau}$.

$\sqrt{\tau}$ range	gluon-gluon	gluon-quark
< 0.1	$\pm 10\%$	$\pm 10\%$
$0.1 - 0.2$	$\pm 20\%$	$\pm 10\%$
$0.2 - 0.3$	$\pm 30\%$	$\pm 15\%$
$0.3 - 0.4$	$\pm 60\%$	$\pm 20\%$

quark luminosity (again normalized to the CTEQ4M result). The uncertainties on the parton-parton luminosities, as a function of $\sqrt{\tau}$, are summarized in Table 1. Note that the region of production of a $100 - 140$ GeV Higgs at the LHC lies in the region where the range of variation in the gg luminosity is $\pm 10\%$.

5 Direct Photons and Jets in Global Fits

5.1 Direct Photons

As mentioned previously in this section and in Reference [25], direct photon production has long been viewed as an ideal vehicle for measuring the gluon distribution in the proton. The quark-gluon Compton scattering subprocess ($gq \to \gamma q$) dominates photon production in all kinematic regions of pp scattering, as well as for low to moderate values of parton momentum fraction x in $\overline{p}p$ scattering. As described previously, the gluon distribution is relatively well constrained at low $x(x < 0.1)$ by DIS and DY data, but less so at higher x. Consequently, fixed target direct photon data have been incorporated in several modern global parton distribution function analyses with the hope of providing a major constraint on the gluon distribution at moderate to high x.

A pattern of systematic deviations of direct photon data from NLO predictions has been observed [26, 27], however, these being particularly striking for the E706 experiment. The origin of the deviations is still quite controversial. One possibility that has been suggested is that the deviations are due to the effects of soft gluon radiation, or k_T [28, 29]. This view, however, is not universally held; see, for example, the discussion in Reference [25] and in Reference [27]. The k_T values needed to describe the data are too large to be viewed as purely 'intrinsic' or non-perturbative in origin. But, as discussed in Reference [25], in the standard formalism for direct photon production there are no double-logs to be resummed. This is in contrast to double-arm observables such as Drell-Yan or diphoton production; since direct photon production is, by definition, a single-arm observable, there is no restriction of phase space for gluon emission, and thus no double logarithmic enhancement to the p_T distribution. The only enhancement effects that survive arise from the purely 'intrinsic' k_T present in the colliding hadrons.

Nonetheless, there is generally a substantial amount of k_T that results from the emission of soft gluons in hard scattering processes. Direct evidence of this k_T has long been evident in Drell-Yan, diphoton and heavy quark measurements. The values of $< k_T >$/parton for these processes vary from 1 GeV at fixed target energies to $3 - 4$ GeV at the Tevatron Collider. The growth is approximately logarithmic with center of mass energy. (The value expected at the LHC for relatively low mass states ($30 - 40$ GeV) is in the range of $6.5 - 7.0$ GeV.)

Perturbative QCD corrections are insufficient to explain the size of the observed k_T and fully resummed calculations are required to explain Drell-Yan, W/Z and diphoton distributions [30]. These resummed calculations qualitatively describe the growth of the $< k_T >$ with center-of-mass energy. Currently there is no rigorous k_T-type resummation calculation available for single photon production, for the reasons cited above. In addition, this calculation is quite challenging in that the final state parton takes part in soft gluon emission and in color exchange with initial state partons, in contrast with the Drell-Yan and diphoton cases. Also, the calculation is complicated by the fact that several overlapping power-suppressed corrections can contribute and, at high x, threshold effects are important.

Nevertheless, there has been recent theoretical progress in single photon resummation [31, 32, 33, 34]. In particular, in Reference [34], a technique has been presented for simultaneously treating recoil and threshold corrections in single photon inclusive cross sections, working within the formalism of collinear factorization. In the preliminary results, substantial en-

hancements have been observed, at moderate p_T and x, from higher order perturbative and power-law non-perturbative corrections. This approach is still quite new and the efficacy of the formalism still has to be evaluated.

There is an intuitive picture that describes the effects of this soft gluon radiation, both perturbative and non-perturbative, on the direct photon cross section. The presence of soft gluon radiation, or k_T, can give a 'kick' in the photon direction. Due to the steeply falling cross sections, the k_T kick can lead to the promotion of photons from lower p_T to higher values of p_T. The more steeply falling the cross section, the larger the resulting enhancement. Using this intuitive picture, the effects of soft gluon radiation can be approximated by a convolution of the NLO cross section with a Gaussian k_T smearing function. The value of $< k_T >$ to be used for each kinematic regime should be taken directly from relevant experimental observables, given the lack of a rigorous formalism, rather than from a theoretical prediction. The behaviour of the k_T smearing correction is quite different for the Tevatron collider and for fixed target experiments. For the Tevatron, there are two points to note: (1) the agreement with the data is improved if the k_T correction is taken into account and (2) the k_T smearing effects fall off roughly as $1/p_T^2$ [29]. The latter behaviour is the expectation for such a power-suppressed type of effect and is the behaviour expected at the LHC, where the effects of the k_T smearing should not be important beyond p_T values of 30 GeV [15].

The k_T correction obtained for E706 at a center-of- mass energy of 31.6 GeV is shown in Figure 8. The value of $< k_T >$ of 1.2 GeV was obtained from measurements of several kinematic observables in the experiment [29]. The k_T smearing effect is much larger here then observed at the collider and does not have the $1/p_T^2$ falloff. Also shown are the k_T corrrections using values of $< k_T >$ of 1.0 and 1.4 GeV (a reasonable estimate of the range of experimental uncertainty in the $< k_T >$ determination). In addition, the k_T correction for the E706 data used in the recent MRST pdfs is shown. The MRST k_T correction, utilizing a different model, is larger leading to a smaller gluon distribution in the relevant x range. (Both the CTEQ4 and MRST pdfs, with their respective k_T corrections, lead to good agreement with the E706 direct photon cross sections.) The differences between the k_T correction from Reference [29] and that from the MRST pdfs can be taken as an indication of the uncertainty in the value of this correction. Good agreement with the E706 direct photon and cross section at $\sqrt{s} = 31.6$ GeV is observed when the nominal k_T correction of 1.2 GeV is used; however, the allowed range of variation of $\langle k_T \rangle$ $(1.0 - 1.4$ GeV) makes quantitative comparisons, and thus an extraction of the gluon distribution, difficult [16]. Since the high p_T E706 data agrees well with CTEQ4M, it would thus disfavor the CTEQ4HJ pdf. As stated before, however, a definitive conclusion must await a more rigorous theoretical treatment.

Other related fixed target processes, such as π^0 production, in the same p_T range as the

[15]Similar k_T smearing effects should be present in all hard scattering cross sections, for example jet production at the Tevatron. The size of the experimental and theoretical systematic errors in the low E_T region make such a confirmation difficult.

[16]NLO QCD predictions for fixed-target direct photon production (as is also true for other fixed target processes) also contain a non-negligible renormalization and factorization scale dependence, as discussed in Reference [25]

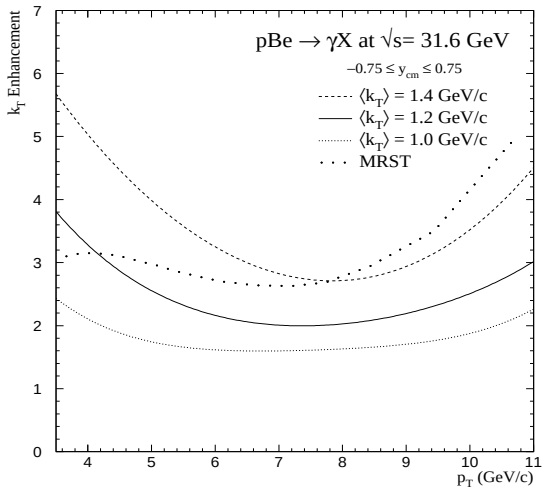

Figure 8: The variation of k_T enhancements (ratio of cross sections with and without the k_T corrections) relevant to E706 direct photon data at 31.6 GeV, for different values of average k_T. In addition, the k_T correction for E706 used in the recent MRST fit is indicated.

measured direct photon cross section, may perhaps shed some light on the puzzle. It has been noted [35] that essentially all of the fixed target π^0 cross sections disagree with NLO predictions, by essentially a constant factor. Thus, there may be a common problem causing the deviations, such as uncertainties in the high z quark and gluon fragmentation functions and possible sizeable higher order corrections. In addition, the importance of the high z fragmentation region implies the need for threshold resummation techniques to be applied, in processes with non-trivial color flow.

It is worthwhile pointing out, though, that the same k_T model used for for single photon production was shown to also provide an adequate description of the experimental π^o cross sections [29, 36]. As in the case of direct photon production, the controversy regarding the theory/data discrepancies is still open. The π^0 cross sections may form a crucial role in the ultimate understanding for a number of reasons: if k_T are important for photon production, they should also have a measureable impact on the π^0 cross sections as well. In addition, π^0's form the primary experimental background to direct photon production.

Finally, it is not clear if any theoretical treatment for photon production is capable of describing all of the current fixed target direct photon data. There are discrepancies between the different experiments which may imply experimental difficulties, which are in addition to any of the theoretical problems discussed above.

5.2 Influence of Jets

An important process that is sensitive to the gluon distribution is jet production in hadron-hadron collisions. Processes responsible for jet production include gluon-gluon, gluon-quark and quark-quark(or anti-quark) scattering. Precise data on jet production at the Fermilab Tevatron are now available over a wide range of transverse energy, and the theoretical uncertainties in most of this range are well-understood. Thus, it is to be expected that jet production can provide a good constraint on the gluon distribution.

The jet data that has been utilized in global pdf fits has been from the CDF and D0 collaborations [17]. The data cover a wide kinematic range (E_T values from 15 to 450 GeV corresponding to an x range of 0.02 to 0.5). The CDF jet data from Run IA were utilized in the CTEQ4HJ pdf fit [37]. Here, a large emphasis was given to the high E_T data points which show a deviation from NLO QCD predictions with "conventional" pdfs. Given the lack of constraints on the high x gluon distribution discussed in Section VI, the extra emphasis on the high E_T region was enough to cause a significant increase in the gluon distribution; for example, the gluon distribution at an x value of 0.5 ($Q = 100$ GeV) increases by a factor of two. Since the dominant jet subprocess in this region is $\overline{q}q$ scattering the increase in the gluon distribution of a factor of two causes only a 20% increase in the jet cross section. This is sufficient to pass through the bottom of the CDF high E_T jet error bars. The preliminary jet cross sections from Run 1B (90 pb^{-1}) from both the CDF and D0 experiments were used in the CTEQ4M fits, but with statistical errors only and only for E_T in the range $50 - 200$ GeV. The points with E_T lower than 50 GeV have substantial systematic errors on both the theoretical and experimental sides while the points with E_T higher than 200 GeV contain the CDF excess. The inclusion of the jet data serves to considerably constrain the gluon distribution over the x range of 0.1 to 0.2. The resulting gluon (CTEQ4M) does not decrease the excess observed by CDF at high E_T.

The published D0 jet cross section [38] along with the (soon-to-be published) CDF jet cross section [39] from Run 1B were used in the recently released CTEQ5 parton distributions. The fits use the full E_T range for the cross sections and use the correlation information on the systematic errors as contained in the covariance matrices for both experiments. The two experiments are in agreement with each other except for a slight normalization shift [18]; the two highest E_T data points for CDF are above those for D0, but both experiments have large statistical errors in this region. As can be seen in Figure 9 the NLO QCD prediction with the CTEQ5M pdf is in good agreement with the CDF data. The conclusions are exactly the same for the D0 jet data. The CTEQ5M gluon is very similar to CTEQ4M, except perhaps at very high x. The CTEQ4HJ pdf has been updated to complement the new CTEQ5M pdf. The CTEQ5HJ pdf gives almost as good a global fit as CTEQ5M to the full set of data on DIS and DY processes, and has the feature that the gluon distribution is significantly enhanced in the high x region, resulting in improved agreement with the

[17] The experimental and theoretical errors associated with the UA2 jet cross section make its use in pdf fits difficult.

[18] A shift on the order of 3% is expected since the two experiments use values for the total inelastic cross section that differ by that amount.

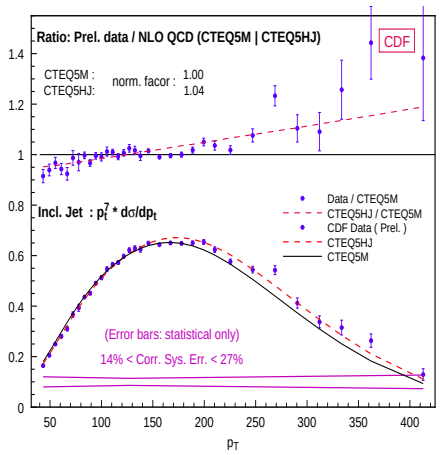

Figure 9: A comparison of the Run 1B CDF inclusive jet cross section to the CTEQ5 fits. The bottom plot shows the measured cross section multiplied by p_T^7 in order to allow a linear display. The top plot shows the ratio of the measured cross section to that calculated with CTEQ5M, as well as the ratios of CTEQ5HJ to CTEQ5M.

observed trend of jet data at high E_T in both the CDF and D0 experiments.

6 Systematic Uncertainties

There is currently an increasing awareness of the need and possibility of propagating errors in the data into error estimates on parton distribution functions [41, 42, 43]. Ideally, one might hope to perform a full error analysis and provide correlated errors for all the parton distributions determined in a global fit. This goal is difficult to carry out for several reasons. Firstly, there is no established way of quantifying the theoretical uncertainties for the diverse physical processes that are used. More pragmatically, only a subset of the experiments usually involved in global analyses provide correlation information on their data sets in a way suitable for the analysis. In these circumstances, comparing data from different experiments becomes very difficult. Furthermore the standard fitting procedure introduces methodological uncertainties due in particular to the necessity of choosing specific choices of parametrization. All of these uncertainties are of course all highly correlated. We discuss each in turn.

6.1 Theoretical Uncertainties

The most important theoretical uncertainty in the determination of parton densities is the truncation of the resummed perturbation series at NLO. Consistent NNLO determinations will require NNLO splitting functions: there has recently been some progress in this direction [45], and it is hoped that NNLO calculations might be available before the LHC

is turned on. Meanwhile there are some 'approximate NNLO' calculations [46], which attempt to reconstruct the NNLO splitting functions from their known integer moments and behaviour at large and small x: these analyses suggest that NNLO corrections might reduce theoretical uncertainties due to truncation of the perturbative expansion by at least a factor of two.

One of the most important consequences of the theoretical uncertainty from unknown NNLO corrections is that it currently limits the accuracy of most of the experimentally more reliable determinations of α_s. This in turn inevitably limits the accuracy of all extrapolations from low to high Q^2: for example one of the largest uncertainties in the prediction of the W and Z cross-sections is that due to the uncertainty in α_s [47].

Uncertainties at low Q^2 due to higher twist may be estimated from phenomenological fits: recent studies [21, 48] have shown that there are important correlations between empirical higher twist and the value of α_s. It has also been shown that the fitted higher twist contribution drops when estimates of NNLO corrections are included [49]. The empirical higher twist is qualitatively consistent with renormalon estimates. Taken together, these observations suggest that it is difficult to disentangle genuine higher twist from higher order perturbative corrections: the true higher twist contribution may be much smaller than is suggested by the fits.

The correct treatment of heavy quarks close to threshold was developed some time ago [10]; more recently it was proven that this procedure works to all orders in perturbation theory [50]. This treatment is now included in some of the CTEQ fits [1, 51]; a closely related but not identical procedure is used by MRS [2]. A simpler version of ACOT, which nonetheless accurately reproduces its essential features, has also been developed [52].

An accurate treatment of heavy quark production, and indeed W and Higgs production, requires the resummation of threshold logarithms. Recently it has been suggested that resummation of soft gluons may solve some of the problems with prompt photons [31, 32, 33, 34]. A fully consistent treatment will require the inclusion of soft gluon resummations in parton determinations, but as yet this has not been attempted. Renormalon studies suggest that such resummations may substantially improve the reliability of perturbation theory at large x. Again there will be strong correlations with higher twist. It would be particularly interesting to see the effect of such resummations on the predictions for the parton-parton luminosities eq.2 in the region relevant for Higgs production at the LHC.

The resummation of high energy (small x) logarithms is more problematic. Present data suggest that their effect on inclusive cross sections must be very small, at least at HERA and the Tevatron if not at the LHC. Furthermore, conventional theoretical approaches [53, 54] based on summations of LLx and NLLx [55] corrections have been shown to break down: the NLLx corrections are overwhelmingly large and negative [56]. Various suggestions for the resummation of these large corrections have been put forward [57, 58, 59, 60]. Hopefully a detailed phenomenological analysis based on one or other of these procedures will eventually provide a reliable estimate of the error due to uncertainties in small x evolution when using parton distributions measured at HERA to predict those to be used at the LHC.

6.2 Combining Different Experiments

On the experimental side, one of the major problems with combining results from different experiments lies in the degree of 'rigour' in the interpretation of the experimental errors. Experimental results may be conveniently expressed as probabilities $P(\text{data}|\text{theory})$, i.e. the probabilities of obtaining the given set of data given a certain theoretical prediction [44]. Often these probabilities are expressed in terms of predictions and (Gaussian) errors: for a given experiment, $P(d|t) = \exp(-\frac{1}{2}\chi^2(d|t))$, where d are the data, t the theoretical predictions and

$$\chi^2(d|t) = \sum_{\text{data}} (d-t)\Sigma^{-1}(d-t) \tag{3}$$

where Σ is the matrix of correlated errors. Maximizing the probability, and thus obtaining the most likely 'prediction', then corresponds to minimizing the χ^2. It should be emphasized that it is not necessary to present experimental results in this way, and in particular some systematics may be completely non-Gaussian; however if the experiment is to be useful it must always provide a (clear) estimate of $P(d|t)$, otherwise the error analysis is at best incomplete and at worst useless.

In the present situation, the predictions will be constrained functionals of the input pdfs (the constraints being the result of perturbative evolution and cross-sections). If the errors have been estimated correctly, and the theory which constrains the predictions is sufficiently accurate, then there should be pdfs for which the χ^2 per degree of freedom is of order unity. Unfortunately for many important datasets this is not the case, and thus if one were to insist on the rigour of the statistical method, then many important experiments would not be included in the analysis [42, 71]. Such a strict criterion is probably unrealistic: rather the emphasis should be placed on using the maximal experimental constraints from experimental data [41]. In this case the standard statistical techniques may not apply, but must be supplemented by physical considerations, taking into account experimental and theoretical limitations [43].

As an example of how this works in practice, we consider a recent CTEQ error analysis of the W-production cross-section [42, 43]. This uses the standard CTEQ5 analysis [1] as the starting point: there are fifteen experimental data sets, with a total of ~ 1300 data points, and experimental errors are generally treated by ignoring correlations and combining statistical and systematic errors in quadrature (so Σ in eq.(3) is taken to be diagonal, with each diagonal entry set to $\sigma^2_{\text{stat}} + \sigma^2_{\text{syst}}$ of the corresponding data point). The initial pdfs are parameterised by 18 parameters $a_i, i = 1, \ldots, 18$: each theoretical prediction is then a function of these parameters. The 'best-fit' distribution (CTEQ5M1 in this case) is then given by the set of parameters a which minimise $\sum_{\text{expts}} \sum_{\text{data}} \chi^2(d|t[f(a)])$, where $t[f(a)]$ are the theoretical predictions for each data point given the pdf $f(a)$ for the fifteen base experimental data sets.

A natural way to find the limits of a physical observable which depends on the pdfs, call it $\mathcal{O}[f(a)]$, such as the W-production cross-section σ_W at $\sqrt{s} = 1.8\,\text{TeV}$, is then to study the dependence of the total χ^2 on $\mathcal{O}$. An efficient way of doing this is to use Lagrange's method

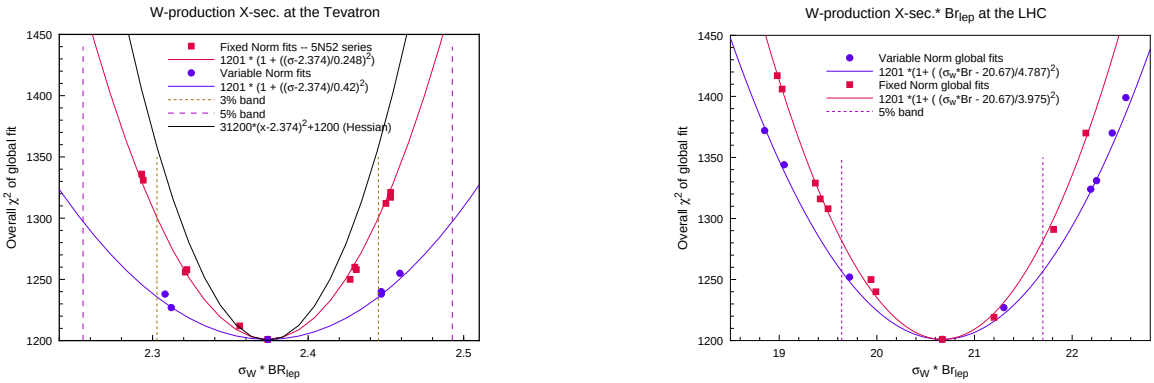

Figure 10: χ^2 of the base experimental data sets vs. the W production cross-section at the Tevatron and LHC.

of undetermined multipliers: one minimizes

$$F(\lambda) = \sum_{\text{expts}} \sum_{\text{data}} \chi^2(d|t[f(a)]) + \lambda \mathcal{O}[f(a)] \tag{4}$$

for fixed λ, and then varies λ in order to map out the χ^2 as a function of $\mathcal{O}$.

Figs. 10a,b show the χ^2 for the fifteen base experimental data sets as a function of σ_W at the Tevatron and LHC energies respectively [42]. Two curves with points corresponding to specific global fits are included in each plot[19]: one obtained with all experimental normalizations fixed; the other with these included as fitting parameters (with the appropriate experimental errors). We see that the χ^2's for the best fits corresponding to various values of the W cross-section are close to being parabolic, as expected. Indicated on the plots are 3% and 5% ranges for σ_W. The two curves for the Tevatron case are farther apart than for LHC, reflecting the fact that the W-production cross-section is more sensitive to the quark/anti-quark distributions and these are tightly constrained by existing DIS data.

The important question is: how large an increase in χ^2 should be taken to define the likely range of uncertainty in $\mathcal{O}$? The elementary statistical theorem that $\Delta\chi^2 = 1$ corresponds to one standard deviation of the measured quantity $\mathcal{O}$ relies on assuming that the errors are gaussian, uncorrelated, and with their magnitudes correctly estimated. Because these conditions do not hold here, this theorem cannot be naively applied quantitatively: rather one must examine in detail how well the fits along the parabolas shown in Fig.10 compare with the individual precision experiments included in the global analysis, in order to arrive at reasonable quantitative estimates on the uncertainty range for the W cross-section. In the meantime, based on past (admittedly subjective) experience with global fits, it seems that a χ^2 difference of $40 - 50$ points represents a 'reasonable' estimate of current uncertainty of parton distributions. This implies that the uncertainty of σ_W is about 3% at the Tevatron, and 5% at the LHC.

[19]The third line in Figs. 10a refers to an alternative technique [42] based on the assumption of Gaussian errors in the parameters a_i.

6.3 Correlated Experimental Systematics

There is now an increasing awareness of the necessity and possibility of carrying out a careful treatment of correlated systematic errors when attempting to determine errors on pdfs. For example a systematic study of the uncertainties in the parton distribution in the small x region has been made recently by experimentalists at H1 and ZEUS [62, 63]. These studies include a proper treatment of correlated systematic errors, and some attempt is made to quantify parametrization uncertainties. Similar studies of the errors in polarized parton densities have been made by the SMC [64]. Besides showing that careful estimates of parton uncertainties are useful and necessary, these studies also show that it is possible to include correlated systematics and combine data sets from different (albeit similar) experiments in a meaningful way. However they also show that doing something similar for a global parton determination would be very difficult and extremely tedious, unless new techniques are developed.

The importance of correlations in experimental systematic errors has been underlined by a recent reanalysis [65] of the F_2 BCDMS data. A more careful treatment of the correlations between data taken at different beam energies, and the correlations between the fitted parton distributions and higher twist, results in a significant increase in the value of $\alpha_s(M_Z^2)$ extracted from the data: Alekhin quotes a value of 0.118 ± 0.002. This is consistent with the current world average and the value 0.119 ± 0.002 recently extracted from the reanalysed CCFR data [66] (though after a more careful treatment of correlated higher twist [67] this rises to 0.122 ± 0.005).

In this context it should be noted that in the usual global analyses, in which correlations between systematic errors are ignored, and higher twist effects are not included, neither the BCDMS or the CCFR F_2 data show a minimum in their χ^2 as α_s is varied [2, 12], despite the fact that when treated separately each is capable of yielding an excellent determination of α_s. Only the minima in the H1 and ZEUS datasets are strong enough to survive this treatment: this may be helped by the fact that empirical higher twists are very small at small x [68]. It will be interesting to repeat the preliminary determination [69] using the 95-97 HERA datasets when these finally become available.

6.4 Methodological Issues

While the issues addressed in the previous three sections are no doubt all important, there are also some methodological issues which need to be considered if we are to achieve our aim of a reliable determination of the errors in a global determination of parton distributions. In particular, we need a technique which can give parton distribution functions and their errors, such that:

(i) there is no inbuilt methodological bias (for example dependence on a particular parametrization of the input distributions)

(ii) it is easy to propagate the effects of correlated systematic errors in the data to correlated uncertainties in the parton distributions

(iii) it is easy to add new data sets or estimate theoretical errors or test models of new

physics without redoing the whole of the analysis.

All of these criteria can be met if we 'quantise' our parton distributions: instead of trying to determine a single 'best fit' set of parameterised parton distributions with an associated error matrix, we construct an ensemble of sets of partons, distributed according to how well they fit the data [42, 70, 71, 73, 74]. The expected result for a parton dependent observable, call it $\mathcal{O}[f]$, would then be given by an ensemble average:

$$\langle \mathcal{O}[f] \rangle = \mathcal{Z}^{-1} \int [\mathcal{D}f]\, \mathcal{O}[f]\, J[f]\, s[f] \prod_{\text{expts}} P(d|t[f]), \tag{5}$$

where $\int [\mathcal{D}f]$ means functional integration over all possible input distributions f (subject to basic constraints such as sum rules and positivity) and $\mathcal{Z} = \langle 1 \rangle$ is a normalization factor. The measure of integration is given essentially by the probability distributions $P(d|t[f])$ for each of the experiments used as input. These probabilities are, as explained above, the essential input of the experimental data used in the fit: they support distributions which fit the data well, and suppress the contribution of distributions which fit badly. If the errors on the data were assumed Gaussian, these probabilities would come in the form of a χ^2, as in eq.(3), though the technique does not depend on such an assumption, and non Gaussian errors could also be incorporated. There is also a Jacobian factor $J[f]$, which turns the integration measure from an integration over theoretical predictions $t[f]$ to one over the pdfs themselves, and enforces the theoretical constraint that the theoretical predictions are related through pQCD. It is also necessary to introduce a 'smoothness' factor $s[f]$ into the measure, to enforce the natural theoretical prejudice that the initial pdfs should be smooth functions of x, without wiggles or jumps: a suitable form for such a factor would be $\exp -\frac{1}{2}\varepsilon \sum_x (\partial_x f)^2$, where ε is a small parameter which quantifies the extent of this prejudice. Final results should be independent of the form of this term, and in particular the parameter ε, provided that it is varied in a suitable range.

The way in which this procedure works should now be clear, since it is similar to the quantum mechanics (or more precisely statistical mechanics) of a particle in a (highly non-local) potential [70]: the parton distributions may be thought of as quantum fields, with, in the case of Gaussian experimental errors, the action

$$\mathcal{S}[f] = \tfrac{1}{2} \sum_{\text{expts}} \sum_{\text{data}} (d - t[f]) \Sigma^{-1} (d - t[f]) + \tfrac{1}{2} \varepsilon \sum_x (\partial_x f)^2. \tag{6}$$

The best fit parton distribution is then the solution of the classical equations of motion (since it minimises the action), while the error bands are given by the 'quantum' fluctuations around the classical field. Since the determination of the classical field is itself nontrivial, the system is best solved numerically: we discretise the field by introducing a parametrization with a finite number of parameters a_i, $i = 1, \ldots, N$, so that $\int [\mathcal{D}f]\, J[f] \to \prod_i da_i\, J(a_i)$, rather as we would for a lattice field theory. Here the best discretization would not necessarily be a naive discretization in x_{Bj} with spline interpolation: rather it might involve expansion of each pdf in sets of orthogonal polynomials, or other sets of (orthogonal) functions, for example eq.(1) and its obvious generalizations. The integration over the parameters a would then be done by Monte Carlo, using an algorithm such as Metropolis or HMC [61] to generate an ensemble

of configurations distributed according to the measure of integration, and thus according to its likelihood given the input datasets. Finding each such configuration will involve a similar computational effort to that of finding a best fit. Finally, we would like to increase the number of parameters N (taking the 'continuum limit') until we are sufficiently close to a truly parametrization independent ensemble, at which stage we can readily compute expectation values of observables and their associated errors as averages over the ensemble of pdfs.

This procedure has several advantages:

(i) it is intrinsically parametrization independent as the number of parameters increases, because of the universality of the continuum limit. Flat directions are no longer the problem that they are in a best fit procedure: the total number of parameters is now limited only by computational resources. Indeed the flat directions are now interesting, since they give the most important uncertainties in the parton distribution functions.

(ii) the propagation of correlated systematics is automatically taken care of by the procedure. The only limitation is the reliability of the probabilities $P(d|t)$ produced by experimentalists. This should give added impetus to the determination of meaningful (and thus comparable) estimates of systematic errors by different experimental collaborations, and their presentation in such a way that they can be readily input into such an analysis. Preliminary explorations of the technique [42] indicate that the errors in the pdf parameters are not only highly correlated, but also in many cases significantly non-Gaussian, even when the errors in the data are assumed to be Gaussian.

(iii) Data from new experiments can be added using the old configurations, since different experiments are (in principle!) statistically independent, so $\mathcal{S}_{\rm tot}[f] = \sum_{\rm expts} \mathcal{S}_{\rm exp}[f]$. Similarly we could estimate theoretical errors due, for example, to NLO truncation, by using the standard configurations reweighted by varying renormalization and factorization scales. Similarly, we could test the effect of resummations by reweighting the configurations generated using standard NLO evolution, or indeed test models for new physics by reweighting the configurations generated using the Standard Model [71].

The main problems to be faced in actually implementing the procedure are computational: we need a fast evolution code, and high performance computing. The advantages of parallelization should be obvious. In fact the computational requirements are very similar to those of the lattice gauge theorists: calculating the 'action' is more difficult, but the 'continuum limit' should be reached much more quickly.

7 From here to the LHC and Beyond

7.1 Progress Before the LHC Turns on

Perturbative QCD has been extremely successful in describing data in DIS, DY and jet production, as well as describing the evolution of parton distributions over a wide range of x and Q^2. From the point of view of pdf determination, the primary problem lies in the calculation of the direct photon cross sections which could serve as a primary probe of the gluon distribution at high x. However, a rigorous theoretical treatment of soft gluon effects

(perhaps requiring both k_T and Sudakov resummation) will be required before the data can be used with confidence in pdf fits. On the experimental side, it will also be necessary to resolve the inconsistency between the WA70 and E706 data.

D0 has recently presented a new result for the measurement of the inclusive jet cross section as a function of the jet rapidity (up to values of three) [72]. Such a measurement probes a greater kinematic range than the central inclusive jet cross sections. In addition, the differential dijet data from the Tevatron explore a wider kinematic range than the inclusive jet cross section. Both CDF and D0 have dijet cross section measurements from Run I which may also serve probe the high x gluon distribution, in regions where new physics is not expected but where any parton distribution shifts should be observable. The ability to perform such cross-checks is essential.

CDF and D0 will accumulate on the order of 2-4 fb^{-1} of data in Run II (from 2000-2003), a factor of 20-40 greater than the current sample. This sample should allow for more detailed information on parton distributions to be extracted from direct photon and DY data, as well as from jet production. Run III (2003-2007) offers a data sample potentially as large as 30 fb^{-1}.

H1 and ZEUS will continue the analysis of the data taken with positrons in 1991-97. HERA switched to electron running in 1998 and plans to deliver approximately 60 In 2000, the HERA machine will be upgraded for high luminosity running, with yearly rates of 150 integrated luminosity of about 1 fb^{-1} by 2005. This will allow for an error of a few percent on the structure function F_2 for Q^2 scales up to 10^4 GeV^2. The gluon density, derived from scaling violations of F_2, should be known to an accuracy of less than 3% in the kinematic range $10^{-4} < x < 10^{-1}$.

It is also hoped that over the next five years the Monte Carlo outlined in the previous section will begin to bear fruit, perhaps to the point where they can make a serious contribution to global pdf error analysis.

7.2 Physics cross sections at the LHC and the role of LHC data in pdf determination

ATLAS measurements of DY (including W and Z), direct photon, jet and top production will be extremely useful in determining pdfs relevant for the LHC. The data can be input to the global fitting programs, where it will serve to confirm/constrain the pdfs in the LHC range. Again, DY production will provide information on the quark (and anti-quark) distributions while direct photon, jet and top production will provide, in addition, information on the gluon distribution.

Other processes might also prove useful. For example diphoton production might be useful for determining the gluon distribution, and this in turn would lead to an improved knowledge of the relevant parton pdfs and parton-parton luminosity functions for the production of the Higgs (which is largely due to gg scattering for low to moderate Higgs' masses).

Another possibility that has been suggested is to directly determine parton-parton luminosities (and not the parton distributions per se) by measuring well-known processes such as W/Z production [40]. This technique would not only determine the product of parton

distributions in the relevant kinematic range but would also eliminate the difficult measurement of the proton-proton luminosity. It may be more pragmatic, though, to continue to separate out the measurements of parton pdfs (through global analyses which may contain LHC data) and of the proton-proton luminosity. The measurement of the latter quantity can be pegged to well-known cross sections, such as that of the W/Z, as has been suggested for the Tevatron.

8 Conclusions

The determination of parton distributions and uncertainties is an important ingredient of our preparations for physics at the LHC. The global fitting techniques used for the past fifteen years may soon be superseded by more sophisticated methods. Developing and exploiting these techniques will be a great challenge to theorists and experimentalists alike.

9 Acknowledgements

RDB would like to thank Sergey Alekhin, John Collins, Tony Doyle, Stefano Forte, Stefane Keller, Tony Kennedy, David Kosower, Brian Pendleton, Dave Soper, James Stirling, Wu-Ki Tung and Andreas Vogt for various stimulating and useful discussions. JH would like to thank James Stirling, Steve Mrenna and his CTEQ colleagues for useful comments. We would also like to thank James Stirling and Lenny Apanasevich for providing many of the figures. This work was supported in part by an EU TMR contract FMRX-CT98-0194 (DG 12 - MIHT) and by the NSF under grant PHY-9901946.

References

[1] H.L. Lai, J. Huston et al., *Eur. Phys. J.* **C12**, 375 (2000), `hep-ph/9903282`.

[2] A. D. Martin, R. G. Roberts, W. J. Stirling and R. Thorne, *Eur. Phys. J.* **C4**, 463 (1998), `hep-ph/9906231`.

[3] H. L. Lai, J. Huston et al., *Phys. Rev.* **D55**, 1280 (1997), `hep-ph/9606399`.

[4] See, for example, the plenary talk given by John Womersley at the XIX International Symposium on Lepton and Photon Interactions at High Energies (LP99), Stanford University, August 1999 `hep-ph/9912009`.

[5] S. Kuhlmann, W.-K. Tung and H. L. Lai, *Phys. Lett.* **409B**, 271 (1997).

[6] We would like to thank James Stirling for providing this plot; it is from his talk on LHC physics at the Feb 1998 workshop on LHC Physics Processes.

[7] J. Blumlein, S. Riemersma, M. Botje, C. Pascaud, F. Zomer, W. L. van Neerven and A. Vogt, `hep-ph/9609400`.

[8] W. J. Stirling, private communication.

[9] M. Gluck, E. Reya, A. Vogt, *Eur. Phys. J.* **C5**, 461 (1998).

[10] M.A.G. Aivazis, J.C. Collins, F.I. Olness and W.-K. Tung, *Phys. Rev.* **D50**, 3102 (1994).

[11] R.G. Roberts and R.S. Thorne, *Phys. Lett.* **B421**, 303 (1998).

[12] G. Marchesini et al., `hep-ph/9607393`.

[13] T. Sjostrand, `hep-ph/9508391`.

[14] J. Botts et al., *Phys. Lett.* **304B**, 159 (1993).

[15] CTEQ internal report (unpublished).

[16] H. L. Lai, J. Huston et al., *Phys. Rev.* **D51**, 4763 (1995).

[17] CDF Collaboration, F. Abe et al., *Phys. Rev. Lett.* **81**, 5754 (1998), `hep-ex/9809001`.

[18] A. Baldit et al., *Phys. Lett.* **332B**, 244 (1994).

[19] E. A. Hawker et al., *Phys. Rev. Lett.* **80**, 3715 (1998), `hep-ex/9803011`.

[20] W. G. Seligman et al., *Phys. Rev. Lett.* **79**, 1213 (1997).

[21] U. K. Yang, A. Bodek, *Phys. Rev. Lett.* **82**, 2467 (1999),`hep-ph/9809480`.

[22] S. Kuhlmann et al., *Phys. Lett.* **B476**, 291 (2000).

[23] M. Bonesini et al., *Z. Phys.* **C38**, 371 (1988); *ibid.* **C37**,535 (1988); *ibid.* **C37**, 39 (1988).

[24] J. Huston et al., *Phys. Rev.* **D58**, 114034 (1998), `hep-ph/9801444`.

[25] S. Catani, in these proceedings.

[26] J. Huston et al., *Phys. Rev.* **D51**, 6139 (1995), `hep-ph/9501230`.

[27] P. Aurenche et al., *Eur. Phys. J* **C9**, 107 (1999), `hep-ph/9811382`.

[28] L. Apanasevich et al., *Phys. Rev. Lett.* **81**, 2642 (1998).

[29] L. Apanasevich, J. Huston et al., *Phys. Rev.* **D59**, 074007 (1999), `hep-ph/9808467`.

[30] C. Balazs, C.-P. Yuan, *Phys. Rev.* **D56**, 5558 (1997) and references therein.

[31] E. Laenen, G. Oderda, G. Sterman, *Phys. Lett.* **438B**, 173 (1998), `hep-ph/9806467`.

[32] S. Catani, M. Mangano, P. Nason, *JHEP* **9807**, 024 (1998), `hep-ph/9806487`; S. Catani, M. Mangano, P. Nason, C. Oleari, W. Vogelsang, *JHEP* **9903**, 025 (1999).

[33] H-n. Li, *Phys. Lett.* **B454**, 328 (1999), hep-ph/9812363; H-n. Li, hep-ph/9811340.

[34] E. Laenen, G. Sterman and W. Vogelsang, hep-ph/0002078.

[35] P. Aurenche et al., *Eur. Phys. J.* **C13**, 347 (2000).

[36] L. Apanasevich et al., paper in preparation.

[37] J. Huston et al., *Phys. Rev. Lett.* **77**, 444 (1996).

[38] B. Abbott et al., *Phys. Rev. Lett.* **82**, 2451 (1999), hep-ex/9807018.

[39] F. Bedeschi, talk at 1999 Hadron Collider Physics Conference, Bombay, India, January, 1999.

[40] M. Dittmar, F. Pauss, D. Zuercher, *Phys. Rev.* **D56**, 7284 (1998); hep-ex/9705004.

[41] D.E. Soper and J.C. Collins, hep-ph/9411214.

[42] Proceedings of the Workshop on *Standard Model Physics (and more) at the LHC*, CERN 1999 (to appear). See: http://home.cern.ch/~mlm/lhc99/lhcworkshop.html

[43] Proceedings of the Workshop on *Physics at the Tevatron in Run II*, Fermilab, 2000 (to appear). See: http://www-theory.fnal.gov/people/ellis/QCDWB/QCDWB.html

[44] G. D'Agostini, hep-ph/9512295.

[45] S. Catani, *Phys. Lett.* **B427**, 161 (1998)161); S. Catani and M. Grazzini, *Phys. Lett.* **B446**, 143 (1999); J.M. Campbell and E.W.N. Glover, *Nucl. Phys.***B527**, 264 (1998); Z. Bern et al, *Phys. Lett.* **B445**, 168 (1998); *Phys. Rev.* **D60**, 116001 (1999)116001; D.A. Kosower, *Nucl. Phys.* **B552**, 319 (1999); D.A. Kosower and P. Uwer, hep-ph/9903515, V.A. Smirnov, hep-ph/9905323.

[46] J. Santiago and F.J. Yndurain, hep-ph/9904344, hep-ph/9907387; W.L. van Neerven and A. Vogt, hep-ph/9907472.

[47] A.D. Martin et al., hep-ph/9907231.

[48] S.I. Alekhin and A.L. Kataev, *Phys. Lett.* **B452**, 402 (1999).

[49] A.L. Kataev, G. Parente and A.V. Sidorov, hep-ph/9904332, hep-ph/9905310.

[50] J.C. Collins, *Phys Rev.* **D58**, 094002 (1998).

[51] H. L. Lai and W.-K. Tung, *Zeit. Phys.* **C74**, 463 (1997).

[52] M. Krämer, F.I. Olness and D.E. Soper, hep-ph/0003035.

[53] T. Jaroszewicz, *Phys. Lett.* **B116**, 291 (1982); S. Catani et al, *Phys. Lett.* **B336**, 18 (1990), *Nucl. Phys.* **B361**, 645 (1991); S. Catani and F. Hautmann, *Phys. Lett.* **B315**, 157 (1993), *Nucl. Phys.* **B427**, 475 (1994).

[54] R.D. Ball and S. Forte, *Phys. Lett.* **B351**, 313 (1995); R.K. Ellis, F. Hautmann and B.R. Webber, *Phys. Lett.* **B348**, 582 (1995).

[55] V.S. Fadin and L.N. Lipatov, *Phys. Lett.* **B429**, 127 (1998); V.S. Fadin et al, *Phys. Lett.* **B359**, 181 (1995), *Phys. Lett.* **B387**, 593 (1996), *Nucl. Phys.* **B406**, 259 (1993), *Phys. Rev.* **D50**, 5893 (1994), *Phys. Lett.* **B389**, 737 (1996), *Nucl. Phys.* **B477**, 767 (1996), *Phys. Lett.* **B415**, 97 (1997), *Phys. Lett.* **B422**, 287 (1998); G. Camici and M. Ciafaloni, *Phys. Lett.* **B412**, 396 (1997), *Phys. Lett.* **B430**, 349 (1998); V. del Duca, *Phys. Rev.* **D54**, 989 (1996), *Phys. Rev.* **D54**, 4474 (1996); V. del Duca and C.R. Schmidt, *Phys. Rev.* **D57**, 4069 (1998); Z. Bern et al, *Phys. Lett.* **B445**, 168 (1998).

[56] R.D. Ball and S. Forte, `hep-ph/9805315` J. Blümlein et al., `hep-ph/9806368`.

[57] S.J. Brodsky et al, *JETP Lett.* **70**, 155 (1999); R.S. Thorne, *Phys. Rev.* **D60**, 054031 (1999).

[58] G. Salam, *Jour. High Energy Physics* **9807**, 19 (1998); M. Ciafaloni et al, *Phys. Lett.* **B452**, 372 (1999), `hep-ph/9905566`.

[59] C.R. Schmidt, `hep-ph/9901397`; J.R. Forshaw et al `hep-ph/9903390`.

[60] R.D. Ball and S. Forte, *Phys. Lett.* **B465**, 271 (1999); G. Altarelli, R.D. Ball and S. Forte, `hep-ph/9911273`; `hep-ph/0001157`.

[61] S. Duane et al, *Phys. Lett.* **B195**, 216 (1987).

[62] See *e.g.* M. Klein, Proceedings of the Lepton-Photon Symposium (Stanford, 1999), *http://www-sldnt.slac.stanford.edu/lp99/pdf/54.pdf*

[63] M. Botje, `hep-ph/9905518`; V. Barone, C. Pascaud and F. Zomer, `hep-ph/9907512`.

[64] B. Adeva et al, *Phys. Rev.* **D58**, 112002 (1998).

[65] S.I. Alekhin, *Phys. Rev.* **D59**, 114016 (1999) and `hep-ph/9907350`.

[66] W.G. Seligman et al, *Phys. Rev. Lett.* **79**, 1213 (1997).

[67] S.I. Alekhin and A.L. Kataev, `hep-ph/9908349`.

[68] R.D. Ball and S. Forte, `hep-ph/9607291`; A.D. Martin et al, `hep-ph/9808371`.

[69] R.D. Ball and S. Forte, *Phys. Lett.* **B358**, 365 (1995).

[70] W. Bialek, C.G. Callan, S.P. Strong, *Phys. Rev Lett.* **77**, 4693 (1996); V. Periwal, *Phys. Rev.* **D59**, 094006 (1999).

[71] W.T. Giele and S. Keller *Phys. Rev.* **D58**, 094023 (1998).

[72] L. Babukhadia, Proceedings of the XXIX International Symposium on Multiparticle Dynamics (ISMD99).

[73] D. Kosower, talk given at 'Les Rencontres de Physique de la Valle d'Aoste', La Thuile, February 1999.

[74] R.D. Ball in the proceedings of the XXXIVth Rencontres de Moriond, *"QCD and Hadronic Interactions"*, Les Arcs, March 1999.

Generalized factorization and resummation

C. Balázs, J.C. Collins, D.E. Soper

Abstract

In this section we summarize the formalism which extends the usual hadronic factorization theorem to the low transverse momentum region for the inclusive production of colorless final states, while resumming logarithms with the ratio of the invariant mass and transverse momentum. Among the various recent applications the calculation of the Z^0 and Higgs boson transverse momentum distributions are highlighted.

1 The Collins-Soper-Sterman formalism

The standard factorization formula fails near kinematic boundaries. We discuss the case of low transverse momentum in Z_0 production, etc; this is an important case because the cross section peaks there. The failure of the factorization formula is symptomized by large corrections involving a factor of $\ln^2 Q/Q_T$ for each power of α_s.

Although the solutions to the problem are all commonly referred to as "resummations", there are in fact two very different approaches. One is resummation in its strict sense: One performs a selective and approximation summation of the largest parts of the perturbative series for the hard scattering in the standard factorization formalism.

The second approach is that of Collins, Soper and Sterman (CSS) [1, 2, 3]. These authors observed that the conventional factorization formalism is in fact wrong at low transverse momentum and they derive a correct factorization for this region. In an intermediate region of transverse momentum, the standard factorization with resummation is applicable with somewhat reduced accuracy, and there is an overlap between the two approaches, which we will discuss later.

In any case, it is essential to improve on the standard fixed-order factorization formalism, and the reward is an improved method that

- includes large, logarithmic QCD corrections up to all orders in the strong coupling,
- improves the renormalization scale dependence of the prediction,
- enables prediction of certain quantities reliably, which cannot be done in a fixed order calculation,
- provides an independent, analytic check for parton shower Monte Carlo's.

1.1 k_T-dependent parton densities

CSS realized that the failure of the standard factorization when $Q_T \ll Q$ occurs because it neglects the transverse motion of the incoming partons in the hard scattering. (Here Q can be the invariant mass of a colorless particle, or set of particles, created in a hard partonic collision, and Q_T is the related transverse momentum.) The approximation of neglecting parton transverse momentum is only valid when the cross section is integrated over a large range of Q_T. But if, for example, Q_T is of order 1 GeV, then we are outside of the domain in which the factorization is applicable.

A fully satisfactory approach must use a factorization theorem that is valid for any Q_T that is small compared to Q. CSS's theorem gives the cross section as a convolution of transverse momentum distributions

$$\frac{d\sigma}{d^4Q} \propto \int d^2k_T P(x_1, k_T) P(x_2, Q_T - k_T), \tag{1}$$

where P is a partonic density distribution that is a function of both longitudinal (x) and transverse (k_T) momenta. The partonic recoil against soft gluons as well as the intrinsic partonic transverse momentum are included in P.

Such a treatment completely formalizes the intuitive notion that partons must have transverse momentum and that this transverse momentum gives rise to transverse momentum of the Drell-Yan pair. There is then no need to convolute a calculated cross section with "intrinsic transverse momentum" for the quarks; this manoeuvre is only necessary as an ad hoc correction to a formalism that is incomplete.

In QCD, complications arise from soft-gluon effects, because these effects do not cancel, in contrast to the case of the cross section integrated over Q_T. A consequence, proved by CSS, is a particular form of the evolution equations for the k_T-dependent parton densities. These equations are *not* the normal DGLAP equations[1]. The kernel of the evolution contains a perturbatively calculable part and non-perturbative part. The non-perturbative part can be summarized by saying that there is a fixed amount of gluon radiation per *unit rapidity*, so that the transverse momentum distribution of the partons broadens in a characteristic way with energy. The non-perturbative part of this energy-dependent radiation is fitted by the g_2 term of Eq.(10) below.

This feature may be the dominant reason why transverse momentum distributions are so broad at high energies, as in Z^0 production: the transverse momentum of the Z^0 has a component due to the recoil against non-perturbative glue emitted into many units of rapidity.

The CSS formalism clearly entails a phenomenological fitting of the non-perturbative part of the k_T-dependent parton densities and the evolution kernel. In principle, this can be done at fairly low energy, and then the evolution equations predict the results for higher energies with no further adjustable parameters. The more conventional resummation formalism is compatible with the CSS formalism, but it is not as complete.

[1] Although all the physics associated with the DGLAP equations is present.

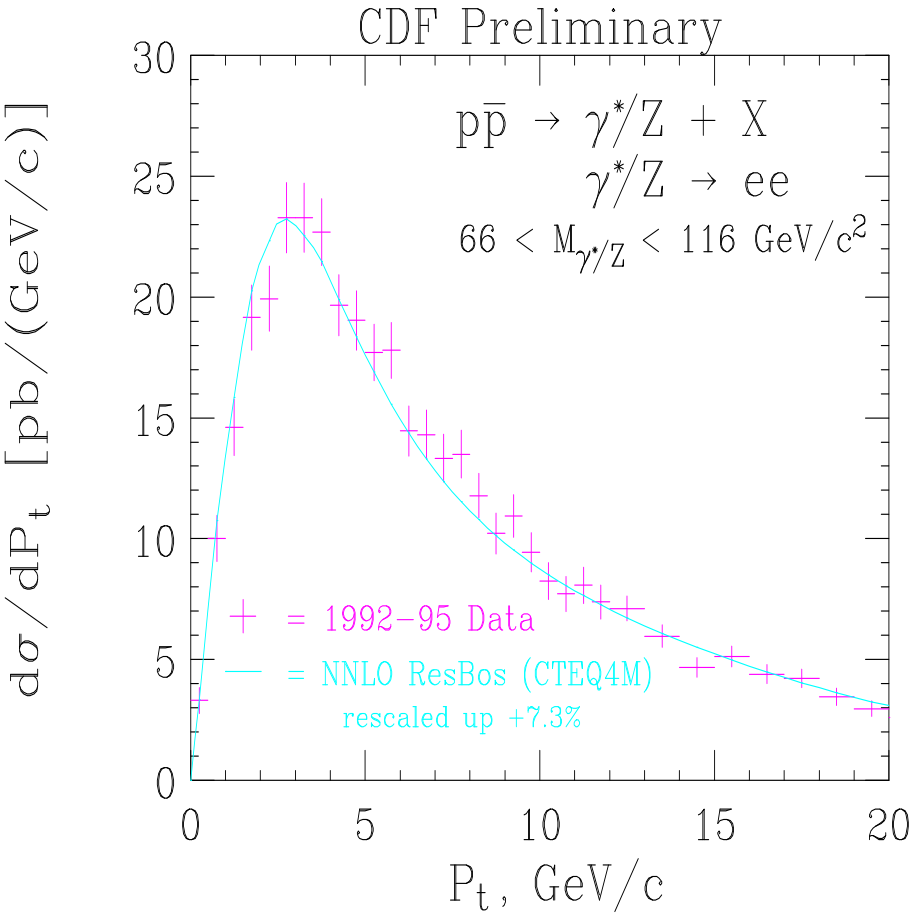

Figure 1: Transverse momentum distribution of electron-positron pairs from decays of (mostly) Z^0 bosons, produced at the Tevatron in $\sqrt{S} = 1.8$ GeV center of mass proton–anti-proton collisions. The data are CDF preliminary [4], and the curve is calculated by the ResBos Monte Carlo event generator [5, 6].

Because the CSS formalism is designed to treat correctly the $Q_T \ll Q$ region, it also provides an appropriate resummation of the large logarithms, $\ln(Q/Q_T)$ in the standard factorization formula.

We can gauge how important these logarithms are in practice by examining the cross section for Z production at the Tevatron. The bulk of the cross section is in the low Q_T region, and, as can be seen from Fig. 1, there is a peak at around $Q_T = 2.7$ GeV, which is much smaller than the invariant mass $Q = m_Z = 91.187$ GeV. This implies that for the bulk of the events $\ln(Q/Q_T)$ is large enough that $\alpha_s(m_Z)\ln^2(Q/Q_T) > 1$. Since we have a double logarithm for each radiated gluon, higher orders in the perturbative series are not suppressed.

1.2 From fixed order to resummed

In this section we show how the results of the standard factorization theorem are related to a resummation in terms of leading logarithms, etc.

When the Z^0 is produced in a hadron-hadron collision its transverse momentum is balanced by some hadronic activity which stems from partons emitted by the initial state partons. (In the first order in the strong coupling a Z^0 and a gluon is produced.) The Q_T distribution given by the usual factorization in the low Q_T region is written as

$$\lim_{Q_T\to 0}\frac{d\sigma}{dQ_T^2} = \sum_{n=1}^{\infty}\sum_{m=0}^{2n-1}\alpha_s^n\ \frac{{}_nv_m}{Q_T^2}\ \ln^m\left(\frac{Q^2}{Q_T^2}\right) + \mathcal{O}\left(\frac{1}{Q_T}\right), \tag{2}$$

where the coefficients ${}_nv_m$ are perturbatively calculable apart from some factors of parton densities. When the two scales Q and Q_T are very different, the logarithmic terms $\ln^m(Q^2/Q_T^2)$ are large, and for $Q_T \ll Q$ the perturbative series is dominated by these terms. For $Q_T \ll Q$ truncation of the perturbative series, i.e. any fixed order calculation, gives an answer which neglects these important all order logarithmic contributions. At the lowest order, $\mathcal{O}(\alpha_s^0)$, the Z^0 boson is produced alone, that is with a Q_T distribution of $\delta(Q_T)$. The singularity at $Q_T = 0$ prevails at any fixed order in α_s, as Eq. (2) shows.

One way of reorganizing the perturbation series is to make the expansion one in terms of $\alpha_s\ln^2(Q/Q_T)$ instead of α_s itself. In this simplified picture, calculating fixed order QCD corrections means calculating the perturbative series

$$\begin{aligned}\lim_{Q_T\to 0}\frac{d\sigma}{dQ_T^2} = \\ Q_T^{-2}\Big\{&\alpha_s({}_1v_1'L + {}_1v_0') + \alpha_s^2({}_2v_3'L^3 + {}_2v_2'L^2) + \alpha_s^3({}_3v_5'L^5 + {}_3v_4'L^4) + \ \ldots \\ &+ \alpha_s^2({}_2v_1'L_2 + {}_2v_0'L^0) + \alpha_s^3({}_3v_3'L^3 + {}_3v_2'L^2) + \ \ldots \\ &+ \ \ldots \qquad\qquad \ldots\Big\},\end{aligned}$$

column by column. In the leading logarithm approach, on the other hand, we calculate the above series line by line [7]. While in the fixed order (column by column) calculation the convergence for low Q_T is spoiled by the higher order uncalculated logs ($L = \ln(Q/Q_T)$), in the resummed (line by line) calculation convergence is preserved in each "order" (by each line), and higher order corrections are systematically included.

1.3 The CSS formula

The improved factorization theorem of CSS together with their evolution equation for the k_T dependent parton distributions, leads [3] to a useful formula[2] for the cross section. For Z^0 production it can be written as

$$\frac{d\sigma(h_1h_2 \to Z^0X)}{dQ^2\,dQ_T^2\,dy} = \sum_j \sigma_{0,j} W_{j\bar{j}}(Q, Q_T, x_1, x_2) \; + \; Y(Q, Q_T, x_1, x_2), \tag{3}$$

where the "resummed" part, $W(Q, Q_T, x_1, x_2)$, is defined as

$$\begin{aligned} W_{j\bar{j}}(Q, Q_T, x_1, x_2) \;\; &= \\ &\frac{1}{(2\pi)^2} \int d^2b\, e^{i\vec{Q}_T\cdot\vec{b}}\, \mathcal{C}_{j/h_1}(Q, b, x_1, \mu) e^{-\mathcal{S}(Q,b_*)} \mathcal{C}_{\bar{j}/h_2}(Q, b, x_2, \mu) \end{aligned} \tag{4}$$

for a given partonic initial state with flavor j.[3] The Fourier integral is introduced because transverse momentum conservation is explicit in the impact parameter, b, space [8].

All the dangerous logarithms are included in the perturbative Sudakov exponent

$$\mathcal{S}(Q, b_*) = \int_{C_0^2/b_*^2}^{Q^2} \frac{d\overline{\mu}^2}{\overline{\mu}^2} \left[A\left(\alpha_s(\overline{\mu})\right) \ln\left(\frac{Q^2}{\overline{\mu}^2}\right) + B\left(\alpha_s(\overline{\mu})\right) \right]. \tag{5}$$

Here C_0 is an arbitrary parameter which cuts off the perturbative low Q_T region.[4] To prevent perturbative calculations from being done in region where perturbation theory is inapplicable, the "impact parameter" b in the Sudakov exponent was replaced by

$$b_* = \frac{b}{\sqrt{1 + (b/b_{\max})^2}}. \tag{6}$$

The errors caused by this replacement are of the same form as the non-perturbative contributions to be discussed below, and are therefore correctly treated by being absorbed into the non-perturbative part of the formula.

The A and B functions are free of large logarithms and can be reliably calculated perturbatively for a given process as

$$A\left(\alpha_s(\bar{\mu})\right) = \sum_{n=1}^{\infty} \left(\frac{\alpha_s(\bar{\mu})}{\pi}\right)^n A^{(n)}, \quad B\left(\alpha_s(\bar{\mu})\right) = \sum_{n=1}^{\infty} \left(\frac{\alpha_s(\bar{\mu})}{\pi}\right)^n B^{(n)}. \tag{7}$$

[2] While solving the RGE, an integro-differential equation, specific choices of integration constants were made (c.f. Ref. [3]): $C_1 = C_3 = 2e^{-\gamma_E} \equiv C_0$ and $C_2 = C_4 = 1$, to optimize logarithmic contributions. This is similar to the $\mu = Q$ choice in case of the ultraviolet renormalization, to make terms like $\ln(\mu/Q)$ vanish.

[3] The lowest order partonic total cross section is $\sigma_{0,j} = \pi^2 g^2((1 - 4Q_j s_w^2)^2 - 1)/(48Q^2 c_w^2)$, where g is the weak coupling constant, s_w^2 (c_w^2) is the sine (cosine) of the weak mixing angle squared, and Q_j is the charge of the quark flavor j.

[4] In practice $C_0 = 2e^{-\gamma_E}$ is used, which is related to the values of the integration constants of the RGE for the k_T dependent PDF's.

The distributions

$$\mathcal{C}_{j/h}(Q,b,x,\mu) = \sum_a \int_x^1 \frac{d\xi}{\xi} C_{ja}\left(b_*, \frac{x}{\xi}, \mu\right) f_{a/h}(\xi,\mu)\, \mathcal{F}_{a/h}(b,x)\, e^{-r(b)\ln Q} \tag{8}$$

depend on virtual and real emission contributions for a given process, via the Wilson coefficients C_{ja}. Just as the A and B functions the Wilson coefficients are expanded in terms of the strong coupling α_s

$$C_{ij}\left(b_*, z, \mu\right) = \sum_{n=0}^{\infty} \left(\frac{\alpha_s(\mu)}{\pi}\right)^n C_{ij}^{(n)}\left(z, b_*\right). \tag{9}$$

Since the Sudakov exponent integrates to unity, the C_{ij} function sets the normalization of the resummed distribution. In particular, if coefficients up to $C_{ij}^{(n)}$ are included in the calculation then the resummed rate will equal the rate calculated in fixed order at $\mathcal{O}(\alpha_s^n)$ [5]. The function $f_{a/h}(x,\mu)$ is the usual renormalized momentum fraction (x) distribution of parton a in hadron h at the energy scale μ. Observe that the impact parameter dependence of the perturbative coefficient functions is cut off by the use of b_* instead of b.

Included in Eq. (8) are two non-perturbative factors, $\mathcal{F}_{a/h}(b,x)$ and $e^{-r(b)\ln Q}$. These implement the parts of the CSS factorization and evolution equation that cannot be implemented as a resummation of the standard factorization theorem. They also compensate for the errors in the resummation at large b. The overall effect is that (8) define k_T-dependent parton densities. The $\mathcal{F}$ factor can be interpreted as allowing for intrinsic transverse momentum, and the $e^{-r(b)\ln Q}$ factor allows for the recoil against soft gluon radiation. The $\ln Q$ in the exponent of the soft-gluon factor comes from the solution of the CSS evolution equation and can be interpreted by saying that soft gluons are emitted uniformly in rapidity.

The perturbative part of the formula uses b_* instead of b, as defined by Eq. (6). The parameter $b_{\max}$ provides an infra-red cutoff on the perturbative part of the formula. In practice the empirically optimal value, $b_{\max} = 1/2\ \mathrm{GeV}^{-1}$, is used. This arbitrary cutoff of the b integration is compensated by the parameterization of the non-perturbative part of the formula, which is

$$\begin{aligned} W_{ij}^{\mathrm{NP}}(Q,b,x_1,x_2) &= \mathcal{F}_{i/h_1}(Q,b,x_1)\mathcal{F}_{j/h_2}(Q,b,x_2)e^{-r(b)\ln Q} \\ &= \exp\left[-g_1 b^2 - g_2 b^2 \ln\left(\frac{Q}{2Q_0}\right) - g_1 g_3 b \ln\left(100 x_1 x_2\right)\right], \end{aligned} \tag{10}$$

where Q_0 is chosen to be the initial scale of the parton evolution[5] and the g_i parameters have to be determined using experimental data.[6]

1.4 Matching

The resummed term, defined by Eq. (4), was derived in the context of a generalized factorization, under the assumption that $Q_T \ll Q$. This assumption will break down within

[5]For recent CTEQ PDF's $Q_0 = 1.6$ GeV.

[6]The $\ln\left(Q^2/Q_0^2\right)$ term is introduced to match the logarithmic term of the Sudakov exponent and its coefficient is expected to be process independent, depending only on the initial partonic state.

and beyond the intermediate $Q_T \lesssim Q$ region. In the high Q_T region (where $Q_T \gtrsim Q$) the conventional perturbative factorization formalism is reliable. To obtain sufficiently accurate results for all Q_T, it is necessary to combine the formalisms.

The Y term in Eq. (3) was introduced by CSS [2] to correct the behavior of the resummed piece in the intermediate and high Q_T regions.[7] It is defined as the difference of the cross section calculated from the standard factorization formula at a fixed order n of perturbation theory and the $Q_T \ll Q$ asymptote of this cross section:

$$Y(Q, Q_T, x_1, x_2) = \left(\frac{d\sigma}{dQ^2\, dQ_T^2 dy}\right)_n - \left(\frac{d\sigma}{dQ^2\, dQ_T^2 dy}\right)_{n, Q_T \ll Q}. \tag{11}$$

Thus, the full CSS formula can be written as

$$\frac{d\sigma}{dQ^2\, dQ_T^2 dy} = \left(\frac{d\sigma}{dQ^2\, dQ_T^2 dy}\right)_{\rm res} + \left(\frac{d\sigma}{dQ^2\, dQ_T^2 dy}\right)_n - \left(\frac{d\sigma}{dQ^2\, dQ_T^2 dy}\right)_{n, Q_T \ll Q}. \tag{12}$$

This method of matching the resummed and fixed order pieces is valid because the low Q_T asymptote used in Eq. (11) is the same as the large Q_T asymptote of the resummed term W. At low Q_T the asymptotic part dominates the Q_T distribution (the logs are large), and the last two terms cancel in Eq.(12), while the resummed term is significant near $Q_T = 0$. At high Q_T the logs are small, and the expansion of the resummed term cancels the Q_T singular terms up to higher orders in α_s.[8] In this situation the first and third terms cancel and CSS formula reduces to the fixed order perturbative result. After matching the resummed and fixed order cross sections in such a "smooth" manner, it is expected that the normalization of the CSS cross section reproduces the fixed order total rate, since when expanded and integrated over Q_T it deviates from the fixed order result only in small higher order terms in α_s [5].

Unfortunately the above argument does not completely work in practice. The problem arises because at large Q_T the W term in Eq. (3) is an extrapolation of the cross section from small Q_T. So it has a $1/Q_T^2$ behavior, modified by logarithms. This falls less steeply than the true cross section, which is subject to kinematic limits. The errors in the CSS formula at large Q_T are indeed suppressed by a power of α_s. But the coefficient of this power is the $1/Q_T^2$ part of the formula, and so the error can be easily larger than the true cross section. A symptom of the problem is that the cross section calculated from Eq. (3) is typically negative at large enough Q_T.

One possible remedy [9] is to abandon the CSS formalism. But we regard this as undesirable, because it also abandons the important physical result of CSS that goes beyond mere resummation: their proper treatment of non-perturbative transverse momentum.

A second, commonly used remedy, is to utilize the fact that in the high Q_T region the fixed order result is a good description of the distribution. So when calculating the Q_T distribution one can simply switch from the CSS to the fixed order distribution whenever they cross for high Q_T's. Since the mismatch between the resummed and the asymptotic

[7] The exact definition of the Y piece for Z^0 production can be found in Refs. [3, 5].

[8] The cancellation is higher order than the order at which the singular pieces were calculated.

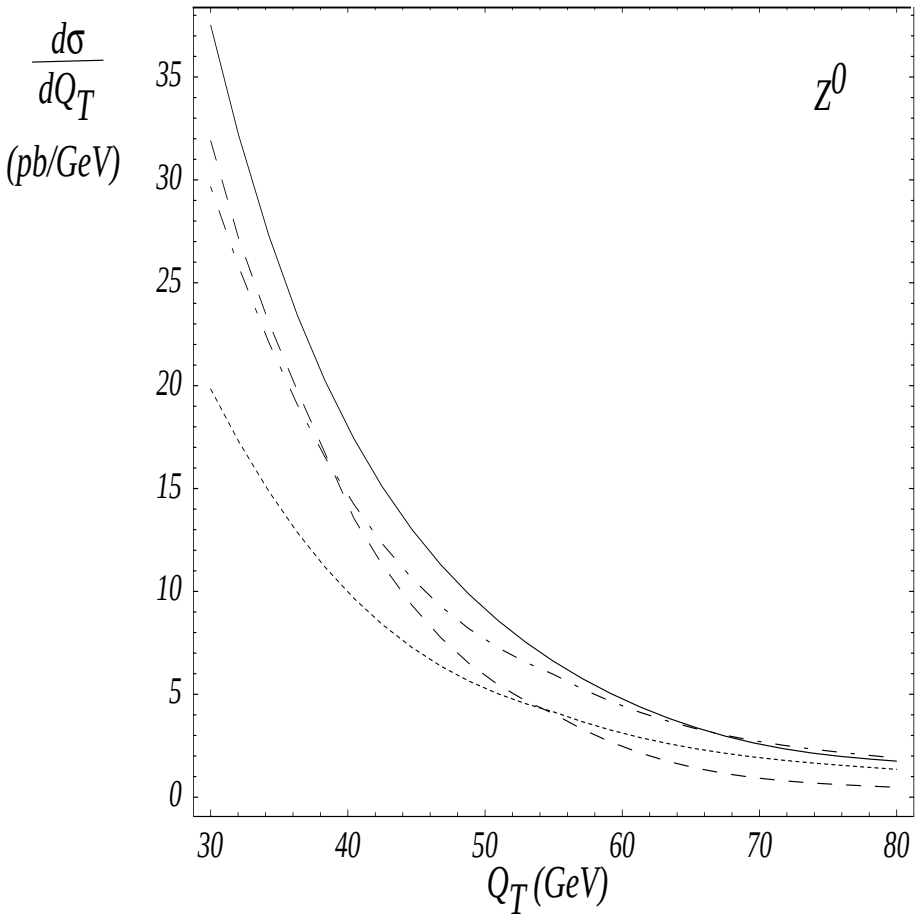

Figure 2: Transverse momentum distributions calculated using the CSS (solid and dashed) and the usual factorization (dot-dashed and dotted) formalisms. The CSS calculation is not switched over to the usual formalism to show the typical "kink" which occurs at a switching point. The solid and dot-dashed curves are calculated at $\mathcal{O}(\alpha_s^2)$, while the dashed and dotted curves are at $\mathcal{O}(\alpha_s)$, illustrating the improvement of the high Q_T behavior of the CSS formula with the perturbative order.

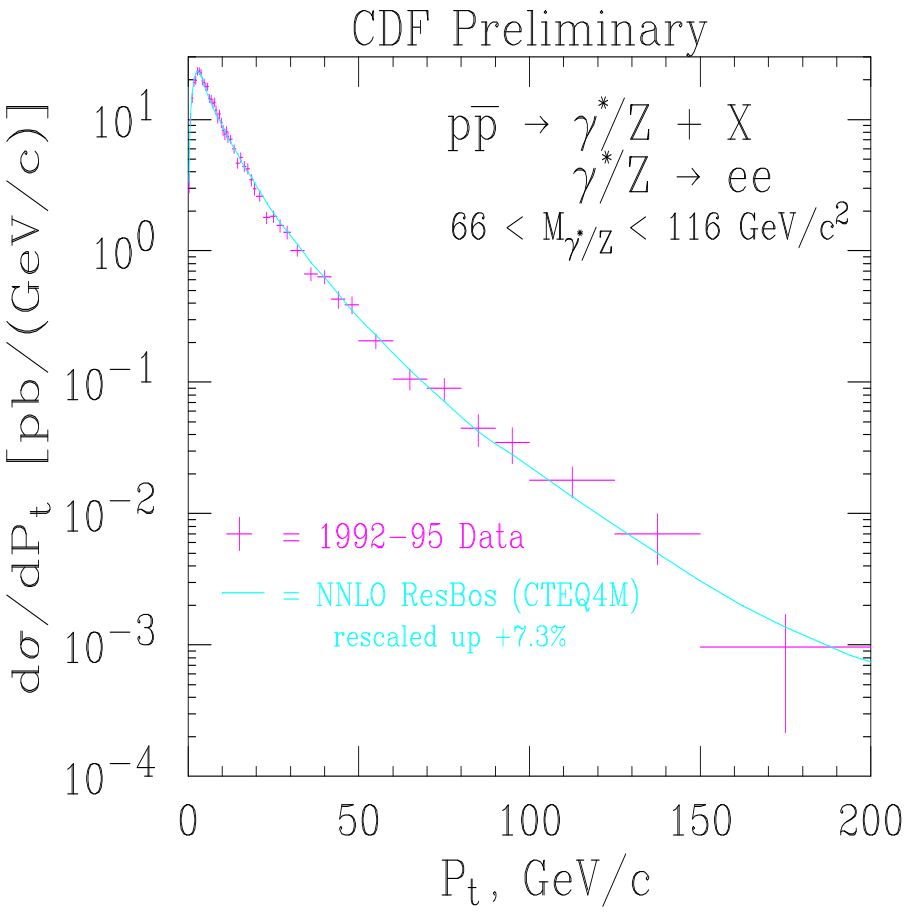

Figure 3: Same as Fig. 1, except shown for the full range of transverse momentum Q_T. Switching from the CSS to the usual factorization formalism in the $60 \lesssim Q_T \lesssim 70$ GeV region (c.f. [5]), results in a smooth Q_T distribution which agrees well with the experiment in the full Q_T range.

terms in Eq.(12) decreases as the perturbative order of the calculation (n) increases, it is expected that the crossing point shifts toward $Q_T = Q$, and the slope of the resummed and fixed order curves approaches each other as n increases (cf. Ref. [5]). Indeed, calculations at $\mathcal{O}(\alpha_s^2)$ blend closer to m_Z, and smoother than at $\mathcal{O}(\alpha_s)$, as shown in Fig. 2.

When this prescription for the switching is followed at the fully differential, $d\sigma/dQ_T dQ dy$, level the result is a smooth and differentiable Q_T distribution, after the invariant mass and rapidity is integrated out. This is illustrated in Fig. 27. It was shown in Ref. [5] that the integral of the Q_T distribution calculated using this prescription recovers the fixed order total rate within an error which is the size of the higher orders, as it is expected.

1.5 Improved matching

Since the calculations of W and Y are done using truncations of perturbation theory, the switching between calculational methods introduces an artificial discontinuity in the slope of the cross section. This practical problem arises in the matching because of a mismatch of the orders of perturbation theory at which W and Y are calculated. From the point of view of a standard factorization calculation, W contains a selective summation of arbitrarily high orders of perturbation theory. The possibility of getting such a resummation relies on performing certain approximations that are only valid at small Q_T. The difficulty of performing complete higher-order calculation means that Y can only be calculated at fixed order.

At large transverse momentum, $|W|$ is much larger than the actual cross section, and so the cross section Eq. (12) is obtained by the cancellation of two almost equal terms. This is clearly a recipe for bad numerical work.

Examination of the lowest-order calculation of Y, for the $q\bar{q}$ annihilation term [2] shows some of the sources of the problems:

$$
\begin{aligned}
Y \;=\; & \frac{C}{Q_T^2}\int \frac{d\xi_1}{\xi_1}\frac{d\xi_2}{\xi_2} f_q(\xi_1) f_{\bar{q}}(\xi_2) \\
& \left\{ \frac{(Q^2-\hat{t})^2+(Q^2-\hat{u})^2}{\hat{s}}\delta(\hat{s}+\hat{t}+\hat{u}-Q^2) \right. \\
& -2\delta(1-x_1/\xi_1)\delta(1-x_2/\xi_2)\left[\ln(Q^2/Q_T^2)-\frac{3}{2}\right] \\
& \left. -\delta(1-x_1/\xi_1)\left[\frac{1+x_2^2/\xi_2^2}{1-x_2/\xi_2}\right]_+ - \left[\frac{1+x_1^2/\xi_1^2}{1-x_1/\xi_1}\right]_+ \delta(1-x_2/\xi_2)\right\}.
\end{aligned}
\tag{13}
$$

Here x_1 and x_2 are the longitudinal momentum fractions of the Drell-Yan pair. The first term contains the usual perturbative calculation of the differential cross section, and the other 3 terms give the negative of its low Q_T asymptote. The intrinsic rate of fall off of the cross section with Q_T is given by the explicit $1/Q_T^2$ factor which is present in the parton cross section. But an extra fall off is caused by the fact that the parton densities are probed at larger fractional momenta when Q_T is increased.

Some symptoms of the problems can already be seen. One is that the first subtraction term, on the second line of Eq. (13), changes sign at large Q_T: the extrapolation of a positive

cross section becomes negative. The second is the plus distribution in the third line; if the parton distributions are steeply falling, the plus distributions give a misleading size for the integrand. This last effect really indicates that there is an additional scale in the process, so that the relevant scales are:

- The transverse momentum Q_T of the Drell-Yan pair.
- The invariant mass Q of the pair.
- The increase ΔQ of Q that is necessary to make the typical parton densities in the factorization formula decrease by a factor 2.

We believe the overall approach of a subtraction method is correct: W correctly represents the physics at low Q_T, and we do not wish to give up a method that uses the intuitive notion of k_T-dependent parton densities. We therefore cannot expect to obtain a perfect estimate of the large Q_T cross section from W alone. The idea of adding a correction term Y is a good way of combining the information in standard fixed order calculations with the resummed calculations.

But improvements in its implementation are needed. We suggest the following strategies that could be tried, individually or even in combination:

- Multiply W by an ad hoc factor $F(Q_T/M)$. Correspondingly the formula for the subtraction term in Y will also have the same factor. The parameter M is in principle arbitrary, and it should be chosen so that the fall off in the modified W term mimics that of the actual cross section. The cut-off function obeys $F(0) = 1$, so that the small Q_T behavior is unchanged, and the function should be zero for large Q_T.
- Change the argument of W from Q_T to some other function of Q_T. One possible choice would be $Q'_T = Q_T/(1 - Q_T/M)$, where M is again a parameter to be chosen. One would replace W by zero if $Q_T > M$. The effect of the variable change is to leave W unaltered at small Q_T and to give a more rapid fall off at large Q_T. Again one would make an identical redefinition in the subtraction term in Y.
- Redefine the + distributions such as those in Eq. (13), by:

$$\int_0^1 dz f(z) \left[\frac{1}{z}\right]_{+,z_0} = \int_0^1 dz \frac{1}{z} \left[f(z) - f(0)\theta(z_0 - z)\right]. \tag{14}$$

  (The usual definition has $z_0 = 1$.)

In each case we have a generalized renormalization-group invariance of the exact cross section under changes of the parameter M or z_0. But approximations obtained by truncation of a perturbation series are invariant only up to a term of order the first uncalculated correction. The aim is to choose the parameters on physical grounds to be such as to keep these higher order terms small, to eliminate their reason(s) for being large.

1.6 Applications

Beyond Z^0 production, in its present form, the CSS formalism can be applied in hadron-hadron collisions whenever the final state is colorless. The phenomenological significance of this "transverse momentum resummation" ranges from Drell-Yan pair production, through lepton pair production via $W^{\pm}$ and Z^0 bosons [5], di-gauge boson (e.g. photon or Z^0 boson pair) production [10, 11], to Higgs production [12, 13, 14]. In recent years it was tested in hadronic processes taking place at fixed target (e.g. in DY photon and diphoton production) [15] and collider energies (e.g. in DY, $W^{\pm}$, Z^0, and diphoton production). It was applied for different hadronic initial states in pion–nucleon, proton–nucleon, and proton–anti-proton collisions. It was also modified and tested for DIS processes [16]. Finally, since was first devised for the calculation of the energy correlation of jets in e^+e^- collisions [1], it can be used in jet production at lepton colliders. Such a wide variety of applicability, and good agreement with existing experimental results for different processes, colliders, center of mass energies, and initial states gives us a confidence in the resummed predictions for the LHC.

2 Higgs production

At the LHC the SM Higgs boson will be mainly produced through the gluon fusion subprocess via a top quark loop: gg (top quark loop) $\rightarrow HX$ [17]. The Higgs boson can be detected in its $H \rightarrow \gamma\gamma$ decay mode, if its mass is in the 100-150 GeV range [18]. If the Higgs mass is higher than about 130 GeV then its $H \rightarrow Z^0 Z^{0*}$ decay mode is the cleanest and most significant [18]. To distinguish these signals from the substantial QCD background, besides the sharp peak in the invariant mass distribution, the most straightforward measurable to use is the transverse momentum. According to earlier studies, a statistical significance on the order of 5-10 can be reached for the inclusive $H \rightarrow \gamma\gamma$ signal, actual values depending on luminosity and background estimates. Once their transverse momentum distribution is reliably predicted, the difference in the Q_T of the signal and background can be utilized to devise kinematic cuts to enhance the statistical significance of the signal. After the discovery, when determining the properties of the Higgs boson, besides the total cross section and the invariant mass distribution, the simplest and most fundamental measurable to use is the transverse momentum. For a recently proposed new detection mode, $H \rightarrow \gamma\gamma$jet, in Ref. [19] it was also found that in order to optimize the significance it is necessary to impose a 30 GeV cut on the transverse momentum of the jet, or equivalently (at NLO precision), on the Q_T of the photon pair. With this cut in place extraction of the signal in the Higgs plus jet mode requires the precise knowledge of both the signal and background distributions in the mid- to high-Q_T region.

To reliably predict the Q_T distribution of Higgs bosons at the LHC, especially in the low to mid Q_T region where the bulk of the rate is, the effects of the multiple soft–gluon emission have to be included. In practice, performing soft gluon resummation within the CSS formalism is equivalent to the determination of the $A^{(n)}$, $B^{(n)}$, and $C^{(n)}$ coefficients and the Y part at some order in α_s. One way to calculate the coefficients is to expand the resummed part in terms of the strong coupling (expanding the exponent an the Wilson

coefficients), and compare the expansion with a fixed order calculation. Luckily, because of its significance, there was much work done on fixed order QCD corrections to Higgs production in the $gg \to HX$ channel. These fixed order QCD corrections are known to substantially increase the rate: by about 70 to 100 percent, depending on the Higgs mass, at $\mathcal{O}(\alpha_s^3)$[20, 21], and by an additional 50 to 70 percent at $\mathcal{O}(\alpha_s^4)$ [22]. It is expected that the calculation of even higher order corrections is important to reliably predict the cross section. In Ref. [23] it was shown that multiple soft–gluon emission dominates the higher order corrections.

2.1 Soft gluon resummation for the $gg \to HX$ channel

Resummed calculations, taking into account the soft–gluon effect, attempted to estimate the size of the non-calculated higher order corrections [23], as well as provide a reliable shape of the Higgs transverse momentum distribution [12, 13]. Our present approach surpasses these by calculating the Q_T distribution while including $\mathcal{O}(\alpha_s^4)$ terms in the Sudakov exponent, using the state of the art matching to the latest fixed order distributions, using a QCD improved gluon-Higgs effective coupling [24], and using an improved non-perturbative function. We utilize the approximation that the object which couples the gluons to the Higgs (the top quark in the SM), is much heavier than the Higgs itself. This approximation is not essential to our calculation and can be released by the calculation of the further Wilson coefficients keeping the relevant masses. The heavy quark approximation in the SM was shown to be reliable within 5 percent for $m_H < 2m_t$ [22, 20, 25], and still reasonable even in the range of $m_H \gtrsim 2m_t$ [23]. It has also been shown that the approximation remains valid for the Q_T distribution in the large Q_T region, provided that $m_H < m_t$ and $Q_T < m_t$ [26]. In this work we assume that the approximation is valid in the whole Q_T region. Unlike the authors of Ref. [23] we do not assume that the QCD corrections to the $gg \to HX$ cross section can be factorized into a multiplicative term in the heavy quark limit in all orders of α_s. We can release this approximation because the CSS formalism, by definition, systematically incorporates higher order fixed order corrections via the definition of the Sudakov exponent and the Wilson coefficients as perturbative expansions [5, 6].

Multiple soft–gluon emission affects the $gg \to HX$ cross section when the transverse momentum of the Higgs is low, while for high transverse momenta the hard gluon radiation is dominant. Thus, using the CSS formalism we resum large logs of the type $\ln(Q/Q_T)$ in the low Q_T region, and we match the resummed result to the fixed order calculation which is valid for high Q_T [5]. We also include the qg and $q\bar{q}$ subprocesses which, depending on the Higgs mass, together constitute 0 to 10 percent of the total rate [20].

The resummed differential cross section of the Higgs boson production in hadronic collisions is written as

$$\frac{d\sigma(h_1 h_2 \to H^0 X)}{dQ^2\, dy\, dQ_T^2} = \sigma_0 \frac{Q^2}{S} \pi\delta(Q^2 - m_H^2)$$
$$\times \left\{ \frac{1}{(2\pi)^2} \int d^2b\, e^{i\vec{Q}_T\cdot\vec{b}} \widetilde{W}_{gg}(b_*, Q, x_1, x_2, C_{1,2,3}) \right.$$

$$\times \widetilde{W}_{gg}^{\rm NP}(b,Q,x_1,x_2) + Y(Q_T,Q,x_1,x_2,C_4)\Big\}\,. \tag{15}$$

The kinematic variables Q, y, and Q_T are the invariant mass, rapidity, and transverse momentum of the Higgs boson in the laboratory frame. The parton momentum fractions are defined as $x_1 = e^y Q/\sqrt{S}$, and $x_2 = e^{-y} Q/\sqrt{S}$, with $\sqrt{S}$ being the center–of–mass (CM) energy of the hadrons h_1 and h_2. The lowest order cross section, with the QCD corrected effective coupling of the Higgs boson to gluons is

$$\sigma_0 = \kappa_\phi(Q) \frac{\sqrt{2} G_F \alpha_s^2(Q^2)}{576\pi}, \tag{16}$$

where G_F is the Fermi constant and κ_ϕ is defined in Ref. [23]. The renormalization group invariant kernel of the Fourier integral $\widetilde{W}_{gg}$ and the regular terms $Y(Q_T, Q, x_1, x_2, C_4)$ (together with the variables b_* and C_1 to C_4) are defined in Ref. [13]. In addition to Ref. [13] we use the process independent coefficient

$$A^{(2)} = C_A \left[\left(\frac{67}{36} - \frac{\pi^2}{12} \right) N_C - \frac{5}{18} N_f \right], \tag{17}$$

in the expansion of the A function ($N_C = 3$ the number of colors and $N_f = 5$ the number of active quark flavors).

2.2 Some numerical results

The resummation formula is coded in the ResBos Monte Carlo event generator [5, 6], which uses the following electroweak input parameters [27]: $G_F = 1.16639 \times 10^{-5}$ GeV^{-2}, $\mathrm{m_Z} = 91.187$ GeV, $\mathrm{m_W} = 80.36$ GeV. The NLO expressions for the running electromagnetic and strong couplings $\alpha(\mu)$ and $\alpha_S(\mu)$ are used, as well as the NLO parton distribution function set CTEQ4M (defined in the modified minimal subtraction, $\overline{MS}$, scheme). The renormalization and factorization scales are set equal to the Higgs invariant mass. In the choice of the non-perturbative parameters we follow Ref. [28]. Since we are not concerned with the decays of Higgs bosons in this work, we do not impose any kinematic cuts.

Fig. 4 displays production cross sections at the LHC, calculated in the SM as the function of the Higgs mass. Our $\mathcal{O}(\alpha_s^3)$ curve agrees well with the result in Ref. [23]. The ratio of the fixed order $\mathcal{O}(\alpha_s^3)$ (dashed) and the lowest order $\mathcal{O}(\alpha_s^2)$ (dotted) curves varies between 2.35 and 2.00. We note that less than 2 percent of the $\mathcal{O}(\alpha_s^3)$ corrections come from the qg and $q\bar{q}$ initial states for Higgs masses below 200 GeV. The resummed curve is slightly (5 to 6 percent) higher than the $\mathcal{O}(\alpha_s^3)$ one, as expected based on the findings that the CSS formalism preserves the fixed order rate within the error of the matching (which is expected to be higher order) [5]. The resummed rate is close to the $\mathcal{O}(\alpha_s^3)$, because we used the $\mathcal{O}(\alpha_s^3)$ fixed order results to derive the Wilson coefficients which are utilized in our calculation. In Ref. [22] the $\mathcal{O}(\alpha_s^4)$ corrections were utilized to show that in the high Q_T region the $\mathcal{O}(\alpha_s^4)$ to $\mathcal{O}(\alpha_s^3)$ K-factor is nearly constant and is about 1.5 (for CTEQ4M parton distributions). Based on this finding we also plot the $\mathcal{O}(\alpha_s^3)$ curve rescaled by 1.5, to illustrate the size of

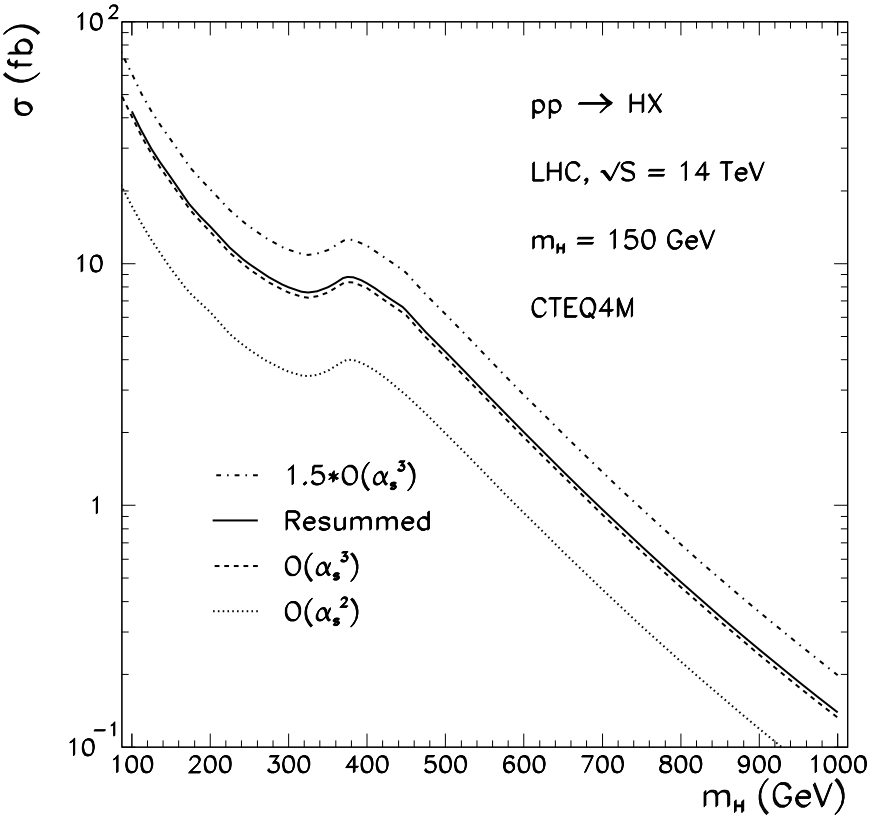

Figure 4: SM Higgs boson production cross sections at the LHC via top quark loop as the function of the Higgs mass, with QCD corrections calculated by soft–gluon resummation (solid), at fixed order $\mathcal{O}(\alpha_s^3)$ (dashed), and without QCD corrections at $\mathcal{O}(\alpha_s^2)$ (dotted). The $\mathcal{O}(\alpha_s^3)$ curve is scaled by 1.5 (dash-dotted, c.f. Ref. [22]) to estimate the $\mathcal{O}(\alpha_s^4)$ result.

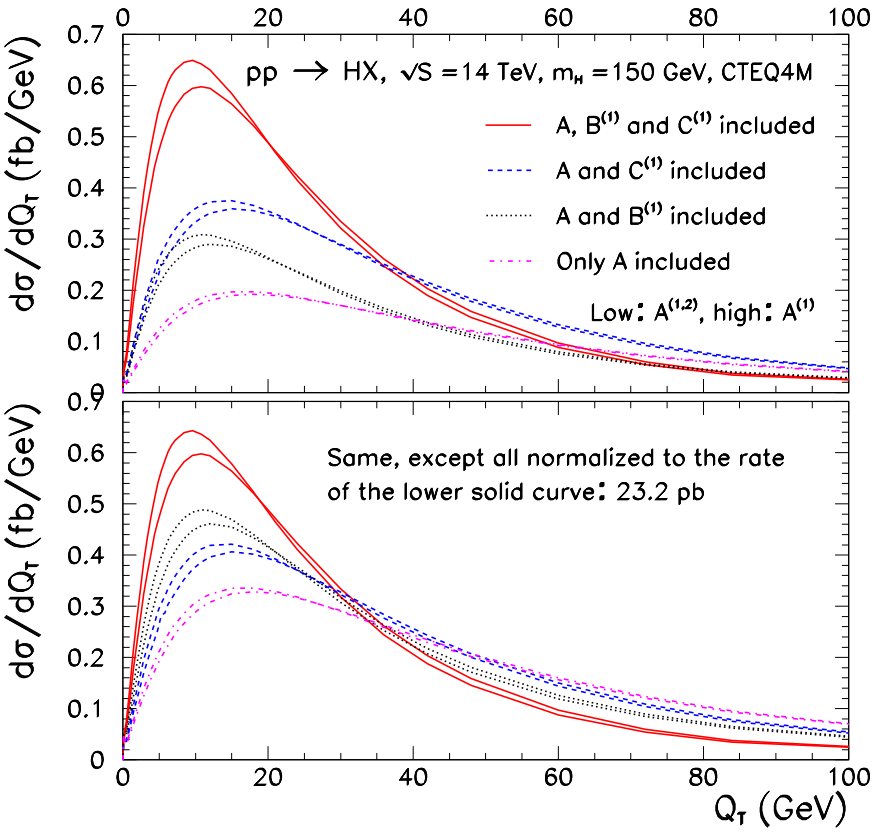

Figure 5: Higgs boson transverse momentum distributions at the LHC, illustrating the effect of various contributions of the CSS formalism. Among the pair of curves the ones which peak lower are calculated by using $A^{(1,2)}$ and the others by $A^{(1)}$. Additionally, the solid curves include $B^{(1)}$ and $C^{(1)}$, the dashed ones $C^{(1)}$, and the dotted ones $B^{(1)}$. The dot-dashed curves only include A coefficients. The lower portion of the figure shows the same curves normalized to the area under the lower peaking solid curve, to compare the changes in the shape.

the $\mathcal{O}(\alpha_s^4)$ corrections and to establish the normalization of our resummed calculation among the fixed order results.

Fig. 5 illustrates the effect of the various contributions of the CSS formalism on the Higgs boson transverse momentum distribution. The lower peaking curves, drawn by the same type line, contain the coefficients $A^{(1,2)}$. The others lack the $A^{(2)}$ coefficient. Comparison of pairs of curves shows that the log multiplied by the $A^{(2)}$ coefficient increases the rate by about 10% around the peak, and decreases it in the mid-Q_T region. The figure also shows that exclusion of the $B^{(1)}$ term leads to about 40% decrease around the peak, and an increase away from it. Finally, the exclusion of the $C^{(1)}$ coefficient decreases the overall rate by about a factor of 2, coupled with some shape change similar to the $B^{(1)}$ case.

Fig. 6 displays transverse momentum distributions of Higgs bosons produced at the LHC. The Q_T distribution is calculated under several different assumptions for the non-perturbative sector of the CSS formalism, in order to span the range of scatter of these different predictions. In Fig. 6a the (solid) curve using the result of the latest 3-parameter fit for the non-perturbative function [28] is shown. (The actual values of the parameters used are: $g_1 = 0.15$ GeV^2, $g_2 = (C_F/C_A) * 0.48$ GeV^2, and $g_3 = -0.58$ GeV^{-1}.) Also shown the (dashed) curve using the result of the latest 3-parameter fit of Ref. [28]. (The values were used are: $g_1 = 0.24$ GeV^2, and $g_2 = (C_F/C_A) * 0.34$ GeV^2.) We plotted the (dotted) curve using the previous 3-parameter fit of Ref. [29], as well. In the lower portion of the figure we show the ratios of the different curves to the solid curve. From this we conclude that the three different parameterizations differ by about 5 percent, at most, in the relevant Q_T region. At $Q_T = 10$ GeV, in the region of the peak of the distribution, the difference is about 2 percent.

In Fig. 6b the solid curve is the same as in Fig. 6a. In this figure results using $g_2 = (C_F/C_A) * 0.33$ GeV^2, and $g_2 = (C_F/C_A) * 0.69$ GeV^2 values are plotted (dashed). These g_2 values are 3 σ deviations from the central value $g_2 = (C_F/C_A) * 0.48$ GeV^2 of the new 3-parameter fit. Also shown a curve with $g_2 = 0.48$ GeV^2, where the assumption that the non-perturbative parameter g_2 scales by C_A/C_F for the gluonic initial state was not utilized. The lower portion of the figure shows that the ratios of the various curves to the solid curve do not deviate from 1 significantly except in the very low Q_T (< 5 GeV) region.

Acknowledgments

We thank the organizers of the les Houches workshop for their hospitality. We are indebted for the CTEQ Collaboration for many invaluable discussions and W. Sakumoto for the CDF results. C.B. thanks M. Spira, and C.-P. Yuan for discussions. This work was supported in part by the DOE under grant DE-FG-03-94ER40833.

References

[1] J.C. Collins and D.E. Soper, Phys. Rev. Lett. **48**, 655 (1982); Nucl. Phys. **B193**, 381 (1981), **B213**, 545(E) (1983).

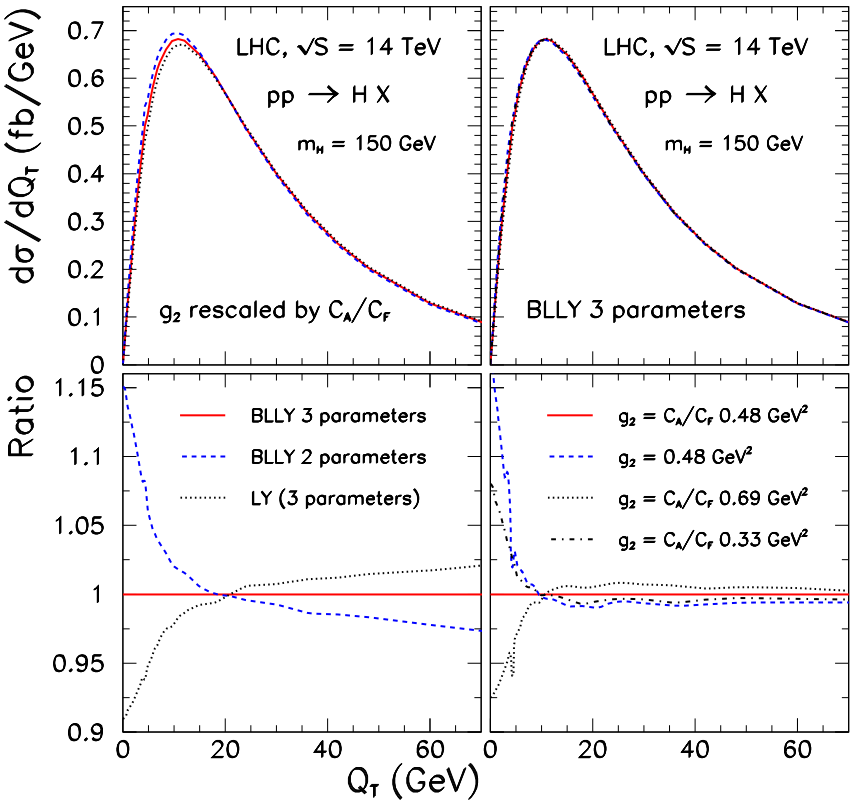

Figure 6: Higgs boson transverse momentum distributions at the LHC, displaying uncertainties arising from the non-perturbative sector of the CSS formalism. a) The solid curve is calculated using the latest 3-parameter fit of the non-perturbative function [28]. The dashed curve uses the new 2-parameter fit [28], and the dotted curve the previous 3-parameter fit [29]. The lower portion shows the ratio of the dashed and the dotted curves to the solid one. b) The solid curve uses the nominal result of the new 3-parameter fit, and the dashed ones are calculated with g_2 parameters deviating by 3 σ from the central value. Also shown in dotted the curve which does not re-scale the g_2 parameter by C_A/C_F. The lower plot shows the ratios with respect to the solid line.

[2] J.C. Collins and D.E. Soper, Nucl. Phys. **B197**, 446 (1982);

[3] J.C. Collins, D.E. Soper and G. Sterman, Nucl. Phys. **B250**, 199 (1985).

[4] The e^+e^- transverse momentum distribution plot is taken from the web-page of the CDF Electroweak Group: http://www-cdf.fnal.gov/physics/ewk/ptz.html

[5] C. Balázs and C.P. Yuan, Phys. Rev. **D56**, 5558 (1997) hep-ph/9704258.

[6] C. Balázs, PhD thesis, Michigan State University (1999) hep-ph/9906422.

[7] P.B. Arnold and R.P. Kauffman, Nucl. Phys. **B349**, 381 (1991).

[8] G. Parisi and R. Petronzio, Nucl. Phys. **B154**, 427 (1979).

[9] R.K. Ellis and S. Veseli, Nucl. Phys. **B511**, 649 (1998) hep-ph/9706526.

[10] C. Balázs, E.L. Berger, S. Mrenna and C.P. Yuan, Phys. Rev. **D57**, 6934 (1998) hep-ph/9712471.

[11] C. Balázs and C.P. Yuan, Phys. Rev. **D59**, 114007 (1999) hep-ph/9810319.

[12] I. Hinchliffe and S.F. Novaes, Phys. Rev. **D38**, 3475 (1988).
R.P. Kauffman, Phys. Rev. **D44**, 1415 (1991); Phys. Rev. **D45**, 1512 (1992);
C. Kao, Phys. Lett. **B328**, 420 (1994) hep-ph/9310206.

[13] C.P. Yuan, Phys. Lett. **B283**, 395 (1992).

[14] C. Balázs and C.P. Yuan, in preparation.

[15] M. Begel, Ph.D thesis, University of Rochester (1999).

[16] P. Nadolsky, D.R. Stump and C.P. Yuan, hep-ph/9906280.

[17] M. Spira, hep-ph/9711394.

[18] ATLAS Collaboration, Technical Proposal,
CERN/LHC/94-43 LHCC/P2 (1994);
CMS Collaboration, Technical Proposal,
CERN/LHC/94-43 LHCC/P1 (1994);
ATLAS Collaboration, Calorimeter Performance,
CERN/LHC/96-40 (1996);
CMS Collaboration, Technical Design Report,
CERN/LHCC/97-33 (1997).

[19] S. Abdullin, M. Dubinin, V. Ilyin, D. Kovalenko, V. Savrin, N. Stepanov, Phys. Lett. **B431**, 410 (1998).

[20] D. Graudenz, M. Spira and P.M. Zerwas, *Phys. Rev. Lett.* **70**, 1372 (1993);

M. Spira, A. Djouadi, D. Graudenz and P.M. Zerwas, *Phys. Lett.* **B 318**, 347 (1993); *Nucl. Phys.* **B 453**, 17 (1995).

[21] A. Djouadi, M. Spira and P.M. Zerwas, *Phys. Lett.* **B 264**, 440 (1991);

S. Dawson, *Nucl. Phys.* **B 359**, 283 (1991);

R.P. Kauffman and W. Schaffer, Phys. Rev. **D49**, 551 (1995);

S. Dawson and R.P. Kauffman, Phys. Rev. **D47**, 1264 (1994).

[22] D. de Florian, M. Grazzini and Z. Kunszt, Phys. Rev. Lett. **82**, 5209 (1999) hep-ph/9902483.

[23] M. Kramer, E. Laenen and M. Spira, Nucl. Phys. **B511**, 523 (1998) hep-ph/9611272.

[24] B.A. Kniehl and M. Spira, Z. Phys. **C69**, 77 (1995) hep-ph/9505225.

[25] Z. Kunszt, S. Moretti and W.J. Stirling, Z. Phys. **C74**, 479 (1997) hep-ph/9611397.

[26] U. Baur and E.W. Glover, Nucl. Phys. **B339**, 38 (1990).

[27] Particle Data Group (C. Caso *et al.*), *The European Physical Journal* **C 3**, 1 (1998).

[28] F. Landry, R. Brock, G. Ladinsky and C.P. Yuan, hep-ph/9905391.

[29] G.A. Ladinsky and C.P. Yuan, Phys. Rev. **D50**, 4239 (1994) hep-ph/9311341.

A Comparison of the Predictions from Monte Carlo Programs and Transverse Momentum Resummation

C. Balázs, J. Huston, I. Puljak

Abstract

Monte Carlo event generators are being increasingly relied upon for predictions of experimental observables at colliders. In this section, the parton shower formalism for Monte Carlos is compared to that of analytic resummation calculations. Predictions for the transverse momentum distribution of Z^0 bosons, photon pairs, and the Higgs boson are compared for the Tevatron and the LHC. [1]

1 Introduction

Parton shower Monte Carlo programs such as `PYTHIA`[2], `HERWIG`[3] and `ISAJET`[4] are commonly used by experimentalists, both as a way of comparing experimental data to theoretical predictions, and also as a means of simulating experimental signatures in kinematic regimes for which there is not yet experimental data (such as the LHC). The final output of the Monte Carlo programs consists of the 4-vectors of a set of final state hadrons; this output can either be compared to reconstructed experimental quantities or, when coupled with a simulation of a detector response, can be directly compared to raw data taken by the experiment, and/or passed through the same reconstruction procedures as the raw data. In this way, the parton shower programs can be more useful to experimentalists than analytic calculations. Indeed, almost all of the physics plots in the ATLAS physics TDR [5] involve comparisons to `PYTHIA` (version 5.7).

For many physical quantities, the predictions from parton shower Monte Carlo programs should be nearly as precise as those from analytic theoretical calculations. This is expected, among others, for calculations which resum logs with the transverse momentum of partons initiating the hard scattering. In the recent literature, most calculations of this kind are either based on or originate from the formalism developed by J. Collins, D. Soper, and G. Sterman (CSS) [2], which we choose as the analytic 'benchmark' of this section. In this case, both the Monte Carlo and analytic calculations should accurately describe the effects of the emission of multiple soft gluons from the incoming partons, an all orders problem in QCD. The initial state soft gluon emission can affect the kinematics of the final state partons. This

[1] A more complete treatment of this subject can be found in Ref. [1].

[2] See, for example, the discussion in the previous section.

may have an impact on the signatures of physics processes at both the trigger and analysis levels and thus it is important to understand the reliability of such predictions. The best method for testing the reliability is the direct comparison of the predictions to experimental data. If no experimental data is available for certain predictions, then some understanding of the reliability may be gained from the comparison of the predictions from the two different methods.

2 Parton Showering and Resummation

For technical reasons, the initial state parton shower proceeds by a *backwards* evolution, starting at the large (negative) Q^2 scale of the hard scatter and then considering emissions at lower and lower (negative) virtualities, corresponding to earlier points on the cascade (and earlier points in time), until a scale corresponding to the factorization scale is reached. The transverse momentum of the initial state is built up from the whole series of splittings (and boosts). The showering process is independent of the hard scattering process being considered (as long as one does not introduce any matrix element corrections), and depends only on the initial state partons and the hard scale of the process.

In the case of parton showering, the leading order collinear singularities factorize for cross sections in the collinear limit

$$\lim_{p_g \to p_b} |\mathcal{M}_{n+1}|^2 = g_s^2 (p_b.p_g)^{-1} P_{g \leftarrow a}(z) |\mathcal{M}_n|^2, \tag{1}$$

where $\mathcal{M}_{n+1}$ is the invariant amplitude for the process producing n partons and a gluon, g_s is the strong coupling constant, p_b and p_g are the 4-momenta of the daughters of the n'th parton a (i.e. a splits into b and g, and when they are collinear then $p_b.p_g \to 0$). Finally $P_{g \leftarrow a}(z)$ is the DGLAP splitting kernel belonging to the $a \to g$ splitting. The leading order collinear singularities can be factorized into a Sudakov form factor: $S = 1 - P(no\ emission) = exp(-\int dp^2/p^2 \int dz P(z))$. The distribution $1-S$ can be used to generate the Q^2 for the first emission and hence for the whole cascade. The formalism can be extended to soft singularities as well by using angular ordering. In this approach, the choice of the hard scattering is based on the use of evolved parton distributions, which means that the inclusive effects of initial-state radiation are already included. What remains is therefore to construct the exclusive showers.

Parton showering resums primarily the leading logs, which are universal, i.e. process independent, and depend only on the given initial state. In this lies one of the strengths of Monte Carlos, since parton showering can be incorporated into a wide variety of physical processes. An analytic calculation, in comparison, can resum all logs. For example, the CSS formalism sums all of the logarithms with Q^2/p_T^2 in their arguments, where (for Higgs boson production) Q is the four momentum of the Higgs and p_T is its transverse momentum. As discussed in the previous section on resummation, all of the 'dangerous logs' are included in the Sudakov exponent, which can be written in the impact parameter (b) space as:

$$\mathcal{S}(p,b) = \int_{1/b^2}^{Q^2} \frac{d\overline{\mu}^2}{\overline{\mu}^2} \left[A\left(\alpha_s(\overline{\mu})\right) \ln\left(\frac{Q^2}{\overline{\mu}^2}\right) + B\left(\alpha_s(\overline{\mu})\right) \right],$$

with the A and B functions being free of large logs and perturbatively calculable:

$$A\left(\alpha_s(\bar{\mu})\right) = \sum_{n=1}^{\infty} \left(\frac{\alpha_s(\bar{\mu})}{\pi}\right)^n A^{(n)}, \quad B\left(\alpha_s(\bar{\mu})\right) = \sum_{n=1}^{\infty} \left(\frac{\alpha_s(\bar{\mu})}{\pi}\right)^n B^{(n)}.$$

These functions contain an infinite number of coefficients, with the $A^{(n)}$ coefficients being universal while the $B^{(n)}$ are process dependent. In practice, the number of towers of logarithms included in the Sudakov exponent depends on the level to which a fixed order calculation was performed for a given process. For example, if only a next-to-leading order calculation is available, only the coefficients $A^{(1)}$ and $B^{(1)}$ can be included. If a NNLO calculation is available, then $A^{(2)}$ and $B^{(2)}$ can be extracted and incorporated into a resummation calculation, and so on. This is the case, for example, for Z^0 boson production. So far, only the $A^{(1)}$, $A^{(2)}$ and $B^{(1)}$ coefficients are known for Higgs production but the calculation of $B^{(2)}$ is in progress. [6] If we try to interpret parton showering in the same language, which is admittedly risky, then we can say that the Monte Carlo Sudakov exponent always contains a term analogous to $A^{(1)}$. It was shown in Reference [7] that a suitable modification of the Altarelli-Parisi splitting function, or equivalently the strong coupling constant α_s, also effectively approximates the $A^{(2)}$ coefficient. [3]

In contrast with the shower Monte Carlos, analytic resummation calculations integrate over the kinematics of the soft gluon emision, with the result that they are limited in their predictive power for inclusive final states. While the Monte Carlo maintains an exact treatment of the branching kinematics, in the original CSS formalism no kinematic penalty is paid for the emission of the soft gluons, although an approximate treatment of this can be incorporated into its numerical implementations, like ResBos [8]. Neither the parton showering process nor the analytic resummation translate smoothly into kinematic configurations where one hard parton is emitted (at large p_T). In the Monte Carlo matrix element corrections, and in the analytic resummation calculation matching is necessary. This matching is standard procedure for resummation calculations and matrix element corrections are becoming increasingly common in Monte Carlos [9, 10].

With the appropriate input from higher order cross sections, a resummation calculation has the corresponding higher order normalization and scale dependence. The normalization and scale dependence for the Monte Carlo, though, remains that of a leading order calculation. The parton showering process redistributes the event particles in phase space, but does not change the total cross section (for example, for the production of a Higgs boson). [4]

In particular, one quantity which should be well-described by both calculations is the transverse momentum (p_T) of the final state electroweak boson in a subprocess such as $q\overline{q} \to WX$, ZX or $gg \to HX$, where most of the p_T is provided by initial state parton showering. The parton showering supplies the same sort of transverse kick as the soft gluon radiation in a resummation calculation. Indeed, very similar Sudakov form factors appear in both approaches, with the caveats about the $A^{(n)}$ and $B^{(n)}$ terms mentioned previously.

[3] This is rigorously true only for the high x or $\sqrt{\tau}$ region.

[4] Technically, one could add the branching for $q \to q$+Higgs in the shower, which would have the capability of increasing somewhat the Higgs cross section; however, the main contribution to the higher order K-factor comes from the virtual corrections and the 'Higgs Bremsstrahlung' contribution is neglible.

This correspondence between the Sudakov form factors in resummation and Monte Carlo approaches may seem trivial, but there are many subtleties between the two approaches relating to both the arguments of the Sudakov factors as well as the impact of subleading logs [11].

At a point in its evolution corresponding to (typically) the virtuality of a few GeV^2, the parton shower is cut off and the effects of gluon emission at softer scales must be parameterized and inserted by hand. This is similar to the (somewhat arbitrary) division between perturbative and non-perturbative regions in a resummation calculation. The parameterization is typically done with a Gaussian formalism similar to that used for the non-perturbative k_T in a resummation program. In general, the value for the non-perturbative $\langle k_T \rangle$ needed in a Monte Carlo program will depend on the particular kinematics being investigated. In the case of the resummation calculation the non-perturbative physics is determined from fits to fixed target data and then automatically evolved to the kinematic regime of interest.

A value for the average non-perturbative k_T of greater than 1 GeV does not imply that there is an anomalous intrinsic k_T associated with the parton size; rather this amount of $\langle k_T \rangle$ needs to be supplied to provide what is missing in the truncated parton shower. If the shower is cut off at a higher virtuality, more of the 'non-perturbative' k_T will be needed.

3 Z^0 Boson Production at the Tevatron

The 4-vector of a Z^0 boson, and thus its transverse momentum, can be measured with great precision in the e^+e^- decay mode. Resolution effects are relatively minor and are easily corrected. Thus, the Z^0 p_T distribution is a great testing ground for both the resummation and Monte Carlo formalisms for soft gluon emission. The (resolution corrected) p_T distribution for Z^0 bosons (in the low p_T region) for the CDF experiment[5] is shown in Figure 1, compared to both the resummed prediction from ResBos, and to two predictions from `PYTHIA` (version 6.125). One `PYTHIA` prediction uses the default (rms)[6] value of intrinsic k_T of 0.44 GeV and the second a value of 2.15 GeV (per incoming parton). [7] The latter value was found to give the best agreement for `PYTHIA` with the data.[8]. All of the predictions use the CTEQ4M parton distributions [12]. The shift between the two `PYTHIA` predictions at low p_T is clearly evident. As might have been expected, the high p_T region (above 10 GeV) is unaffected by the value of the non-perturbative k_T. Note that much of the k_T 'given' to the incoming partons at their lowest virtuality, Q_0, is reduced at the hard scatter due to the number of gluon branchings preceding the collision. The emitted gluons carry off a sizeable fraction of the original non-perturbative k_T. This point will be investigated in more detail later for the case of Higgs production.

[5] We thank Willis Sakumoto for providing the figures for CDF Z^0 production

[6] For a Gaussian distribution, $k_T^{rms} = 1.13\langle k_T \rangle$.

[7] A previous publication [9] indicated the need for a substantially larger non-perturbative $\langle k_T \rangle$, of the order of 4 GeV for the case of W production at the Tevatron. The data used in the comparison, however, were not corrected for resolution smearing, a fairly large effect for the case of $W \to e\nu$ production and decay.

[8] A similar conclusion has been reached for comparisons of the CDF Z^0 p_T data with `HERWIG` [13]

As an exercise, one can transform the resummation formula in order to bring it to a form where the non-perturbative function acts as a Gaussian type smearing term. Using the Ladinsky-Yuan parameterization [14] of the non-perturbative function in ResBos leads to an rms value for the effective k_T smearing parameter, for Z^0 production at the Tevatron, of 2.5 GeV. This is similar to that needed for `PYTHIA` and `HERWIG` to describe the Z^0 production data at the Tevatron.

In Figure 1, the normalization of the resummed prediction has been rescaled upwards by 8.4%. The `PYTHIA` prediction was rescaled by a factor of 1.3-1.4 (remember that this is only a leading order comparison) for the shape comparison.

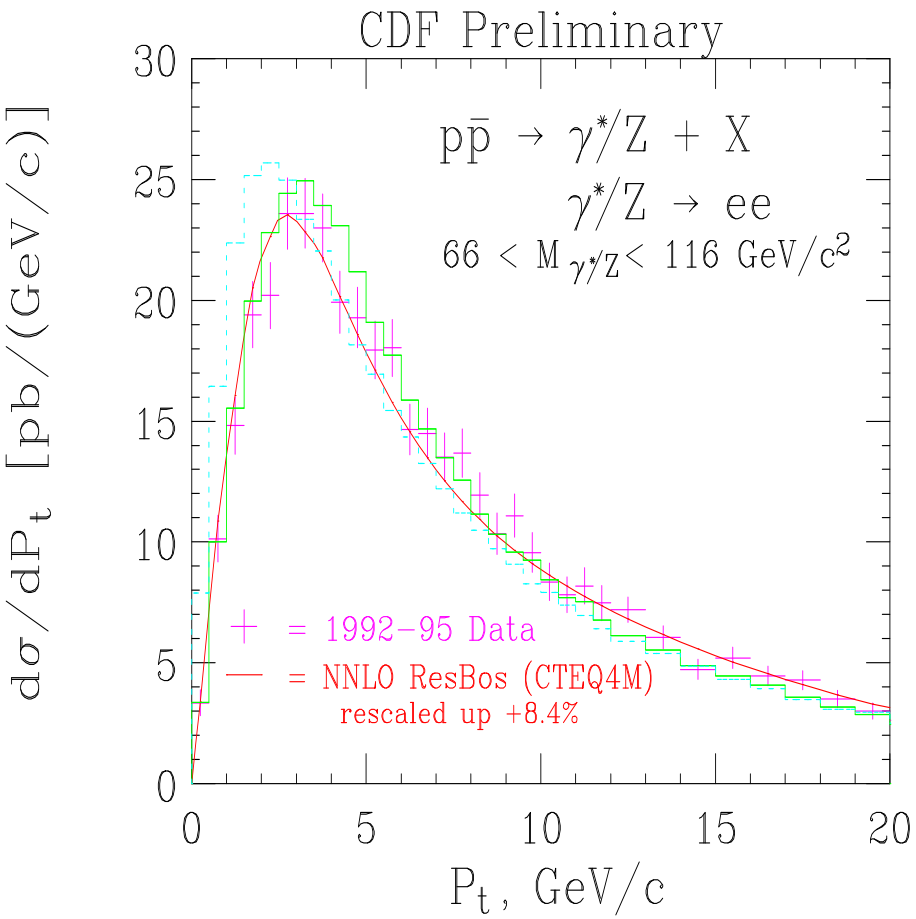

Figure 1: The Z^0 p_T distribution (at low p_T) from CDF for Run 1 compared to predictions from ResBos and from `PYTHIA`. The two `PYTHIA` predictions use the default (rms) value for the non-perturbative k_T (0.44 GeV) and the value that gives the best agreement with the shape of the data (2.15 GeV).

As stated previously, the resummed prediction correctly describes the shape of the Z^0 p_T distribution at low p_T, even with the optimal non-perturbative k_T, although there is still

a noticeable difference in shape between the Monte Carlo and the resummed prediction. It is interesting to note that if the process dependent coefficients ($B^{(1)}$ and $B^{(2)}$) were not incorporated into the resummation prediction, the result would be an increase in the height of the peak and a decrease in the rate between 10 and 20 GeV, leading to a better agreement with the PYTHIA prediction [15].

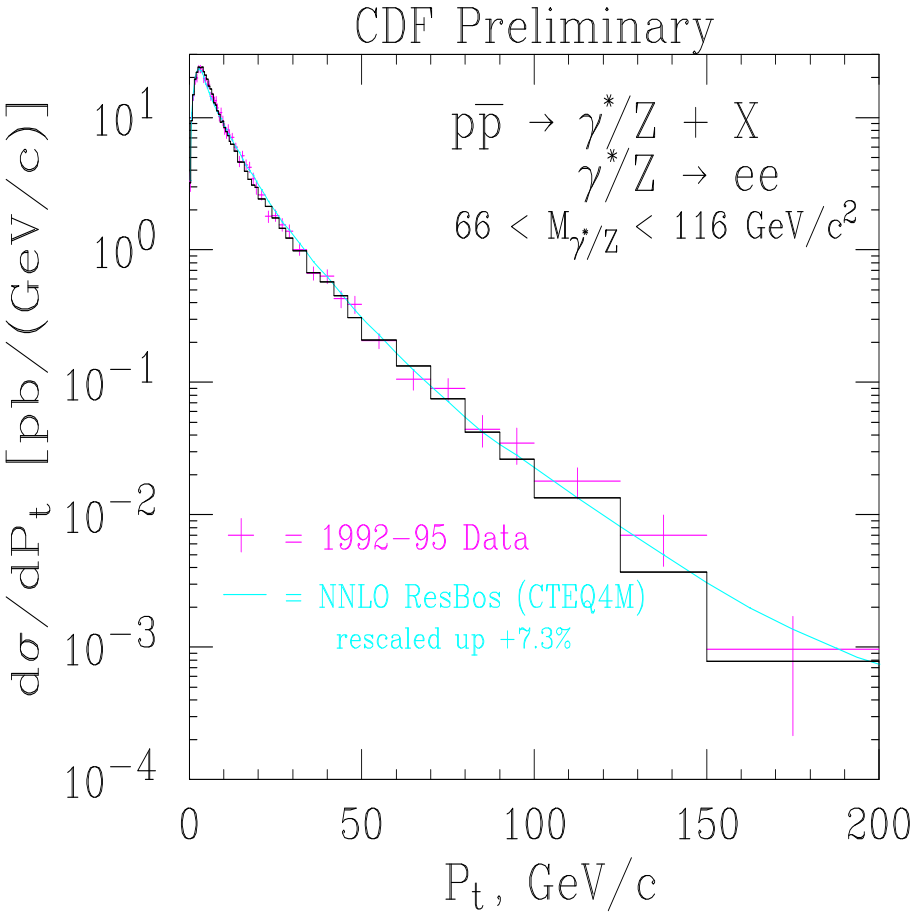

Figure 2: The Z^0 p_T distribution (for the full range of p_T) from CDF for Run 1 compared to predictions from ResBos (curve) and from PYTHIA (histogram).

The Z^0 p_T distribution is shown over a wide p_T range in Figure 2. The PYTHIA and ResBos predictions both describe the data well. Note especially the agreement of PYTHIA with the data at high p_T, made possible by explict matrix element corrections (from the subprocesses $q\overline{q} \rightarrow Z^0 g$ and $gq \rightarrow Z^0 q$) to the Z^0 production process.[9]

[9]Slightly different techniques are used for the matrix element corrections by PYTHIA [9] and by HERWIG [10]. In PYTHIA, the parton shower probability distribution is applied over the whole phase space and the exact matrix element corrections are applied only to the branching closest to the hard scatter. In HERWIG, the corrections are generated separately for the regions of phase space unpopulated by HERWIG (the 'dead zone')

4 Diphoton Production

Most of the experience that we have for comparisons of data to resummation calculations/Monte Carlos deals with Drell-Yan production, i.e. $q\overline{q}$ initial states. It is important then to examine diphoton production at the Tevatron, where a large fraction of the contribution at low mass is due to gg scattering. The prediction for the diphoton k_T distribution at the Tevatron, from `PYTHIA` (version 6.122), is shown in Figure 3, using the experimental cuts applied in the CDF analysis [16]. It is interesting to note that about half of the diphoton cross section at the Tevatron is due to the gg subprocess, and that the diphoton p_T distribution is noticeably broader for the gg subprocess than the $q\overline{q}$ subprocess.

A comparison of the p_T distributions for the two diphoton subprocesses ($q\overline{q}, gg$) in `PYTHIA` versions 5.7 and 6.1 is shown in Figure 4. There seems to be little difference in the p_T distributions between the two versions for both subprocesses.

In Figure 5 are shown the ResBos predictions for diphoton production at the Tevatron from $q\overline{q}$ and gg scattering compared to the `PYTHIA` predictions (using the same experimental cuts). The gg subprocess predictions in ResBos agree well with those from `PYTHIA` while the $q\overline{q}$ p_T distribution is noticebly broader in ResBos. The latter behavior is due to the presence of the Y piece in ResBos at moderate p_T, and the matching of the $q\overline{q}$ cross section to the fixed order $q\overline{q} \rightarrow \gamma\gamma g$ at high p_T. The corresponding matrix element correction is not in `PYTHIA`. It is interesting to note that the `PYTHIA` and ResBos predictions for $gg \rightarrow \gamma\gamma$ agree in the moderate p_T region, even though the ResBos prediction has the Y piece present and is matched to the matrix element piece $gg \rightarrow \gamma\gamma g$ at high p_T, while there is no such matrix element correction for `PYTHIA`. This shows the smallness of the Y piece for the gg subprocess, which is the same conclusion that was reached in Ref. [17]. One way to understand this is recalling that the gg parton-parton luminosity falls very steeply with increasing partonic center of mass energy, $\sqrt{\hat{s}}$. This falloff tends to suppress the size of the Y piece since the production of the diphoton pair at higher p_T requires larger x_1, x_2 values. In the default CSS formalism, there is no such kinematic penalty in the resummed piece since the soft gluon radiation comes for "free". (Larger x_1 and x_2 values are not required.)

A comparison of the CDF diphoton data to NLO [18] and resummed (ResBos) QCD predictions is shown in Figure 6. Plotted are the diphoton mass, the angle $\Delta\phi$ between the two photons and the transverse momentum k_T of the diphoton pair. The transverse momentum distribution, in particular, is sensitive to the effects of the soft gluon radiation and better agreement can be observed with the ResBos prediction than with the NLO one. The data shown in this figure is from an integrated luminosity of 87 pb^{-1}. A much more precise comparison with the effects of soft gluon radiation will be possible with the 2 fb^{-1} or greater data sample that is expected for both CDF and D0 in Run 2.

The prediction for the diphoton production cross section, as a function of the diphoton p_T and using cuts appropriate to ATLAS and CMS, is shown in Figure 7. Note that, as at the Tevatron, about half of the cross section is due to gg scattering and the diphoton p_T

and the populated region. In the dead zone, the radiation is generated according to a distribution using the first order matrix element calculation, while the algorithm for the already populated region applies matrix element corrections whenever a branching is capable of being 'the hardest so far'.

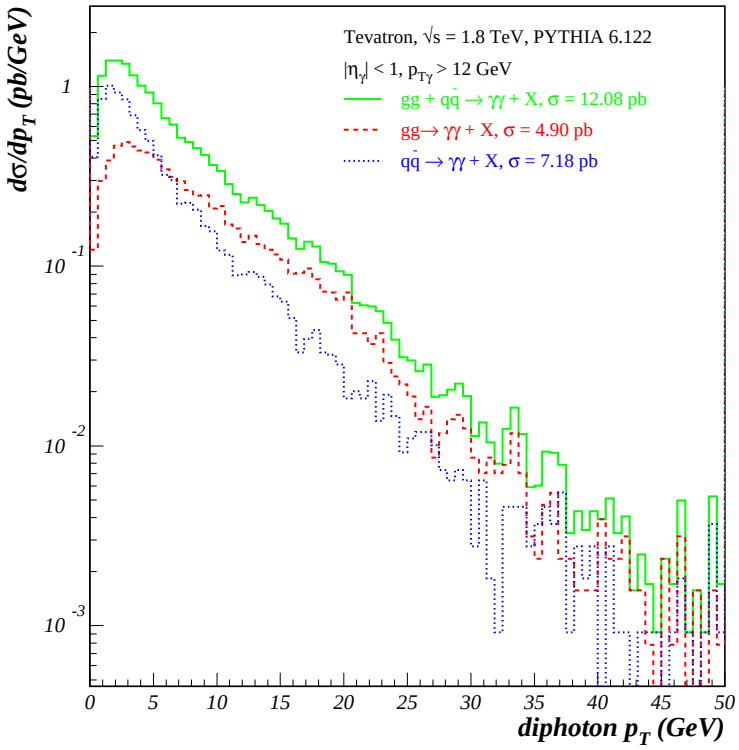

Figure 3: A comparison of the PYTHIA predictions for diphoton production at the Tevatron for the two different subprocesses, $q\overline{q}$ and gg. The same cuts are applied to PYTHIA as in the CDF diphoton analysis.

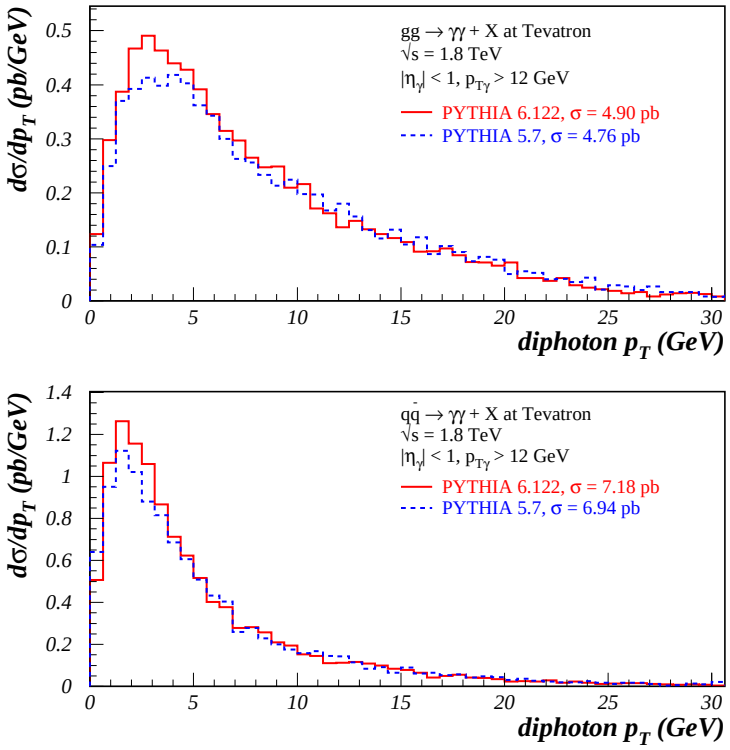

Figure 4: A comparison of the PYTHIA predictions for diphoton production at the Tevatron for the two different subprocesses, $q\overline{q}$ and gg, for two recent versions of PYTHIA. The same cuts are applied to PYTHIA as in the CDF diphoton analysis.

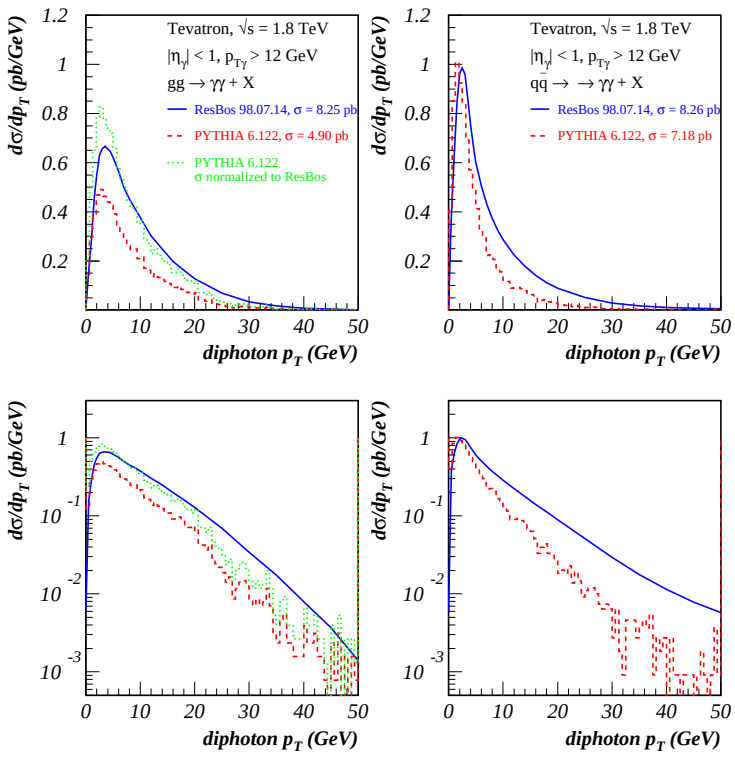

Figure 5: A comparison of the PYTHIA and ResBos predictions for diphoton production at the Tevatron for the two different subprocesses, $q\overline{q}$ and gg. The same cuts are applied to PYTHIA and ResBos as in the CDF diphoton analysis.

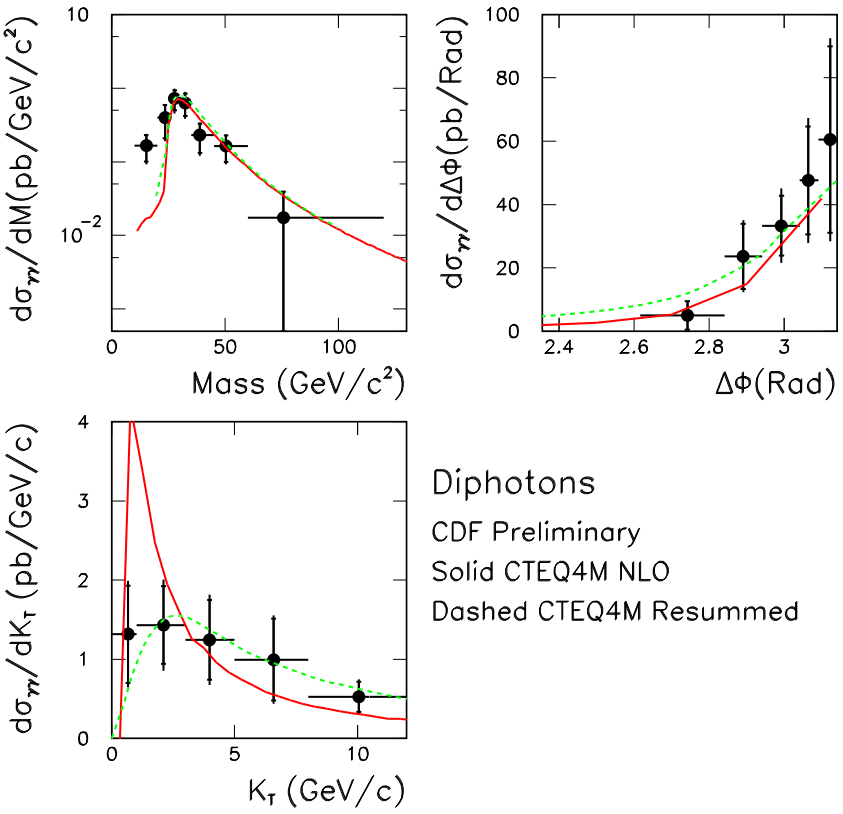

Figure 6: A comparison of the NLO and ResBos predictions for diphoton production at the Tevatron for the diphoton mass, the angle $\Delta\phi$ and the transverse momentum of the photon pair K_T.

distribution from gg scattering is noticeably broader than that from $q\overline{q}$ production.

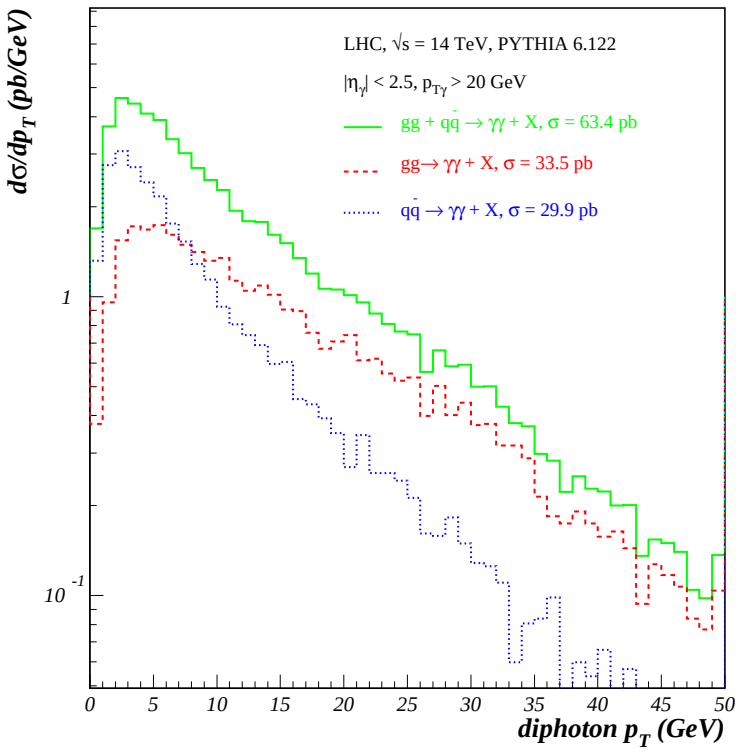

Figure 7: A comparison of the PYTHIA predictions for diphoton production at the LHC for the two different subprocesses, $q\overline{q}$ and gg. Similar cuts are applied to the diphoton kinematics as those used by ATLAS and CMS.

In Figure 8 is shown a comparison of the diphoton p_T distribution for two different versions of PYTHIA, for the two different subprocesses. Note that the p_T distribution in PYTHIA version 5.7 is somewhat broader than that in version 6.122 for the case of gg scattering. The effective diphoton mass range being considered here is lower than the 150 GeV Higgs mass that will be considered in the next section. As will be seen, the differences in soft gluon emission between the two versions of PYTHIA are larger in that case.

In Figure 9 are shown the ResBos predictions for diphoton production at the LHC from $q\overline{q}$ and gg scattering compared to the PYTHIA predictions (using the same experimental cuts). Again, the gg subprocess predictions in ResBos agree well with those from while the $q\overline{q}$ p_T distribution is noticebly broader in ResBos, for the reasons cited previously.

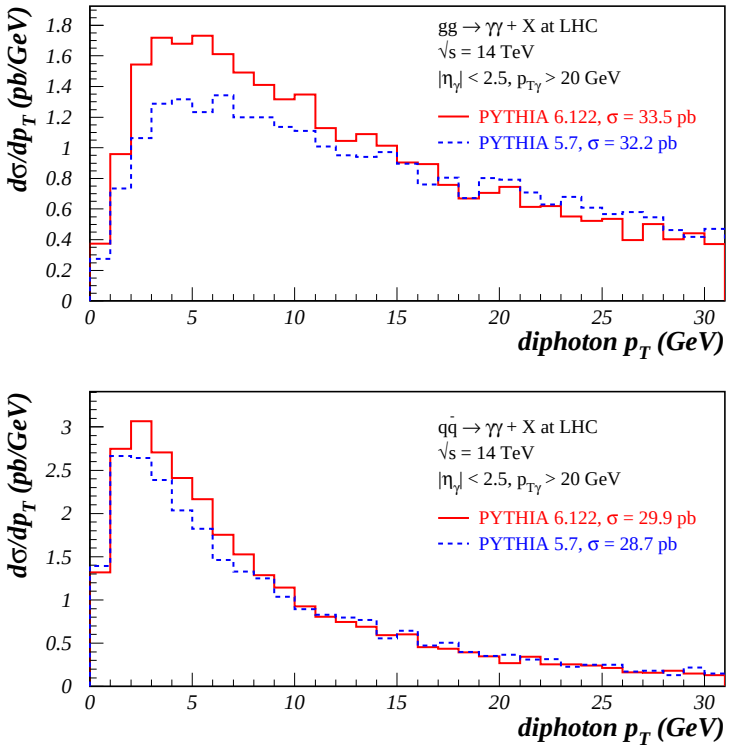

Figure 8: A comparison of the PYTHIA predictions for diphoton production at the LHC for the two different subprocesses, $q\overline{q}$ and gg, for two recent versions of PYTHIA. Similar cuts are applied to the diphoton kinematics as are used by ATLAS and CMS.

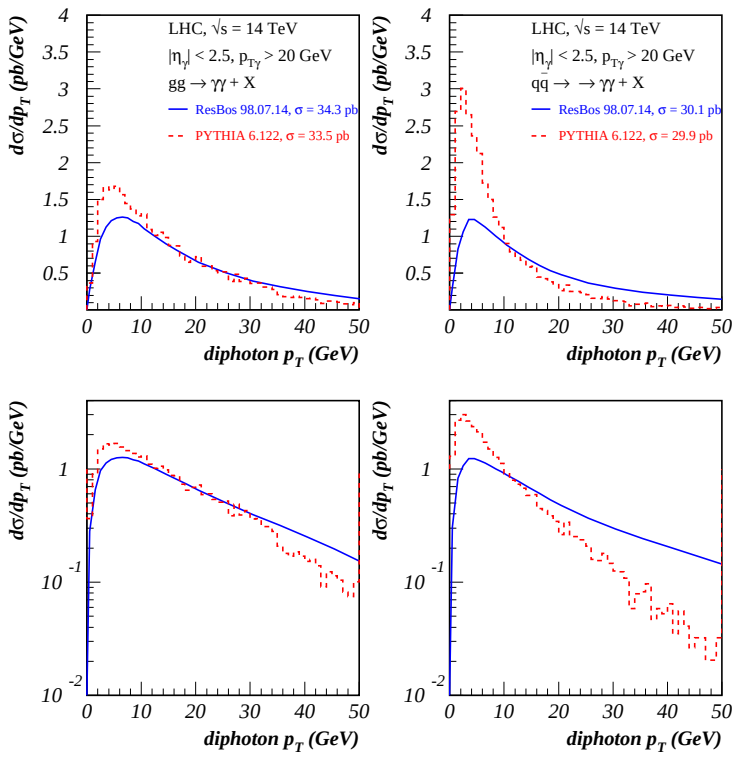

Figure 9: A comparison of the PYTHIA and ResBos predictions for diphoton production at the LHC for the two different subprocesses, $q\overline{q}$ and gg. Similar cuts are applied to PYTHIA and ResBos as in the ATLAS and CMS diphoton analyses.

5 Higgs Boson Production

A comparison of the Higgs p_T distribution at the LHC, for a Higgs mass of 150 GeV, is shown in Figure 10, for ResBos and the two recent versions of PYTHIA. As before, PYTHIA has been rescaled to agree with the normalization of ResBos to allow for a better shape comparison. Note that the peak of the resummed distribution has moved to $p_T \approx 11$ GeV (compared to about 3 GeV for Z^0 production at the Tevatron). This is partially due to the larger mass (150 GeV compared to 90 GeV), but is primarily because of the larger color factors associated with initial state gluons ($C_A = 3$) rather than quarks ($C_F = 4/3$), and also because of the larger phase space for initial state gluon emission at the LHC.

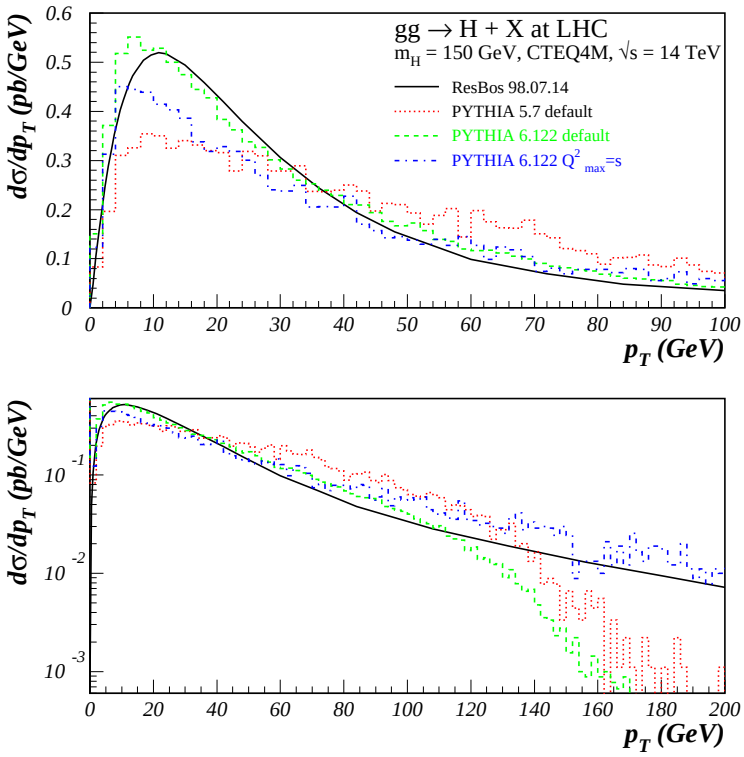

Figure 10: A comparison of predictions for the Higgs p_T distribution at the LHC from ResBos and from two recent versions of PYTHIA. The ResBos and PYTHIA predictions have been normalized to the same area.

The newer version of PYTHIA agrees well with ResBos at low to moderate p_T, but falls below the resummed prediction at high p_T. This is easily understood: ResBos switches to the

NLO Higgs + jet matrix element at high p_T while the default PYTHIA can generate the Higgs p_T distribution only by initial state gluon radiation, using as maximum virtuality the Higgs mass squared. High p_T Higgs production is another example where a $2 \rightarrow 1$ Monte Carlo calculation with parton showering can not completely reproduce the exact matrix element calculation, without the use of matrix element corrections. The high p_T region is better reproduced if the maximum virtuality Q^2_{max} is set equal to the squared partonic center of mass energy, s, rather than m^2_H. This is equivalent to applying the parton shower to all of phase space. However, this has the consequence of depleting the low p_T region as 'too much' showering causes events to migrate out of the peak. The appropriate scale to use in PYTHIA (or any Monte Carlo) depends on the p_T range to be probed. If matrix element information is used to constrain the behavior, the correct high p_T cross section can be obtained while still using the lower scale for showering. The incorporation of matrix element corrections to Higgs production (involving the processes $gq \rightarrow qH$,$q\overline{q} \rightarrow gH$, $gg \rightarrow gH$) is the next logical project for the Monte Carlo experts, in order to accurately describe the high p_T region.

A comparison of the two versions of PYTHIA and of ResBos is also shown in Figure 11 for the case of Higgs production (at a Higgs mass of 100 GeV) at the Tevatron with center-of-mass energy of 2.0 TeV. The same qualititative features are observed as at the LHC: the newer version of PYTHIA agrees better with ResBos in describing the low p_T shape, and there is a falloff at high p_T unless the larger virtuality is used for the for the parton showers. The default (rms) value of the non-perturbative k_T (0.44 GeV) was used for the PYTHIA predictions for Higgs production.

The older version of PYTHIA produces too many Higgs events at moderate p_T (in comparison to ResBos) at both the Tevatron and the LHC. Two changes have been implemented in the newer version. The first change is that a cut is placed on the combination of z and Q^2 values in a branching: $\hat{u} = Q^2 - \hat{s}(1-z) < 0$, where $\hat{s}$ refers to the subsystem of the hard scattering plus the shower partons considered to that point. The association with $\hat{u}$ is relevant if the branching is interpreted in terms of a $2 \rightarrow 2$ hard scattering. The corner of emissions that do not respect this requirement occurs when the Q^2 value of the spacelike emitting parton is little changed and the z value of the branching is close to unity. This effect is mainly for the hardest emission (largest Q^2). The net result of this requirement is a substantial reduction in the total amount of gluon radiation [19]. [10] In the second change, the parameter for the minimum gluon energy emitted in spacelike showers is modified by an extra factor roughly corresponding to the $1/\gamma$ factor for the boost to the hard subprocess frame [19]. The effect of this change is to increase the amount of gluon radiation. Thus, the two effects are in opposite directions but with the first effect being dominant.

This difference in the p_T distribution between the two versions of PYTHIA could have an impact on the analysis strategies for Higgs searches at the LHC. For example, for the CMS detector, the higher p_T activity associated with Higgs production in version 5.7 would have allowed for a more precise determination of the event vertex from which the Higgs (decaying into two photons) originated. Vertex pointing with the photons is not possible in the CMS

[10] Such branchings are kinematically allowed, but since matrix element corrections would assume initial state partons to have $Q^2 = 0$, a non-physical $\hat{u}$ results (and thus no possibility to impose matrix element corrections). The correct behavior is beyond the predictive power of leading log Monte Carlos.

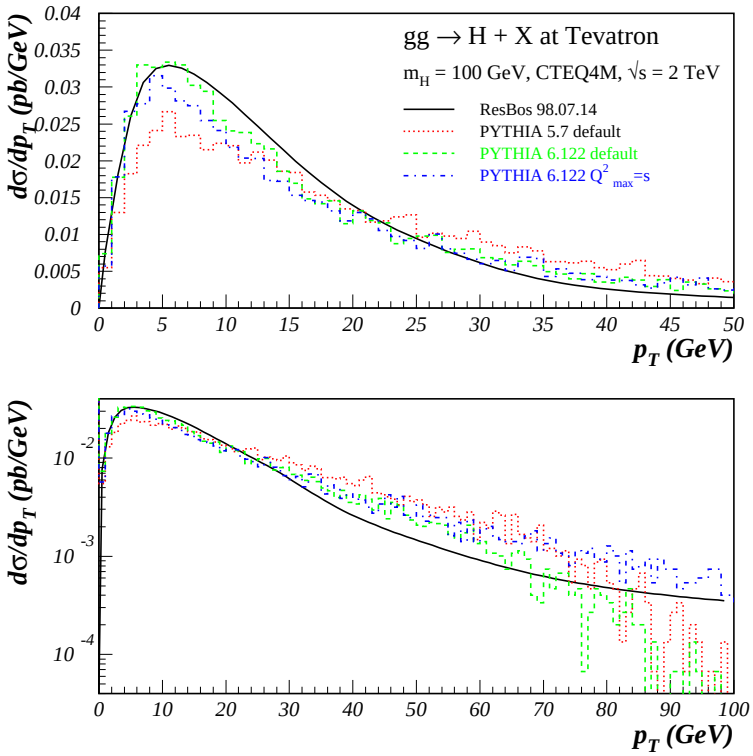

Figure 11: A comparison of predictions for the Higgs p_T distribution at the Tevatron from ResBos and from two recent versions of PYTHIA. The ResBos and PYTHIA predictions have been normalized to the same area.

barrel region, and the large number of interactions occuring with high intensity running will mean a substantial probability that at least one of the interactions will produce jets at low to moderate E_T. This could lead to the wrong vertex being chosen for the Higgs, leading to a significant degradation in the $\gamma\gamma$ effective mass resolution. [20] In principle, this problem could affect the p_T distribution for all PYTHIA processes. In practice, it affects only gg initial states, due to the enhanced probability for branching with such an initial state.

As an exercise, an 80 GeV W and an 80 GeV Higgs were generated at the Tevatron using PYTHIA5.7 [21]. A comparison of the distribution of values of $\hat{u}$ and the virtuality Q for the two processes indicates a greater tendency for the Higgs virtuality to be near the maximum value and for there to be a larger number of Higgs events with positive $\hat{u}$ (than W events).

6 Comparison with HERWIG

The variation between versions 5.7 and 6.1 of PYTHIA gives an indication of the uncertainties due to the types of choices that can be made in Monte Carlos. The requirement that $\hat{u}$ be negative for all branchings is a choice rather than an absolute requirement. Perhaps the better agreement of version 6.1 with ResBos is an indication that the adoption of the $\hat{u}$ restrictions was correct. Of course, there may be other changes to PYTHIA which would also lead to better agreement with ResBos for this variable.

Since there are a variey of choices that can be made in Monte Carlo implementations, it is instructive to compare the predictions for the p_T distribution for Higgs production from ResBos and PYTHIA with that from HERWIG (version 5.6, also using the CTEQ4M parton distribution functions). The HERWIG prediction is shown in Figure 12 along with the PYTHIA and ResBos predictions, all normalized to the ResBos prediction. [11] (In all cases, the CTEQ4M parton distribution was used.) The predictions from HERWIG and PYTHIA 6.1 are very similar, with the HERWIG prediction matching the ResBos shape somewhat better at low p_T. For reference, the absolutely normalized predictions from ResBos, PYTHIA and HERWIG for the p_T distribution of a 150 GeV Higgs at the LHC are shown in Figure 13.

7 Non-perturbative k_T

A question still remains as to the appropriate value of non-perturbative k_T to input in the Monte Carlos to achieve a better agreement in shape, both at the Tevatron and at the LHC. In Figures 14 and 15 are shown comparisons of ResBos and PYTHIA predictions for the Higgs p_T distribution at the Tevatron and LHC. The PYTHIA prediction (now version 6.1 alone) is shown with several values of non-perturbative k_T. Suprisingly, no difference is observed between the predictions with the different values of k_T, with the peak in PYTHIA always being somewhat below that of ResBos. This insensitivity can be understood from the plots at the bottom of the two figures which show the sum of the non-perturbative initial state k_T (k_{T1}+k_{T2}) at Q_0 and at the hard scatter scale Q. Most of the k_T is radiated away. with

[11] The normalization factors (ResBos/Monte Carlo) are PYTHIA (both versions)(1.68) and HERWIG (1.84).

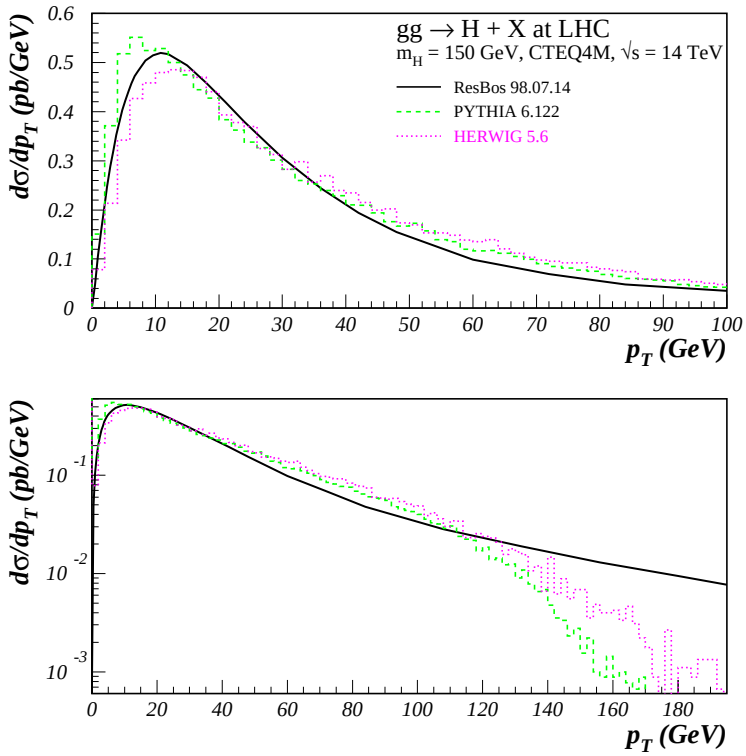

Figure 12: A comparison of predictions for the Higgs p_T distribution at the LHC from ResBos, two recent versions of PYTHIA and HERWIG. The ResBos, PYTHIA and HERWIG predictions have been normalized to the same area.

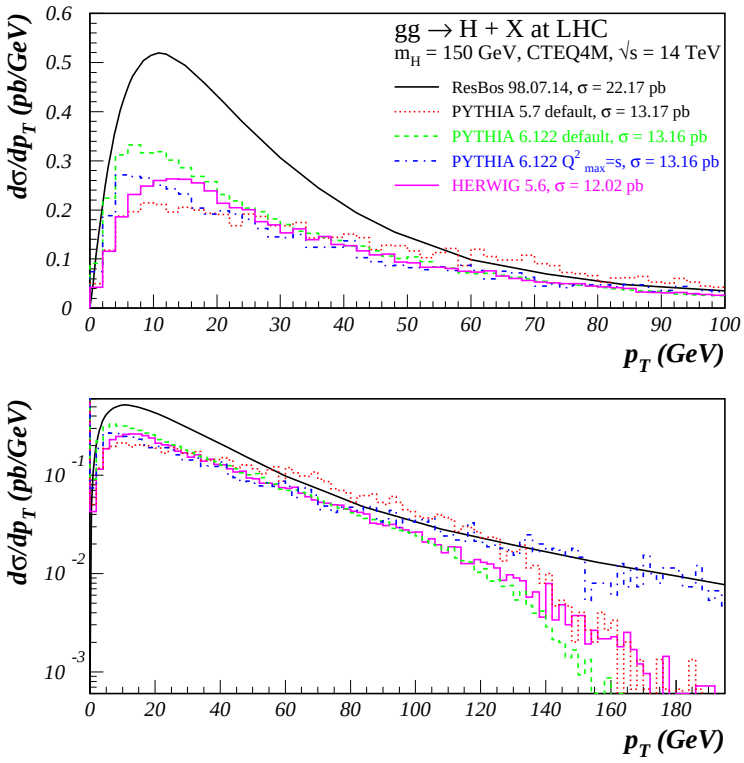

Figure 13: A comparison of predictions for the Higgs p_T distribution at the LHC from ResBos and from two recent versions of PYTHIA. The ResBos and PYTHIA predictions have their absolute normalizations.

this effect being larger (as expected) at the LHC. The large gluon radiation probability from a gluon-gluon initial state (and the greater phase space available at the LHC) lead to a stronger degradation of the non-perturbative k_T than was observed with Z^0 production at the Tevatron.

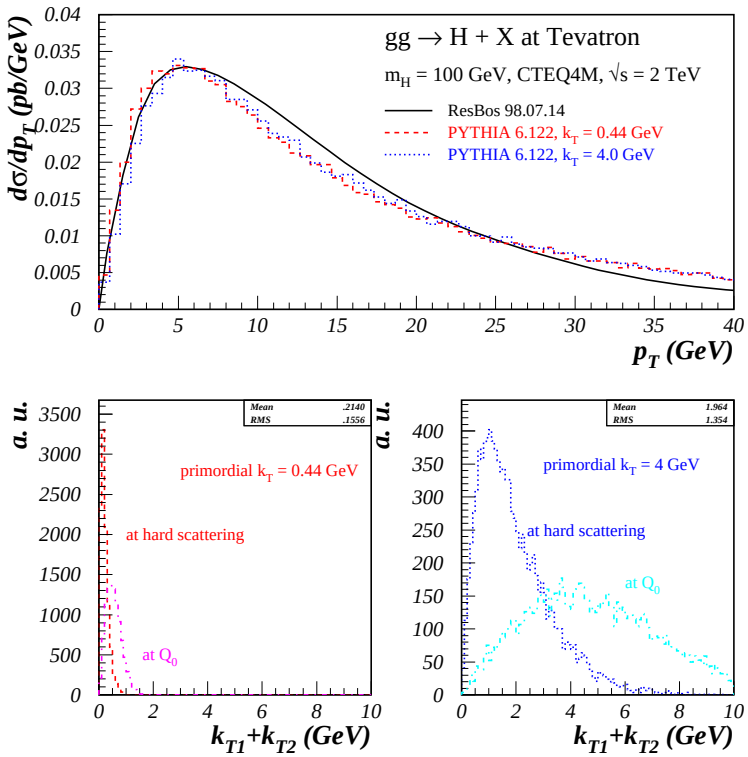

Figure 14: (top) A comparison of the PYTHIA predictions for the p_T distribution of a 100 GeV Higgs at the Tevatron using the default (rms) non-perturbative k_T (0.44 GeV) and a larger value (4 GeV), at the initial scale Q_0 and at the hard scatter scale. Also shown is the ResBos prediction (bottom) The vector sum of the intrinsic k_T (k_{T1}+k_{T2}) for the two initial state partons at the initial scale Q_0 and at the hard scattering scale for the two values of intrinsic k_T.

For completeness, a comparison of PYTHIA and ResBos is shown in Figure 16 for Z^0 boson production at the LHC. There are two points that are somewhat surprising. There is still a very strong sensitivity to the value of the non-perturbative k_T used in the smearing, and the best agreement with ResBos is obtained with the default value (0.44 GeV), in contrast to the 2 GeV needed at the Tevatron. Note again the agreement of PYTHIA with ResBos at the highest values of Z^0 p_T due to the explicit matrix element corrections applied.

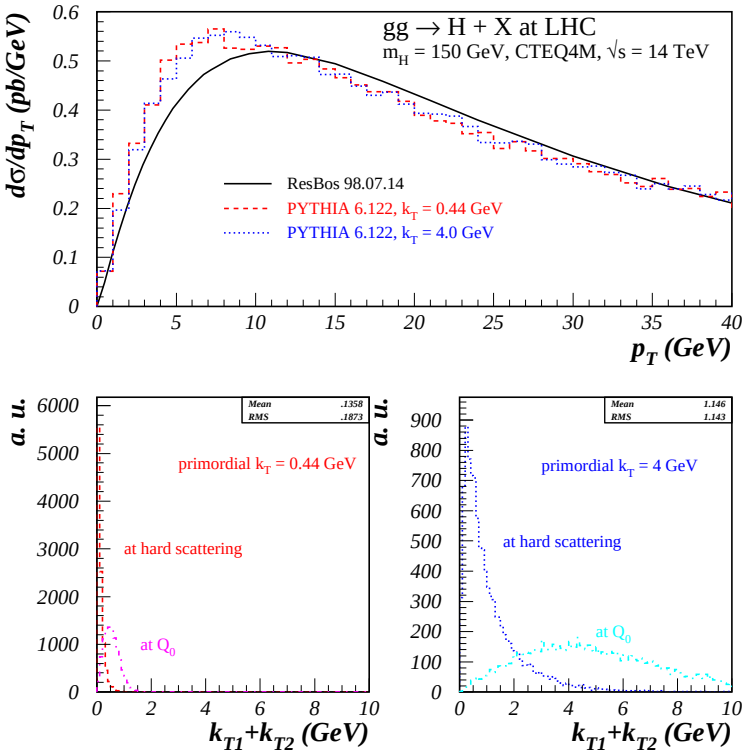

Figure 15: (top) A comparison of the PYTHIA predictions for the p_T distribution of a 150 GeV Higgs at the LHC using the default (rms) non- perturbative k_T (0.44 GeV) and a larger value (4 GeV), at the initial scale Q_0 and at the hard scatter scale. Also shown is the ResBos prediction. (bottom) The vector sum of the intrinsic k_T (k_{T1}+k_{T2}) for the two initial state partons at the initial scale Q_0 and at the hard scattering scale for the two values of intrinsic k_T.

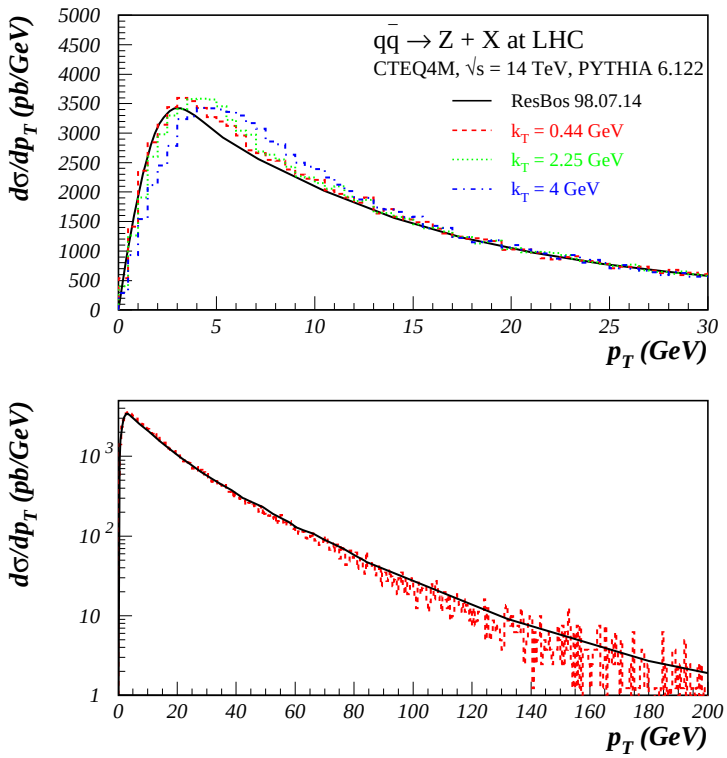

Figure 16: A comparison of the predictions for the p_T distribution for Z^0 production at the LHC from PYTHIA and ResBos, where several values of k_T have been used to make the PYTHIA predictions.

The sum of the incoming parton k_T distributions, both at the scale Q_0 and at the hard scattering scale, are shown in Figure 17 for several different starting (rms) values of primordial k_T (per parton). There is substantially less radiation for a $q\overline{q}$ initial state than for a gg initial state (as in the case of the Higgs), leading to a noticeable dependence of the Z^0 p_T distribution on the primordial k_T distribution.

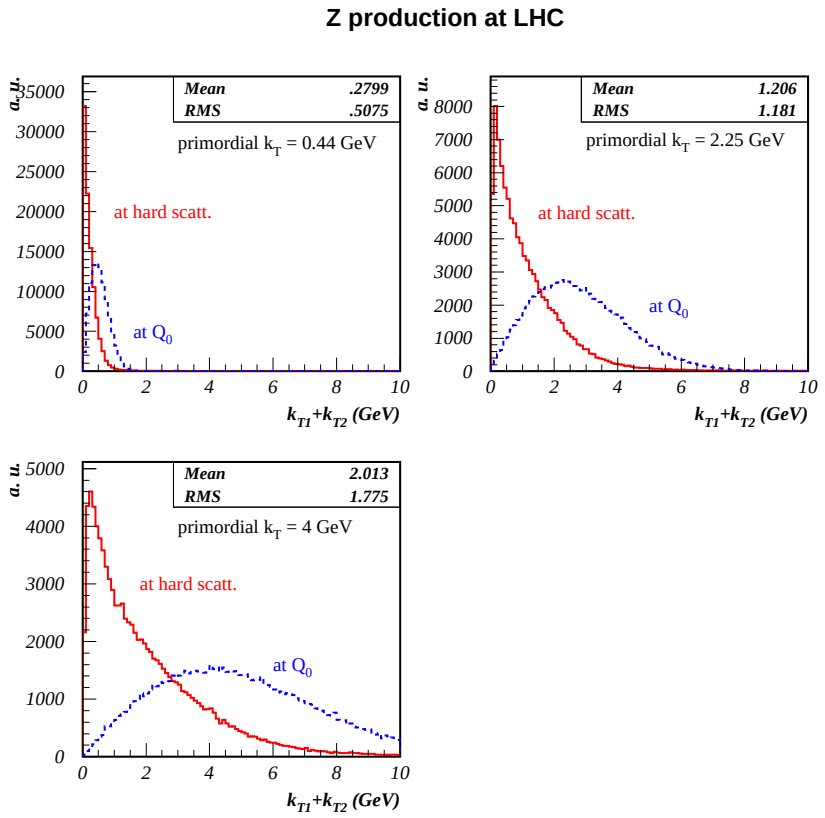

Figure 17: A comparison of the total initial state k_T ($k_{T1} + k_{T2}$) distributions for Z^0 production at the LHC from PYTHIA, both at the initial scale Q_0 and at the hard scattering scale, for several (rms) values of the initial state k_T. The mean and rms numbers refer to the values at the hard scattering scale.

8 Conclusions

An understanding of the signature for Higgs boson production at either the Tevatron or LHC depends upon the understanding of the details of soft gluon emission from the initial

state partons. This soft gluon emission can be modelled either in a Monte Carlo or in a k_T resummation program, with various choices possible in both implementations. A comparison of the two approaches is useful to understand the strengths and weaknesses of each. The data from the Tevatron that either exists now, or will exist in Run 2, will be extremely useful to test both approaches.

9 Acknowledgements

We would like to thank Claude Charlot, Gennaro Corcella, Steve Mrenna, Willis Sakumoto, Torbjorn Sjostrand and Valeria Tano for useful conversations and plots. This work was supported in part by the NSF under grant PHY-9901946 and by the DOE under grant DE-FG-03-94ER40833.

References

[1] C. Balazs, J. Huston and I. Puljak, hep-ph/0002032, submitted to *Nucl. Phys.* **B**.

[2] T. Sjostrand, *Computer Phys. Commun.* **82**, 74 (1994).

[3] G. Marchesini, B.R. Webber, G. Abbiendi, I.G. Knowles, M.H. Seymour and L. Stanco, *Computer Phys. Commun.* **67**, 465 (1992).

[4] F.E. Paige, S.D. Protopescu, H. Baer and X. Tata, hep-ph/9810440.

[5] ATLAS Detector and Physics Performance Technical Design Report, CERN/LHCC/99-14.

[6] C. Schmidt, private communication.

[7] S. Catani and B.R. Webber, *Nucl. Phys.* **B349**, 635 (1991).

[8] C. Balazs and C. P. Yuan, Phys. Rev. **D56**, 5558 (1997) hep-ph/9704258; C. Balazs and C. P. Yuan, hep-ph/0001103.

[9] G. Miu and T. Sjostrand, *Phys. Lett.* **B449**, 313 (1999).

[10] G. Corcella and M.H. Seymour, RAL-TR-1999-051 and hep-ph/9908388.

[11] S. Mrenna, hep-ph/9902471.

[12] H.L. Lai, J. Huston, S. Kuhlmann, F. Olness, J. Owens, D. Soper, W.K. Tung, H. Weerts, *Phys. Rev.* **D55**, 1280 (1997).

[13] G. Corcella, talk at the LHC workshop, October 1999.

[14] G. Ladinsky, C.P. Yuan, *Phys. Rev.* **D50**, 4239 (1994).

[15] C. Balazs, J. Collins and D. Soper, these proceedings.

[16] F. Abe et al., *Phys. Rev. Lett.* **70**, 2232 (1993); T. Takano, Ph.D. thesis, U. Tsukuba (1998); CDF Collaboration, paper in preparation.

[17] C. Balazs, P. Nadolsky, C. Schmidt and C.–P. Yuan, hep-ph/9905551.

[18] P. Aurenche, A. Douri, R. Baier, M. Fontannaz, *Z. Phys.* **C29**, 423 (1985); B. Bailey, J. Owens, J. Ohnemus, *Phys. Rev.* **D46**, 2018 (1992); T. Binoth, J.P. Guillet, E. Pilon, M. Werlen, hep-ph/9911340.

[19] `PYTHIA` manual update for version 6.1.

[20] D. Denegri, private communication.

[21] S. Mrenna, talk at the Run 2 workshop, Nov 1999, Fermilab; C. Balazs, J. Huston, S. Mrenna, I. Puljak, Proceedings of the Run 2 Workshop.

Automatic Computation of LHC Processes

E. Boos, V. Ilyin, K. Kato, A. Pukhov, A. Semenov, A. Skatchkova

Automatic computation is a new approach to HEP computing. The first such systems, GRACE [1], FeynArt/FeynCalc [2] and CompHEP [3], were reported at the 1st International Workshop AIHENP held on March, 1990 in Lyon-Villeurbanne (France). Under this terminology, *automatic computation system (ACS)*, we assume, as a distinguishing feature, the generation of the computing code for a specific collision process with the aid of another code.

ACS's are now used widely by phenomenologists for the calculation of many collision processes. For example, the GRACE and CompHEP systems were used in the LEP2 Workshop [4], and for evaluation of processes at TeV linear colliders [5]. With ACS one can calculate *all* collision processes within a given physical model, where by physical model we mean the set of Feynman rules. Recent developments with the LanHEP package [11] have opened a possibility to derive Feynman rules in the form of the ACS intrinsic physical model in a fully automatic way, starting from the Lagrangian. Now, not only the Standard Model but a number of its extensions, like SUSY models, are implemented in ACS. A general review of this new approach is given in these Proceedings by K.Kato together with discussion of main directions of the ACS development. Here, we discuss in more detail specifics of the ACS applications in LHC phenomenology, and in particular to the evaluation of QCD processes.

To close this preview we list below the main ACS options in order to provide an idea for users of what is available:

i) selection of physical model (Lagrangian) and hard subprocess,

ii) Feynman diagram generation,

iii) generation of the code for matrix element,

iv) convolution with parton distributions,

v) generation of kinematics (phase space parameterization) with regularization of kinematical peaks,

vi) integration over the phase space (evaluation of cross section),

vii) generation of events at partonic level, including the interface to hadronization tools.

1 The problem of multiparticle final states: why automatic computations?

We start from the problem of the accurate evaluation of hard subprocesses in the case of multiparticle final states.

When physicists simulate HEP processes with such generators as PYTHIA [6], ISAJET [7] or HERWIG [8] they use a data base of hard subprocesses implemented in these packages. It means that a) matrix elements are stored as formulas, and b) a knowledge about the behaviour of matrix elements as phase space integrands are coded in the form of modelling functions in order to get a fast generation of the partonic events. One can note that these data bases include a rather simple variety of subprocesses, mainly of the $2 \to 2$ type.

If one tries to include a hard subprocesses with 3, 4 and more particles in the final state, large problems appear. Indeed, the size of matrix elements increases very fast. For example, in the $2 \to 4$ case, the size of the code for evaluation of helicity amplitudes for one subprocess is at the 100's of Kbyte level. However, the main problem lies elsewhere; it is impossible to construct an analytical formula for matching peaks and other structures of the rather singular behaviour of matrix elements. In the $2 \to 3$ case, phase space has 4 dimensions plus two for convolution with the PDF's; in the $2 \to 4$ case 7+2 dimensions are present, and so on. As a result, the set of kinematical singularities has, as a rule, a very complicated positioning in the multidimensional phase space. This particular problem was not solved accurately, e.g., when the Zbb final state was implemented in PYTHIA 5.7.

Let us discuss further this somewhat delicate point. It is necessary to integrate the squared matrix element over the phase space in order to obtain the cross section. Precise information about the behaviour of the integrand then is necessary for further event generation. This information can be obtained at the step of the phase space integration. The problem is that the integrand, as a rule, has a singular behaviour with sharp kinematical peaks connected with different denominators (propagators) of Feynman diagrams. This problem is caused, in particular, by the circumstance that one has to take into account nonzero masses of particles in many important cases, especially if accurate calculations are needed. The masses of elementary particles can have extremely small values, e.g. the masses of the 1st generation quarks (few MeV), and can also be zero (for the photon and gluon). At the same time, other parameters are of the order of a hundred GeV, e.g. masses of W and Z bosons and t-quark. Moreover the collision energy can also have a very large value, e.g. 14000 GeV for LHC processes, and some other important variables, like the transverse energy of jets, are at the hundred GeV scale or even greater. This huge scale interval for different parameters causes serious computational problems which result in the appearance of sharp peaks for the integrand. So, at the step of phase space parameterization, one has to include a regularization of the integration measure in order to smooth the singularities of the integrand.

LHC phenomenology requires the computation of a wide spectrum of hard subprocesses with 3,4 and even more particles (partons) in the final state. This is a common need for all of the physics working groups: QCD, EW, Higgs, SUSY etc. These requirements are especially common for new physics searches. Furthermore, a major challenge results from background

analyses, where QCD subprocesses play a major role with, in many cases, multiparton final states. As a rule, for each LHC discovery reaction, one should calculate several QCD processes giving both irreducible and reducible backgrounds. The parton-shower generation of multiparticle final states is usually utilized in this situation. However, this can be too crude an approximation for many important studies leading to sometimes grossly unreliable predictions.

We emphasize that ACS can give the possibility to compute accurately a variety of LHC processes (and in particular QCD processes) with 3, 4 and more bodies in the final partonic state. Indeed, the first problem (the size of the matrix element computing code and the difficulty to obtain the exact matrix elements) is solved in ACS by the automatic generation of the corresponding code. This step is fast and pain-free from the viewpoint of the user. The second problem (the accurate integration over the multidimensional phase space) is solved in ACS by the generation of kinematics where the necessary regularizations are included. For example, in CompHEP the user has to list a set of singular propagators using the menu system. After that, the code for kinematics (with regularizations) is generated automatically. In GRACE, a library of kinematics (with regularizations) is used and the user has to make the necessary choices. Thus, the high art (mathematics and programming), needed to elaborate the sharp peaks, is enclosed in a form hidden from the user, giving him a possibility to compute complicated processes.

At the step of integration over the phase space, ACS uses adaptive Monte Carlo integrators (VEGAS [12] in CompHEP, and BASES [13] in GRACE). To match the complete set of singularities, the multichannel MC approach [10] is utilized. As a result, the phase space grid is created with an accurate mapping of the singular behaviour of the matrix element. This complex body of information (let us call it *MEgrid*) has a rather large size that rapidly increases with the number of phase space dimensions. One can consider *MEgrid* as a multidimensional analog of the modelling function used in PYTHIA and other similar packages for the effective generation of partonic events. Of course, this information can not be expressed in analytical form. It is necessary to point out also that the convolution with parton distributions should be made at the same stage as the integration over the phase space. Indeed, the contributions of different subspaces (in particular different kinematical peaks) can depend largely on the partonic collison energy, $\hat{s}$, resulting from the information stored in *MEgrid*.

ACS can be considered as a tool for the automatic generation of the data base of hard subprocesses for physical generators like PYTHIA, ISAJET and HERWIG. However, it is difficult to imagine that the data base created can be implemented in the code of these generators. This is due, first of all, to the size of the generated codes. Thus, we propose a *two stage* approach. At the first stage, ACS is used resulting in a cross section and *MEgrid* for the subprocess under evaluation. This can be stored in a special LHC data base. This data base can be used for the effective generation of partonic events. In GRACE, it is available with the SPRING [13] generator, and in CompHEP by a relatively straightforward procedure and an effective generator is under construction). The output is a partonic event flow that can be used as an input for physical generators like PYTHIA, ISAJET and HERWIG; this is second stage of the full simulations. At this stage partons (quarks and gluons) should be

hadronized and unstable particles decayed. We note that in PYTHIA there exists a rather flexible interface for such a *two stage* approach, the option for inclusion of external processes through the routine PYUPEV.

This is a general view on the way in which ACS (GRACE and CompHEP in particular) can be used for the simulation of LHC processes. Below we discuss some specific features of this technology with special attention to QCD aspects.

2 General Considerations about GRACE and CompHEP

With CompHEP and GRACE the user can evaluate hard subprocesses at the tree level, i.e. Feynman diagrams are generated without loops. This corresponds to the basic request for LHC phenomenology. However, it is well known that QCD next-to-leading corrections are large, as a rule, for LHC processes. In many cases these corections can be accounted for in the form of so-called K-factors and one can include them easily in tree level calculations. Nevertheless, in many important cases an explicit evaluation of higher order corrections is necessary. At this moment it is not clear how to automate calculations of LHC processes at NLO level. The problem is connected, in particular, with the circumstance that different resummations of large logarithms should be included in order to get reliable NLO predictions. The interface between resummation techniques and event generators is under intensive discussion now, and at the present Workshop also. We note in this respect, that the GRACE package includes the code for the generation and evaluation of one-loop diagrams.

The user interface should provide the possibility to calculate complicated processes for users not experienced in programming. CompHEP has a (graphical) menu driven system where the user proceeds through all steps of the calculation without any programming. In GRACE, the user needs to write a few simple interface routines.

The information on the GRACE system and its products can be found at

http://www-sc.kek.jp/minami/

The code of CompHEP is free for users and one can take it from the following Web page

http://theory.npi.msu.su/comphep

where the user's manual is available in PS format (see also hep-ph/9908288). The CompHEP package, adapted for LHC processes (see next section) is installed on the SUN platform

/afs/cern.ch/cms/physics/COMPHEP/v33-SUN

and on the PC/Linux platform

/afs/cern.ch/cms/physics/COMPHEP/v33-Linux

The interface between CompHEP and PYTHIA has beencreated with the corresponding code available from the address:

/afs/cern.ch/cms/physics/comp-pyth

where one can find a short description in the file README. With this interface, the partonic event flow for any processes calculated with CompHEP can be sent to PYTHIA to generate physical events.

3 QCD aspects in automatic computations

In this section we discuss the treatment of QCD effects in the case of automatic computations, and consider CompHEP options as an example. As has been discussed above, CompHEP calculates only at tree level, and so at leading order (LO). Thus, the main problems concerning an accurate accounting of QCD effects are outside the discussion. Nevertheless, some important QCD dependencies can not be avoided even at tree level and the corresponding options are available for users. These aspects are: a) parton distributions, b) QCD scale, and c) running strong coupling constant.

Parton distributions.

In CompHEP the specification of initial states in the collision process under evaluation can include the convolution with structure function. So, in the case of hadron collisions, the cross section is evaluated as an integral

$$\sigma(s) \;=\; \int_0^1 dx_1 dx_2 f_i(x_1,Q) f_j(x_2,Q) \hat{\sigma}_{ij}(x_1 x_2 s)$$

where f_i are the corresponding parton distributions, $\hat{\sigma}$ is the partonic cross section and Q is the QCD scale.

In CompHEP v.33, installed at CERN (see address above), parton distributions from two pdf families are implemented, MRS and CTEQ, and in particular the following versions: 1) MRS(A') and MRS(G) [14], 2) CTEQ4l and CTEQ4m [15]. Note that CTEQ4l is a LO parametrization, while in all others the evolution of parton distributions is realized in the next-to-leading (NLO) approximation.

In addition, a special interface is available to include a user's defined parton distribution. By this way one can implement the most recent parametrizations (at this moment CTEQ5 and MSRT). See the CompHEP user's manual for the corresponding procedure (section 3.6.2).

Choice of QCD scale.

The factorization theorem states that parton distributions depend not only on the Bjorken variable x but also on some parameter Q which characterizes the energy (or momentum) scale at which the QCD effects give the main contribution to the hard subprocess. This parameter is set by the user for each specific QCD process. It is possible to set a fixed scale or a running scale. In the later case, Q^2 can be a squared linear combination of any set of initial and outgoing particles momenta, for example, $(p_1-p_3)^2$, $(p_1-p_3-p_4)^2$, $(p_3+p_4)^2$ and so on (initial and outgoing momenta enter with opposite signs). The corresponding settings are made through the option QCD SCALE of the numerical menu.

Running α_s.

It is the nature of strong interactions that there is no absolute normalization of the corresponding coupling constant. This is in contrast to the value 1/137 for the electromagnetic constant known with high accuracy from classical electrodynamical experiments. Instead, we have a function for α_s rather than a constant. Even in the leading order approximation, $\alpha_s^{LO} = 6\pi/[(33-2n_f)\log Q/\Lambda^{(n_f)}]$, where Q is the QCD scale of the hard subprocess under

the evaluation with Λ the so-called QCD fundamental parameter. Then, n_f is the number of parton flavours with masses lower than Q. The n_f dependence in QCD parameter Λ matches the quark mass threshold effects.

In the version of CompHEP installed at CERN, the running α_s is realized in LO, NLO and NNLO. All of the corresponding formulas are based on the choice of $\Lambda^{(6)}$ (see *Review of Particle Physics* [16] p.81. The user can find the corresponding switch in the option QCD SCALE in the numerical menu.

Therefore, to evaluate QCD processes with CompHEP, one has, first of all, to fix the normalization of α_s. The popular normalization point is the mass of Z boson, $Q = M_Z$. By changing the parameter $\Lambda^{(6)}$, the user should set the strong coupling at the appropriate value, say $\alpha_s(M_Z) = 0.118$. Then, the user has to choose the order for the running α_s (LO, NLO or NLO). Finally, the user has to define the QCD scale Q, which will be used both for the evaluation of α_s at this scale and in the parton distributions.

Thus, the complete LO calculations of LHC processes are available, with the matrix element, parton distributions and running strong coupling constant calculated in the lowest order of the perturbation theory. This is a self-consistent starting point in the phenomenological analysis; when/where higher order corrections are available, all elements of the calculation can be calculated at the higher order and then compared to the leading order result.

However, it is also common for phenomenologists use a mixed approach, with the matrix element evaluated at LO but the parton distributions and running α_s taken in NLO approximation. Surely, only a part of the NLO corrections is accounted for in this case. We note that this option is also available for users in CompHEP calculations.

4 Partonic Subprocesses

When hadronic collision processes are evaluated, especially in the case of a large number of final state particles, one serious problem is the large number of contributing partonic subprocesses. This occurs because of the quark and gluon content of the initial hadrons and CKM quark mixing. For example, at LHC energies, 180 subprocesses contribute to the $W+2jets$ and 292 subprocesses to the $W+3jets$ production (taking into account only quarks of the first two generations). During this workshop a new method has been proposed to avoid a multiplication of channels due to the mixture of quark states [17]. The method leads to a simple modification of the rules for the evaluation of the cross sections and distributions. It is based on the unitary rotation of down quarks, thus providing the transportation of mixing matrix elements from vertices of Feynman diagrams to the parton distribution functions. As a result, one can calculate cross sections with a significantly smaller number of subprocesses contributing. For the examples mentioned above, one needs to evaluate (with the new rules) only 21 and 33 subprocesses, respectively, in order to compute the cross sections for the $W+2jets$ and $W+3jets$ processes. The matrix elements of the subprocesses are calculated without quark mixing, but with a modified PDF convolution which now depends on the quark

mixing angle and the topologies of the gauge invariant classes of diagrams contributing to the subprocesses. The method proposed has been incorporated into the CompHEP program and checked with many examples.

5 PEVLIB - library of LHC processes

Now the library of CompHEP based event generators for LHC processes has been started at the address:

/afs/cern.ch/cms/physics/PEVLIB

The following QCD processes are stored already in this library: $Zb\bar{b}$, $Wb\bar{b}$, $t\bar{t}b\bar{b}$ and some others. In the corresponding directories (with the names literally corresponding to the final states) unweighted events are stored (see the files README in these directories for details about evaluation of the corresponding samples of events).

Together with the CompHEP-PYTHIA interface code (see discussion above) these event files can be used for full LHC simulations with the help of PYTHIA package and detector simulation software in the standard way.

Let us discuss the process $Zb\bar{b}$ in order to supply more details. In the directory

/afs/cern.ch/cms/physics/PEVLIB/Z_b_b

the file __pevZbb includes about 200000 unweighted events with the final state $Zb\bar{b}$. Each event includes the Lorentz momenta of all particles in the initial and final states. In the present version of this library, there is no information about the color flow in the event. Thus, only the Independent Fragmentation Model can be used for the hadronization. Of course, the user can use the Lund model; for this one has to define the corresponding color flows by hand in the routine PYUPEV. The same remark is valid also for FSR (final state radiation), what is switched off by default in CompHEP-PYTHIA interface. In the same time ISR (initial state radiation) is switched on automatically.

Note that the user can generate more events than stored in the library. In the corresponding subdirectories (indicated in the file README) the generators are stored in the form of the executable code (at this moment for SUN platform only). These generators are the corresponding CompHEP codes for the process with the proper set of kinematical regularizations.

The library PEVLIB is under construction now. New processes will be added. The structure and user's interface will be developed.

6 Acknowledgements

The work of V.I., A.P., A.S, E.B. and A.S. was partially supported by the CERN-INTAS grant 377 and RFBR-DFG grant 99-02-04011.

References

[1] *New Computing Techniques in Physics Research*, ed. D.Perret-Gallix and W.Wojcik, Ed. CNRS, Paris, 1990, p.555.

T.Tanaka, T.Kaneko and Y.Shimizu, *Comp. Phys. Commun.* **64**, 149 (1991).

T.Ishikawa et al., *GRACE manual*, KEK Report 92-19, 1993.

[2] *New Computing Techniques in Physics Research*, ed. D.Perret-Gallix and W.Wojcik, Ed. CNRS, Paris, 1990, p.565.

[3] *New Computing Techniques in Physics Research*, ed. D.Perret-Gallix and W.Wojcik, Ed. CNRS, Paris, 1990, p.573.

P.A.Baikov et al., In: Proc.of X Workshop on High Energy Physics and Quantum Field Theory (QFTHEP-95), ed.by B.Levtchenko and V.Savrin, Moscow, 1996, p.101, `hep-ph/9701412`.

E.E.Boos, M.N.Dubinin, V.A.Ilyin, A.E.Pukhov and V.I.Savrin, `hep-ph/9503280`.

A.E.Pukhov et al., *CompHEP user's manual, v.3.3.* Preprint INP MSU 98-41/542, 1998, `hep-ph/9908288`.

[4] "Physics at LEP2", ed. by G.Altarelli, T.Sjöstrand and F.Zwirner, CERN report 96-01, vol. 1, 2.

[5] E.Accomando et al., *Physics with e^+e^- linear colliders*, *Phys. Rep.* **C299**, 1 (1998).

[6] T.Sjostrand, *Comp. Phys. Commun.* **82**, 74 (1994).

[7] F.E.Paige et al., *ISAJET 7.40: a Monte Carlo event generator for pp, $\bar{p}p$, and e^+e^- reactions*, BNL-HET-98-39, Oct 1998, hep-ph/9810440.

[8] G.Marchesini et al., *HERWIG VERSION 5.9.*, `hep-ph/9607393`.

[9] H.Tanaka, *Comput. Phys. Commun.* **58**, 153 (1990).

[10] F.A.Berends. R.Pittau and R.Kleiss, *Comp. Phys. Commun.* **85**, 437 (1995).

V.A.Ilyin, D.N.Kovalenko and A.E.Pukhov, *Int.J.Mod.Phys.* **C7**, 761 (1996).

A.E.Pukhov and D.N.Kovalenko, Talk on 5th Int. Workshop AIHENP'96 (September 1996, Lauzanne). *Nucl.Inst. and Meth.* **A393**, 299 (1997).

[11] A.Semenov, Talk on 5th Int. Workshop AIHENP'96 (September 1996, Lauzanne). *Nucl.Inst. and Meth.* **A393**, 293 (1997).

A.Semenov, *Comp. Phys. Commun.* **115**, 124 (1998).

[12] G.P.Lepage, *J. Comp. Phys.* **27**, 192 (1978).

[13] S.Kawabata, *Comp. Phys. Commun.* **41**, 127 (1986).

S.Kawabata, *Comp. Phys. Commun.* **88**, 309 (1995).

[14] A.D.Martin, R.G.Roberts and W.J.Stirling, *Phys. Lett.* **B354**, 155 (1995).

[15] H.L.Lai et al., *Phys. Rev.* **D55**, 1280 (1997).

[16] Particle Data Book, *Europ. Phys. J.* **C3** (1998).

[17] E. E. Boos, V. A. Ilyin and A. N. Skachkova, `hep-ph/0004194` .

Monte Carlo Event Generators at NLO

J. Collins

Abstract

I am concerned here with QCD calculations for processes with a hard scattering — production of heavy particles, jets, etc. The most accurate calculations are by the "analytic" methods. But the most useful calculations for direct comparison with data are done by Monte-Carlo event generators, and these are limited in accuracy. In particular, there is as yet no known method of systematically improving the Monte-Carlo calculations by incorporating the non-logarithmic parts of higher order perturbative corrections. This creates limitations on the analysis of future data. Therefore I summarize some ideas for remedying the situation.

Factorization for inclusive processes

- Normal proofs of factorization are for inclusive cross sections.
- To get the simplifications in the factorization formula, as compared with the exact cross section, one makes suitable approximations.
- The approximation is to the hard scattering part H of a cross section, as in:

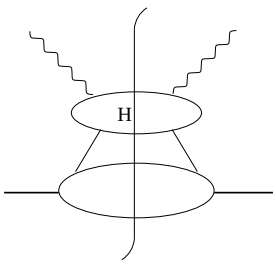

Figure 1:

which is a graph for the DIS cross section. The kinematics of the external lines of H are changed to massless on-shell partons with zero transverse momentum. Also the internal (light parton) lines of H are made massless.

- The approximation is correct to the leading power of m^2/Q^2, where m is a typical hadronic scale and Q is the scale of the hard scattering (e.g., Q^2 is the virtuality of the virtual photon in DIS).

- Subtractions are applied to the hard scattering to cancel double counting. A high-order graph for the hard scattering has subtractions that correspond to smaller hard subgraphs (and hence smaller regions of momentum space).

- The exact form of the subtractions corresponds to the approximations made for the smaller regions.

Monte-Carlo event generators at NLO (and beyond) Current event generators essentially use the leading order for the hard-scattering coupled to an algorithm that approximates the exclusive structure of the low virtuality parts of graphs for the cross section. The algorithm is in an improved leading logarithm approximation.

With the exception of the recent paper by Friberg and Sjöstrand [1], previous attempts, e.g., [2], at incorporating NLO corrections have tended to implement them by a reweighting of the events generated by showering from the LO matrix elements. Normal NLO "analytic" calculations for the hard-scattering coefficients for inclusive scattering are not usable as they stand in a Monte-Carlo event generator, because they involve singular distributions.

Here I summarize some ideas [3] to remedy this situation. I have applied them to one specific case in DIS in Ref. [4], but I think they can be generalized:

- Separate groups of events are generated with LO and NLO hard scattering coefficients.

- To obtain the NLO coefficients, the same general ideas are used as in inclusive hard scattering.

- The methods are applied both to the hard scattering itself and to the showering kernels.

- However, because we are now working with *exclusive* processes, the form of the approximations is different. The approximated graphs must satisfy the following requirements:

  - Exact 4-momentum conservation must be obeyed for each subprocess (hard scattering or one stage of the showering). I.e., $p_i^\mu = p_f^\mu$, where p_i^μ and p_f^μ are the total initial and final momenta the the subprocess.

  - The approximation may change the momenta of the internal lines but it must preserve the momenta of the external lines. This avoids the problem with having singular distributions.

- A cut-off is applied, for otherwise the approximated graphs give ultra-violet divergences when integrated to large transverse momentum. The kinematics associated with exact momentum conservation do provide a cutoff, but such a cutoff tends to violate factorization of the momentum-space integrals. So a separate artificial cutoff is better, and probably makes for a better implementation of the algorithm.

- Conventionally, in a Monte-Carlo a sharp cutoff is used. But a smooth cut-off will probably be better for numerical work. It will also make it easier to get positive cross sections.

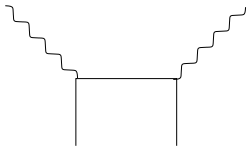

Figure 2: Born graph for DIS

- The dependence on the cutoff is a generalized renormalization-group transformation, and the exact cross section is independent of the form of the cutoff.
- Separate explicit soft factors are needed, as in the factorization theorem for the q_T distribution for the Drell-Yan process; unlike the case of an inclusive cross section the cancellation of the soft region is not complete. This issue is not treated in Refs. [4, 3], but will need further work, which is in progress.

Example of application to DIS [4] The parton model graph of Fig. 2 is combined with showering to give a LO cross section that can be summarized as

$$\sigma_{\rm LO} = \text{Born graph} \times \text{initial-state showering} \times \text{final-state showering}. \tag{1}$$

The NLO cross section is obtained from subtracted one-loop graphs, and the hard-scattering coefficient is of the form

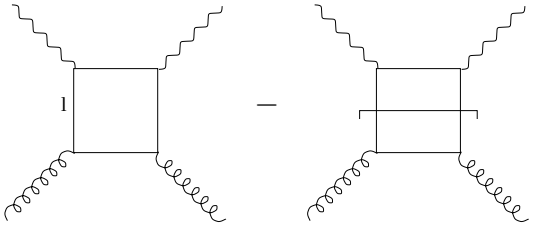

$\times$ Jacobian $\times$ cutoff function. (2)

The first term is an unsubtracted NLO graph. The subtraction corresponds to the approximation made in LO. Above the horizontal line, the following replacement for the internal momentum l^μ is made:

$$l \;\rightarrow\; \text{massless on-shell, zero transverse momentum} \tag{3}$$
$$\;\rightarrow\; \text{Lorentz-transformed momentum with correct final state.} \tag{4}$$

The first step is the standard approximation. The second step is needed to obtain the correct kinematics with conservation of 4-momentum. It is somewhat non-trivial to implement consistently since the subtraction term is needed when it is far from the collinear region. The bulk of my work in Refs. [4, 3] is about constructing a definite correct and consistent implementation. Correctness here means that the subtraction term is the order α_s approximation to the showering in the LO Monte Carlo algorithm.

Differences between conventional "analytic" method and Monte-Carlo method These differences can be illustrated by the following mathematical example. *Warning: In a number of respects this example is over-simplified.* For example, it does not take account of the parton densities. As explained in Ref. [4], the parton densities in the Monte Carlo are not in the usual $\overline{\rm MS}$ scheme. However, they are related to them by definite formulae.

Let the unapproximated unsubtracted integrand at NLO be

$$\frac{d\hat{\sigma}}{d^2k_T} = \frac{Q^2}{(Q^2+k_T^2+m^2)(k_T^2+m^2)}. \tag{5}$$

The conventional approach obtains the hard-scattering coefficient by setting the mass m to zero. The integral is then infinite, and a subtraction is inserted which consists of a delta function at $k_T = 0$ with an infinite coefficient. The result is a + distribution, which has a finite integral:

$$\frac{d\hat{\sigma}}{d^2k_T} \;=\; \frac{Q^2}{Q^2+k_T^2}\left(\frac{1}{k_T^2}\right)_+ \;=\; \frac{Q^2}{(Q^2+k_T^2)\,k_T^2} - C\delta^{(2)}(k_T), \tag{6}$$

where C is an infinite constant, defined with the aid, for example, of dimensional regularization.

In my new approach the subtracted integrand is

$$\frac{d\hat{\sigma}}{d^2k_T} \;=\; \frac{Q^2}{(Q^2+k_T^2)\,k_T^2} - \frac{f(k_T/\mu)J(k_T)}{k_T^2}, \tag{7}$$

where $f(k_T/\mu)$ is the previously mentioned cutoff function, which is unity for small k_T and zero for large k_T. As usual μ is the factorization scale. The factor $J(k_T)$ symbolizes the Jacobian that is necessary in the transformation from the variables appropriate for generation of events and the variables for the measured particles.

References

[1] C. Friberg and T. Sjöstrand, "Some thoughts on how to match Leading Log Parton Showers with NLO Matrix Elements", hep-ph/9906316, in Proceedings of the DESY Workshop on Monte Carlo Generators for HERA Physics, A.T. Doyle, G. Grindhammer, G. Ingelman, and H. Jung (eds.), (DESY, Hamburg, 1999) ISSN 1435-8077.

[2] For example,
M.H. Seymour, Comput. Phys. Commun. **90**, 95 (1995), hep-ph/9410414;
J. André and T. Sjöstrand, Phys. Rev. **D57**, 5767 (1998), hep-ph/9708390;
G. Corcella and M.H. Seymour, Phys. Lett. **B442**, 417 (1998), hep-ph/9809451;
G. Miu and T. Sjöstrand, Phys. Lett. **B449**, 313 (1999), hep-ph/9812455;
G. Corcella and M.H. Seymour, hep-ph/9908388.
S. Mrenna, hep-ph/9902471.

[3] J.C. Collins, "Monte-Carlo Event Generators at NLO", preprint in preparation.

[4] J. Collins, "Subtraction method for NLO corrections in Monte-Carlo event generators for leptoproduction", e-Print Archive: hep-ph/hep-ph/0001040.

NLO and NNLO Calculations

V. Del Duca and G. Heinrich

1 The NLO and NNLO program

QCD calculations of multijet rates beyond the leading order (LO) in the strong coupling constant α_s are usually quite involved. Nowadays we know (see Section 1.2) how to perform in general calculations of the next-to-leading order (NLO) corrections to multijet rates, and almost every process of interest has been computed to that accuracy. Instead, the calculation of the next-to-next-to-leading order (NNLO) corrections is still at an organizational stage and represents a main challenge. Why should we perform calculations which are technically so complicated ?

The general motivation is that the calculation of the NLO corrections allows us to estimate reliably a given production rate, while the NNLO corrections allow us to estimate the theoretical uncertainty on the production rate. This is achieved by reducing the dependence of the cross section on the renormalization scale, μ_R, and for processes with strongly-interacting incoming particles the dependence on the factorization scale, μ_F, as well.

An example is the determination of α_s from event shape variables in $e^+e^- \to 3$ jets [1]. Although the NLO contributions to $e^+e^- \to 3\,jets$ have been computed for some time now [2, 3], the NNLO contributions have yet to be obtained. A calculation of these NNLO contributions would be needed to further reduce the theoretical uncertainty in the determination of α_s.

We present in Section 1.1 an additional motivation for performing QCD calculations at NNLO, which is specific to the LHC program, and we outline in Section 1.2 how QCD calculations at NLO are implemented and in Section 1.3 how QCD calculations at NNLO could be performed.

1.1 Higgs production

The main goal of the LHC physics program is the investigation of the mechanism of the electroweak symmetry breaking, and namely the search and detection of the Higgs boson. If the Higgs boson is light (100 GeV $\leq m_H \leq$ 140 GeV), the rare decay channel in two photons, H$\to \gamma\gamma$, provides the best signature [4, 5, 6, 7]. Since the signal-to-background ratio is quite low ($\sim 7\%$), the analysis of this channel promises to be demanding. Our theoretical understanding of signal and background is still preliminary: the NLO QCD corrections to

the signal are known to be quite large ($\mathcal{O}(100\%)$) [8]. Also the QCD background $pp \to \gamma\gamma$, given at LO by the parton subprocess $q\bar{q} \to \gamma\gamma$, is known to NLO [9], with the full NLO fragmentation contributions having just been evaluated [10]. However, $pp \to \gamma\gamma$ receives a sizeble contribution from NNLO corrections because of the large gluon luminosity of the subprocess $gg \to \gamma\gamma$ appearing first at NNLO [11]. Thus in order to have a reliable theoretical estimate both the signal and the background need to be determined at least to NNLO accuracy.

In order to improve the signal-to-background ratio, Higgs production in association with a high transverse energy (E_T) jet, $p\,p \to H\,jet \to \gamma\gamma\,jet$, has been considered [12]. This production rate offers the advantage of being more flexible in choosing suitable acceptance cuts to curb the background. $p\,p \to H\,jet$ is known to LO exactly [13], while the NLO corrections [14] have been computed in the infinite top-mass limit. The NLO corrections to the signal are large. However, it is believed that the background, $p\,p \to \gamma\gamma\,jet$, can be more reliably calculated because LO production is dominated by the parton subprocess $q\,g \to q\,\gamma\gamma$, which benefits from the large gluon luminosity, while the subprocess $gg \to g\gamma\gamma$, which is believed to dominate the NNLO contribution, yields a comparatively smaller contribution [11, 15]. Thus, even though the signal, $p\,p \to H\,jet$, likely needs be computed at NNLO accuracy, it should suffice to evaluate the background, $p\,p \to \gamma\gamma\,jet$, at NLO. The NLO corrections to the background, though, have yet to be computed, with the appropriate QCD amplitudes having just been evaluated [16].

1.2 NLO algorithms and one-loop amplitudes

In recent years it has become clear how to construct general-purpose algorithms for the calculation of multijet rates at NLO accuracy. The crucial point is to organise the cancellation of the infrared (i.e. collinear and soft) singularities of the QCD amplitudes in a universal, i.e. process-independent, way. The universal terms in a NLO calculation are given by the tree-level splitting [17] and eikonal [18, 19] functions, and by the universal structure of the poles of the one-loop amplitudes [20, 21, 22]. The universal NLO terms and the process-dependent amplitudes are combined into effective matrix elements, which are devoid of singularities. The various NLO algorithms (phase-space slicing [20, 23], subtraction method [21, 24], dipole formalism [25] and subtraction-improved slicing [26]) provide different methods to construct the effective matrix elements. These can be integrated, analytically or otherwise numerically, in four dimensions. The integration can be performed with arbitrary experimental acceptance cuts.

Then the remaining work to be performed to calculate a production rate at NLO is to compute the appropriate tree and one-loop amplitudes. To compute n-jet production at NLO, two sets of amplitudes are required: *a*) n-particle production amplitudes at tree level and one loop; *b*) $(n+1)$-particle production amplitudes at tree level. If the one-loop amplitudes are regularised through dimensional regularization (DR) by evaluating them in $d = 4-2\epsilon$ dimensions, it suffices at NLO to compute them to $\mathcal{O}(\epsilon^0)$. As an example, in Fig. 1 we show the squared matrix elements which are required to calculate the NLO corrections to $e^+e^- \to 3\,jets$.

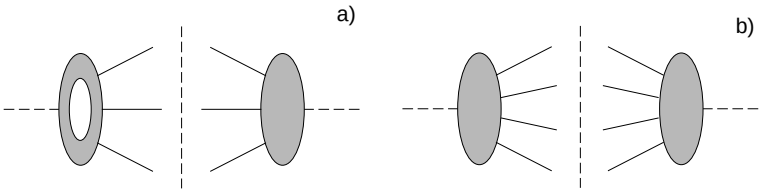

Figure 1: Squared matrix elements which contribute the NLO corrections to $e^+e^- \to 3\,jets$. The dashed line represents a massive vector boson, γ^*, W, Z. a) interference term between one-loop and tree amplitudes. The final-state partons are a $q\bar{q}$ pair and a gluon. b) square of a tree amplitude. The final-state partons are a $q\bar{q}$ pair and two gluons, or two $q\bar{q}$ pairs. In figure b) one of the partons is unresolved.

Efficient methods based on the color decomposition [27, 28, 29, 30] of an amplitude in color-ordered subamplitudes, which are then projected onto the helicity states of the external partons, have largely enhanced the ability of computing tree [31] and one-loop [32] amplitudes. Accordingly, tree amplitudes with up to seven massless partons [31, 33] and with a vector boson and up to five massless partons [34] have been computed analytically. In addition, efficient techniques to evaluate numerically tree multi-parton amplitudes have been introduced [35, 36], and have been used to compute tree amplitudes with up to eleven massless partons [36]. The calculation of one-loop amplitudes can be reduced to the calculation of one-loop n-point scalar integrals [37, 38]. The reduction method [37] allowed the computation of one-loop amplitudes with four massless partons [39] and with a vector boson and three massless partons [40]. However, one-loop scalar integrals present infrared divergences, induced by the massless external legs. For one-loop multi-parton amplitudes, the infrared divergences hinder the reduction methods of ref. [37, 38]. This problem has been overcome in ref. [41]. Accordingly, one-loop amplitudes with five massless partons [42, 43] and with a vector boson and four massless partons [44] have been computed analytically. The reduction procedure of ref. [41] has been generalised in ref. [45], where it has been shown that any one-loop n-point scalar integral, with $n > 4$, can be reduced to box scalar integrals, and that in the reduction of n-point tensor integrals, all higher dimensional ($d > 4 - 2\epsilon$) n-point integrals with $n > 4$ drop out. The calculation of one-loop multi-parton amplitudes thus can be pushed a step further in the near future.

1.3 NNLO calculations

Eventually, a procedure similar to the one followed at NLO will permit the construction of general-purpose algorithms at NNLO accuracy. It is mandatory then to fully investigate the infrared structure of the phase space at NNLO. The universal pieces needed to organise the cancellation of the infrared singularities are given by the tree-level double-splitting [46, 47, 29], double-eikonal [19, 48] and splitting-eikonal [46, 48] functions, by the one-loop splitting [49, 50] and eikonal [49] functions, and by the universal structure of the poles of the two-loop amplitudes [51]. These universal pieces have yet to be assembled together, to show the cancellation of the infrared divergences at NNLO.

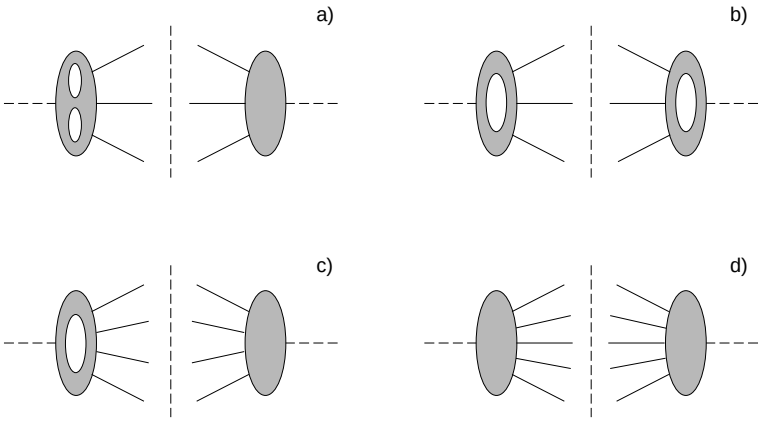

Figure 2: Squared matrix elements which contribute the NNLO corrections to $e^+e^- \to 3\,jets$. The dashed line represents a massive vector boson, γ^*, W, Z. $a)$ interference term between two-loop and tree amplitudes, and $b)$ square of a one-loop amplitude. In figures $a)$ and $b)$ the final-state partons are a $q\bar{q}$ pair and a gluon. $c)$ interference term between one-loop and tree amplitudes. The final-state partons are a $q\bar{q}$ pair and two gluons or two $q\bar{q}$ pairs. One of the partons is unresolved. $d)$ square of a tree amplitude. The final-state partons are a $q\bar{q}$ pair and three gluons, or two $q\bar{q}$ pairs and a gluon. Two of the partons are unresolved.

Then to compute n-jet production at NNLO, three sets of amplitudes are required: $a)$ n-particle production amplitudes at tree level, one loop and two loops; $b)$ $(n+1)$-particle production amplitudes at tree level and one loop; $c)$ $(n+2)$-particle production amplitudes at tree level. In Fig. 2 we show the squared matrix elements which are required to calculate the NNLO corrections to $e^+e^- \to 3\,jets$. In DR at NNLO, the two-loop amplitudes need be computed to $\mathcal{O}(\epsilon^0)$, while the one-loop amplitudes must be evaluated to $\mathcal{O}(\epsilon^2)$ [49, 52]. The main challenge is the calculation of the two-loop amplitudes. At present, the only amplitude known at two loops is the one for $V \leftrightarrow q\bar{q}$ [53], with V a massive vector boson, which depends only on one kinematic variable. It has been used to evaluate the NNLO corrections to Drell-Yan production [54] and to deeply inelastic scattering (DIS) [55]. No two-loop computations exist for configurations involving more than one kinematic variable, except in the case of maximal supersymmetry [56]. One of the main obstacles for configurations involving two kinematic variables is the analytic computation of the two-loop four-point functions with massless external legs, where significant progress has just been achieved. These consist of planar double-box integrals [57], non-planar double-box integrals [58], single-box integrals with a bubble insertion on one of the propagators [59] and single-box integrals with a vertex correction [60]. The two-loop four-point functions with massless external legs are needed for the computation of two-loop amplitudes in parton-parton scattering. Finally, the topical processes considered above, i.e. $e^+e^- \to 3\,jets$ and $pp \to H\,jet$ sport configurations involving three kinematic variables and require the analytic computation of two-loop four-point functions with a massive external leg. The two-loop four-point functions of this kind with up to five different denominators have been derived recently [61], while those with six and seven different propagators are still missing. Another obstacle is the

color decomposition of two-loop amplitudes, which is not known yet. Substantial progress is expected in the next future on all the issues outlined above, which should make the present note soon outdated.

Finally, we mention that in the factorization of collinear singularities [62] for strongly-interacting incoming particles, the evolution of the parton distribution functions (*pdf*'s) in the jet cross section should be determined to an accuracy matching the one of the parton cross section. For hadroproduction of jets computed at NLO, one needs the NLO, or two-loop, evolution of the *pdf*'s [63, 64, 65]. Accordingly for hadroproduction at NNLO the evolution of the *pdf*'s should be computed to NNLO, or three-loop, accuracy. Except for the lowest five (four) even-integer moments of the three-loop non-singlet (singlet) splitting functions [66], no calculation of the NNLO evolution of the *pdf*'s exists yet. However, NNLO analysis based on the finite set of known moments have been performed for xF_3 [67, 68] and F_2 (non-singlet [69] and singlet [70]). Furthermore, in ref. [71] a quantitative assessment of the importance of the yet unknown higher-order terms has been performed, with the conclusion that they should be numerically significant only for Bjorken-scaling $x < 10^{-2}$.

The computation of the evolution of the *pdf*'s at NNLO accuracy is a main challenge in QCD. The NLO computation was performed with two different methods, one using the operator product expansion (OPE) in a covariant gauge [63], the other using the light-cone axial (LCA) gauge with principal value prescription [64]. However, the prescription used in ref. [64] has certain shortcomings. Accordingly, the calculation has been repeated in the LCA gauge using a generally correct prescription [72], which makes it amenable to extensions beyond NLO. On the other hand, using the OPE method, there had been a problem with operator mixing in the singlet sector, which has been fixed[65] only recently, and the result finally coincides with the one obtained in the LCA gauge in ref. [64]. Thus the calculation of the *pdf* evolution at NLO accuracy is fully under control. Recent proposals for a calculation beyond NLO include extensions of the OPE technique, which have been used to recompute the NNLO corrections to DIS [73], and a computation of the *pdf* evolution by combining the universal gauge-invariant collinear pieces [74]. For the two-loop *pdf* evolution, e.g., they are the collinear pieces mentioned at the beginning of this section.

References

[1] By P.N. Burrows, et. al., in *New Directions for High Energy Physics: Proceedings Snowmass 96*, Eds., D.G. Cassel, L. Trindle Gennari and R.H. Siemann [hep-ex/9612012];
M. Schmelling, *Proc. of 28*$^{\rm th}$ *International Conf. on High Energy Physics*, Warsaw, eds. Z. Ajduk and A.K. Wroblewski, (World Scientific, 1997) [hep-ex/9701002];
S. Catani, Proc. of the 18th Symposium on Lepton-Photon Interactions, *LP97*, Hamburg, Germany, A. De Roeck and A. Wagner ed., World Scientific pub., 1998, [hep-ph/9712442].

[2] R.K. Ellis, D.A. Ross and A.E. Terrano, *Nucl. Phys.* **B178**, 421 (1981);
K. Fabricius, I. Schmitt, G. Kramer and G. Schierholz, *Phys. Lett.* **B97**, 431 (1980); *Z. Phys.***C11**, 315 (1981).

[3] P. Nason and Z. Kunszt, in *Z Physics at LEP1*, CERN Yellow report 89-08 (1989); G. Kramer and B. Lampe, *Z. Phys.* **C34**, 497 (1987); **C42**, 504(E) (1989); *Fortschr. Phys.* **37**, 161 (1989).

[4] ATLAS Collaboration, Technical Proposal, CERN/LHCC 94-43 (1994).

[5] ATLAS Collaboration, "Detector and Physics Performance", Technical Design Report, vol. II (1999).

[6] CMS Collaboration, Technical Proposal, CERN/LHCC 94-38 (1994).

[7] CMS Collaboration, Technical Design Report, CERN/LHCC 97-33 (1997).

[8] D. Graudenz, M. Spira and P. Zerwas, *Phys. Rev. Lett.* **70** (1993) 1372; A. Djouadi, D. Graudenz, M. Spira and P. Zerwas, *Nucl. Phys.* **B453** (1995) 17.

[9] B. Bailey, J.F. Owens and J. Ohnemus, *Phys. Rev. D* **46** (1992) 2018; B. Bailey and J.F. Owens, *Phys. Rev. D* **47** (1993) 2735.

[10] T. Binoth, J.Ph. Guillet, E. Pilon and M. Werlen, `hep-ph/9911340`.

[11] D. de Florian and Z. Kunszt, *Phys. Lett.* **B460**, 184 (1999) [hep-ph/9905283].

[12] S. Abdullin, et al., *Phys. Lett.* **B431** (1998) 410 [hep-ph/9805341].

[13] R.K. Ellis, I. Hinchliffe, M. Soldate and J.J. van der Bij, *Nucl. Phys.* **B297** (1988) 221.

[14] D. de Florian, M. Grazzini and Z. Kunszt, *Phys. Rev. Lett.* **82**, 5209 (1999) [hep-ph/9902483].

[15] C. Balazs, P. Nadolsky, C. Schmidt and C.P. Yuan, `hep-ph/9905551`.

[16] V. Del Duca, W.B. Kilgore and F. Maltoni, `hep-ph/9910253`.

[17] V.N. Gribov and L.N. Lipatov, *Yad. Fiz.* **15**, 781 (1972) [*Sov. J. Nucl. Phys.* **15**, 438 (1972)];
L.N. Lipatov, *Yad. Fiz.* **20**, 181 (1974) [*Sov. J. Nucl. Phys.* **20**, 94 (1975)];
G. Altarelli and G. Parisi, *Nucl. Phys.* **126**, 298 (1977);
Yu. L. Dokshitzer, *Zh. Eksp. Teor. Fiz.* **73**, 1216 (1977) [*Sov. Phys. JETP* **46**, 641 (1977)].

[18] D.R. Yennie, S.C. Frautschi and H. Suura, *Ann. Phys.* **13**, 379 (1961); A. Bassetto, M. Ciafaloni and G. Marchesini, *Phys. Rep.* **100**, 201 (1983).

[19] F.A. Berends and W.A. Giele, *Nucl. Phys.* **B313**, 595 (1989).

[20] W.T. Giele and E.W.N Glover, *Phys. Rev.* **D46**, 1980 (1992).

[21] Z. Kunszt and D.E. Soper, *Phys. Rev.* **D46**, 192 (1992).

[22] Z. Kunszt, A. Signer and Z. Trocsanyi, *Nucl. Phys.* **B420** (1994) 550 [hep-ph/9401294].

[23] W.T. Giele, E.W.N. Glover and D.A. Kosower, *Nucl. Phys.* **B403** (1993) 633 [hep-ph/9302225]; S. Keller and E. Laenen, *Phys. Rev.* **D59**, 114004 (1999) [hep-ph/9812415].

[24] S. Frixione, Z. Kunszt and A. Signer, *Nucl. Phys.* **B467**, 399 (1996) [hep-ph/9512328]; Z. Nagi and Z. Trocsanyi, *Nucl. Phys.* **B486**, 189 (1997) [hep-ph/9610498]; S. Frixione, *Nucl. Phys.* **B507**, 295 (1997) [hep-ph/9706545].

[25] S. Catani and M.H. Seymour, *Phys. Lett.* **B378**, 287 (1996) [hep-ph/9602277]; *Nucl. Phys.* **B485**, 291 (1997) (Erratum-*ibid.* **B510**, 503 (1998)) [hep-ph/9605323]; D.A. Kosower, *Phys. Rev.* **D57**, 5410 (1998) [hep-ph/9710213].

[26] W.T. Giele and W.B. Kilgore, *Phys. Rev.* **D55**, 7183 (1997) [hep-ph/9610433].

[27] J.E. Paton and H.-M. Chan, *Nucl. Phys.* **B10** (1969) 516; P. Cvitanovic, P.G. Lauwers, and P.N. Scharbach, *Nucl. Phys.***B186** (1981) 165; F.A. Berends and W.T. Giele, *Nucl. Phys.* **B294** (1987) 700; D.A. Kosower, B.-H. Lee and V.P. Nair, *Phys. Lett.* **B201** (1988) 85; M. Mangano, S. Parke and Z.Xu, *Nucl. Phys.* **B298** (1988) 653; M. Mangano, *Nucl. Phys.* **B309** (1988) 461; D. Zeppenfeld, *Int. J. Mod. Phys.* **A3** (1988) 2175; D.A. Kosower, *Nucl. Phys.* **B315**, 391 (1989).

[28] Z. Bern and D.A. Kosower, *Nucl. Phys.* **B362** (1991) 389.

[29] V. Del Duca, A. Frizzo and F. Maltoni, `hep-ph/9909464`.

[30] V. Del Duca, L. Dixon and F. Maltoni, `hep-ph/9910563`.

[31] M. Mangano and S.J. Parke, *Phys. Rep.* **200**, 301 (1991).

[32] Z. Bern, L. Dixon and D.A. Kosower, *Ann. Rev. Nucl. Part. Sci.* **46**, 109 (1996) [hep-ph/9602280].

[33] F.A. Berends, W.T. Giele and H. Kuijf, *Nucl. Phys.* **B333**, 120 (1990); H. Kuijf, Ph.D. Thesis (unpublished).

[34] F.A. Berends, W.T. Giele and H. Kuijf, *Nucl. Phys.* **B321**, 39 (1989).

[35] P. Draggiotis, R.H. Kleiss and C.G. Papadopoulos, *Phys. Lett.* **B439**, 157 (1998) [hep-ph/9807207].

[36] F. Caravaglios, M.L. Mangano, M. Moretti and R. Pittau, *Nucl. Phys.* **B539**, 215 (1999) [hep-ph/9807570].

[37] G. Passarino and M. Veltman, *Nucl. Phys.* **B160**, 151 (1979).

[38] W.L. van Neerven and J.A.M. Vermaseren, *Phys. Lett.* **B137**, 241 (1984); G.J. van Oldenborgh and J.A.M. Vermaseren, *Z. Phys.* **C46**, 425 (1990).

[39] R.K. Ellis and J.C. Sexton, *Nucl. Phys.* **B269**, 445 (1986).

[40] R.K. Ellis, D.A. Ross and A.E. Terrano, *Nucl. Phys.* **B178**, 421 (1981).

[41] Z. Bern, L. Dixon, D.A. Kosower, *Phys. Lett.* **B302**, 299 (1993) (Erratum-*ibid.* **B318**, 649 (1993)) [hep-ph/9212308]; *Nucl. Phys.* **B412**, 751 (1994) [hep-ph/9306240].

[42] Z. Bern, L. Dixon, D.A. Kosower, *Phys. Rev. Lett* **70**, 2677 (1993) [hep-ph/9302280]; *Nucl. Phys.* **B437**, 259 (1995) [hep-ph/9409393].

[43] Z. Kunszt, A. Signer and Z. Trocsanyi, *Phys. Lett* **B336**, 529 (1994) [hep-ph/9405386].

[44] Z. Bern, L. Dixon, D.A. Kosower, *Nucl. Phys. Proc. Suppl.* **51C**, 243 (1996) [hep-ph/9606378]; *Nucl. Phys.* **B513**, 3 (1998) [hep-ph/9708239]; Z. Bern, L. Dixon, D.A. Kosower and S. Weinzierl, *Nucl. Phys.* **B489**, 3 (1997) [hep-ph/9610370]; E.W.N. Glover and D.J. Miller, *Phys. Lett.* **B396**, 257 (1997) [hep-ph/9609474]; J.M. Campbell, E.W.N. Glover and D.J. Miller, *Phys. Lett.* **B409**, 503 (1997) [hep-ph/9706297].

[45] T. Binoth, J.Ph. Guillet and G. Heinrich, `hep-ph/9911342`.

[46] J.M. Campbell and E.W.N. Glover, *Nucl. Phys.* **B527**, 264 (1998) [hep-ph/9710255].

[47] S. Catani and M. Grazzini, *Phys. Lett.* **B446**, 143 (1999) [hep-ph/9810389].

[48] S. Catani and M. Grazzini, `hep-ph/9908523`.

[49] Z. Bern, V. Del Duca and C.R. Schmidt, *Phys. Lett.* **B445**, 168 (1998) [hep-ph/9810409]; Z. Bern, V. Del Duca, W.B. Kilgore and C.R. Schmidt, *Phys. Rev.* **D60**, 116001 (1999) [hep-ph/9903516].

[50] D.A. Kosower, *Nucl. Phys.* **B552**, 319 (1999) [hep-ph/9901201]; D.A. Kosower and P. Uwer, `hep-ph/9903515`.

[51] S. Catani, *Phys. Lett.* **B427**, 161 (1998) [hep-ph/9802439].

[52] Z. Bern and G. Chalmers, *Nucl. Phys.* **B447**, 465 (1995) [hep-ph/9503236].

[53] T. Matsuura, S.C. van der Marck, and W.L. van Neerven, *Phys. Lett.* **B211**, 171 (1988); R. Hamberg, T. Matsuura and W.L. van Neerven, *Nucl. Phys.* **B359**, 343 (1991).

[54] W.L. van Neerven and E.B. Zijlstra, *Nucl. Phys.* **B382**, 11 (1992).

[55] E.B. Zijlstra and W.L. van Neerven, *Nucl. Phys.* **B383**. 525 (1992); *Phys. Lett.* **B297**, 377 (1992).

[56] Z. Bern, J.S. Rozowsky, B. Yan, *Phys. Lett.* **B401**, 273 (1997) [hep-ph/9702424]; Z. Bern , L. Dixon, D.C. Dunbar, M. Perelstein and J.S. Rozowsky, *Nucl. Phys.* **B530**, 401 (1998) [hep-th/9802162].

[57] V.A. Smirnov, *Phys. Lett.* **B460**, 397 (1999) [hep-ph/9905323]; V.A. Smirnov and O.L. Veretin, `hep-ph/9907385`.

[58] J.B. Tausk, `hep-ph/9909506`.

[59] C. Anastasiou, E.W.N. Glover and C. Oleari, `hep-ph/9907523`.

[60] C. Anastasiou, E.W.N. Glover and C. Oleari, `hep-ph/9912251`.

[61] T. Gehrmann and E. Remiddi, `hep-ph/9912329`.

[62] J.C. Collins, D.E. Soper and G. Sterman in *Perturbative Quantum Chromodynamics*, ed. A.H. Mueller, World Scientific, Singapore, 1989.

[63] E.G. Floratos, D.A. Ross and C.T. Sachrajda, *Nucl. Phys.* **B129**, 66 (1977); Erratum-*ibid.* **B139**, 545 (1978); *ibid.* **B152**, 493 (1979); A. Gonzales-Arroyo, C. Lopez and F.J. Yndurain, *Nucl. Phys.* **B153**, 161 (1979); A. Gonzales-Arroyo and C. Lopez, *Nucl. Phys.* **B166**, 429 (1980); E.G. Floratos, C. Kounnas and P. Lacaze, *Phys. Lett.* **98B**, 89, 285 (1981).

[64] G. Curci, W. Furmanski and R. Petronzio, *Nucl. Phys.* **B175**, 27 (1980); W. Furmanski and R. Petronzio, Phys. Lett. **97B**, 437 (1980).

[65] R. Hamberg and W.L. van Neerven, *Nucl. Phys.* **B379**, 143 (1992); J.C. Collins and R.J. Scalise, *Phys. Rev.* **D50**, 4117 (1994) [hep-ph/9403231]; Y. Matiounine, J. Smith and W.L. van Neerven, *Phys. Rev.* **D57**, 6701 (1998) [hep-ph/9801224].

[66] S.A. Larin, T. van Ritbergen and J.A.M. Vermaseren, *Nucl. Phys.* **B427**, 41 (1994); S.A. Larin, P. Nogueira, T. van Ritbergen and J.A.M. Vermaseren, *Nucl. Phys.* **B492**, 338 (1997) [hep-ph/9605317].

[67] A. L. Kataev, A. V. Kotikov, G. Parente, A. V. Sidorov, *Phys. Lett.* **B388**, 179 (1996) [hep-ph/9605367]; *ibid.* **B417**, 374 (1998) [hep-ph/9706534]; S. I. Alekhin, A. L. Kataev, *Phys. Lett.* **B452**, 402 (1999) [hep-ph/9812348].

[68] A. L. Kataev, G. Parente, A. V. Sidorov, `hep-ph/9905310`.

[69] G. Parente, A. V. Kotikov, V. G. Krivokhizhin, *Phys. Lett.* **B333**, 190 (1994).

[70] J. Santiago, F.J. Yndurain, `hep-ph/9904344` and `hep-ph/9907387`.

[71] W.L. van Neerven and A. Vogt, `hep-ph/9907472`.

[72] G. Heinrich and Z. Kunszt, *Nucl. Phys.* **B519**, 405 (1998) [hep-ph/9708334]; A. Bassetto, G. Heinrich, Z. Kunszt and W. Vogelsang, *Phys. Rev.* **D58**, 094020 (1998) [hep-ph/9805283].

[73] S. Moch and J.A.M. Vermaseren, `hep-ph/9912355`.

[74] P. Uwer, Talk at the Europhysics Conference on High Energy Physics (EPS-HEP99), Tampere, Finland.

Jet Algorithms

S. Catani and D. Zeppenfeld

1 Jet algorithms

Jet algorithms have the task to assign streams of hadrons in hard scattering processes to a jet, who's energy, mass and momentum can then be related to a collection of partons in a perturbative QCD calculation. Although, at the experimental level, jets can be defined by using rather general and intuitive procedures, if we would like to compute jet cross sections and properties by using QCD perturbation theory, the definition of jets should fulfil stronger constraints to guarantee its perturbative safety. Perturbative safety means that the definition has to be infrared safe (jet properties cannot depend on the presence of arbitrarily soft partons), collinear safe (jet properties cannot change by replacing a parton with a set of collinear partons carrying the same total momentum) and collinearly factorizable (jet properties should be insensitive to partons radiated collinearly to the beam direction). If the jet definition is not perturbative safe, we cannot perform calculations order-by-order in perturbation theory because they are affected by uncancelled infrared divergences. Of course, in the full QCD theory (i.e. beyond perturbation theory) the perturbative divergences are regularized by small physical cutoffs related to hadron masses and the finite experimental resolution (size of calorimeter cells, energy thresholds, etc.). The physical cutoffs are always present, independently of the jet definition. However, in the case of a perturbative safe definition, their effects are suppressed by some inverse power of the jet transverse energy E_T, and thus they can be made small by sufficiently increasing E_T. This power suppression is not at work in perturbative unsafe jet definitions, where the effects of the small physical cutoffs can amount to large corrections (of order unity) to the perturbative results. Thus, perturbative safe definitions are preferred.

Jet algorithms start from a list of "particles" which we would like to freely associate with calorimeter cells or hadrons at the experimental level, and with partons in a QCD calculation. Each particle i carries a 4-momentum p_i^μ, which we take to be massless. The task is to select a set of particles which are emitted close to each other in angle and combine their momenta to form the momentum of a jet. The selection process is called the "jet algorithm", the momentum addition rule is called the "recombination scheme".

Let us start with a discussion of recombination schemes. In a hadron collider environment the arbitrary boost of the hard scattering system along the beam axis needs to be taken into account in the definition of angles to ensure collinear factorizability. This is achieved by using

transverse momentum, $p_T = \sqrt{p_x^2 + p_y^2}$, rapidity $y = 1/2 \log(E + p_z)/(E - p_z)$ and azimuthal angle ϕ of the massless particles as the kinematic variables. When adding the massless 4-vectors of particles we obtain massive objects which only approximately correspond to the massless partons which we would like to associate with jets at tree level.

One popular choice, the Snowmass convention [1], leaves the question of jet mass open, by only defining total transverse energy, rapidity and azimuthal angle of a set of parton momenta, as the E_T weighted sums of the individual particle variables. For the original massless particles $E_{Ti} = p_{Ti}$ and $\eta_i = y_i$. The corresponding recombined variables for a cluster of particles are then given by the total transverse energy

$$E_T = \sum_i E_{Ti} \ , \tag{1.1}$$

the cluster pseudorapidity

$$\eta = \sum_i \frac{E_{Ti}}{E_T} \ \eta_i \ , \tag{1.2}$$

and the azimuthal angle of the cluster

$$\phi = \sum_i \frac{E_{Ti}}{E_T} \ \phi_i \ . \tag{1.3}$$

Note that the designation of η as pseudorapidity is purely conventional. It corresponds to neither the pseudorapidity nor the rapidity of the massive cluster and is approximately equal to either only in the limit of small cluster mass ($<< E_T$). The concomitant loss of Lorenz invariance is a serious disadvantage of the Snowmass convention. Another serious problem appears in resummation calculations (see Sect. 2): the kinematic boundary of jet E_T shifts (from $\sqrt{\hat{s}}/2$ in e.g. dijet kinematics) when including additional final state partons.

Because of these shortcomings we formulate all jet algorithms in the 4-momentum recombination scheme (also called E-scheme) in the following, i.e. the kinematic variables of a cluster of particles is given by direct addition of the 4-momenta of the individual massless particles:

$$p^\mu = (E, p_x, p_y, p_z) = \sum_i p_i^\mu \ . \tag{1.4}$$

Since the resulting clusters have a clearly defined mass, we must distinguish transverse energy E_T from transverse momentum p_T, and pseudorapidity η from rapidity y. We define

$$p_T = \sqrt{p_x^2 + p_y^2} \ , \qquad \phi = \tan^{-1} \frac{p_x}{p_y} \ , \qquad y = \frac{1}{2} \log \frac{E + p_z}{E - p_z} \ , \tag{1.5}$$

The rapidity y and azimuthal ϕ should be used as the legoplot position of the jet when calculating its separation from other particles or jets. Auxiliary quantities are

$$\theta = \cos^{-1} \frac{p_z}{\sqrt{p_x^2 + p_y^2 + p_z^2}} \ , \qquad E_T = E \ \sin\theta \ , \qquad \eta = -\log \tan \frac{\theta}{2} \ . \tag{1.6}$$

1.1 The k_T algorithm

The k_T algorithm [2] is a successive recombination algorithm. The idea is to recombine particles with nearly parallel momenta, beginning with the softest particles in the sample. This recombination stops once all clusters of particles are separated by a distance larger than D in the legoplot. The k_T algorithm starts from a list of protojets and their momenta, p_i^μ, which in the beginning consists of the list of all particles:

(1) For each protojet i define

$$d_i = E_{Ti}^2 \tag{1.7}$$

and for each pair of protojets i, j define a distance

$$d_{ij} = \min(E_{Ti}^2, E_{Tj}^2)\frac{(y_i - y_j)^2 + (\phi_i - \phi_j)^2}{D^2} \ . \tag{1.8}$$

(2) Find the smallest of all d_i and d_{ij} and call it d_{min}.

(3) If d_{min} is d_{ij} then merge protojets i and j to form a new protojet k of momentum

$$p_k^\mu = p_i^\mu + p_j^\mu \tag{1.9}$$

(4) If d_{min} is d_i then remove protojet i from the protojet list and move it to the list of completed jets.

(5) Continue with step 1 until the list of protojets is empty.

The algorithm is infrared safe because it renders all soft partons harmless: it either takes them off the protojet list or it combines them with nearby harder partons. The only effect of the soft parton then is a shift in the momentum of the recombined cluster. However, this shift is small, disappearing in the infrared limit, which guarantees infrared safety. Also for collinear emission the algorithm is safe, because in the limit of zero angle between two partons, these two will have the smallest d_{ij} and will thus be combined early on in the recombination process, thus restoring the momentum of the almost on-shell parton from which they originated by splitting. Finally, every original particle is assigned to exactly one jet, i.e. there are no splitting/merging issues to be resolved for the k_T algorithm.

1.2 ILCA: an infrared safe cone algorithm

Cone algorithms are intended to cluster all energy within a given radius, R, around a point in the legoplot, to form jets. Naively, this procedure is both infrared and collinear safe: the effect of infrared radiation on the cluster momentum vanishes in the infrared limit, and the energy measured for the jet is the same whether a single particle is at the core of the cone or whether there has been collinear splitting. This naive expectation can easily be violated, however, by the prescription for selecting cones. Two examples illustrate this point [3].

Assume that cones are constructed around actual energy depositions only. In Fig. 1(a) two particles are emitted at a distance greater than the cone radius R but smaller than $2R$ and therefore are assigned to separate cones, which are then identified as two distinct jets. The only difference in Fig. 1(b) is the emission of a third soft particle (a "soft gluon") between the original two particles. Now the additional cone around the soft energy deposition encompasses all three particles and they will be classified as a single jet. The presence of a soft particle changes the classification of a hard event: this is an example for an infrared unsafe algorithm. In perturbation theory, at sufficiently high order, an arbitrary number of soft gluons will be radiated, hence, cones should be allowed anywhere in phase space to anticipate this feature of higher order corrections. An arbitrary restriction on allowed cone positions may lead to an infrared unsafe algorithm.

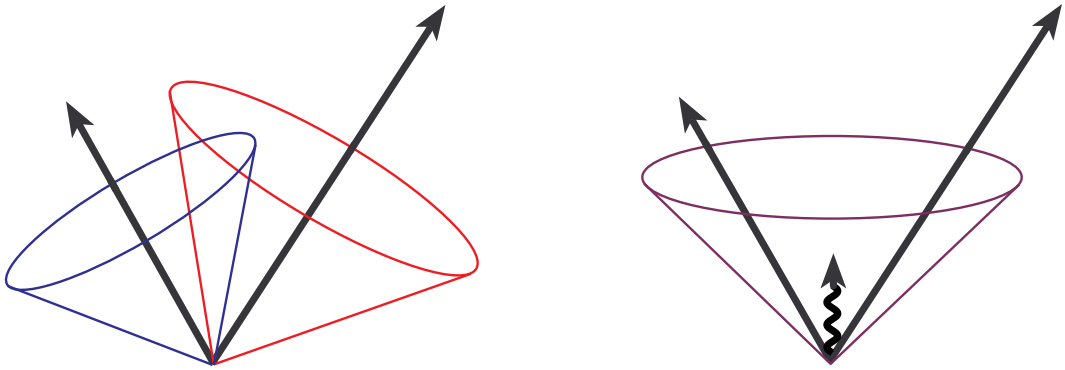

Figure 1: Example for a situation which can lead to infrared problems in an unsafe cone algorithm.

Similarly, an infinite number of collinear splittings occurs at higher order in perturbation theory. A possible collinear problem, resulting from E_T ordering of particles, is illustrated in Fig. 2. The difference between the two situations is that the central (hardest) parton may split into two almost collinear partons. On the left-hand-side the distance between the lateral partons is larger than R but the three hard partons all fall within a cone of radius R around the central parton, which happens to have the largest E_T. As a result, all three partons are recombined to a single jet. Collinear splitting renders the right hand parton to be the one with the largest E_T. Drawing the first cone around the highest E_T parton will recombine it with the two central partons and a separate jet is likely to be assigned to the remaining fourth parton. A differing jet number which depends on the presence or absence of collinear splitting must be avoided because the incomplete cancellation of the logarithmic divergences of real emission and virtual contributions will lead to a collinear unsafe jet algorithm. One can eliminate such ambiguities by making the selection or ordering of jet definition cones independent of the E_T of individual particles. Also, allowing trial cones anywhere in phase space would have made the two situations in Fig. 2 more similar: allowing cones centered between the central and the outside partons from the start would lead to a more similar jet

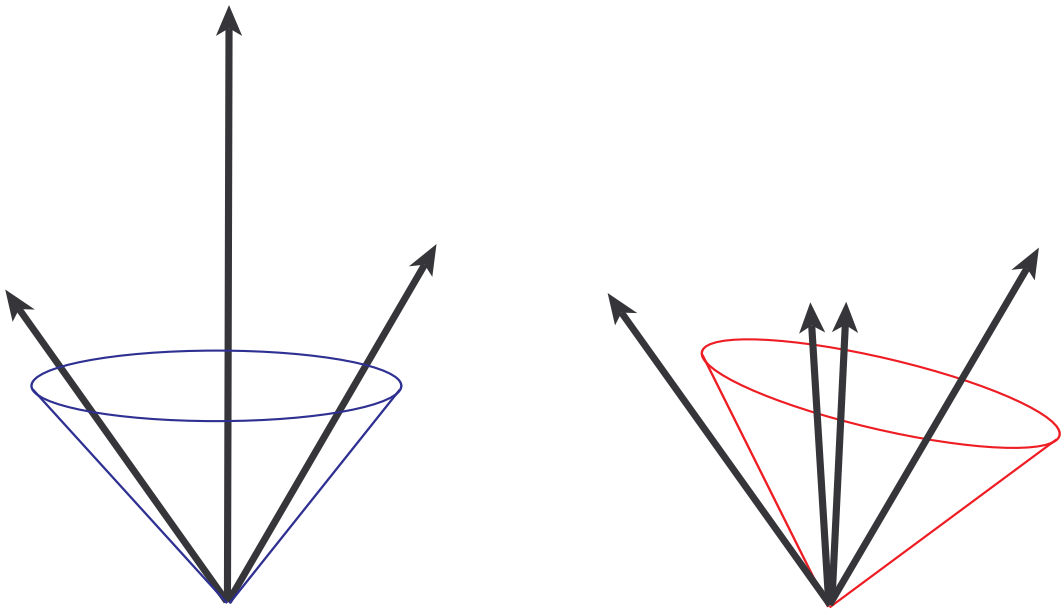

Figure 2: Example for a situation which can lead to collinear problems in an unsafe cone algorithm.

identification in the two cases.

The above considerations lead us to consider a cone algorithm which allows trial cones to be positioned anywhere in phase space, irrespective of the transverse momentum carried by individual particles or calorimeter cells. We start by formulating this seed-less algorithm at the calorimeter level, where the basic entities are calorimeter towers.

(0) Make a list of all calorimeter towers.

(1) Select the next tower on the list as the center of a trial cone of radius R.
Goto (4) if the list of towers is exhausted.

(2) Add the momenta of all towers inside the trial cone and determine the legoplot position (y, ϕ) corresponding to this momentum.

(3) If this position is outside the selected tower, discard the trial cone and go to (1).
If (y, ϕ) is inside the selected tower, add the set of towers inside the trial cone as a new entry to the list of protojets.

At this stage we have a list of protojets, and we need to split/merge them to make jets.

(4) Select the highest E_T protojet remaining on the list. (If the list is exhausted jet identification for the event is complete.)

(5) Does the selected protojet share any towers with other protojets?

(5.a) No: Move protojet to list of jets and continue with (4).

(5.b) Yes: Find the highest E_T protojet that shares towers with the selected protojet. (Call this the neighbor protojet.) Decide whether the E_T in the shared cells is greater than a fraction f of the E_T in the neighbor protojet.

(5.b.1) No: Split the shared towers.

(5.b.1.a) Allocate shared towers to either the selected or the neighbor protojet depending on which jet center is closer.

(5.b.1.b) Calculate the new momenta for the modified protojets, i.e. their E_T, and legoplot positions (y, ϕ). Continue with step (4).

(5.b.2) Yes: Merge the selected and neighbor protojets to form a new protojet. Add the momenta of both protojets and determine the total E_T and and the legoplot position (y, ϕ). Continue with step (4).

The procedure that defines the list of protojets is infrared and collinear safe. The additional steps completely define how to solve the problem of overlapping cones. The critical overlap fraction f is a free parameter of the algorithm and may be chosen as 50%, similar to the D0 choice in run I of the Tevatron (CDF uses 75%). The E_T-ordering of protojets in this split/merge step does not introduce collinear problems provided the cone size R is chosen sufficiently large.

The definition of calorimeter towers, i.e. a discretization of (y, ϕ) space, would be cumbersome in a theoretical calculation, and is indeed not necessary. In a perturbative calculation at fixed order, the maximal number, n, of partons is fixed. The only possible positions of stable cones are then given by the partitions of the n parton momenta, i.e. there are at most $2^n - 1$ possible locations of protojets. They are given by the legoplot positions of individual partons, all pairs of partons, all combinations of three partons etc. In a perturbative calculation, e.g. via a NLO Monte Carlo program, the protojet selection of the seedless algorithm (steps (0) to (3) above) can then be replaced as follows:

(0) Make a list of all possible cone centers. These are the legoplot coordinates of all parton momenta p_i, of all pairs of parton momenta $p_i + p_j$, of all triplets of parton momenta $p_i + p_j + p_k$, etc. For each cone center record which set of partons defines it.

(1) Select the next cone center on the list as the center of a trial cone of radius R. Goto (4) if the list of cone centers is exhausted.

(2) Add the momenta of all partons inside the trial cone and determine the legoplot position (y, ϕ) corresponding to this momentum.

(3) If this position is different from the trial cone center, i.e. if the cone center record and the list of partons inside the trial cone disagree, discard the trial cone and go to (1). If (y, ϕ) is the trial cone center, add the set of partons inside the trial cone as a new entry to the list of protojets.

As before, different protojets may share partons, i.e. they may overlap. The required split/merge step is then identical to the calorimeter level steps (4) and (5), with towers replaced by partons as elements of protojets.

In an actual experiment the number of calorimeter towers may be very large (order 6000 for tower sizes of $\Delta\eta \times \Delta\phi = 0.1 \times 0.1$ and an η coverage of ± 5 units of pseudorapidity). The calorimeter level algorithm may then be rather slow computationally. The question arises whether an acceptable approximation of the seedless algorithm can be constructed, analogous to the parton level short-cut, by considering only those towers which have energy depositions above a minimal seed threshold. One would like to replace the list of parton momenta above by the list of tower momenta with

$$p_{Ti} > E_{T,seed} \, . \tag{1.10}$$

Since the algorithm is infrared and collinear safe when $E_{T,seed} = 0$, it is always possible to chose the seed threshold $E_{T,seed}$ low enough so that variations of $E_{T,seed}$ lead to negligeable variations in any observable under consideration.

One would like to include in the determination of jet momenta all towers, of course, which lie inside the cone of radius R around the protojet axis. This requires an additional iteration of the cone axis in the parton level algorithm when a seed threshold is imposed. The steps leading to the definition of protojets can then be modified as follows:

(0) Make a list of all possible cone centers. These are the legoplot coordinates of all parton/tower momenta p_i with $p_{Ti} > E_{T,seed}$, of all pairs of such parton/tower momenta $p_i + p_j$, of all triplets $p_i + p_j + p_k$, etc.

(1) Select the next cone center on the list as the center of a trial cone of radius R. Goto (3) if the list of cone centers is exhausted.

(2) Add the momenta of all partons/towers inside the trial cone (also those with $p_{Ti} < E_{T,seed}$) and determine the legoplot position (y, ϕ) corresponding to this cone momentum. Use (y, ϕ) as the new center of the trial cone and iterate this step until the position is stable. The set of all towers/partons inside the final trial cone constitutes a new protojet. Continue with step (1).

(3) Eliminate all duplicate protojets, i.e. protojets with an identical set of towers/partons.

With these changes, the resulting algorithm (named Improved Legacy Cone Algorithm or ILCA) is quite close to those used in run I of the Tevatron. The main change is the inclusion of midpoints of seeds (the $p_i + p_j$ pairs) and of centers of larger numbers of seeds as additional seed locations for trial cones. Including these additional midpoints is absolutely crucial in perturbative calculations in order to achieve infrared safety (see discussion on Fig. 1). When dealing with data, these effects are somewhat diminished, because with sufficiently low seed thresholds $E_{T,seed}$, a large number of trial cones will be generated from actual soft energy depositions in the calorimeter. However, because these soft energy depositions will decide how many jets are reconstructed, one potentially introduces a high sensitivity of jet

observables to soft hadrons, Monte Carlo modelling of soft particles etc. The inclusion of the extra midpoints eliminates these soft effects because observables no longer depend on whether soft emission actually took place.

2 Resummed calculations

The ILCA and k_T-algorithm eventually lead to jets whose topology is not extremely different from that expected on the basis of a naive definition in terms of cones in azimuth-rapidity space. This is obviously true for the ILCA, where jets can contain particles whose distance is smaller than $2R$ and have a shape that differs from a cone-shape only because of the merging/splitting procedure. In the k_T-algorithm, jets have no sharp boundaries, but opening angles of particles within each jet are, typically, smaller than D and all opening angles between jets are larger than D. The detailed jet structure is, however, different in the two algorithms. Although both algorithms are perturbative safe, the differences show up in higher-order perturbative calculations.

Higher-order perturbative computations and, in particular, resummed calculations can be necessary in special kinematics configurations that lead to large logarithmically-enhanced contributions at any fixed order in perturbation theory. Typical examples are calculations of jet cross sections near the phase-space boundary and of the fine internal structure of jets (shape variables, subjets, etc.). These quantities can be strongly dependent on the jet definition. The corresponding perturbative calculations do strongly depend on the jet definition, because they are the result of the integration of the QCD matrix elements (which do not depend on jets) over phase-space regions whose boundaries depend on the fine details of jet kinematics.

As an example of this strong sensitivity, we can consider the one-jet inclusive cross section as a function of the transverse momentum p_T of the jet. *If* the jet variable p_T is defined by using the 4-momentum recombination scheme (see Eqs. (1.4)–(1.6)), the kinematical boundary is $x_T \leq 1$, where $x_T = 2p_T/\sqrt{S}$. Close to the boundary $x_T \sim 1$, the perturbative contributions are enhanced by large logarithmic corrections $(\alpha_S \log^2(1-x_T))^n$ that need to be resummed to all orders in α_S. Techniques to perform this resummation can be developed (see below). However, *if* the jet variable p_T is defined by using a recombination scheme that does not conserve the 4-momentum (e.g. the true p_T in Eq. (1.5) is replaced by the variable E_T in Eq. (1.1)), the kinematical boundary for x_T, although close to $x_T = 1$, is not fixed: the corresponding large logarithms cannot be resummed because the x_T-boundary shifts in a complicated manner depending on the number of final-state partons in the calculation [4].

The feasibility of resummed calculations depends not only on the recombination scheme but also on the jet algorithm, as is well known for jets in e^+e^- annihilation [5]. The jet definition of the k_T-algorithm is inspired by the parton shower picture of jet fragmentation [2]. Thus resummed calculations can be carried out by using the analytic version of the recurrence techniques used to generate multiparton final states in Monte Carlo parton showers. This is demonstrated by explicit calculations of subjet multiplicity and rates in hadron collisions [6]. The ILCA has still to be investigated in this respect. The two algorithms differ only slightly

at highly inclusive level [2]. Thus, in these cases (such as the large-x_T behaviour of the one-jet inclusive cross section), resummed calculations in the ILCA should be feasible as in the k_T-algorithm. Studies of the internal structure of ILCA jets may instead be more difficult since it depends on the procedure to merge/split overlapping jets.

3 Conclusions

During the Les Houches workshop discussions were centered on the general properties of jet algorithms, in particular their infrared and collinear safety at the perturbative level. The k_T-algorithm and the seedless cone algorithm described in Section 1.2 fulfil these requirements. Beyond these theoretical concerns there are many experimental issues which need to be addressed to obtain a practical algorithm. Among these are ease of energy calibration, effects of underlying event and overlapping events in a high luminosity hadron collider environment, high jet reconstruction efficiency, and efficient use of computer resources in reconstructing jets. These issues have been addressed in a parallel study, during the Run II QCD Workshop at Fermilab [7]. In particular it has been shown that the ILCA produces small corrections only, when compared with the jet algorithms used in run I of the Tevatron. We refer the reader to the Proceedings of the Run II Workshop for a detailed study of these effects.

References

[1] J. Huth et al., Proc. of the 1990 DPF Summer Study on High Energy Physics, Snowmass, CO, ed. by E. L. Berger (World Scientific, Singapore, 1992), p.134.

[2] S. Catani, Y. L. Dokshitzer, M. H. Seymour and B. R. Webber, Nucl. Phys. **B406**, 187 (1993); S. D. Ellis and D. E. Soper, Phys. Rev. **D48**, 3160 (1993).

[3] M.H. Seymour, Nucl. Phys. **B513**, 269 (1998).

[4] S. Catani and B. R. Webber, JHEP **9710**, 005 (1997) [hep-ph/9710333].

[5] N. Brown and W. J. Stirling, Phys. Lett. **B252**, 657 (1990); S. Catani, Y. L. Dokshitzer, M. Olsson, G. Turnock and B. R. Webber, Phys. Lett. **B269**, 432 (1991).

[6] M. H. Seymour, Phys. Lett. **B378**, 279 (1996) [hep-ph/9603281]; J. R. Forshaw and M. H. Seymour, JHEP **9909**, 009 (1999) [hep-ph/9908307].

[7] G. C. Blazey et al., *Run II Jet Physics*, contribution of the "Jet Physics" group to the proceedings of the workshop on *QCD and Weak Boson Physics* in preparation of Run II at the Fermilab Tevatron, March - November, 1999.

A Study of the Underlying Event in Jet and Minimum Bias Events

J. Huston and V. Tano

Abstract

In order to determine more accurately the energy contribution in a jet cone due to the underlying event, and in order to understand better the ambient event environment at both the Tevatron and the LHC, we have studied the energy distribution in a cone of radius 0.7 in both jet and in minimum bias events. We have compared the results from CDF data from Run 1b with results from `HERWIG` passed through the detector simulation program QFL [1].

1 Introduction

Due to the importance of the inclusive jet cross section as a test of perturbative QCD over a wide range of Q^2 values, it is necessary to carefully consider all systematic effects that influence its measurement. In addition to the hard interaction that produces the jets in the final state there is also an underlying event, originating mostly from $soft$ spectator parton interactions. Because of the softness of the scale, their contribution cannot be perturbatively calculated. There may also be a contribution due to $semi-hard$ interactions between spectator partons, which create $mini-jets$ at transverse momenta almost large enough for perturbative calculations, but much smaller than that of the primary interaction responsible for the highest E_T jets in the event. This process is known as double parton scattering. Both of the above processes, as well as higher order radiation from the 2→2 hard subprocess [2], contribute to the underlying event.

The experimental cross sections are most commonly compared to theoretical calculations at next-to-leading order (NLO) in the coupling constant α_s, such as JETRAD [3] or EKS [4]. At NLO, there can be at most 3 partons in the final state, leading to the presence of either 2 or 3 jets, depending on whether the third parton is present in the final state and whether it ends up being clustered with one of the other two partons. As the jet clustering is based on a fixed cone algorithm, the contribution due to the underlying event must be subtracted from the jet cone, in order to compare the results with NLO QCD calculations. As will be seen below, one of the largest sources of systematic error for the inclusive jet cross section at low E_T is due to the uncertainty on the subtraction of this underlying event.

The current 'paradigm' [1] is that the underlying event in jet events is similar to the average energy level found in 'active' minimum bias events. Thus, this energy level needs to be determined and subtracted from the energy in a jet cone before the jet data is compared to NLO theory predictions. CDF assumes an uncertainty of 30% on this underlying event subtraction which makes it the dominant error at low E_T.

The flip side of the above 'paradigm' is that the underlying event energy in a jet event (once the two leading jets have been subtracted) should be the sum of the minimum bias level contribution and the third parton in the NLO calculation. The preliminary results of a study in CDF designed to test the accuracy of these assumptions are described in this section.

In this section, the experimental results will be compared to the HERWIG [5] Monte Carlo which has the $2 \rightarrow 2$ matrix elements for jet production, parton showering in the initial and final state, and a model for the underlying event. The ultimate result from HERWIG consists of the 4-vectors of the final state hadrons. In HERWIG the soft underlying event in the hadron-hadron collision is assumed to be a soft collision between the two 'beam clusters', which contain the spectators from the incoming hadrons. The model for the simulation of underlying event uses the $p\bar{p}$ event generator from the UA5 Collaboration, which is modified to make use of the HERWIG fragmentation algorithm.

The results from HERWIG can be quoted at the parton level (excluding the soft underlying event portion), the hadron level and/or comparisons can be made at the detector level after the Monte Carlo hadrons are passed through the CDF detector simulation program QFL [6]. For most of the results that we will be reporting, the QFL comparisons will be crucial.

To summarize, the purpose of this analysis is to examine in detail the underlying event in jet events and to understand whether the amount subtracted from the jet cones is correct and whether the uncertainty assumed can be reduced. In addition, a test will be made as to how well HERWIG models the underlying event energy in jet events as well as in minimum bias events.

2 Underlying Energy at 90^0 in jet events

Events generated with HERWIG were passed through QFL. The HERWIG code was adapted to produce the same information as found in the data samples. This information includes the energy, the position and the number of calorimeter towers of the jets in the event, together with the energy and the number of towers in two cones situated at $\pm 90^0$ in ϕ and at the same η as the leading jet. ϕ and η are respectively the azimuthal and polar angle.

For each jet event, two cones of radius 0.7 at $\eta = \eta_{LeadJet}$ and $\phi = \phi_{LeadJet} \pm \frac{\pi}{2}$ were examined. The energy in each cone was determined for two different calorimeter tower thresholds: 50 and 100 MeV. A cut of 100 MeV on tower energies is typically used for jet analyses. For most of the comparisons to follow, a 50 MeV cut was used, though, since we are interested in possible contributions to the tower energies from a number of different sources. The two cones were used to study the underlying event energy because they are

[1] Dave Soper claims that this term is vastly overused but we choose to employ it anyway.

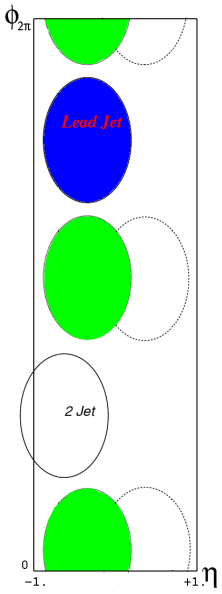

Figure 1: An example of the cones under investigation in the central calorimeter region. The dotted cones are at $\eta = \eta_{LeadJet}$ and $\phi = \phi_{LeadJet} \pm \frac{\pi}{2}$, while dashed cones are at $\eta = -\eta_{LeadJet}$ and $\phi = \phi_{LeadJet} \pm \frac{\pi}{2}$. $|\eta| < 1.$, $0^0 < \phi < 360^0$.

supposed to be in a semi-quiet region, far away from the two leading jets, but still in the central rapidity region. Given the non-uniform response of the CDF detector as a function of rapidity, the latter criterion is essential. The leading jet was required to be in the central region, $|\eta| < 0.7$, the same as in the inclusive jet analysis. No requirement was made on the location of the second jet. In Fig 1 the calorimeter central region is shown as 'unrolled'; η ranges are between -1 and +1, while ϕ goes from 0^0 to 360^0. The leading jet cone and the two cones under study are shown.

The E_T distributions inside the two cones provide an idea of the contribution of the underlying event in the jet cone. For each event the cone which has the maximum energy and the cone with the minimum energy were labelled. This is useful because NLO perturbative corrections to the $2 \rightarrow 2$ hard scattering can contribute only to one of these two regions [8]. The difference between the maximum and the minimum cone provides information on this contribution, while the minimum cone gives an indication of the amount of underlying event. The (roughly constant) underlying event contribution should be suppressed in the difference.

The data were required to have one and only one vertex in order to insure that there is only one interaction per event. A similar cut was made in the simulation. In Figure 2 the transverse energy inside the two cones (max and min) is plotted as a function of the E_T of the leading jet. It can be clearly observed that `HERWIG` and the data have a similar behaviour for the max and min cone; the min cone stays flat while the max cone increases with the E_T of the leading jet. The increase of the max cone energy with increasing jet E_T is easily understandable. What may be surprising is the flatness of the min cone energy as the lead

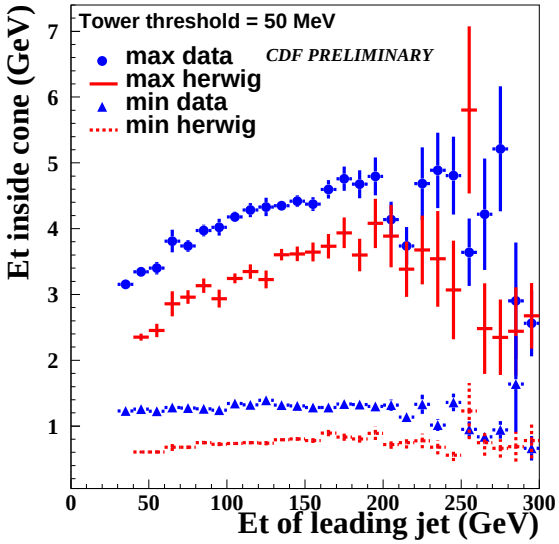

Figure 2: E_T inside the max and min cones as a function of the E_T of leading jet. Both the data and HERWIG distributions are plotted.

jet transverse energy increases. Contrary to the pronouncements of some of the politicians of our day, a rising tide does not raise all boats (or cones), but instead favors the cone in the highest tax bracket. Of course, the division into a max and min cone partially encourages this effect through selection. However, the level of flatness is still somewhat surprising.

It is evident that there is an offset between data and the HERWIG+QFL simulation of about 800 MeV for the max cone and 500 MeV for the min cone. If the tower threshold is increased from 50 to 100 MeV, the transverse energy decreases by about 180 MeV in the data (both cones), while in HERWIG the transverse energy decreases by about 70 MeV in the max cone and 40 MeV in the min cone.

The difference between the transverse energy in the max and in the min cones has a similar trend in both data and simulation(Figure 3). There is still an offset but the offset decreases to about 300 MeV. It appears that the max-min distribution starts going down again at very high E_T (perhaps due to kinematic suppression), although the statistics become poor.

In Figure 4 the E_T frequency distributions for data and HERWIG+QFL are compared for four different jet sub-samples. In this plot, the E_T values for max-min are plotted, for both data and HERWIG+QFL. The number of entries is scaled to easily allow a direct comparison. The E_T distribution of the max-min cone for HERWIG+QFL looks very similar to that of the data. Here the contribution of the underlying event as minimum bias data is presumably removed.

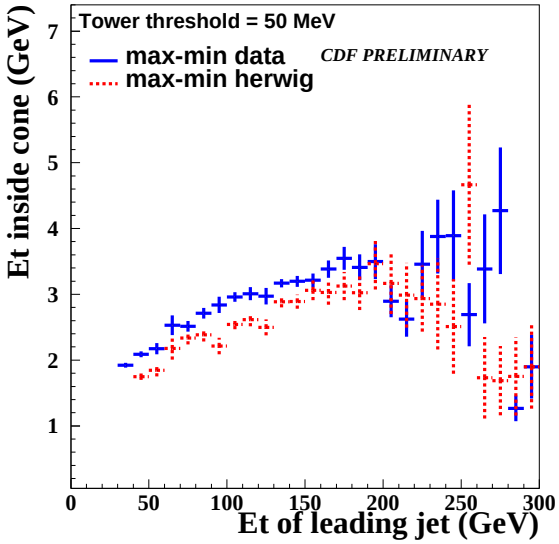

Figure 3: The difference between E_T inside the max and min cones as a function of the E_T of the leading jet. Both the data and HERWIG distributions are plotted.

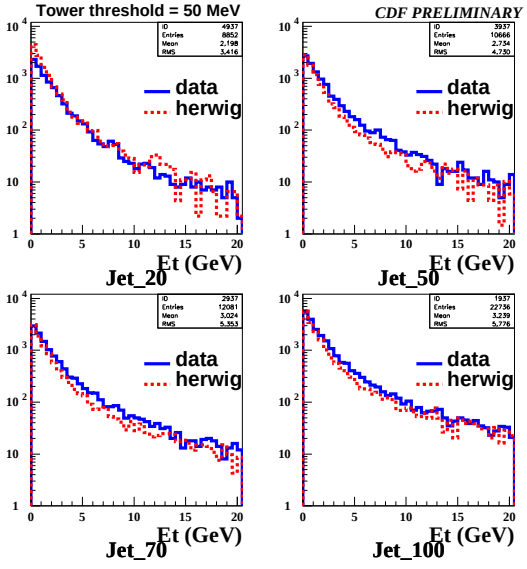

Figure 4: The frequency distribution for the difference between E_T in the max cone and E_T in the min cone. Solid line: data, dashed line: HERWIG. The calorimeter tower energy threshold is 50 MeV.

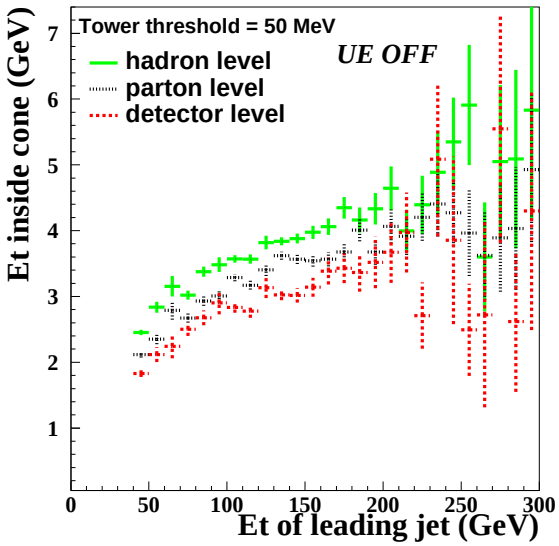

Figure 5: The parton-hadron-detector level for E_T in the max cone is plotted as a function of the E_T of the leading jet. The underlying event in HERWIG is switched off.

2.1 Parton-Hadron-Detector level

With HERWIG (unlike the data), we have the advantage of being able to examine the energy distributions not only at the detector level, but also at the hadron and parton levels. The HERWIG model for the soft underlying event, though, does not show any effect at the parton level because the energy contribution is calculated directly at the hadron level. In the following discussion, in order to examine the differences between hadron, detector and parton level, the underlying event in HERWIG has been switched off.

Figures 5 and 6 show the transverse energy inside the max and min cones at $\eta = \eta_{LeadJet}$ and $\phi = \phi_{LeadJet} \pm \frac{\pi}{2}$ as a function of the leading jet transverse energy at the parton, hadron and detector level. The lead jet is always in the central region. Because of the degradation due to the detector response, the amount of energy is higher at the hadron level than at the detector level.

It is also interesting to note that the hadron level energy is larger than the parton level energy, by the order of several hundred MeV. This is due to hadronization effects of the partons produced in or near the lead and second jet cones. Most of the hadronization effects come from resonance production ($\rho, A_1, A_2, ...$) and their subsequent decays. The hadronization effects from the partons inside the jet cone have previously been termed "splashout". It is important to note that this splashout is not currently taken into account in either the CDF or D0 jet analyses. Both experiments implicitly assume that the hadron and parton levels produce the same energy in the jet cone. This is especially relevant for low E_T jet production.

In order to evaluate to what level resonance decays influence the energy inside the two

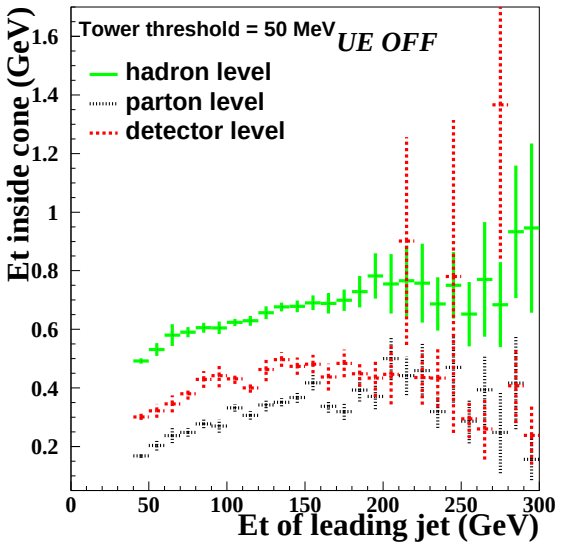

Figure 6: The hadron-parton-detector level for E_T in the min cone is plotted as a function of the E_T of the leading jet. The underlying event in HERWIG is switched off. Note that the E_T at the hadron level is always greater than the E_T at the parton level.

cones at 90^0 from the leading jet, all resonance decays are switched off and the energy in the cones were examined at both the parton and the hadron level. The difference of E_T inside the min cone (between hadron and parton level) decreases from an average of 300 MeV to 100 MeV, while the difference in the max cone goes from 500 MeV to 100 MeV.

3 Underlying Energy in minimum bias events

The model used in HERWIG to simulate minimum bias events is the same as used for the soft underlying energy in hard scattering events. Minimum bias events were studied in order to see if the reason for the offset observed between the data and simulation results from the HERWIG description of the soft underlying event. The minimum bias events generated with HERWIG were passed through the detector simulation program QFL and the information on the energy released in the calorimeter towers stored.

The amount of transverse energy in the calorimeter, in a random cone of radius 0.7 that is required to be in the central region ($|\eta| < 0.7$), was determined. The transverse energy distributions for the two different tower thresholds are summarized in Table 1 where a comparison with data also can be found.

The offset of about 650 MeV between data and HERWIG is slightly higher than the one found comparing the min cones in the jet events.

Table 1: A comparison of data and HERWIG for minimum bias events. The average amount of transverse energy in a cone of radius 0.7 is shown. Thresholds are in Mev, results are in GeV.

Thresholds	DATA	HERWIG	DATA-HERWIG
50	1.05	.37	.68
100	.92	.35	.57

4 E_T summed in the central region (Swiss Cheese)

For these comparisons, the transverse energy in every calorimeter tower in the central region ($|\eta| < 1$) is summed, excluding the towers in a radius 0.7 from the center of the two (or three) most energetic jets in the event:

$$Sum\ of\ E_T = \sum_{towers} E_T^{towers} - \sum_{2/3jets} \left[\sum_{towers} E_T^{towers_{jet}} \right]$$

where $E_T^{towers_{jet}}$ are all the towers in a radius 0.7 from the center of the jet. We require $E_{TJet} > 5$ GeV. This configuration has been labelled 'Swiss cheese' [2].

There are an average of between 2 and 2.5 jets in the central rapidity region, with this average having a slight slope as a function of the lead jet transverse energy. The Swiss cheese energy in the central region is plotted in Fig 7 at the hadron, parton and detector level. The approximate minimum bias level for HERWIG and data is shown with a flat line on the picture. In the simple picture presented earlier, and on which the CDF and D0 jet analyses are based, the difference between the Swiss cheese energy with two jets subtracted and the minimum bias level should be proportional to the NLO (third parton) contribution. The Swiss cheese level with three jets subtracted should have little or no NLO contribution and can be directly compared to the minimum bias data level. The 3-jet subtracted Swiss cheese energy is larger than the minimum bias level and there is a small slope as a function of the lead jet E_T (the offset varies from 6-8 GeV over the E_T range). This indicates perhaps that there is more complexity here than in the simple picture. Other possible contributions to the Swiss cheese energy include hadronization from the jets ("splashout"), double parton scattering and higher order radiation effects.

As was done for the min and max cone studies, the underlying event in HERWIG can be switched off and the hadron/detector level in the Swiss Cheese plots compared when the resonance decay is not allowed. At the hadron level, when the resonance decay is not allowed, we find about 1.5 GeV energy less then when allowing the resonance decay. This implies a 600-700 MeV contribution of splashout per jet (again at the detector level) to the Swiss cheese energy.

The comparison of the Swiss cheese results for the data and HERWIG+QFL is complex and its interpretation is continuing.

[2] Or specifically Emmental

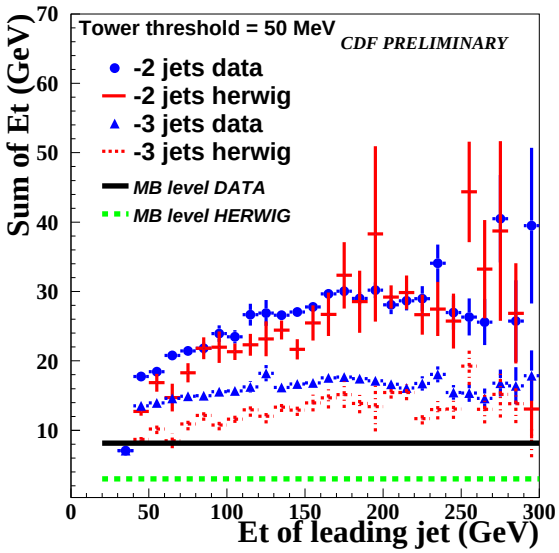

Figure 7: Sum of E_T. The two and three most energetic jets in the events are subtracted from the total transverse energy in the central calorimeter region. Both data and HERWIG results are shown.

5 Conclusions and where do we go from here

The energy from the underlying event is not perturbatively calculable and must be subtracted from a jet cone in order for comparisons to be made to NLO calculations. Because of the ambiguous definition of what constitutes this underlying event, a relatively large uncertainty has been assigned to the value of this subtraction. In order to study the underlying event, we have considered two cones in the calorimeter far away from the leading jet and we examined the energy in the cones, both in the CDF data and with the HERWIG simulation. We discovered that both the data and HERWIG exhibited a similar behaviour for the max and the min cone; the min cone stays flat, while the max cone increases as a function of the leading jet E_T. There is an offset, however, of about 500 MeV for the min and of 800 MeV for the max cone between data and HERWIG. If we examine the difference between the max and min cones, where the underlying event energy contribution should be minimized, we find very similar distributions for data and HERWIG. In minimum bias, the HERWIG model predicts a level of energy substantially below the one found in minimum bias data (400 MeV compared to 1 GeV). Part of this difference is due to the lack of any kind of hard interaction in the minimum bias model.

With HERWIG we investigated max/min cone distributions at the parton, hadron and detector level and we found out that the energy inside the cones is higher at the hadron then at the parton level. This is mainly due to resonance decay.

An improved understanding of the underlying event is desired for a number of reasons:

- The underlying event subtraction is the largest uncertainty for the jet cross section

at low transverse energy (below 60 GeV). In order to have a good comparison of the data with theory, a better understanding of the proper level of this subtraction must be obtained. This uncertainty is especially important for the measurement of the jet cross section at 630 GeV, since most of the data points are below 60 GeV, and similar considerations to those at 1800 GeV also apply.

- This analysis probes the interface between perturbative and non-perturbative QCD, an arena where a great deal of work still needs to be done.
- The authors of the Monte Carlo programs are trying to predict the environments for physics measurements at the LHC. This can be difficult/uncertain without the proper understanding of what is happening at the Tevatron.

This analysis will be extended to the jet and minimum bias data taken at 630 GeV by CDF. It will be especially interesting to observe the level of agreement of the `HERWIG` minimum bias predictions with the CDF data, given that the `HERWIG` model parameters were determined from the UA5 taken at a similar energy. It may be that there is an increase in the semi-hard component of minimum bias energy when going from 630 to 1800 GeV. After the comparisons at 630 and 1800 GeV are complete, extrapolations will made made to LHC energies for the underlying event in both jet and minimum bias events.

6 Acknowledgements

This work was performed in conjunction with our colleagues on CDF, Anwar Bhatti and Eve Kovacs.

References

[1] More details on this analysis can be found at the CDF QCD website: http://www-cdf.fnal.gov/physics/new/qcd/QCD.html .

[2] Jon Pumplin, *Phys. Rev.* **D57**, 5787 (1998); `hep-ph/9708464`.

[3] W.T. Giele, E.W.N. Glover, David A. Kosower, *Nucl. Phys.* **B403**, 633 (1993).

[4] S. Ellis, Z. Kunszt, D. Soper, *Phys. Rev. Lett.* **69**, 3615 (1992).

[5] `HERWIG`, G. Marchesini, B.R. Webber, G. Abbiendi, I.G. Knowles, M.H. Seymour and L.Stanco, *Computer Phys. Commun.* **67**, 465 (1992).

[6] M. Shapiro et al., CDF-1810 (1992).

[7] Anwar Bhatti, CDF-4440 (1998).

[8] G. Marchesini and B.R. Webber, *Phys. Rev.* **D38**, 3419 (1988).

[9] Jon Pumplin, (private communication).

Isolated Photon Production

S. Frixione and W. Vogelsang

1 Isolated-photon production

1.1 General features of photon production at colliders

When mentioning the photon in the framework of high-energy collider physics, one is immediately led to think – with good reasons – to Higgs searches through the gold-plated channel $H \to \gamma\gamma$. However, the production of photons also deserves attention on its own. Firstly, a detailed understanding of the continuum two-photon production is crucial in order to clearly disentangle any Higgs signals from the background. Secondly, in hadronic collisions, where a very large number of strong-interacting particles is produced, photon signals are relatively clean, since the photon directly couples only to quarks. Therefore, prompt-photon data can be used to study the underlying parton dynamics, in a complementary way with respect to analogous studies performed with hadrons or jets. For the same reason, these data represent a very important tool in the determination of the gluon density in the proton, $g(x)$. Indeed, in recent years almost all the *direct* information (that is, not obtained through scaling violations as predicted by Altarelli-Parisi equations) on the intermediate- and high-x behaviour of $g(x)$ came from prompt-photon production, $pp \to \gamma X$ and $pN \to \gamma X$, in fixed-target experiments. The main reason for this is that, at leading order, a photon in the final state is produced in the reactions $qg \to \gamma q$ and $q\bar{q} \to \gamma g$, with the contribution of the former subprocess being obviously sensitive to the gluon and usually dominant over that of the latter. It is the 'point-like' coupling of the photon to the quark in these subprocesses that is responsible for a much cleaner signal than, say, for the inclusive production of a π^0, which proceeds necessarily through a fragmentation process.

There is, however, a big flaw in the arguments given above. In fact, photons can also be produced through a fragmentation process, in which a parton, scattered or produced in a QCD reaction, fragments into a photon plus a number of hadrons. The problem with the fragmentation component in the prompt-photon reaction is twofold: first, it introduces in the cross section a dependence upon non-perturbative fragmentation functions, similar to those relevant in the case of single-hadron production, which are not calculable in perturbative QCD and are, at present, very poorly determined by the sparse LEP data available. Secondly, *all* QCD partonic reactions contribute to the fragmentation component; thus, when

addressing the problem of the determination of the gluon density, the advantage of having a priori only one partonic reaction ($q\bar{q} \to \gamma g$) competing with the signal ($qg \to \gamma q$) is lost, even though some of the subprocesses relevant to the fragmentation part at the same time result from a gluon in the initial state.

The relative contribution of the fragmentation component with respect to the direct component (where the photon participates in the short-distance, hard-scattering process) is larger the larger the center-of-mass energy and the smaller the final-state transverse momentum [1]: at the LHC, for transverse momenta of the order of few tens of GeV, it can become dominant. However, here the situation is saved by the so-called 'isolation' cut, which is imposed on the photon signal in experiments. Isolation is an experimental necessity: in a hadronic environment the study of photons in the final state is complicated by the abundance of π^0's, eventually decaying into pairs of γ's. The isolation cut simply serves to improve the signal-to-noise ratio: if a given neighbourhood of the photon is free of energetic hadron tracks, the event is kept; it is rejected otherwise. Fortunately, by requiring the photon to be isolated, one also severely reduces the contribution of the fragmentation part to the cross section. This is because fragmentation is an essentially collinear process: therefore, photons resulting from parton fragmentation are usually accompanied by hadrons, and are therefore bound to be rejected after the imposition of an isolation cut.

Thus, the fragmentation contribution, that threatened to spoil the cleanliness of the photon signals at colliders, is relatively well under control in the case of isolated-photon cross sections. There is of course a price to pay for this gain: the isolation condition poses additional problems in the theoretical computations, which are not present in the case of fully-inclusive photon cross sections. This topic will be the argument of the next subsection.

1.2 Isolation prescriptions

Consistently with what written above, we write the cross section for the production of an isolated-photon in hadronic collisions as follows:

$$
\begin{aligned}
&d\sigma_{AB}(K_A, K_B; K_\gamma) = \\
&\quad \int dx_1 dx_2 f_a^{(A)}(x_1, \mu_F) f_b^{(B)}(x_2, \mu_F) d\hat{\sigma}^{isol}_{ab,\gamma}(x_1 K_A, x_2 K_B; K_\gamma; \mu_R, \mu_F, \mu_\gamma) \\
&+ \int dx_1 dx_2 dz f_a^{(A)}(x_1, \mu'_F) f_b^{(B)}(x_2, \mu'_F) d\hat{\sigma}^{isol}_{ab,c}(x_1 K_A, x_2 K_B; K_\gamma/z; \mu'_R, \mu'_F, \mu_\gamma) D_\gamma^{(c)}(z, \mu_\gamma) \qquad (1.1)
\end{aligned}
$$

where A and B are the incoming hadrons, with momenta K_A and K_B respectively, and a sum over the parton indices a, b and c is understood. In the first term on the RHS of eq. (1.1) (the direct component) the subtracted partonic cross sections $d\hat{\sigma}^{isol}_{ab,\gamma}$ get contributions from all the diagrams with a photon leg. On the other hand, the subtracted partonic cross sections $d\hat{\sigma}^{isol}_{ab,c}$ appearing in the second term on the RHS of eq. (1.1) (the fragmentation component), get contribution from the pure QCD diagrams, with one of the partons eventually fragmenting

[1] Actually, in the fixed-target $pp \to \gamma X$ reaction, one can see the fragmentation component increasing relatively to the direct one also at very *large* $p_{T\gamma}$, because of the direct cross section dying out very quickly at such momenta. This effect is of no phenomenological relevance at the LHC.

in a photon, in a way described by the parton-to-photon fragmentation function $D_\gamma^{(c)}$. As the notation in eq. (1.1) indicates, the isolation condition is embedded into the partonic cross sections.

It is a well-known fact that, in perturbative QCD beyond leading order, and for all the isolation prescriptions known at present, with the exception of that of ref. [2], neither the direct nor the fragmentation components are *separately* well defined at any fixed order in perturbation theory: only their sum is physically meaningful. In fact, the direct component is affected by quark-to-photon collinear divergences, which are subtracted by the bare fragmentation function that appears in the unsubtracted fragmentation component. Of course, this subtraction is arbitrary as far as finite terms are concerned. This is formally expressed in eq. (1.1) by the presence of the same scale μ_γ in both the direct and fragmentation components: a finite piece may be either included in the former or in the latter, without affecting the physical predictions. The need for introducing a fragmentation contribution is physically better motivated from the fact that a QCD hard scattering process may produce, again through a fragmentation process, a ρ meson that has the same quantum numbers as the photon and can thus convert into a photon, leading to the same signal.

As far as the isolation prescriptions are concerned, here we will restrict to those belonging to the class that can be denoted as 'cone isolations' [1]. In the framework of hadronic collisions, where the need for invariance under longitudinal boosts suggests not to define physical quantities in terms of angles, the cone is drawn in the pseudorapidity–azimuthal angle plane, and corresponds to the set of points

$$\mathcal{C}_R = \left\{ (\eta, \phi) \mid \sqrt{(\eta - \eta_\gamma)^2 + (\phi - \phi_\gamma)^2} \leq R \right\}, \tag{1.2}$$

where η_γ and ϕ_γ are the pseudorapidity and azimuthal angle of the photon, respectively, and R is the aperture (or half-angle) of the cone. After having drawn the cone, one has to actually impose the isolation condition. We consider here two sub-classes of cone isolation, whose difference lies mainly in the behaviour of the fragmentation component. Prior to that, we need to define the total amount of hadronic transverse energy deposited in a cone of half-angle R as

$$E_{T,had}(R) = \sum_{i=1}^{n} E_{Ti} \theta(R - R_{\gamma i}), \tag{1.3}$$

where

$$R_{\gamma i} = \sqrt{(\eta_i - \eta_\gamma)^2 + (\phi_i - \phi_\gamma)^2}, \tag{1.4}$$

and the sum runs over all the hadrons in the event (or, alternatively, i can be interpreted as an index running over the towers of a hadronic calorimeter). For both the isolation prescriptions we are going to define below, the first step is to draw a cone of fixed half-angle R_0 around the photon axis, as given in eq. (1.2). We will denote this cone as the isolation cone.

Definition A. The photon is isolated if the total amount of hadronic transverse energy in the isolation cone fulfils the following condition:

$$E_{T,had}(R_0) \leq \epsilon_c p_{T\gamma}, \tag{1.5}$$

where ϵ_c is a small number, and $p_{T\gamma}$ is the transverse momentum of the photon.

Definition B. The photon is isolated if the following inequality is satisfied:

$$E_{T,had}(R) \leq \epsilon_\gamma p_{T\gamma} \mathcal{Y}(R), \tag{1.6}$$

for *all* the cones lying inside the isolation cone, that is for $R \leq R_0$. The function $\mathcal{Y}$ is arbitrary to a large extent, but must at least have the following property:

$$\lim_{R\to 0} \mathcal{Y}(R) = 0, \tag{1.7}$$

and being different from zero everywhere except for $R = 0$.

Definition A was proven to lead to an infrared-safe cross section at all orders of perturbation theory in ref. [3]. The smaller ϵ_c, the tighter the isolation. Loosely speaking, for vanishing ϵ_c the direct component behaves like $\log \epsilon_c$, while the fragmentation component behaves like $\epsilon_c \log \epsilon_c$. Thus, for $\epsilon_c \to 0$ eq. (1.1) diverges. This is obvious since the limit $\epsilon_c \to 0$ corresponds to a fully-isolated-photon cross section, which cannot be a meaningful quantity, whether experimentally (because of limited energy resolution) or theoretically (because there is no possibility for soft particles to be emitted into the cone).

Definition B was proposed and proven to lead to an infrared-safe cross section at all orders of perturbation theory in ref. [2]. Eq. (1.7) implies that the energy of a parton falling into the isolation cone $\mathcal{C}_{R_0}$ is correlated to its distance (in the η–ϕ plane) from the photon. In particular, a parton becoming collinear to the photon is also becoming soft. When a quark is collinear to the photon, there is a collinear divergence; however, if the quark is also soft, this divergence is damped by the quark vanishing energy. When a gluon is collinear to the photon, then either it is emitted from a quark, which is itself collinear to the photon – in which case, what was said previously applies – or the matrix element is finite. Finally, it is clear that the isolation condition given above does not destroy the cancellation of soft singularities, since a gluon with small enough energy can be emitted anywhere inside the isolation cone. The fact that this prescription is free of final-state QED collinear singularities implies that the direct part of the cross section is finite. As far as the fragmentation contribution is concerned, in QCD the fragmentation mechanism is purely collinear. Therefore, by imposing eq. (1.6), one forces the hadronic remnants collinear to the photon to have zero energy. This is equivalent to saying that the fragmentation variable z is restricted to the range $z = 1$. Since the parton-to-photon fragmentation functions do not contain any $\delta(1 - z)$, this means that the fragmentation contribution to the cross section is zero, because an integration over a zero-measure set is carried out. Therefore, only the first term on the RHS of eq. (1.1) is different from zero, and it does not contain any μ_γ dependence.

We stress again that the function $\mathcal{Y}$ can be rather freely defined. Any sufficiently well-behaved function, fulfilling eq. (1.7), could do the job, the key point being the correlation between the distance of a parton from the photon and the parton energy, which must be strong enough to cancel the quark-to-photon collinear singularity. Throughout this paper, we will use

$$\mathcal{Y}(R) = \left(\frac{1 - \cos R}{1 - \cos R_0}\right)^n, \qquad n = 1. \tag{1.8}$$

We also remark that the traditional cone-isolation prescription, eq. (1.5), can be recovered from eq. (1.6) by setting $\mathcal{Y} = 1$ and $\epsilon_\gamma = \epsilon_c$.

1.3 Isolated photons at the LHC

In this section, we will present results for isolated-photon cross sections in pp collisions at 14 TeV. These results have been obtained with the fully-exclusive NLO code of ref. [4], and are relevant to the isolation obtained with definition B; the actual parameters used in the computation are given in eq. (1.8), together with $\epsilon_\gamma = 1$. We let $R_0 = 0.4$. We will comment in the following on the outcome of definition A.

Any sensible perturbative computation should address the issue of the perturbative stability of its results. A rigorous estimate of the error affecting a cross section at a given order can be given if the next order result is also available. If this is not the case, it is customary to study the dependence of the physical observables upon the renormalization (μ_R) and factorization (μ_F) scales. It is important to stress that the resulting spread should not be taken as the 'theoretical error' affecting the cross section; to understand this, it is enough to say that the range in which μ_R and μ_F are varied is arbitrary. Rather, one should compare the spread obtained at the various perturbative orders; only if the scale dependence decreases when including higher orders the cross section can be regarded as perturbatively stable and sensibly compared to data.

Usually, μ_R and μ_F are imposed to have the same value, μ, which is eventually varied. However, this procedure might hide some problems, because of a possible cancellation between the effects induced by the two scales. It is therefore desirable to vary μ_R and μ_F independently. Here, an additional problem arises at the NLO. The expression of any cross section in terms of μ (that is, when $\mu_R = \mu_F$) is not ambiguous, while *it is* ambiguous if $\mu_R \neq \mu_F$. In fact, when $\mu_R \neq \mu_F$, the cross section can be written as the sum of a term corresponding to the contribution relevant to the case $\mu_R = \mu_F$, plus a term of the kind:

$$\alpha_{\rm S}(\mu_A)\,\mathcal{B}(\alpha_{\rm S}(\mu_R))\,\log\frac{\mu_R}{\mu_F}, \tag{1.9}$$

where $\mathcal{B}$ has the same power of $\alpha_{\rm S}$ as the LO contribution, say $\alpha_{\rm S}^k$. The argument of the $\alpha_{\rm S}$ in front of eq. (1.9), μ_A, can be chosen either equal to μ_R or equal to μ_F, since the difference between these two choices is of NNLO. Thus, it follows that the dependence upon μ_R or μ_F of a NLO cross section reflects the arbitrariness of the choice made in eq. (1.9), which is negligible only if the NNLO ($\alpha_{\rm S}^{k+2}$) corrections are much smaller than the NLO ones ($\alpha_{\rm S}^{k+1}$). This leads to the conclusion that a study of the dependence upon μ_R or μ_F *only* can be misleading. In other words: $\mathcal{B}$ in eq. (1.9) is determined through RG equations in order to cancel the scale dependence of the cross section up to terms of order $\alpha_{\rm S}^{k+2}$. This happens regardless of the choice made for μ_A in eq. (1.9). However, here we are not discussing the cancellation to a given perturbative order of the effects due to scale variations; we are concerned about the coefficient in front of the $\mathcal{O}(\alpha_{\rm S}^{k+2})$ term induced by such variations, whose size is dependent upon the choice made for μ_A and therefore, to some extent, arbitrary. We have to live with this arbitrariness, if we decide to vary μ_R or μ_F only. However, we

	MRST99					CTEQ5		
	1	2	3	4	5	M	HJ	$(\delta\sigma/\sigma)_\pm$
NLO, $\lvert\eta_\gamma\rvert < 2.5$	23.78	23.20	24.19	22.07	25.49	25.10	24.61	$^{+0.068}_{-0.057}$
LO, $\lvert\eta_\gamma\rvert < 2.5$	10.34	10.07	10.52	9.875	10.78	10.91	10.66	$^{+0.090}_{-0.072}$
NLO, $\lvert\eta_\gamma\rvert < 1.5$	14.59	14.23	14.88	13.66	15.53	15.35	15.01	$^{+0.068}_{-0.056}$
LO, $\lvert\eta_\gamma\rvert < 1.5$	6.457	6.270	6.583	6.212	6.657	6.771	6.596	$^{+0.091}_{-0.073}$

Table 1: *Isolated-photon cross sections (nb), with $40 < p_{T\gamma} < 400$ GeV, in two different rapidity ranges, for various parton densities. The scale dependence, evaluated according to eq. (1.10), is also shown.*

can still vary μ_R and μ_F independently, but eventually putting together the results in some sensible way, that reduces the impact of the choice made for μ_A. In this section, we will consider the quantities defined as follows:

$$\left(\frac{\delta\sigma}{\sigma}\right)_\pm = \pm\left\{\left[\frac{\sigma(\mu_R=\mu_0,\mu_F=\mu_0)-\sigma(\mu_R=a_\pm\mu_0,\mu_F=\mu_0)}{\sigma(\mu_R=\mu_0,\mu_F=\mu_0)+\sigma(\mu_R=a_\pm\mu_0,\mu_F=\mu_0)}\right]^2 + \left[\frac{\sigma(\mu_R=\mu_0,\mu_F=\mu_0)-\sigma(\mu_R=\mu_0,\mu_F=a_\pm\mu_0)}{\sigma(\mu_R=\mu_0,\mu_F=\mu_0)+\sigma(\mu_R=\mu_0,\mu_F=a_\pm\mu_0)}\right]^2\right\}^{\frac{1}{2}}, \qquad (1.10)$$

where a_+ and $a_- = 1/a_+$ are two numbers of order one, which we will take equal to 1/2 and 2 respectively; the $\pm$ sign in front of the RHS of eq. (1.10) is purely conventional. We can evaluate $(\delta\sigma/\sigma)_\pm$ by using $\mu_A = \mu_R$ or $\mu_A = \mu_F$ in eq. (1.9). The reader can convince himself, with the help of the definition of the QCD β function, that the difference between these two choices is of order α_S^4 in the expansion of *the contribution to* $(\delta\sigma/\sigma)^2_\pm$ *due to eq. (1.9)*; on the other hand, this difference is only of order α_S^3 in each of the two terms under the square root in the RHS of eq. (1.10). This is exactly what we wanted to achieve: a suitable combination of the cross sections resulting from independent μ_R and μ_F variations is less sensitive to the choice for μ_A made in eq. (1.9) with respect to the results obtained by varying μ_R or μ_F *only*.

In table 1 we present the results for the total isolated-photon rates, both at NLO and at LO. The latter cross sections have been obtained by retaining only the lowest order terms ($\mathcal{O}(\alpha_{\rm em}\alpha_S)$) in the short-distance cross section, and convoluting them with NLO-evolved parton densities. Also, a two-loop expression for α_S has been used. There is of course a lot of freedom in the definition of a Born-level result. However, we believe that with this definition one has a better understanding of some issues related to the stability of the perturbative series. In order to obtain the rates entering table 1, we required the photon transverse momentum to be in the range $40 < p_{T\gamma} < 400$ GeV, and we considered the rapidity cuts $|\eta_\gamma| < 1.5$ and $|\eta_\gamma| < 2.5$, in order to simulate a realistic geometrical acceptance of the LHC detectors. We first consider the scale dependence of our results (last column), evaluated according to eq. (1.10). We see that the NLO results are clearly more stable than the LO

ones; this is reassuring, and implies the possibility of a sensible comparison between NLO predictions and the data. Notice that the size of the radiative corrections (K factor, defined as the ratio of the NLO result over the LO result) is quite large. From the table, we see that the cross sections obtained with different parton densities differ by 6% at the most (relative to the result obtained with MRST99-1 [5], which we take as the default set). MRST99 sets 2 and 3 are meant to give an estimate of the effects due to the current uncertainties affecting the gluon density, whereas sets 4 and 5 allow to study the sensitivity of our predictions to the value of $\alpha_{\rm S}(M_Z)$ (sets 1, 4 and 5 have $\Lambda_5^{\overline{\rm MS}}$ =220, 164 and 288 MeV respectively). On the other hand, the difference between MRST99-1 and CTEQ5M [6] results is due to the inherent difference between these two density sets (CTEQ5M has $\Lambda_5^{\overline{\rm MS}}$ =226 MeV, and therefore the difference in the values of $\alpha_{\rm S}(M_Z)$ plays only a very minor role).

From inspection of table 1, we can conclude that isolated-photon cross section at the LHC is under control, both in the sense of perturbation theory and of the dependence upon non-calculable inputs, like $\alpha_{\rm S}(M_Z)$ and parton densities. The relatively weak dependence upon the parton densities, however, is not a good piece of news if one aims at using photon data to directly access the gluon density. On the other hand, the expected statistics is large enough to justify attempts of a direct measurement of such a quantity. In the remainder of this section, we will concentrate on this issue. We will consider

$$\mathcal{R}_x = \frac{d\sigma_0/dx - d\sigma/dx}{d\sigma_0/dx + d\sigma/dx}, \tag{1.11}$$

where x is any observable constructed with the kinematical variables of the photon and, possibly, of the accompanying jets. σ and σ_0 are the cross sections obtained with two different sets of parton densities, the latter of which is always the default one (MRST99-1). We can imagine a gedanken experiment, where it is possible to change at will the parton densities; in this way, we can assume the relative statistical errors affecting σ and σ_0 to decrease as $1/\sqrt{N}$ and $1/\sqrt{N_0}$, N and N_0 being the corresponding number of events. It is then straightforward to calculate the statistical error affecting $\mathcal{R}_x$; by imposing $\mathcal{R}_x$ to be larger than its statistical error, one gets

$$\mathcal{R}_x \;>\; (\mathcal{R}_x)_{min} \;\equiv\; \frac{1}{\sqrt{2\mathcal{L}\epsilon\sigma(x,\Delta x)}}, \tag{1.12}$$

where $\mathcal{L}$ is the integrated luminosity, $\epsilon \leq 1$ collects all the experimental efficiencies, and

$$\sigma(x,\Delta x) = \int_{x-\Delta x/2}^{x+\Delta x/2} dx\, \frac{d\sigma}{dx} \tag{1.13}$$

is the total cross section in a range of width Δx around x.

In fig. 1 we present our predictions for $\mathcal{R}_x$. In the left panel of the figure we have chosen $x = p_{T\gamma}$, while in the right panel we have $x = x_{\gamma j}$, where

$$x_{\gamma j} = \frac{p_{T\gamma}\exp(\eta_\gamma) + p_{Tj}\exp(\eta_j)}{\sqrt{S}}. \tag{1.14}$$

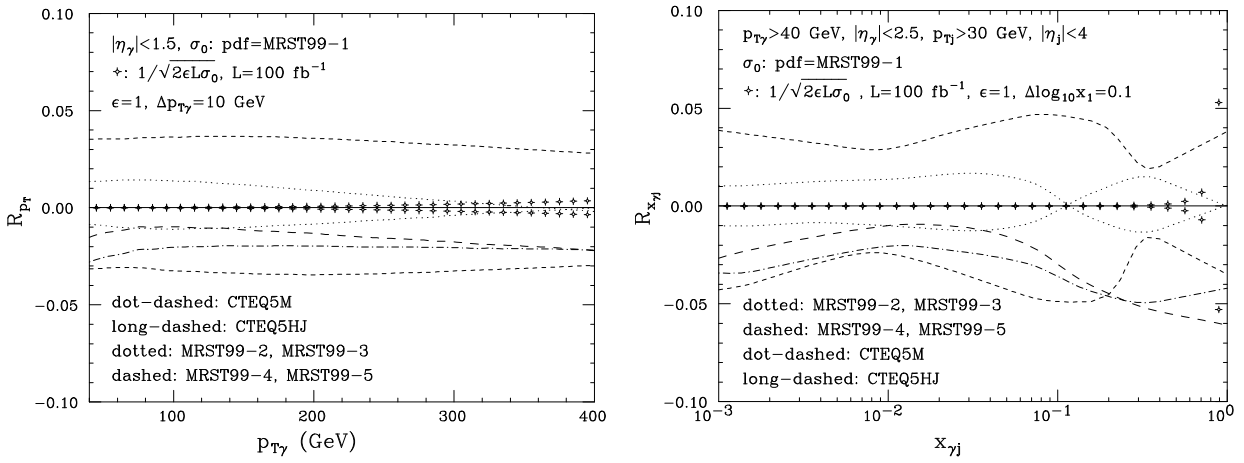

Figure 1: *Dependence of isolated-photon and isolated-photon-plus-jet cross section upon parton densities, as a function of $p_{T\gamma}$ and $x_{\gamma j}$.*

In this equation $\sqrt{S}$ is the center-of-mass energy of the colliding hadrons, and p_{Tj} and η_j are the transverse momentum and rapidity of the hardest jet recoiling against the photon. In order to reconstruct the jets, we adopted here a k_T-algorithm, namely that proposed in ref. [7], with $D = 1$. Notice that $x_{\gamma j}$ exactly coincides at the leading order with the Bjorken-x of the partons in one of the incoming hadrons; NLO corrections introduce only minor deviations. For all the density sets considered, the dependence of $\mathcal{R}$ upon $p_{T\gamma}$ is rather mild. The values in the low-$p_{T\gamma}$ region could also be inferred from table 1, since the cross section is dominated by small $p_{T\gamma}$'s. Analogously to what happens in the case of total rates, the sets MRST99-4 and MRST99-5 give rise to extreme results for $\mathcal{R}_{p_{T\gamma}}$, since the value of Λ_{QCD} is quite different from that of the default set. From the figure, it is apparent that, by studying the transverse momentum spectrum, it will not be easy to distinguish among the possible *shapes* of the gluon density. On the other hand, it seems that, as far as the statistics is concerned, a distinction between any two sets can be performed. Indeed, the symbols in the figure display the quantity defined in eq. (1.12), for $\mathcal{L} = 100$ fb^{-1}, $\Delta p_{T\gamma} = 10$ GeV and $\epsilon = 1$. Of course, the latter value is not realistic. However, a smaller value (leading to a larger $(\mathcal{R})_{min}$), can easily be compensated by enlarging $\Delta p_{T\gamma}$ and by the fact that the total integrated luminosity is expected to be much larger than that adopted in fig. 1.

Turning to the right panel of fig. 1, we can see a much more interesting situation. Actually, it can be shown that the pattern displayed in the figure is rather faithfully reproduced by plotting the analogous quantity, where one uses the gluon densities instead of the cross sections. This does not come as a surprise. First, $x_{\gamma j}$ is in an almost one-to-one correspondence with the x entering the densities. Secondly, photon production is dominated by the gluon-quark channel, and therefore the cross section has a linear dependence upon $g(x)$, which can be easily spotted. It does seem, therefore, to be rather advantageous to look at more exclusive variables, like photon-jet correlations (this is especially true if one considers

the procedure of unfolding the gluon density from the data: in the case of single-inclusive variables, the unfolding requires a de-convolution, which is not needed in the case of correlations). Of course, there is a price to pay: the efficiency ϵ will be smaller in the case of photon-jet correlations, with respect to the case of single-inclusive photon observables, mainly because of the jet-tagging. However, from the figure it appears that there should be no problem with statistics, except in the very large $x_{\gamma j}$ region.

Finally, we would like to comment on the fact that, for the case of single-inclusive photon observables, we also computed the cross section by isolating the photon according to definition A, using $\epsilon_c = 2$ GeV$/p_{T\gamma}$. The two definitions return a $p_{T\gamma}$ spectrum almost identical in shape, with definition B higher by a factor of about 9%. It is only at the smallest $p_{T\gamma}$ values that we considered, that definition B returns a slightly steeper spectrum. The fact that such different definitions produce very similar cross sections may be surprising. This happens because, prior to applying the isolation condition, partons tend to be radiated close to the photon; therefore, most of them are rejected when applying the isolation, no matter of which type. This situation has already been encountered in the production of photons at much smaller energies. The reader can find a detailed discussion on this point in ref. [8].

References

[1] H. Baer, J. Ohnemus and J. F. Owens, *Phys. Rev.* **D42** (1990) 61 ;
P. Aurenche, R. Baier and M. Fontannaz, *Phys. Rev.* **D42** (1990) 1440 ;
E.L. Berger and J. Qiu, *Phys. Rev.* **D44** (1991) 2002 ;
E. W. N. Glover and W. J. Stirling, *Phys. Lett.* **B295** (1992) 128 ;
Z. Kunszt and Z. Trocsanyi, *Nucl. Phys.* **B394** (1993) 139 ;
L.E. Gordon and W. Vogelsang, *Phys. Rev.* **D50** (1994) 1901.

[2] S. Frixione, *Phys. Lett.* **B429** (1998) 369 .

[3] S. Catani, M. Fontannaz and E. Pilon,*Phys. Rev.* **D58** (1998) 094025 .

[4] S. Frixione, `hep-ph/9809397`, Proc. of the '29th International Conference on High-Energy Physics (ICHEP 98)', Vancouver, Canada, July 1998.

[5] A.D. Martin, R.G. Roberts, W.J. Stirling and R.S. Thorne, `hep-ph/9907231`.

[6] CTEQ Collaboration (H.L. Lai et al.), `hep-ph/9903282`.

[7] S.D. Ellis and D. Soper, *Phys. Rev.* **D48** (1993) 3160 .

[8] S. Frixione and W. Vogelsang, `hep-ph/9908387`, to appear in *Nucl. Phys.* **B**.

Direct photon pair production at colliders, an irreducible background to Higgs boson searches at the LHC

T. Binoth, J.P. Guillet, V.A. Ilyin, E. Pilon and M. Werlen

Abstract

Direct [1] photon pairs with large invariant mass are the so-called irreducible background in the search for Higgs bosons at the LHC in the channel $h \to \gamma\gamma$, in the mass range $80 - 140$ GeV/c^2. This huge background requires an understanding and quantitative evaluation. Photon pair production at the Tevatron offers the opportunity to already test our understanding of this process. In the same mass range, the production of a Higgs boson ($hrightarrow\gamma\gamma$) in association with a hard jet at the LHC is a promising channel, as the corresponding $\gamma\gamma+$ jet background may be under better control.

1 Role and relevance of higher order corrections

Our theoretical understanding of direct photon pair production (as any hard hadronic process, cf. [1]) is based on the QCD improved parton model, according to which long and short distance effects factorize from each other. Short distance subprocesses are safely computed in perturbative QCD. Long distance effects cannot be completely calculated from QCD at present, although their scaling violations can be. Instead, they are extracted from experimental data and encoded into non-perturbative quantities, such as the parton distribution functions in incoming hadrons and, if necessary, inclusive fragmentation functions of partons into observed outgoing particles, e.g. photons. Yet these quantities are universal, i.e. independent of the hard subprocess: schematically they can be measured in one process, then transported to predict another one.

However, the border between short and long distance scales is arbitrary. The separation requires the introduction of unphysical parameters; e.g. the factorization scale M^2, and similarly the fragmentation scale M_f^2 in the case of a fragmentation process. In an ideal exact calculation, the dependence on these spurious parameters (as well as on the arbitrary renormalization scale μ^2) would cancel between the short and long distance parts. In an actual expansion in powers of α_s truncated at some finite order, this cancellation is only

[1] "Direct" or "prompt" mean that these photons do not result from the decay of π^0 and η.

partial; it holds up to a term of the lowest uncalculated order. As the order of truncation increases, theoretical estimates become flatter and flatter over broader and broader ranges of these spurious scales. The uncertainty induced by this actual dependence restricts the accuracy and predictive character of QCD calculations. In particular, the result of a lowest order calculation is plagued by a large monotonic dependence with respect to M^2, M_f^2 and μ^2. It changes by a large factor (two or more) when these scales are varied around the typical hard scale of the process; such a lowest order estimate is *not at all quantitative*. This is the first reason why any tentatively accurate QCD calculation has to be carried out to at least next-to-leading order (abbreviated below as NLO).

Another important motivation is that higher order corrections to some given process may reveal new mechanisms, whose rates may be not necessarily negligible compared to the leading order contribution. The production of photons is a typical example of this phenomenon, as will be explained below. This amounts to large higher order corrections, which affect substantially both the magnitude and the shape of the distributions, not due to poor apparent convergence of the first terms in the perturbative expansion, but for physically understood reasons.

Finally, finite order calculations may not be accurate enough, as in the case of infrared sensitive observables, i.e. observables controlled by multiple soft gluon emission [2]. Yet, in some less well-known cases of infrared sensitivity, they may reveal perturbative instabilities or even divergences plaguing the calculation at any further order *inside* the physical spectrum [4]. This is, for example, the case for the transverse momentum distribution of pairs of isolated photons, as will be discussed below. The calculation of higher order corrections is therefore the first step towards a deeper understanding of what happens in such cases.

2 Mechanisms of production.

Schematically, three possible mechanisms may produce prompt photon pairs with large invariant mass: one (which may be called "two direct") in which both photons take part directly in the hard subprocess, another one ("one fragmentation") in which one of the photons undergoes the hard subprocess while the other results from the fragmentation of a hard parton (quark or gluon), itself produced at large tranverse momentum, and yet another mechanism ("two fragmentation") in which both photons result from such a fragmentation. This schematical splitting into these three contributions emerges from a factorization procedure sketched in what follows. Although this splitting provides a convenient picture, one must however keep in mind that it is arbitrary; none of these contributions can be measured separately. Only their sum is physical.

2.1 Direct vs. fragmentation mechanisms

From a topological point of view, a photon produced from fragmentation is with a high probability accompanied by a jet of hadrons. From a technical point of view, the lowest order of

[2] See for example [1, 2, 3]

the "one fragmentation" contribution emerges in the calculation of higher order perturbative corrections to the "two direct" contribution given by the Born process $q\bar{q} \to \gamma\gamma$. Some of these higher order corrections, such as $qg \to q\gamma\gamma$, are plagued by final state collinear singularities associated with the collinear splitting $q \to q\gamma$. The latter have to be factorized and absorbed into quark and gluon fragmentation functions to a photon, $D_{\gamma/q \text{ or } g}(z, M_f^2)$ defined at some fragmentation scale [3] M_f^2. Analogously to the so-called anomalous component of the photon structure function, a collinear logarithmic enhancement occurs, induced by the pointlike quark-photon coupling. To all orders in α_s, this phenomenon results in $D_{\gamma/q \text{ or } g}(z, M_f^2)$ behaving asymptotically [4] as $\alpha/\alpha_s(M_f^2)$. This compensates the one extra power of α_s involved in the short distance subprocess, so that fragmentation contributions are asymptotically of the same order as the Born term, by power counting in α_s. What is more, given the high gluon density at LHC, the gq (or $\bar{q}$) initiated process involving one photon from fragmentation even dominates the inclusive production rate in the range $80 - 140$ GeV.

In turn, higher order corrections to "one fragmentation" reveal the "two fragmentation" mechanism. Similarly, a collinear enhancement associated with each photon fragmentation compensates two extra powers of α_s in the short distance subprocess, so that the power counting in α_s is here also asymptotically the same as for the Born and "one fragmentation" parts. Higher order corrections to both fragmentation contributions have in principle to be computed in order to provide a consistent NLO study. This has been done in [6]. The actual quantitative significance of these contributions is discussed in sect. 4.

2.2 The box contribution

Beyond this, the gluon-gluon fusion contribution $gg \to \gamma\gamma$, of the "two direct" type, cannot be neglected. Indeed, although it is an $\mathcal{O}(\alpha^2\alpha_s^2)$ i.e. next-to-next-to-leading order contribution, the suppression due to higher powers of α_s is compensated by the large gluon luminosity at colliders. This is especially true at LHC in the relevant range for Higgs search, where the so-called box contribution has the same magnitude as the Born term, roughly 50 to 80 %.

Moreover it is the lowest order of a new mechanism, whose spurious scale dependences are thus monotonic, and only higher corrections to it would reduce the sensitivity with respect to spurious scale dependences. Finally, this lowest order is a $2 \to 2$ process which yields only back to back photons in the direction transverse to the beam axis; it gives no contribution to the tail of the transverse momentum distribution of photon pairs. An evaluation of the distortion of the transverse momentum distribution of photon pairs due to the process of gluon-gluon fusion requires the computation of at least the next order correction [3]. The sum "two direct + box" will be refered to as the "direct" contribution.

[3] and in some given factorization scheme. Here we use the $\overline{MS}$ scheme, [5].

[4] i.e. when the fragmentation scale M_f^2 (chosen of the order of the hard scale of the subprocess) is large compared to any typical hadronic scale ~ 1 GeV^2.

3 Isolation

At TeV colliders, the fragmentation contributions are far from negligible. In particular, the "one fragmentation" component dominates the inclusive production of photon pairs in the lower range of the invariant mass spectrum; in the range of interest for Higgs search at LHC it happens to be 2 to 5 times larger than the "two direct" contribution, depending on choice of scales [5] [6]. A NLO evaluation of the fragmentation contribution is thus necessary to have a tentatively reliable prediction.

Actually, collider experiments do not measure *inclusive* photon pairs. Isolation cuts [6] are imposed experimentally to drastically reduce the gigantic background coming from decays of π^0 and η mesons. Schematically, a candidate-photon is considered isolated if, in some given cone in azimuthal angle and rapidity about the photon defined by

$$(\phi - \phi_\gamma)^2 + (y - y_\gamma)^2 \leq R^2, \tag{3.1}$$

the deposited hadronic transverse energy E_T^{had} is smaller than some maximal amount E_T^{max},

$$E_T^{had} \leq E_T^{max} \tag{3.2}$$

R and E_T^{max} being fixed by the experiments. Such isolation cuts affect also the production rate of direct photon pairs, especially the "single-" and "two fragmentation" contributions, whose topologies are similar to the one of the background. Those are severely reduced when E_T^{max} is chosen to be very small compared to the transverse momenta of the photons.

Yet a NLO evaluation of fragmentation contributions is still relevant for various reasons. First, the actual isolation cuts used by collider experiments may be quite more complicated than the schematical criterion given by eqns. (3.1,3.2). Higher order partonic calculations are not designed to account for such criteria accurately, contrary to Monte-Carlo event generators such as `PYTHIA` [8] or `HERWIG` [9]. Since these Monte-Carlos and NLO partonic calculations are based on different QCD approximations, it is worthwhile to compare these two approaches whenever possible, as for the inclusive production rate, as well as with rather simple isolation cuts such as the one of eqns. (3.1,3.2). Secondly, the above cone-type isolation criterion induces infrared sensitivity *inside* the physical spectrum for observables such as the q_T spectrum of photon pairs. This effect appears at the NLO - and every higher order - in the "one fragmentation" component, as will be shown in the next section.

4 Phenomenology

In earlier works on di-photon production [10], only the "two direct" contribution was calculated at NLO, while the fragmentation contribution included only the lowest order "one fragmentation" part [7]. Moreover, these works were not implemented in a form suited to compute observables such as the invariant mass relevant for Higgs search, nor flexible enough to

[5] As already mentioned in the beginning of sect. 2, this statement is strongly fragmentation scale dependent.

[6] More about isolation issues in processes involving direct photons is discussed in [7].

[7] The "box" contribution was included too.

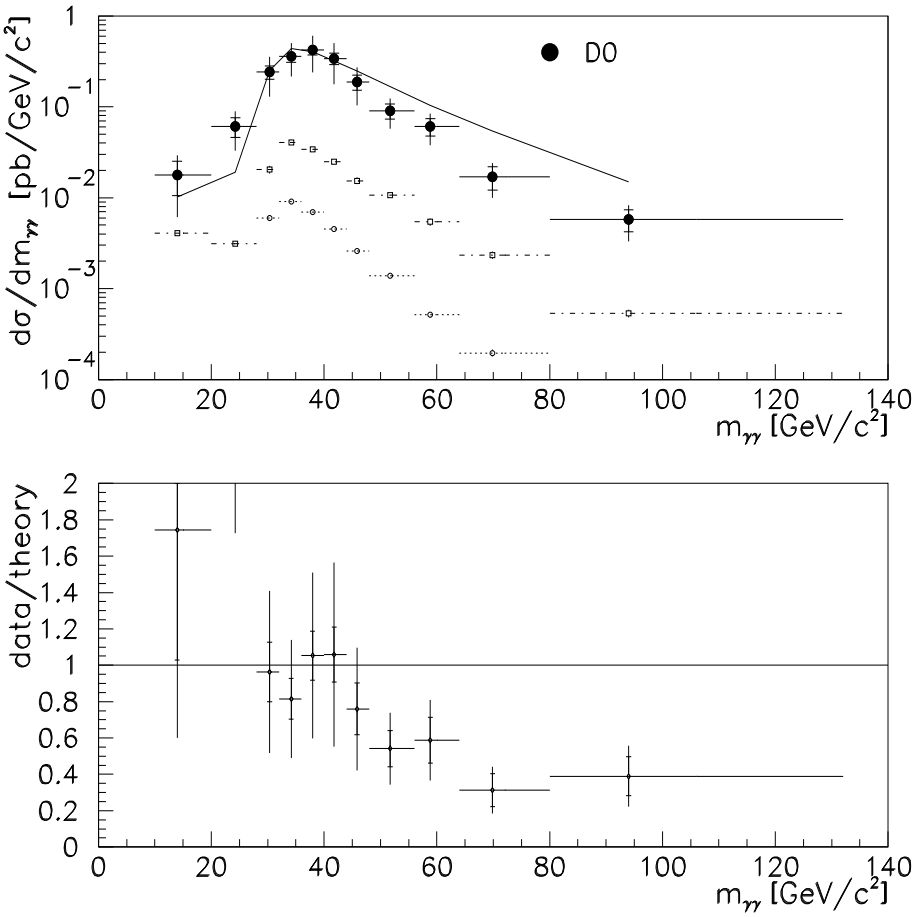

Figure 1: Diphoton differential cross section $d\sigma/dm_{\gamma\gamma}$ vs. $m_{\gamma\gamma}$, the mass of the photon pair, at the Tevatron, $\sqrt{S} = 1.8$ TeV. Preliminary data points (statistical errors and systematics in quadrature) from the D0 collaboration [12] are compared to the theoretical predictions; the full NLO prediction is shown as the solid line while open squares (open circles) represent the single (double) fragmentation contribution.

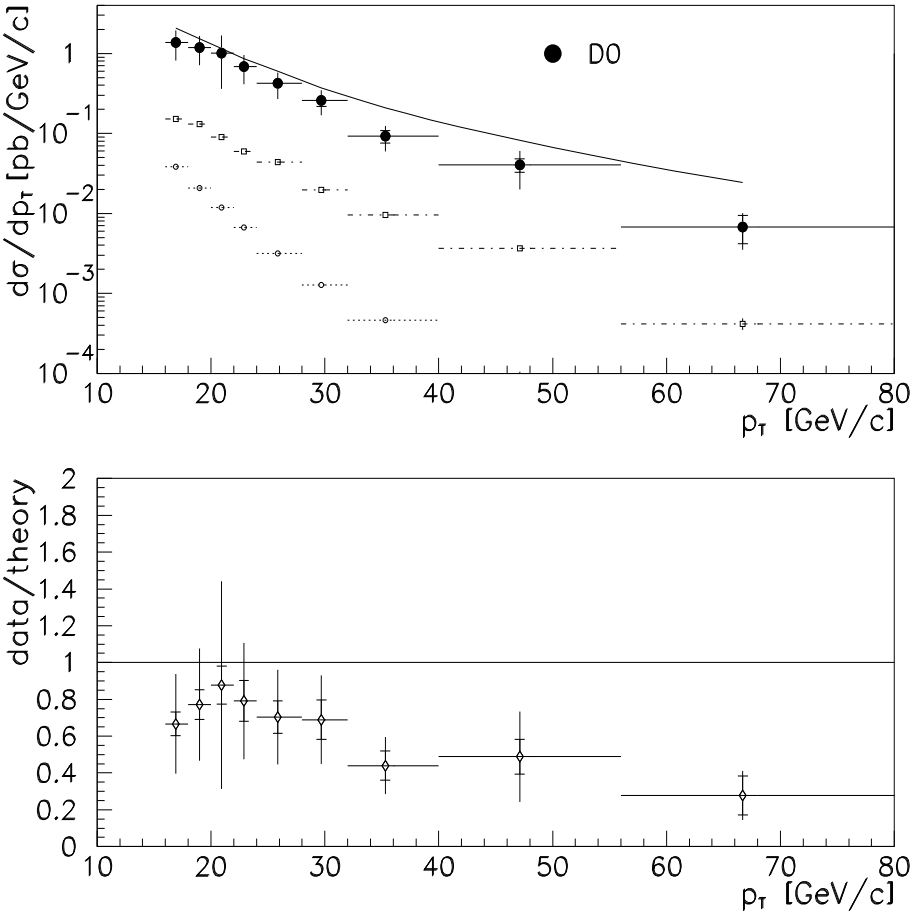

Figure 2: Diphoton differential cross section $d\sigma/dp_T$ vs p_T, the transverse energy of each photon, at Tevatron, $\sqrt{S} = 1.8$ TeV. Preliminary data points (statistical errors and systematics in quadrature) from the D0 collaboration [12] are compared to the theoretical predictions; the full NLO prediction is shown as the solid line while open squares (open circles) represent the single (double) fragmentation contribution. The ratio data/(full NLO theory) is shown below.

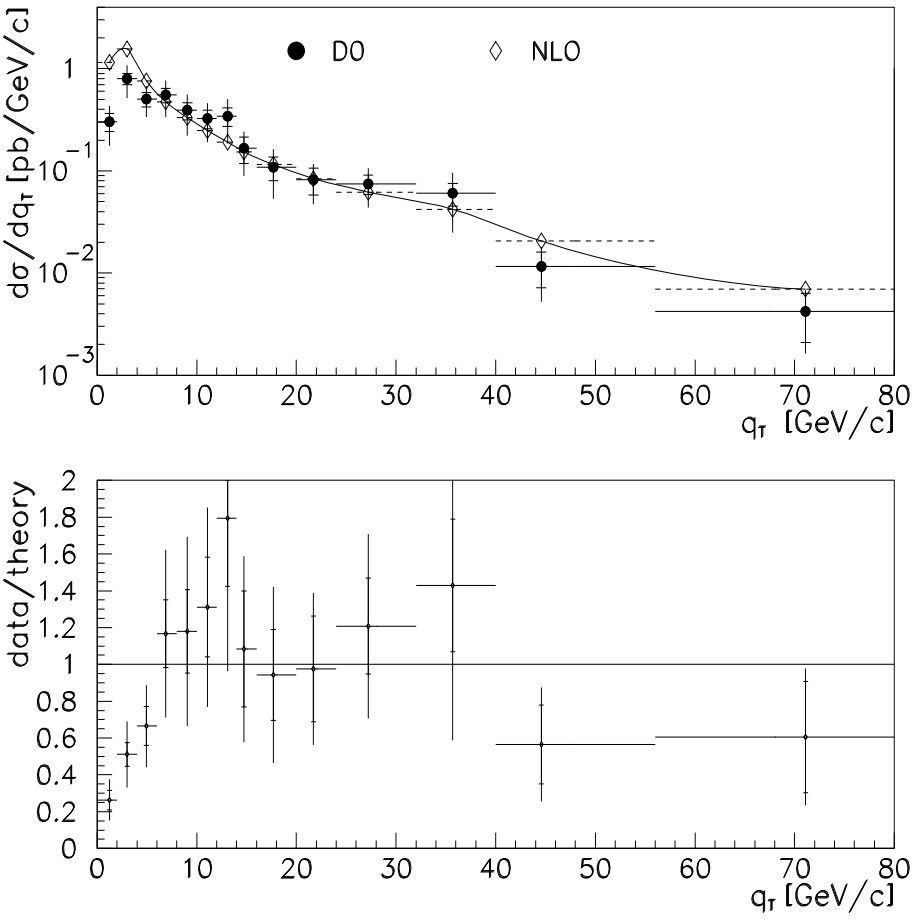

Figure 3: Diphoton differential cross section $d\sigma/dq_T$ vs. q_T, the transverse momentum of the photon pair, at the Tevatron, $\sqrt{S} = 1.8$ TeV. Preliminary data points (statistical errors and systematics in quadrature) from the D0 collaboration [12] are compared to the theoretical predictions; the full NLO prediction is shown as the solid line.

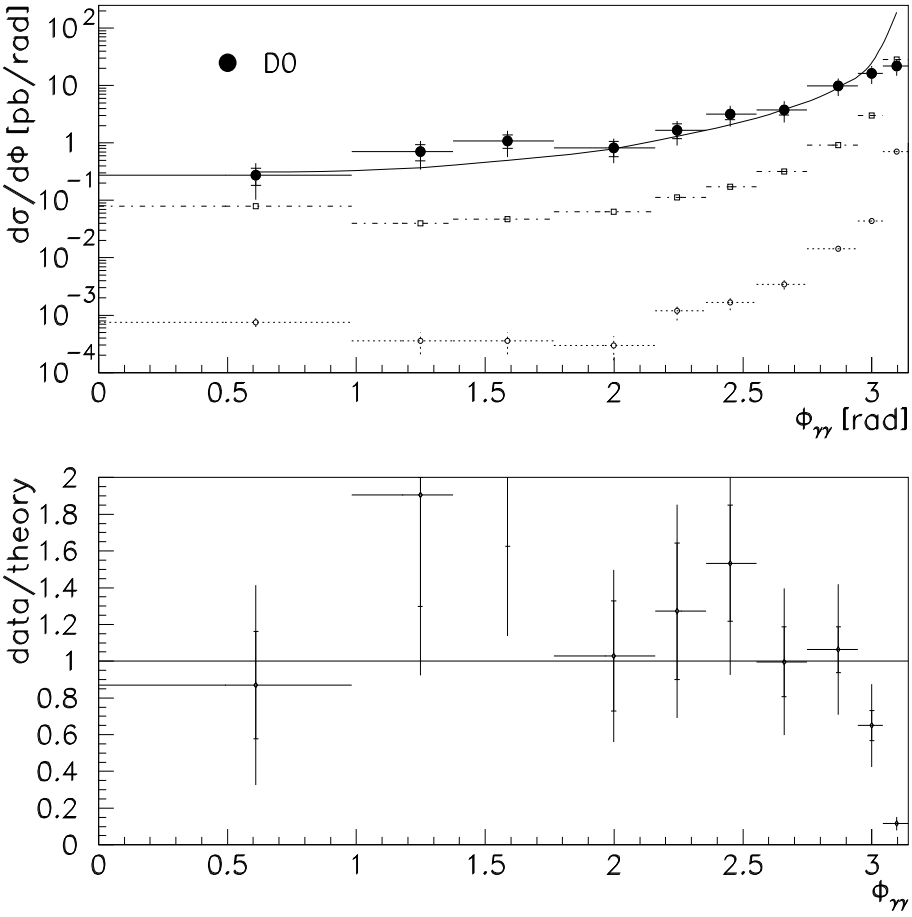

Figure 4: Diphoton differential cross section $d\sigma/d\phi_{\gamma\gamma}$ vs. $\phi_{\gamma\gamma}$, the azimuthal angle between the two photons, at the Tevatron, $\sqrt{S} = 1.8$ TeV. Preliminary data points (statistical errors and systematics in quadrature) from the D0 collaboration [12] are compared to the theoretical predictions; the full NLO prediction is shown as the solid line. The direct contribution is shown as the dashed line while open squares (open circles) represent the single (double) fragmentation contribution.

accomodate experimental selection cuts. A further refinement [11] has implemented the same approximation in a more flexible approach combining analytical and Monte-Carlo integration techniques, thus allowing the computation of several observables within the same calculation, and the possibility to account for selection/isolation cuts. Two recent developments are presented in this workshop (see also C. Balazs' contribution).

We have implemented the "two direct", "single-" and "double fragmentation" contributions at NLO accuracy, together with the box gluon-gluon contribution, into a general purpose computer program of "partonic event generator" type (*DIPHOX*) presented in detail in [6]. The results which we present here are derived from this analysis.

4.1 Comparison with Tevatron data

The NLO results agree with the preliminary D0 data [12] reasonably, as seen in Figs. (1-4), except for the tails of each photon's transverse momentum distribution $d\sigma/dE_T$ and the invariant mass distribution of pairs $d\sigma/dM_{\gamma\gamma}$ at large E_T and $M_{\gamma\gamma}$ respectively, where the three highest data points are affected by correlated systematic uncertainties due to background evaluation in both cases. However, more instructive conclusions will be drawn after a finalized understanding of the systematics, and even more so after the Tevatron Run II with the statistics improved by a factor of 20.

4.2 Estimates for LHC

We now give some theoretical estimates in the domain relevant for Higgs search at the LHC, for the invariant mass distribution cf. Fig. (5) with and without isolation. One has to keep in mind that the theoretical uncertainties are still large. Firstly these results are still plagued by rather large scale uncertainties, as discussed below. Secondly, for a given scale choice, they may still underestimate the actual background to Higgs search.

4.3 Critical examination of various theoretical issues

4.3.1 Scale uncertainties

As mentioned above all results depend on three unphysical scales. Varying these between $M^2_{\gamma\gamma}/4$ and $4M^2_{\gamma\gamma}$ along the first diagonal $\mu^2 = M^2 = M_f^2$, the NLO results for the invariant mass distribution appear surprisingly stable, since they change by about 5% only. Alternatively, anti-diagonal variations of μ^2 and $M^2 = M_f^2$ in the same interval about the central value $M^2_{\gamma\gamma}$ lead to a variation still rather large (up to 20 %). This is because variations with respect to μ^2 and M^2 act in opposite ways. When μ^2 is increased, $\alpha_s(\mu^2)$ and hence the NLO corrections decrease; on the other hand the relevant values of the momentum fraction of incoming partons are small, $\sim \mathcal{O}(10^{-3}$ to $10^{-2})$, so that the gluon and sea quark distribution functions increase when M^2 is increased. Scale changes with respect to μ^2 and M^2 thus nearly cancel again each other along the first diagonal but add up in the other case. Actually,

the stability along the first diagonal is accidental at this order [8]. These observations hold separately for the box contribution.

In conclusion, the μ^2, M^2 dependences are thus not completely under control yet. On the other hand, accounting for the NLO corrections to the fragmentation components provides stability with respect to M_f^2 variations about orthodox choices of the fragmentation scale.

4.3.2 Quantitative importance of fragmentation contributions

For orthodox choices of the fragmentation scale, M_f^2 of order $M_{\gamma\gamma}^2$, the "single fragmentation" contribution is small at Tevatron, given the stringent isolation cuts used, and the "two fragmentation" one is even smaller. For example, as can be seen in Figs. (1,2) the "one fragmentation" contribution is about one order of magnitude less than the "two direct" one. It may still have a small visible effect, as in the tail of the azimutal angle distribution $d\sigma/d\phi_{\gamma\gamma}$ ($\phi_{\gamma\gamma}$ being the azimutal angle between the two photons of a pair) in the low $\phi_{\gamma\gamma}$ range, cf. Fig. (4).

The situation is the same for LHC predictions, see Fig. (6). Contributions from fragmentation are drastically reduced when very stringent cuts are imposed, e.g. $E_T^{max} = 2.5$ GeV in $R = 0.4$. However, in practice such isolation cuts will be nearly saturated by underlying events: their veto on the hard event itself is thus even more severe, allowing almost no transverse energy leakage from the hard process inside the cone. This may be experimentally most suitable. However, requiring that *no transverse energy* be deposited in a cone of fixed size about a photon is *not* infrared safe order by order in perturbation. It means that finite but very stringent isolation cuts imposed in fixed order partonic calculations would lead to unreliable results. When less severe isolation cuts are used, the "one-", and to a lesser extend, "two fragmentation" components are subdominant but not negligible.

4.3.3 Infrared sensitive distributions

Being based on a finite order calculation, our computer code is not suited for the study of observables controled by multiple soft gluon emission [1, 2]. Among those, one may distinguish the following examples, most of which would require an improved account of soft gluon effects.

The transverse momentum distribution of pairs $d\sigma/dq_T$ near $q_T = 0$
The problematics of the "two direct" contribution is similar to the well-known Drell-Yan process, see [3]. On the other hand, the fragmentation contributions do not diverge order by

[8] In processes for which the lowest order involves some power of α_s, an explicit μ^2 dependence appears in next-to-leading order correction, which partially compensates the μ^2 dependence in $\alpha_s(\mu^2)$. Unlike this, in the two direct component which dominates the cross section when a drastic isolation is required, the lowest order involves no α_s. The explicit μ^2 dependence would thus appear only at $\mathcal{O}(\alpha_s^2)$, i.e. at next-to-next-to leading order. At next to leading order, the μ^2 dependence occurs only through the monotonous decrease of the $\alpha_s(\mu^2)$ weighting the first correction: there is no partial cancellation of μ^2 dependence. The mechanism is more complicated in the fragmentation components, and the situation becomes mixed up between all components when the severity of isolation is reduced.

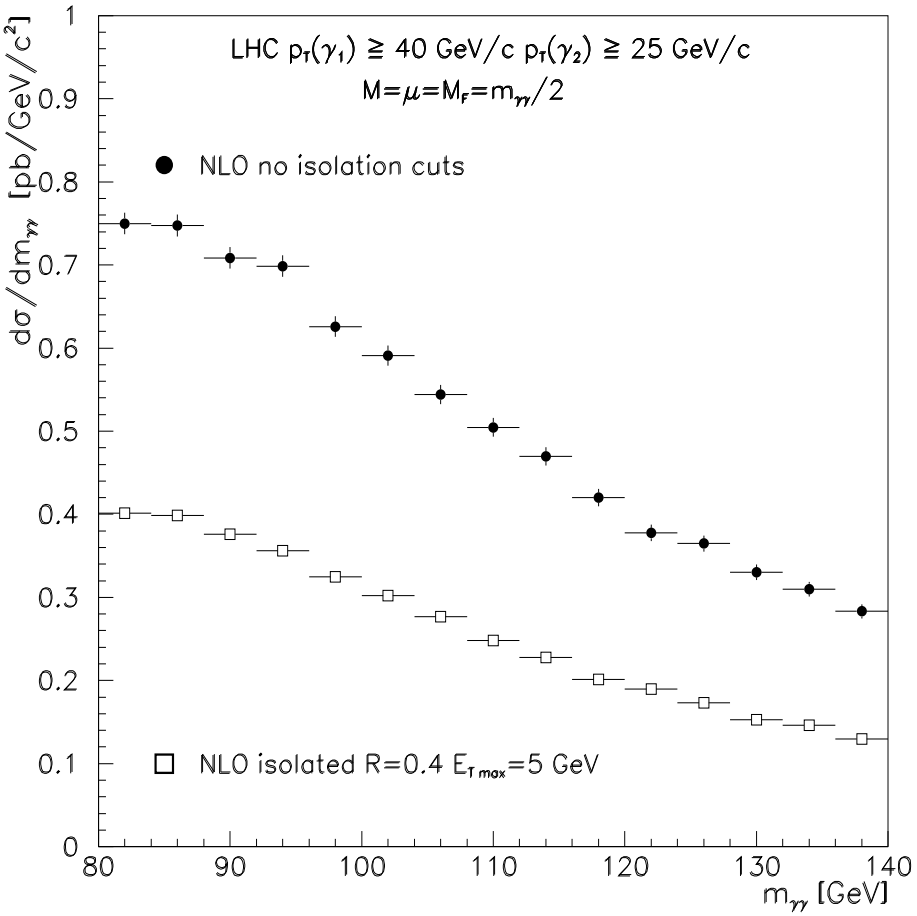

Figure 5: Diphoton differential cross section $d\sigma/dm_{\gamma\gamma}$ vs. $m_{\gamma\gamma}$ at the LHC, $\sqrt{S} = 14$ TeV, without and with isolation criterion $E_{Tmax} = 5$ GeV in $R = 0.4$. Same kinematic cuts as in Fig. (6). The scale choice is $M = M_f = \mu = m_{\gamma\gamma}/2$.

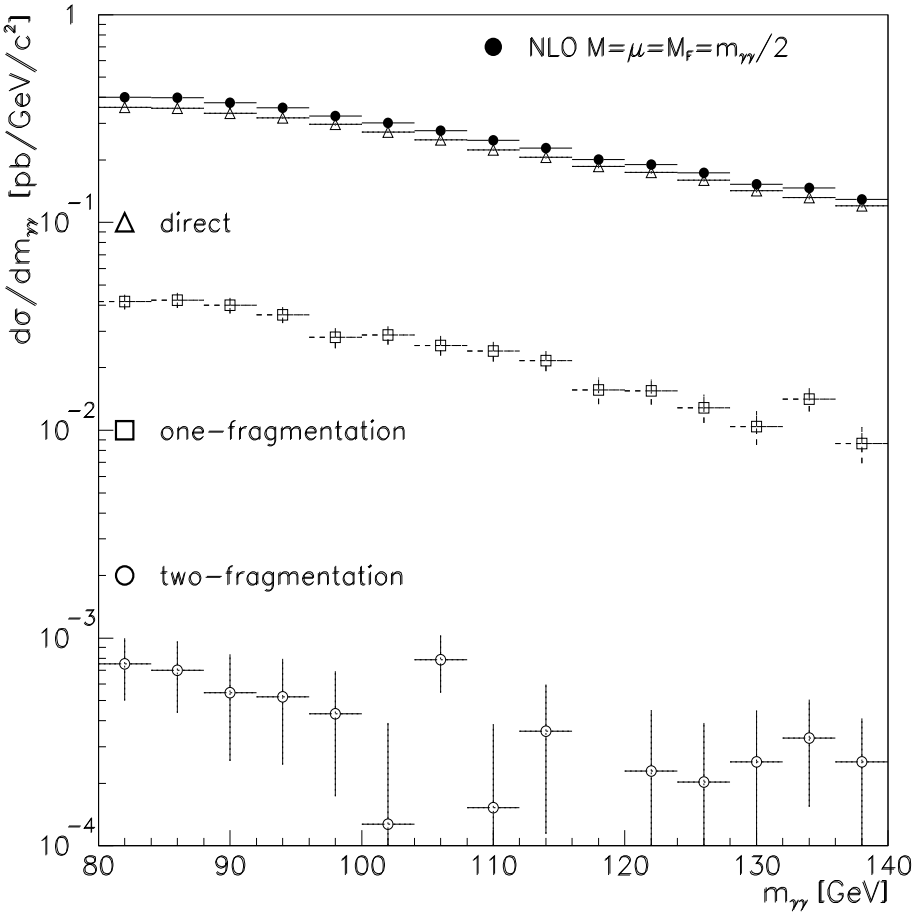

Figure 6: Splitting of the diphoton differential cross section $d\sigma/dm_{\gamma\gamma}$ at the LHC, $\sqrt{S} = 14$ TeV with isolation criterion $E_{Tmax} = 5$ GeV in $R = 0.4$, into the "direct","one fragmentation" and "two fragmentation" components, shown for the scale choice $\mu = M = M_f = m_{\gamma\gamma}/2$. The following kinematic cuts are applied: $p_T(\gamma_1) \geq 40$ GeV, $p_T(\gamma_2) \geq 25$ GeV, $|y(\gamma_{1,2})| \leq 2.5$.

order when $q_T \to 0$. Indeed, in the "one fragmentation" case,

$$\text{parton } 1 + \text{parton } 2 \;\to\; \gamma_1 + \text{parton } 3 \tag{4.1}$$
$$\text{parton } 3 \;\to\; \gamma_2 + X \tag{4.2}$$

the NLO contribution to the hard subprocess (4.1) yields a double logarithm

$$\sim \alpha_s \ln^2 \|\mathbf{p}_T(\gamma_1) + \mathbf{p}_T(\text{parton } 3)\| \tag{4.3}$$

when $\mathbf{p}_T(\gamma_1) + \mathbf{p}_T(\text{parton } 3) \to 0$. However the extra convolution associated with the fragmentation (4.2) involves an integral over $z_2 = p_T(\gamma_2)/p_T(\text{parton } 3)$ which smears out this integrable singularity. The "two fragmentation" contribution involves two such convolutions, and hence one more smearing.

The azimuthal angle distribution $d\sigma/d\phi_{\gamma\gamma}$ near $\phi_{\gamma\gamma} = \pi$
This case differs from the previous one for two reasons. Firstly, not only the "two direct" contribution diverges order by order when $\phi_{\gamma\gamma} \to \pi$, but also both "single-" and "double-fragmentation" contributions do, as can be seen in Fig. (4). Moreover, in both fragmentation cases, soft gluons may couple to both initial- and final-state hard emitters. Indeed, consider the example of the "one fragmentation case", cf. eqns. (4.1). Selecting $\phi_{\gamma\gamma} \to \pi$ emphasizes $\phi(\text{parton } 3) - \phi(\gamma_1) \to \pi$, so that all the emitted partons besides parton 3 have to be collinear to either of the incoming or outgoing particles, and/or soft, which yields double logarithms

$$\sim \alpha_s \ln^2 [\pi - (\phi(\text{parton } 3) - \phi(\gamma_1))] \tag{4.4}$$

associated with each of the hard partons 1,2,3 - plus single logarithms as well. For the observable $d\sigma/d\phi_{\gamma\gamma}$ near $\phi_{\gamma\gamma} = \pi$, the integral involved in the convolution of the hard subprocess with the fragmentation functions does not smear these logarithmic divergences, since the fragmentation variable $z_2 = p_T(\gamma_2)/p_T(\text{parton } 3)$ is decoupled from the azimutal variable $\phi(\text{parton } 3)$ equal to $\phi(\gamma_2)$ in the soft and collinear limits. A similar explanation holds for the "double fragmentation component". An analagous problem affects the q_T distribution of a pair photon + jet at low q_T.

The azimuthal angle distribution $d\sigma/d\phi_{\gamma\gamma}$ near $\phi_{\gamma\gamma} = 0$
Both fragmentation contributions to $d\sigma/d\phi_{\gamma\gamma}$ diverge also order by order when $\phi_{\gamma\gamma} \to 0$. Here also soft gluons may couple to both initial- and final-state hard emitters. Actually, given the large invariant mass of the pairs, the vicinity of $\phi_{\gamma\gamma} = 0$ is never probed, so that an improved treatment of soft gluon effects is not needed in this case. Yet, as a consequence, an increase of the "single-fragmentation" contribution can be seen [9] in the lower range of the $\phi_{\gamma\gamma}$ spectrum, cf. Fig. (4).

An infrared divergence for $d\sigma/dq_T$ *inside* the physical spectrum
Besides the well-known issue at $q_T = 0$, another infrared sensitive point appears in the q_T

[9] A similar behaviour occurs also for the "two fragmentation" contribution, which is however too tiny to have any significant effect.

spectrum due to isolation, at the critical value $q_T = E_T^{max}$. Indeed, at lowest order the "one fragmentation" component is not smooth, it instead behaves as a step function [13],

$$\left(\frac{d\sigma}{dq_T}\right)^{\text{“single fragm”},(LO)} \propto \Theta\left(E_T^{max} - q_T\right) \tag{4.5}$$

Consequently, in agreement with the general study of [4], the NLO - and every higher order - correction has a double logarithmic divergence at the critical point. Such singularities are very sensitive to the kinematical constraints and the observable considered. The present case has a double logarithm *below* the critical point,

$$\left(\frac{d\sigma}{dq_T}\right)^{\text{“single fragm”},(NLO)} \propto -\alpha_s \ln^2\left(E_T^{max} - q_T\right)\Theta\left(E_T^{max} - q_T\right) + \cdots \tag{4.6}$$

The infrared sensitive behaviour at this critical point can be infered on Fig. (7), where a rather large value for E_T^{max} is used in order to split this critical point from the small q_T region.

This effect is not visible on the theoretical prediction of Fig. (3) because of the low value $E_T^{max} = 4$ GeV used by the D0 collaboration. The two infrared sensitive regions ($q_T \to 0$ and $q_T \sim E_T^{max}$) are not separated enough, and the bin smearing averages over both effects. The phenomenon is thus camouflaged. An all order summation of this soft gluon effect has to be carried out to restore a sensible shape to the q_T distribution. A similar observation would be made about the q_T distribution of a pair {photon + jet}.

5 Perspectives

Future improvements of the theoretical understanding of di-photon production will require various inputs. Next-to-next to leading order corrections would hopefully stabilize the scale dependences and correct the normalisations. Another important quantitative improvement would be the higher order corrections to the box contribution, which is within reach thanks to some recent achievements. Progresses in this direction are reported on elsewhere in these proceedings [14].

This accounting of multiple soft gluon effects, already implemented in [3] for the "two direct" contribution in absence of isolation cuts, is needed in the *DIPHOX*-based study to provide correct distributions in the infrared sensitive regions. This affects the q_T distribution at low q_T. It also concerns the $\phi_{\gamma\gamma}$ distribution when $\phi_{\gamma\gamma} \to \pi$, which has been less studied, and for which the soft gluon effects in the fragmentation cases are more involved than in the "two direct" case [15, 16]. It is also important for the q_T distribution in the vicinity of the critical point $q_T = E_T^{max}$, induced by the fixed cone type isolation criterion.

The understanding of the background to the Higgs search is quantitatively not yet on the same footing as for the signal. Hence, accounting for the higher order correction to the signal in numerical simulations might be instructive, but the results should be considered with care in order to avoid statements that are too optimistic.

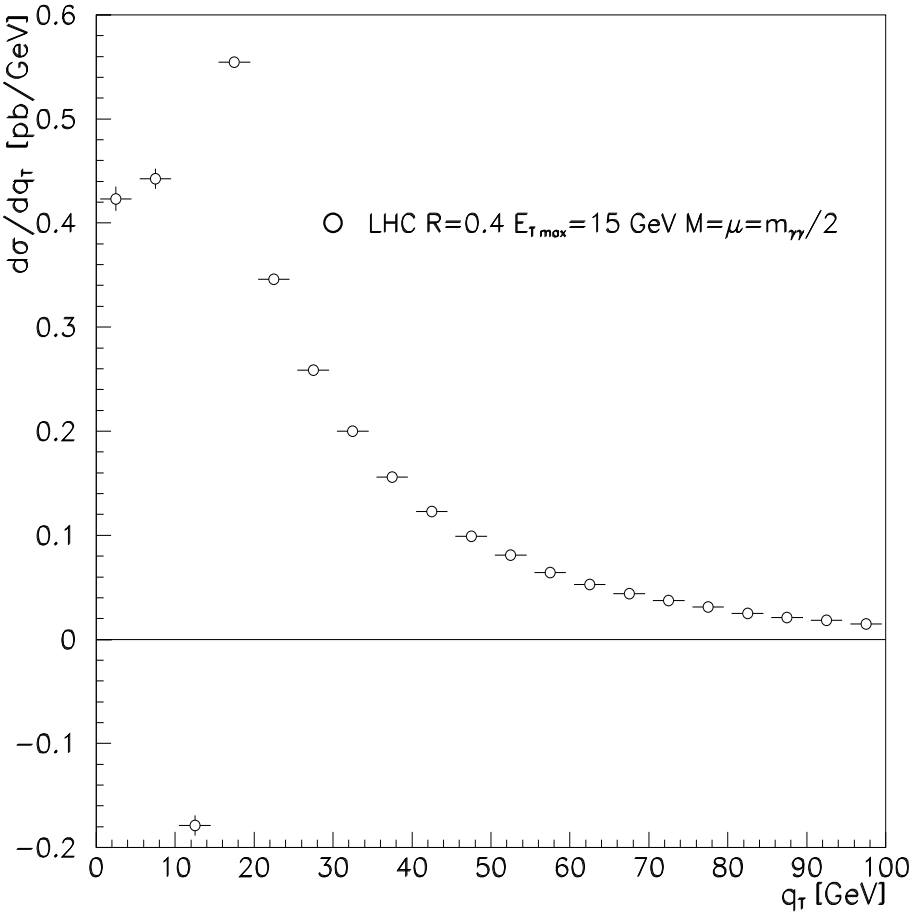

Figure 7: Diphoton differential cross section $d\sigma/dq_T$ at LHC, $\sqrt{S} = 14$ TeV, with isolation criterion $E_{Tmax} = 15$ GeV in $R = 0.4$.

6 Higgs search in association with a hard jet

In order to overcome the present insufficient control of higher order corrections in inclusive production, it has been suggested [17] to study the associated production of $h(\to \gamma\gamma)+$ jet, for which both signal S and background B are lower (but still at the level of hundred signal events at low luminosity). The lowest order estimate has shown that the S/B ratio is improved critically (up to $1/2 - 1/3$) with the same level of the significance $S/\sqrt{B}$. Furthermore, higher order corrections to the background have been shown recently [18] to be under better control than in the inclusive (i.e. unassociated) case.

6.1 Background: associated vs. inclusive

Indeed, in the inclusive case, the magnitude of the NNLO box contribution is comparable to the LO cross section essentially because the latter is initiated by $q\bar{q}$, whereas the former involves gg. The gg luminosity, much larger than the $q\bar{q}$ one, compensates numerically the extra α_s^2 factor of the box. On the contrary, in the channel $\gamma\gamma$ + jet, the LO cross-section is dominated by a qg initiated subprocess. The qg luminosity is sizeably larger than the $q\bar{q}$ one, so that the corresponding NNLO remains small compared to the LO result [18]. Thus, expecting that the subprocess $gg \to \gamma\gamma g$ gives the main NNLO correction, a quantitative description of the background with an accuracy better than 20% could be achieved already at NLO in the $\gamma\gamma+$ jet channel for a high p_T ($\geq$ 30 GeV) jet. All the helicity amplitudes needed for the implementation of the ("direct" contribution to the) background to NLO accuracy [10]are now available [19, 20, 21].

6.2 Signal vs. background

The origin of this improvement of the S/B ratio is the following. At LO, the signal of associated $h(\to \gamma\gamma)+jet$ production has basically a 2-body kinematics, due to the extremely small Higgs width (a few MeV). On the contrary, the LO background contributions $q\bar{q} \to \gamma\gamma g$ and $gq \to \gamma + \gamma + q$ (as well as the NNLO $gg \to \gamma\gamma g$ one) have 3-body kinematics. This is in contrast to the inclusive channel where both signal and background LO subprocesses have 2-body kinematics. This circumstance opens the room for more refined cuts to suppress the background more efficiently [17]. The contributions $q\bar{q} \to \gamma\gamma g$ and $gg \to \gamma\gamma g$ are suppressed down to 40% of the signal (to be compared with $S/B \sim 1/7$ for the inclusive channel). Unfortunately, as found in [17], the contribution of the other subprocess $gq \to \gamma\gamma q$, which dominates, yields the overall ratio $S/B \sim 1/2 - 1/3$.

The cuts which allow this efficient suppression of the irreducible background at LO are based on the differences in the shapes of the angular distributions in the partonic c.m.s.. Due to helicity and total angular momentum conservation, the S-wave does not contribute

[10]We remind the reader unfamiliar with the LO, NLO, NNLO, etc, terminology that this terminology does not refer to the absolute power of α_s involved, but instead to the relative power with respect to the Born term of the process considered. Hence, NLO corrections to $\gamma\gamma+$ jet are also part of the NNLO corrections to $\gamma\gamma$ inclusive (converse not true, cf. box).

to the dominant signal subprocess $gg \to Hg$. On the contrary, all angular momentum states contribute to the subprocesses $gq \to \gamma\gamma q$ and $q\bar{q} \to \gamma\gamma g$. Therefore, the signal has a more suppressed threshold behaviour compared to the background. The S/B ratio can thus be improved by increasing the partonic c.m.s. energy $\sqrt{\hat{s}}$ far beyond threshold, and a cut $\sqrt{\hat{s}} > 300$ GeV has been found to give the best S/B ratio for the LHC. Actually, the effect can not be fully explained by the threshold behavior only, since that would result in a uniform suppression factor. It was shown in [17, 22] (see Figs. 5 and 6 there) that the dependences of the background and the signal on the c.m.s. angular variables are quite different; therefore, the strong $\hat{s}$ cut affects them with different suppression factors (see [17, 22] for more details). This effect can be exploited to enhance the significance $S/\sqrt{B}$ at the same level as S/B. If the cut $\cos(\vartheta^*)(j\gamma) < -0.87$ on the jet-photon in the partonic c.m.s. is applied for $\sqrt{\hat{s}} < 300$ GeV and combined with the cut $\sqrt{\hat{s}} > 300$ GeV, the change on S/B is rather small, while the significance is improved by a factor ~ 1.3. The same effect can be observed with the cut on the jet angle in the partonic c.m.s. ($\vartheta^*(j)$, cf. Fig. 5 of [17, 22], but one should notice that the two variables, $\vartheta^*(j\gamma)$ and $\vartheta^*(j)$, are correlated. Therefore, it is desirable to perform a multi-variable optimization of the event selection. Notice that the present discussion is based on a LO analysis, and concerns only what was defined above as the "direct" component of the irreducible background. One now has to understand how this works at NLO.

Other, reducible, sources of background are potentially dangerous. The above-defined "one fragmentation" component to the so-called irreducible background, and the reducible background coming from misidentification of jet events were treated on a similar footing in the LO analysis of [17, 22] as a *de facto* reducible background. In [17, 22], a rough analysis found that this reducible background is less than 20% of the irreducible one after cuts are imposed. The misidentification rate is given mainly by the subprocesses $gq \to \gamma gq$, $gg \to \gamma q\bar{q}$ and $qq' \to \gamma q(g)q'(g)$, when the final state parton produces an energetic isolated photon but other products of the hadronization escape the detection as a jet. There, a $\gamma(\pi^0)/jet$ rejection factor equal to 2500 for a jet misidentified as a photon and 5000 for a well separated $\gamma(\pi^0)$ production by a jet were used. No additional π^0 rejection algorithms were applied. Furthermore, this reducible background is expected to be suppressed even more strongly than the irreducible background of "direct" type when a cut on $\sqrt{\hat{s}}$ is applied.

In summary, the associated channel $H(\to \gamma\gamma)+$ jet with jet transverse energy $E_T > 30$ GeV and rapidity $|\eta| < 4.5$ (thus involving forward hadronic calorimeters) opens a promising possibility for discovering the Higgs boson with a mass of 100-140 GeV at LHC even at low luminosity. However, to perform a quantitative analysis, the NLO calculations, namely of the background, have to be completed, and included in a more realistic final state analysis.

7 Acknowledgements

T. B. is a EU fellow supported by the EU Fourth Programme "Training and Mobility of Researchers", Network "Quantum Chromodynamics and the Deep Structure of Elementary Particles", contract FMRX-CT98-0194 (DG12 - MIHT). V.A. I. acknowledges support by the CERN-INTAS grant 377 and RFBR-DFG grant 99-02-04011. LAPTH is a *Unité Mixte*

de Recherche (UMR 5108) associée au CNRS et à l'Université de Savoie.

References

[1] S. Catani, these proceedings, and references therein.

[2] C. Balazs, J. Collins and D. Soper, these proceedings, and references therein.

[3] C. Balazs, J. Huston and I. Puljak, these proceedings, and references therein.

[4] S. Catani and B. Webber, JHEP 9710:005 (1997).

[5] L. Bourhis, M. Fontannaz and J.Ph. Guillet, Eur. Phys. J. **C2** (1998) 529.

[6] T. Binoth, J.P. Guillet, E. Pilon and M. Werlen, hep-ph/9911340, submitted to Eur. Phys. J **C**.

[7] S. Frixione and W. Vogelsang, these proceedings, and references therein.

[8] H.-U. Bengtsson and T. Sjöstrand, Comp. Phys. Comm. **46** (1987) 43;
T. Sjöstrand, Comp. Phys. Comm. **82** (1994) 74;
T. Sjöstrand, LU TP 95-20, hep-ph/9508391.

[9] G. Marchesini and B.R. Webber, Nucl. Phys **B 310** (1988) 461;
G. Marchesini, B.R. Webber, G. Abbiendi, I.G. Knowles, M.H. Seymour and L. Stanco, hep-ph/9607393.

[10] P. Aurenche, R. Baier, A. Douiri, M. Fontannaz and D. Schiff, Nucl. Phys. **B 286** (1987) 553;
P. Aurenche *et al.*, Proceedings of the ECFA workshop, Aachen 1989.

[11] B. Bailey, J. Ohnemus and J.F. Owens, Phys. Rev. **D46** (1992) 2018.

[12] Wei Chen, PhD Thesis (Univ. New-York at Stony Brook), Dec. 1997, unpublished;
D0 Collaboration (P. Hanlet for the collaboration), Nucl. Phys. Proc. Suppl. **64** (1998) 78.

[13] C. Balazs, E.L. Berger, S. Mrenna and C.P. Yuan, Phys. Rev. **D57** (1998) 6934.

[14] V. Del Duca and G. Heinrich, these proceedings, and references therein.

[15] R. Bonciani, S. Catani, M. Mangano and P. Nason, Nucl. Phys. **B529** (1998) 424.

[16] N. Kidonakis, G. Oderda and G. Sterman, Nucl. Phys. **B531** (1998) 365.

[17] M. Dubinin and V. Ilyin, CMS Note 97/101, 1997;
S. Abdullin *et al.*, Phys. Lett. **B431** (1998) 410.

[18] D. de Florian and Z. Kunszt, Phys. Lett. **B460** (1999) 184.

[19] Z. Bern, L. Dixon and D. A. Kosower, Nucl. Phys. **B437** (1995) 259.

[20] A. Signer, Phys. Lett. **B357** (1995) 204.

[21] V. Del Duca, W. B. Kilgore and F. Maltoni, Nucl. Phys. **B566** (2000) 252.

[22] S. Abdullin, M. Dubinin, V. Ilyin, D. Kovalenko, V. Savrin and N. Stepanov, Phys. Lett. **B431** (1998) 410.